SURFACE MODIFICATIONS TO MITIGATE REFRACTORY DEGRADATION IN HIGH-TEMPERATURE BLACK LIQUOR GASIFIERS

A Thesis
Presented To
The Academic Faculty

by

Krista J. Pallay

In Partial Fulfillment
of the Requirements for the Degree
Master of Science in Chemical Engineering

Georgia Institute of Technology
May 2006

Surface Modification to Mitigate Refractory Degradation in High-Temperature Black Liquor Gasifiers

Approved By:

Dr. Preet M. Singh
Department of Materials Science & Engineering
Georgia Institute of Technology

Dr. Jeff Empie
Department of Chemical and Biomolecular Engineering
Georgia Institute of Technology

Dr. Yulin Deng
Department of Chemical and Biomolecular Engineering
Georgia Institute of Technology

Date Approved: March 6, 2006

ACKNOWLEDGEMENTS

First and foremost I would like to thank my advisors Dr. Preet M. Singh and Dr. Jeff Empie. The patience, guidance, and encouragement of Dr. Singh greatly contributed to the success of my research. I would also like to thank Dr. Yulin Deng for taking the time to be a part of my thesis defense committee. Many thanks go out to Dr. Hiroki Nanko for the use of some important equipment for my research.

I would also like to thank all of the others that assisted me in the completion of my research. Specifically, I would like to thank Patrick Hazlewood for willingly answering countless questions and helping in the laboratory if needed (all without too many complaints) and Jamshad Mahmood for his time and knowledge along the way.

I would like to thank my parents for always encouraging and supporting me. I cannot begin to properly express my gratitude for all that you have done for me. Finally, I would like to thank all of my friends that are near and dear to my heart. Megan, thanks for always being just a phone call away and willing to offer some much needed advice. Akua, Ayanna, and Ryan, thanks to all of you for offering me a couch (or futon) whenever I was in need. You definitely got to see all the highs and the lows and stuck with me anyway. I appreciate that more than you know. Without you, my experience at Georgia Tech definitely would not have been the same. I will miss you all very much! I just have one word of advice, always be careful what you wish for, you may just get it!

TABLE OF CONTENTS

LIST OF TABLES

LIST OF FIGURES

SUMMARY

Ceria (CeO_2), chromia (Cr_2O_3), yttria-stabilized zirconia (Y_2O_3-ZrO_2), and sodium cerium oxide (Na_2CeO_3) were used as barrier coatings on Ufala®, an alumina-based ceramic refractory, to determine if they were effective at increasing the life of the refractory in a high-temperature black liquor gasification environment. The ceria, chromia, and yttria-stabilized zirconia coatings were applied at atmospheric pressure using a coating applicator at the Institute of Paper Science and Technology at the Georgia Institute of Technology. The sodium cerium oxide coatings in addition to the three other coating types were applied under atmospheric pressure at C^3™ International Technologies in Alpharetta, GA. The coated refractory, as well as a set of uncoated refractory used for baseline analysis, were tested using molten synthetic smelt at 1000°C for 36 hours. Uncoated refractory samples were also tested for 12, 72, 120, and 168 hours in order to make a kinetic reaction rate determination. The refractory were analyzed using gravimetric and dimensional analysis, X-ray diffraction, scanning electron microscopy, and energy dispersive X-ray spectroscopy to determine the severity of the physical changes that occurred after exposure to molten smelt. The data gathered from these experiments were not able to conclude that barrier coatings are sufficient to impede corrosion of the Ufala® refractory material in molten smelt.

Chapter 1

INTRODUCTION

Black liquor is the waste product from the Kraft pulping process which contains the remaining inorganic chemicals after cooking the pulp and a large variety and quantity of organic chemicals from the pulped wood chips. For every one ton of pulp that is manufactured, nearly seven tons of black liquor are produced [1]. With such a large amount of waste liquor being produced and containing important pulping chemicals and organic material which can be turned into energy, it is essential to have a recycle and recovery process to reduce the amount of waste and increase a mill's efficiency. The process by which the inorganic cooking chemicals are recovered and regenerated into fresh pulping chemicals and large amounts of heat energy are generated via burning of the organic materials is called chemical recovery [1]. To maximize heat recovery during the chemical recovery process, it is necessary to concentrate the black liquor to 65-80% solids before spraying it into the recovery boiler to be burned. After the combustion of the organics, the inorganic material that remains is referred to as smelt [1]. Smelt is composed of about two-thirds Na_2CO_3, one-third Na_2S, and small amounts of other sodium/sulfur compounds such as Na_2SO_4 and $Na_2S_2O_3$ [2]. It is also important to consider the chemicals that are found in the Kraft liquors since they are found in the recovery process. These chemicals include Na_2S, NaOH, Na_2CO_3, and Na_2SO_4 and are extremely important due to their addition of Na_2O into the recovery system [1].

With the high capital cost of recovery boilers and the fact that they are not easily expanded incrementally, replacement costs are extremely high. This is due to the fact that they are not only the largest, but the also the most expensive unit in the mill at over $100 million dollars a piece. Consequently, recovery boilers tend to be the limiting factor in the production rate of a mill [1] with nearly two-thirds of them already operating at capacity [3]. With changing environmental standards and the desire to increase production rates, the current Kraft recovery cycle needs to be altered. With these new environmental challenges, a greater amount of water, total solids, and organic fuel will need to be sent to the recovery cycle which will only serve to compound the existing bottlenecking problem in current mills [3]. One option would be to modify the current process by replacing the existing Tomlinson boilers with high temperature black liquor gasifiers.

Black liquor gasification is used to convert the organic material in black liquor into combustible gases for eventual power generation while recycling and transforming the inorganics into compounds that can be used to regenerate necessary pulping chemicals [4]. The main advantages to new high temperature black liquor gasification technology are lower capital costs, equipment that can be built modularly so as to allow for incremental mill expansion, and higher energy efficiency [5]. Gasification of black liquor would also reduce the mill emissions making it more environmentally friendly and therefore more feasible for long-term usage. High temperature gasifiers, while providing good sulfate reduction rate and high operating efficiency rates, run at nearly 1000°C inside the reactor. This temperature is above the melting temperature of smelt and as

such the smelt becomes molten [4]. Smelt, because of the sodium salt content, is extremely corrosive to most engineering materials at temperatures above its melting point [6]. The melting point of smelt is approximately 710°C [7]. Due to the problem with corrosion of the recovery boiler lining, there are only a few commercial scale high temperature black liquor gasifiers, one of which is at Weyerhaeuser's New Bern, NC mill. In 1999, the refractory material used in the gasifier at New Bern had a service lifetime of less than one year and was one of the major problems in plant operation [8]. Although alumina (Al_2O_3) has been identified by Saviharju [6] as the most promising material for high temperature black liquor gasification, it is not without its problems. Because alumina-based ceramic refractory material is inherently porous, the molten smelt is able to penetrate through the material via diffusion and react with and corrode the refractory throughout the interior of the material as well as at the surface. The chemical reaction moves the fuse cast alumina towards sodium aluminate in the sodium rich environment. The fact that the volume of the reaction products is larger than the reactants causes localized stresses within the material which leads to spalling of the refractory [9]. This refractory degradation poses a problem because in order to replace the gasifier lining, the equipment must be shut down and the refractory material completely replaced which makes for limited availability and production rates that suffer [8]. Without a gasifier lining that has a service life of at least one year, the viability of high temperature black liquor gasification significantly decreases.

A major problem in the implementation of high temperature black liquor gasification is that the material identified as the best refractory lining, alumina, still does not perform at

a sufficient level. In an attempt to modify the alumina to perform at a higher standard while still being reasonably priced at an industrial scale, the option of surface coatings and treatments must be seriously considered. A primary advantage of surface coatings is that you can use an inexpensive or less expensive substrate material and apply a surface treatment to provide the necessary surface properties such as corrosion resistance [10]. In this case, it is hoped that upon application of the barrier coating, the pore size will be decreased or completely eliminated. By limiting the number and size of the open pores, the molten smelt should have fewer avenues by which to penetrate the refractory. If the molten smelt is prevented from entering the core of the refractory, the problem with spalling and severe refractory degradation should be substantially decreased. Limiting corrosion of the refractory to the surface would not only extend the life of the refractory, it would also simplify lining repairs. If simple re-coating or re-treating instead of replacing the entire refractory lining can easily repair the material that is only altered at the surface level, the downtime and repair costs can be significantly reduced.

The main purpose of surface modification techniques is to create an impenetrable or less permeable surface to slow mass transfer into the refractory. Different types of surface modifications are available; however, the focus of this research is solely on protective barrier coatings. The sodium cerium oxide barrier coatings were applied solely by C^3™ International Technologies, Alpharetta, Georgia, that has a patented dipping and curing process. The remaining three metal oxide barrier coatings were applied by C^3™ International Technologies and under this project at the Institute of Paper Science and Technology (IPST) at Georgia Institute of Technology (GTech) using dip-coating and

curing process. The coatings done at the IPST at GTech included yttria-stabilized zirconium oxide, cerium oxide, and chromium oxide. The refractory materials used in the testing process are Jargal®M and Ufala®, both of which were supplied by Oak Ridge National Laboratories in Oak Ridge, Tennessee. Jargal®M is a high-purity alumina-based fused cast refractory consisting of more than 95% Al_2O_3, 4% Na_2O, 0.05% SiO_2, and less that 0.05% contaminants. Ufala®, on the other hand, is a more porous, less pure, and consequently much less expensive, alumina-based refractory with 58.1% Al_2O_3, 38.2% SiO_2, 2.2% TiO_2, 1.2% Fe_2O_3, and 0.3% other contaminants. Although uncoated Jargal®M performs much better in the high temperature black liquor gasification environments, the main focus was on surface modifications to the Ufala® refractory. The severe deformation that occurs to uncoated Ufala® made simple visual observations of the effectiveness of the surface coatings easier then if the same experiment were carried out on the less reactive Jargal®M. Also, in industrial applications an effective surface modification would more than likely be applied to the less expensive base material to decrease the overall cost of the equipment.

Both types of refractory were cut, weighed and measured, and microhardness tests were performed on the Jargal®M samples. Once the barrier coatings were applied and cured (if called for), the coated refractory samples were exposed to molten synthetic smelt in an oxygen-deficient atmosphere for 7 days for the Jargal®M samples and 36 hours for the Ufala® samples at 1000°C in an attempt to mimic the typical environment within a black liquor gasifier. Uncoated samples were also exposed to the same environment for 7 days or 36 hours, depending on refractory type, in order to provide an appropriate basis for

comparison to determine the corrosion resistance, if any, of the coatings. After exposure, all refractory samples were measured and weighed for dimensional and gravimetric analysis, x-ray diffraction (XRD) was performed to identify any reaction products on the sample surface, scanning electron microscopy (SEM) allowed for visual assessment of the damage done to the refractory in the corrosive environment, and the reaction depth was determined using energy dispersive x-ray spectroscopy (EDS). The microhardness was tested for all Jargal®M samples. Severe deformation occurred to the Ufala® samples upon exposure to molten smelt and as such the microhardness tests were not performed on those samples. After evaluation of results obtained during the research, it can be concluded that different oxide coatings used in this study that were selected due to their better performance in other systems, did not provide sufficient protection or impediment to mitigate refractory degradation in molten smelt environments found in high-temperature black liquor gasifiers. The yttria-stabilized zirconia and chromia coatings performed the best out of the coatings tested. Both coating types showed a marked decrease in weight and volume gain. The chromia coated samples also showed the smallest penetration depth. Ceria coatings performed significantly worse than the other coatings and actually experienced a greater weight gain and volume increase then the uncoated samples. Whether the coatings were applied commercially or in laboratory did not appear to affect the performance of the coatings.

Chapter 2

REVIEW OF LITERATURE

2.1 Kraft Chemical Recovery Process

The current technology being used in pulp and paper mills is the Kraft process with a Tomlinson recovery boiler. The main purpose for the recovery boiler is to recover the inorganic chemicals to regenerate fresh pulping chemicals for the process while also allowing the organics to be burned off. This combustion not only decreases the environmental effects by decreasing mill emissions, it also helps in producing energy to run the mill [1]. There are, however, many different problems that exist with the current system. At over $100 million, the capital costs of installing a Tomlinson furnace are extremely high and they are not easily expanded incrementally [1]. Approximately two thirds of the paper mills in the United States are currently operating at capacity and the recovery boiler is the bottleneck of the process [3]. Unfortunately, with the high capital cost, mills are hesitant to replace existing recovery boilers with larger sized reactors. Smelt-water explosions are another potential problem that exists [7]. These explosions are caused by the rapid vaporization that occurs when water contacts the molten smelt. By 1992 in North America there were more than 140 recovery boiler explosions caused by smelt-water interaction some so severe as to cause death of operators and major structural damage [11]. Also, with restrictions from the Environmental Protection Agency becoming increasingly strict, it is important to take into consideration emissions from the mills when determining how to replace the current technology. The changes that would need to be implemented to the Kraft process to meet with changing

restrictions would cause additional bottlenecking problems because of increasing fuel loads being sent to the recovery boiler. That fuel would contain not only more total solids and more organic fuel, but also more water meaning the evaporators would need to perform more work causing a potential bottleneck there as well [3].

The Kraft pulping process was patented in 1884 by C.F. Dahl and was first used commercially in Sweden in 1885. At the time, it was noted that it was essential to recover the pulping chemicals in order to make the Kraft process an economically viable option instead of the sulfite process [12]. The Tomlinson recovery furnace, created by Tomlinson in conjunction with Babcock and Wilcox, entered the pulping scene in the 1930s allowing the Kraft pulping process to dominate. The Tomlinson recovery boiler was able to combine final evaporation and burning of spent liquor, heat recovery, and chemical recovery into one unit [12]. Within the recovery boiler there are three distinct zones. The top of the recovery boiler is the oxidizing zone, the middle is the drying zone where the black liquor is sprayed into the boiler, and the bottom is the reducing zone [1]. Figure 1 shows the design of a typical recovery boiler [1] and Figure 2 shows a schematic of the recovery boiler system [13]. After 70 years, the Tomlinson boiler is still used in the Kraft recovery process today.

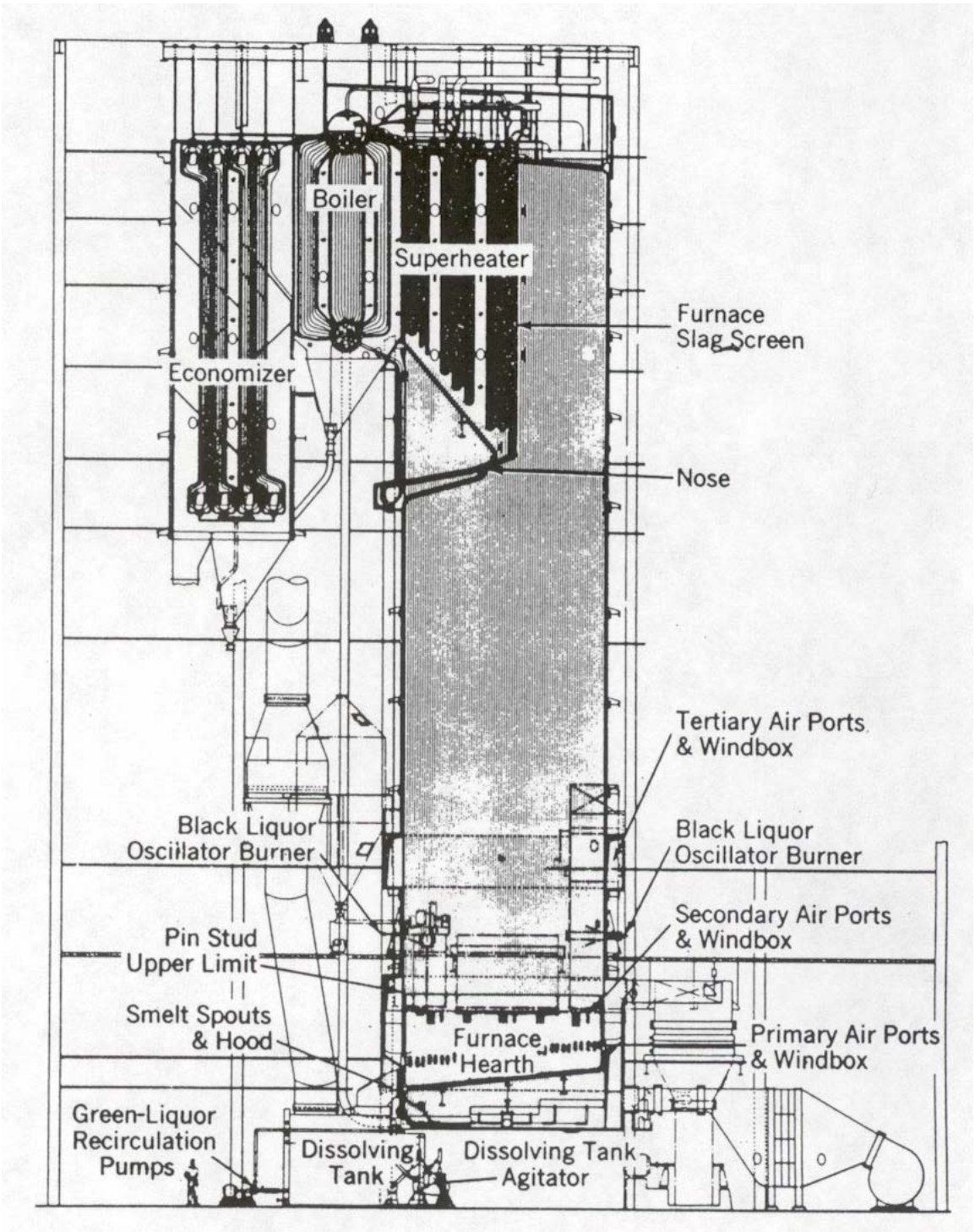

Figure 1: Schematic of a Typical Tomlinson Recovery Boiler [1]

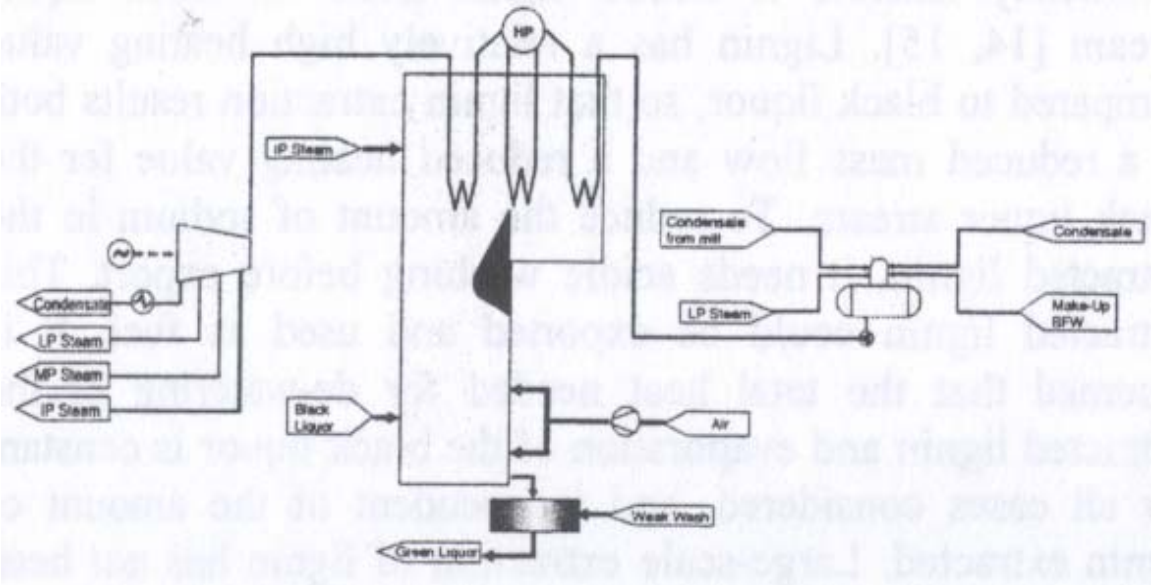

Figure 2: Schematic of Entire Recovery Boiler System [13]

The inorganics are able to be recovered as smelt and regenerated into fresh Kraft pulping chemicals and the organic material gets burned off and the subsequent heat recovered as steam [1]. Smelt is composed of about two-thirds Na_2CO_3, one-third Na_2S, and the marginal balance contains Na_2SO_4, $Na_2S_2O_3$, and other sodium/sulfur compounds [2]. Figure 3 shows a simple schematic of the Kraft liquor cycle whereas Figure 4 depicts the entire Kraft pulping and recovery process [12].

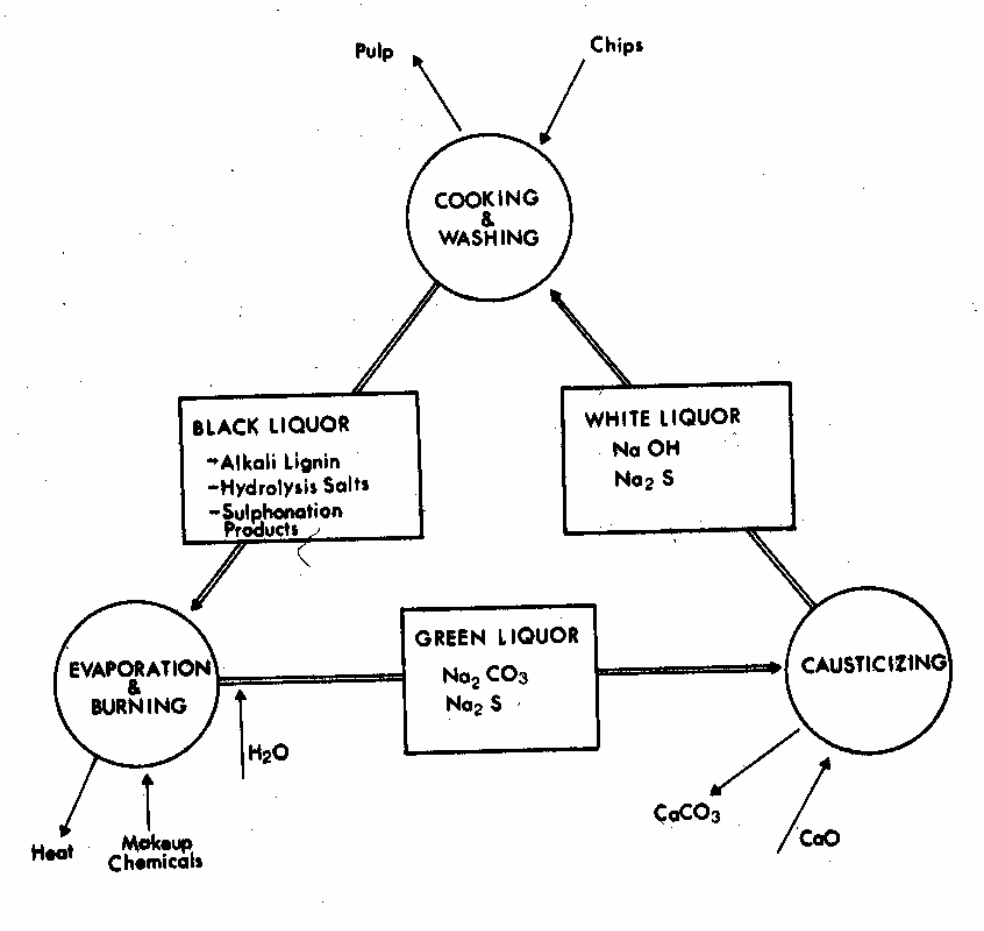

Figure 3: Simple Schematic of the Kraft Liquor Cycle [12]

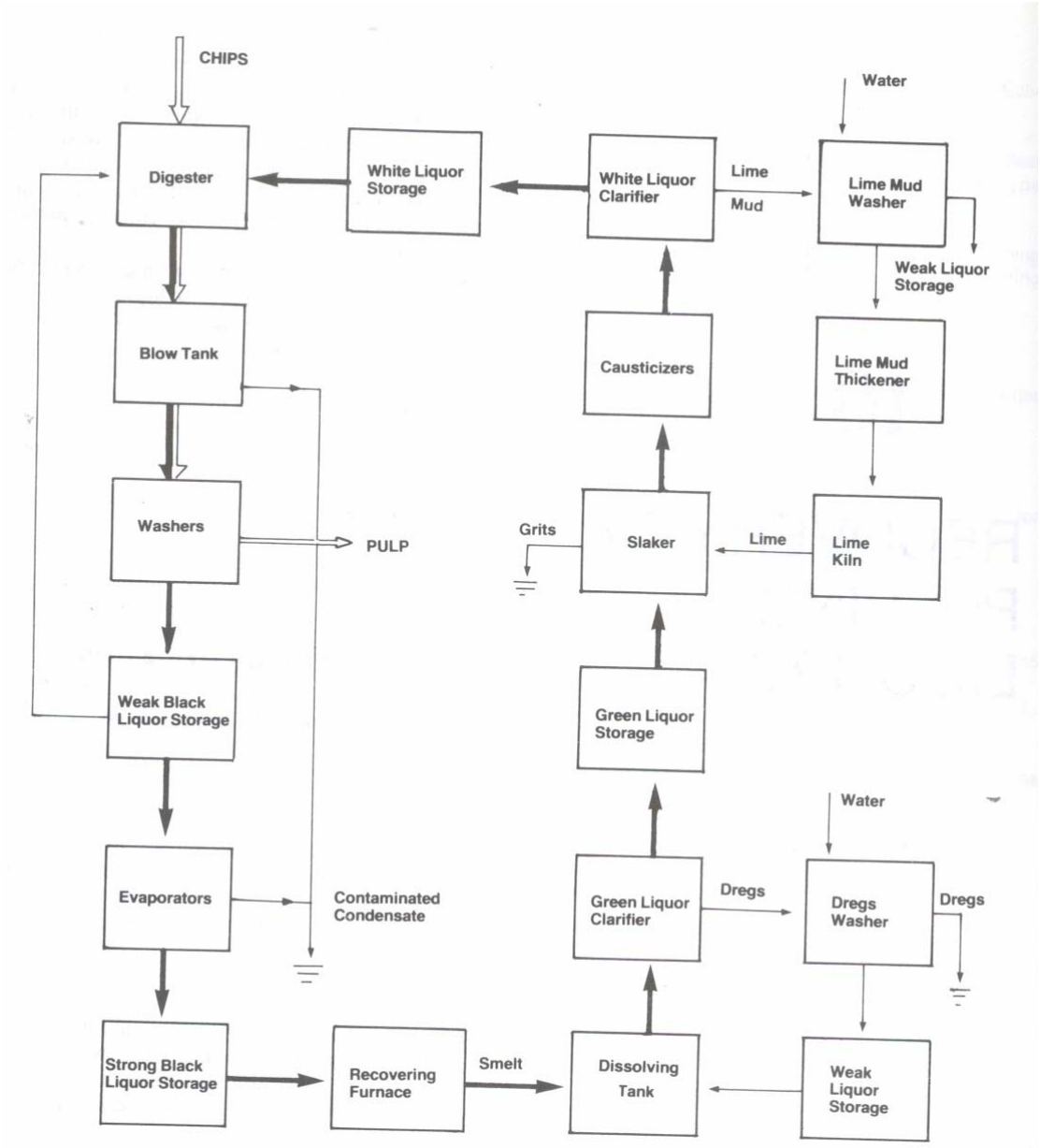

Figure 4: Schematic of the Entire Kraft Pulping and Recovery Process [12]

The white liquor, which is used to cook the chips, consists of sodium hydroxide and sodium sulfide, the active cooking chemicals. Black liquor, on the other hand, is a residual product containing the reaction products of lignin solubilization that are concentrated and burned in the recovery furnace [12]. An inorganic molten smelt containing mainly sodium carbonate and sodium sulfide is formed upon concentration, to increase heat production, and burning of the black liquor [12]. Although there is a dramatic increase in viscosity after concentrating the black liquor to more than 73% solids [1]. That smelt is then dissolved to form green liquor and combined with CaO (lime) in the slaker and reacted in the causticizer to produce NaOH from Na_2CO_3 to be reused as white liquor [1]. The major reactions and the piece of equipment in which they occur during the Kraft process are shown in Equations 1-5.

Recovery Boiler

Conversion of Sodium Salts [1]:

$$2NaOH + CO_2 \rightarrow Na_2CO_3 + H_2O \quad (1)$$

Reduction of Make-up Chemical [1]:

$$Na_2SO_4 + 4C \leftrightarrow Na_2S + 4CO \quad (2)$$

Slaker

Slaking Reaction [1]:

$$CaO + H_2O \rightarrow Ca(OH)_2 \quad (3)$$

Causticizing Reaction [1]:

$$Ca(OH)_2 + Na_2CO_3 \leftrightarrow 2NaOH + CaCO_{3(s)} \quad (4)$$

Lime Kiln

Calcining Reaction [1]:

$$CaCO_3 \ (\Delta\rightarrow) \ CaO + CO_{2(g)} \quad (5)$$

After digestion, the spent black liquor is washed from the pulp and sent through the chemical recovery process. A process known as brown stock washing is used to separate the residual liquor and cooked pulp. The pulp is then screened and cleaned to produce a

high quality Kraft pulp. The low solids content black liquor from the brown stock washing then undergoes a six step process [12]. The black liquor is oxidized to reduce odor generation from the recovery furnace. It is then concentrated into a "strong" black liquor in a multiple-effect evaporator followed by further concentration to a "heavy" black liquor. "Heavy" black liquor contains about 60% solids whereas "strong" black liquor is only about 50% solids. Sodium sulfate (Na_2SO_4) is added to replace lost chemicals to the black liquor in the recovery furnace where the mixture is burned. Green liquor is formed when the smelt from the furnace is dissolved in water. That green liquor is clarified and then causticized with reburned lime to form white liquor which is recycled and used in future digestion processes [12].

In a Kraft mill, chemical and energy recovery from residual black liquor and reformation and reuse of chemicals for white liquor is an integral part of operations [12]. Attempting to minimize pollution is also an important consideration in the Kraft process. The recovery boiler evaporates residual moisture from the liquor solids, burns the organic constituents with maximum combustion efficiency, supplies heat for steam generation, reduces oxidized sulfur compounds to sulfide, recovers inorganic chemicals in molten form, and conditions the products of combustion to minimize chemical carryover [12].

It is expected that within the very near future a large number of pulp and paper mills will need to increase recovery boiler capacity due to the age of the current equipment in the mills and changes and/or expansions in the mill fiberlines. This change to the mill process will have to occur by either adding new equipment and changing the process or

by simply replacing the old recovery boiler with a new, larger one to increase the capacity [14]. Recovery boilers are the largest in size and single most expensive piece of equipment with regards to capital costs in a typical Kraft pulp mill [1] and as such it becomes increasingly difficult to replace such a piece of equipment. Other major concerns with recovery boilers are boiler plugging, boiler integrity (corrosion), air emissions, liquor burnability which may affect operating stability [3], surface fouling in steam generators, steam cycle limitations, and safety hazards [15]. There is a strong interest in the industry to find a more efficient means of recovering energy from the paper-making process. A combination of the current large capital investment and the need for mills to become more self-sufficient for their energy is causing an in depth investigation into the prospect of improving recovery boiler performance or changing the process by implementing different technologies into the mill [16]. "Perhaps most telling, most of the recovery boiler manufacturers also are actively involved in developing black liquor gasification technology [3]."

2.2 Black Liquor Gasification

For over 20 years black liquor gasification has been emerging as a potential replacement technology for chemical recovery [17]. Black liquor gasification is used to convert the organic material in black liquor into combustible gases for eventual power generation while recycling and transforming the inorganics into compounds that can be used to regenerate necessary pulping chemicals [4]. A significant increase in electricity production in future chemical pulp mills is possible with black liquor gasification, especially in those mills that have biomass in excess. Possible black liquor chemical

recovery techniques include the current conventional Tomlinson recovery boiler method and black liquor gasification [13].

The difference between current combustion methods and gasification is that in gasification the organic material in black liquor is converted to a fuel gas instead of being burned into carbon dioxide and water vapor. The fuel gas that is produced using gasification technology can then be burned in a gas turbine to produce electricity and the hot gases that exit the turbine are used to generate steam at high pressure. This ability of combined cycle gasifiers to create energy allows it to be much more efficient then even the best Tomlinson boiler systems. The electricity generation from black liquor gasification reduces the need for fossil fuel usage and provides a subsequent reduction in the amount of carbon dioxide that is released into the environment [17]. The expected rate of reduction in air emissions with black liquor gasification implementation is 90% [18]. Converting carbon to combustible gases is one of the important objectives in black liquor gasification. The reduction of sulfur compounds to Na_2S and H_2S is also an important factor in gasification which dictates the need for temperatures in the reactor of nearly 1000°C to achieve good sulfate reduction [19]. The high temperature inside the reactor, however, is above the melting temperature of smelt and as such it becomes molten [4].

The operating temperature of the black liquor gasifier is used to categorize the different types of gasifiers. There exists both high and low-temperature black liquor gasifiers where the former operates at about 1000°C, above the melting point of smelt, so it

produces molten smelt within the reactor. Low temperature black liquor gasifiers operate below 700°C, allowing the inorganics to leave as dry solids [20]. Options for black liquor gasification configuration include combined cycle, steam-injected gas turbines, and simple cycle gas turbines. The combined cycle gasification technology tends to be the most efficient with simple-cycle gas turbine gasification with maximum biofuel export also being a more effective process then using traditional recovery boilers [13]. The potential to use the product gas from black liquor gasification for combined-cycle gas generation is one of the driving forces behind the interest in this application of gasification technology in the paper-making process [4]. In addition, gasification provides a more compact and flexible design and has better environmental performance than traditional recovery boilers [21].

While one of the problems with the Tomlinson recovery boiler is the difficulty in incremental expansion, gasifiers can also be used to increase the recovery capacity while the product gas is burned in a boiler. Another potential benefit of gasification is that there exists a natural separation of the sulfur from the sodium. This separation allows for the possibility of implementing any number of pulping enhancements in the mill. The high electric generating efficiency of the BLGCC systems can result in double or triple the net power output of a conventional Tomlinson powerhouse [20].

The potential for commercialization and implementation of black liquor gasification with combined cycle (BLGCC) technology is much more realizable today than it ever has been in the past courtesy of new developments in the technology. Another factor

contributing to the potential for implementation of BLGCC technology is the fact that there is an industry-wide need to replace a high amount of the current recovery boilers within the next 10 years. Black liquor gasification with combined cycle has many potential advantages over the traditional Tomlinson recovery boiler, including greater powerhouse electricity generation, improved capital effectiveness, more environmentally friendly, improved safety, direct causticizing possibilities, and flexibility in chemical preparation (chemical and bleaching). There are, however, also a few reasons why BLGCC may not be a feasible implementation option [20].

Although gasification technology is currently successfully used in other industries, there are specific issues that must be considered while attempting to implement black liquor gasification into the paper-making process. These concerns must be properly addressed and reconciled before this technology will be able to seamlessly replace the current recovery boilers [17]. Included in these problems are refractory degradation due to molten smelt, the production of heavy organic compounds, and sulfur separation from sodium. Also, increasing safety by minimizing the chance of explosion due to smelt-water contact is an important concern.

In high temperature black liquor gasification, the "high alkali concentrations and high temperatures result in a significant loss of refractory material and metal components, creating structural and safety issues, thermal efficiency losses, and unacceptable maintenance costs and downtime." The current 6-month refractory lifetimes need to be increased to a service life of at least one year. Figure 5 shows not only a schematic of a

high temperature black liquor gasifier but it also includes a picture of the internal structure of the gasifier and lists some advantages of gasification [22]. A more in depth picture of the internal structure of the reactor is shown in Figure 6 along with a description of the design [23]. There are two separate layers of refractory material in this reactor design. The internal layer in contact with the molten smelt is constructed of high alumina refractory whereas the additional background refractory is a much less expensive and inferior material.

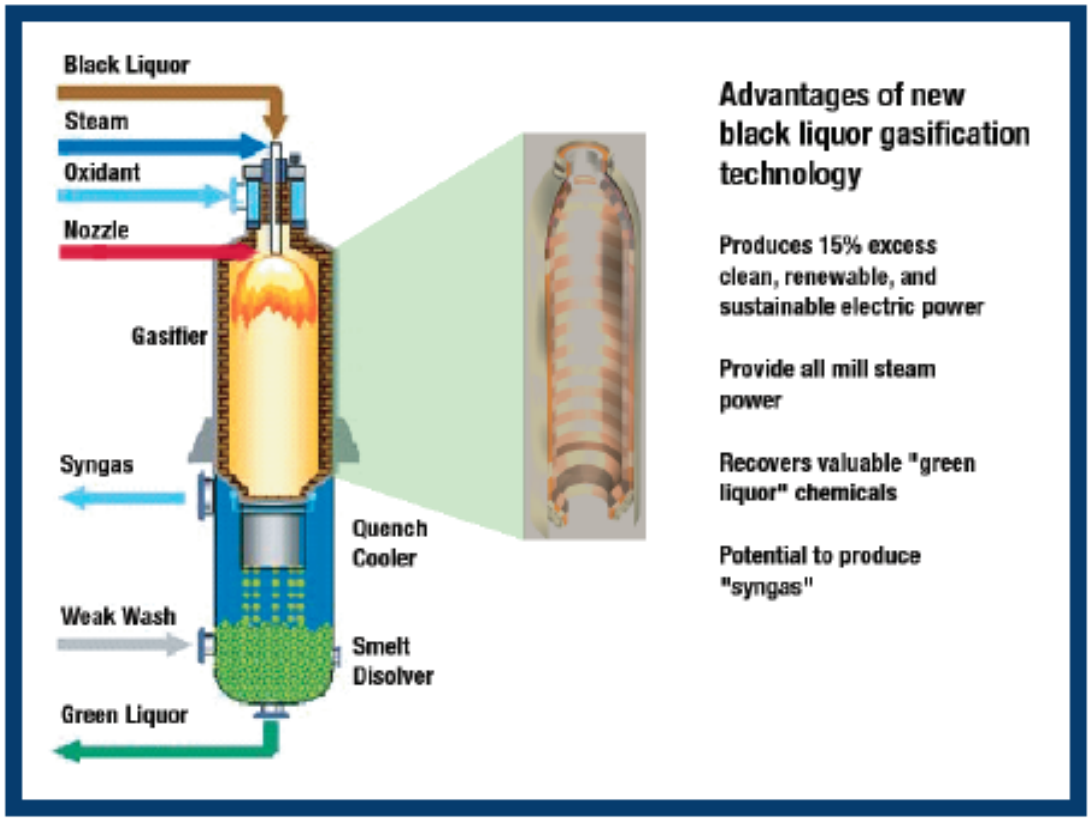

Figure 5: Schematic of a High Temperature Black Liquor Gasifier [22]

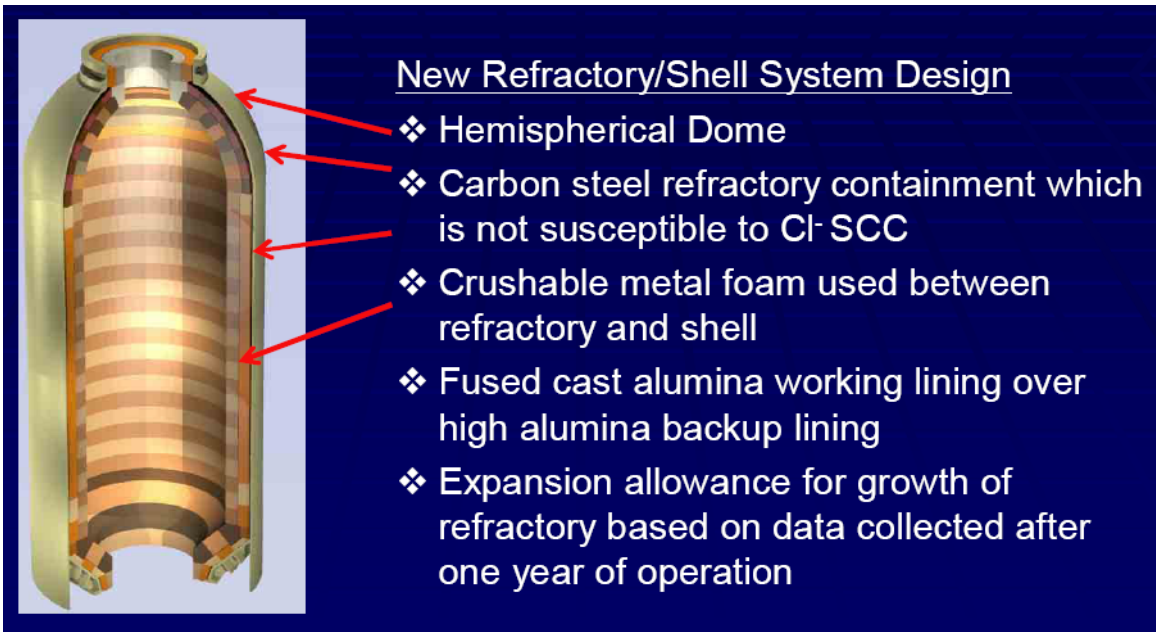

Figure 6: Advanced Gasifier Reactor Structure [23]

2.2.1 High Temperature Black Liquor Gasification

As previously mentioned, high-temperature black liquor gasifiers operate above the melting point of smelt creating molten salts and hence causing severe degradation issues with the lining materials. As such, there are currently only a few commercial scale black liquor gasifiers in existence; the first of which was installed in August 1991 at AssiDomän's Frövifors, Sweden mill [20]. This Frövifors mill was built using the CHEMREC™, a Kvaerner Pulping technology, recovery system. The CHEMREC™ gasification process is a partial combustion in short-residence-time entrained-flow reactor [4]. Tampella and Ahlstrom gasification processes are also high temperature black liquor gasifiers that use entrained flow reactors [4]. The CHEMREC™ unit at the Frövifors mill was built for 75 metric tons of dry solids/day [20].

In December 1996, the first North American commercial-scale black liquor gasification plant was started up at Weyerhaeuser's New Bern, NC pulp mill. The New Bern gasifier plant design and development was based off of the Frövifors gasification system. Weyerhaeuser's gasifier has a 330 metric tons of dry solids/day capacity, more than four times that of the Frövifors mill, and was essentially a straight geometric scaleup of the Frövifors reactor. There are, however, three notable differences: 1) The New Bern plant uses steam instead of air to atomize the black liquor which reduced the plugging tendency of the liquor nozzle. 2) A separately fired indirect air heater is used in New Bern instead of the flue gas heat exchanger. 3) Weyerhaeuser's gasifier product gas is fired in a multifuel power boiler instead of a small dedicated fire tube boiler. The CHEMREC™ gasifier has the ability to provide incremental production capacity independent of the recovery boiler [24]. A heat and mass balance for the traditional Tomlinson recovery boiler system is shown in Figure 7 [20]. The gasification technology at the mill in New Bern uses an air-blown technique versus others such as the one in Piteå, Sweden which is oxygen-blown. An illustrative heat and mass balance for an air-blown gasifier is shown in Figure 8. Conversely, the heat and mass balance for the oxygen-blown gasifier is shown in Figure 9 [20]. Due to the need for the oxygen plant, the oxygen-blown systems have a higher capital cost and consume more auxiliary power than its air-blown counterpart; however, the oxygen-blown system converts a higher fraction of fuel input into electricity but a smaller portion of the fuel input into process steam [20].

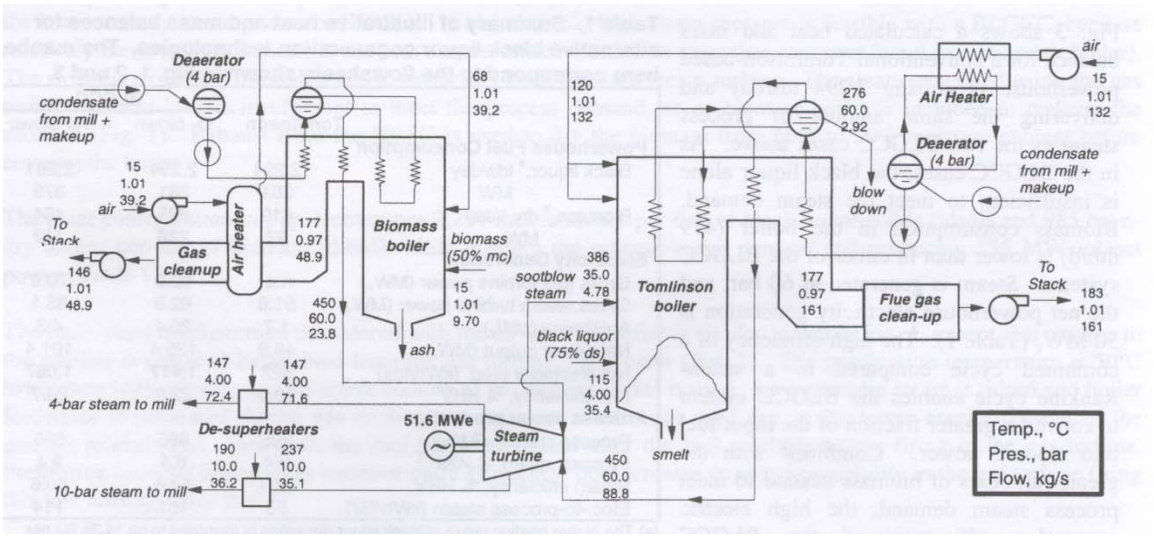

Figure 7: Heat and Mass Balance Schematic for Tomlinson Recovery Boiler System [20]

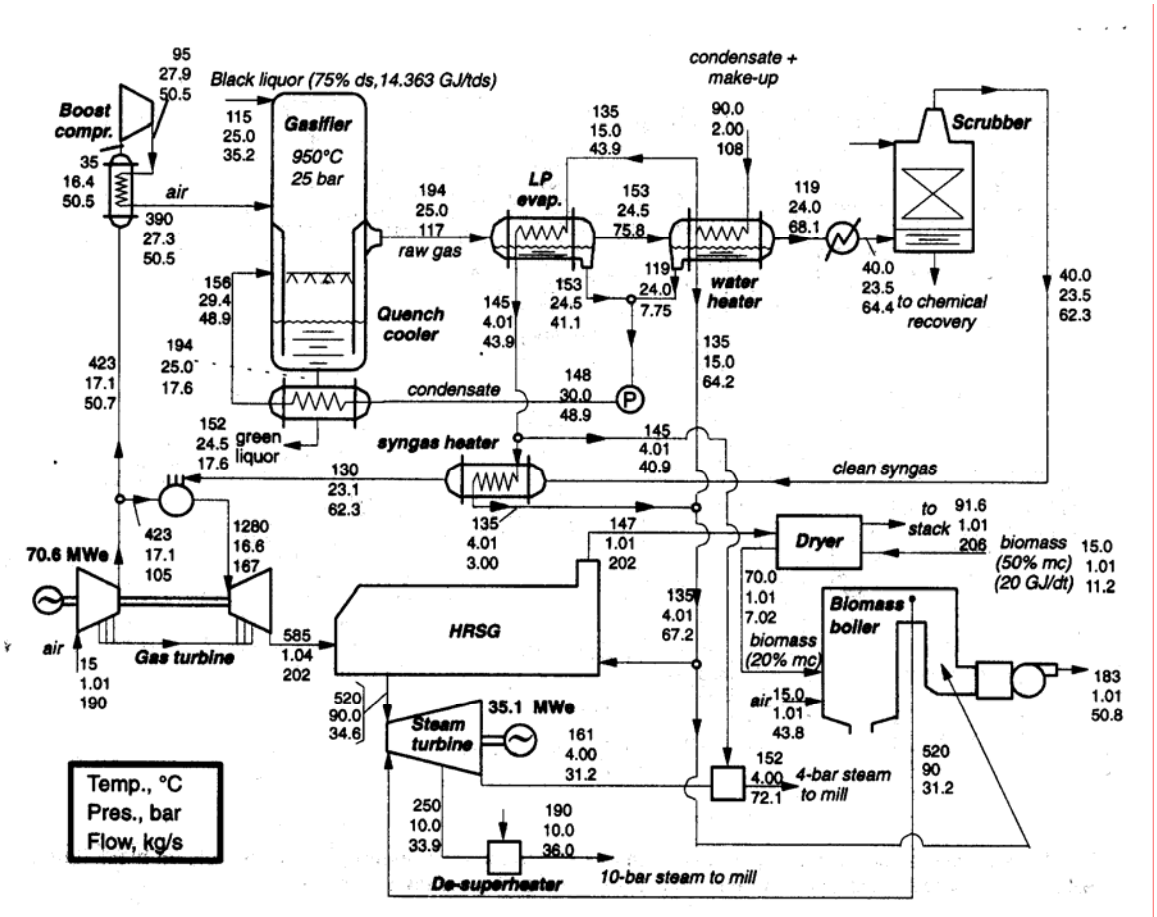

Figure 8: Heat and Mass Balance Schematic for Air-Blown Combined Cycle High-Temperature Black Liquor Gasifier [20]

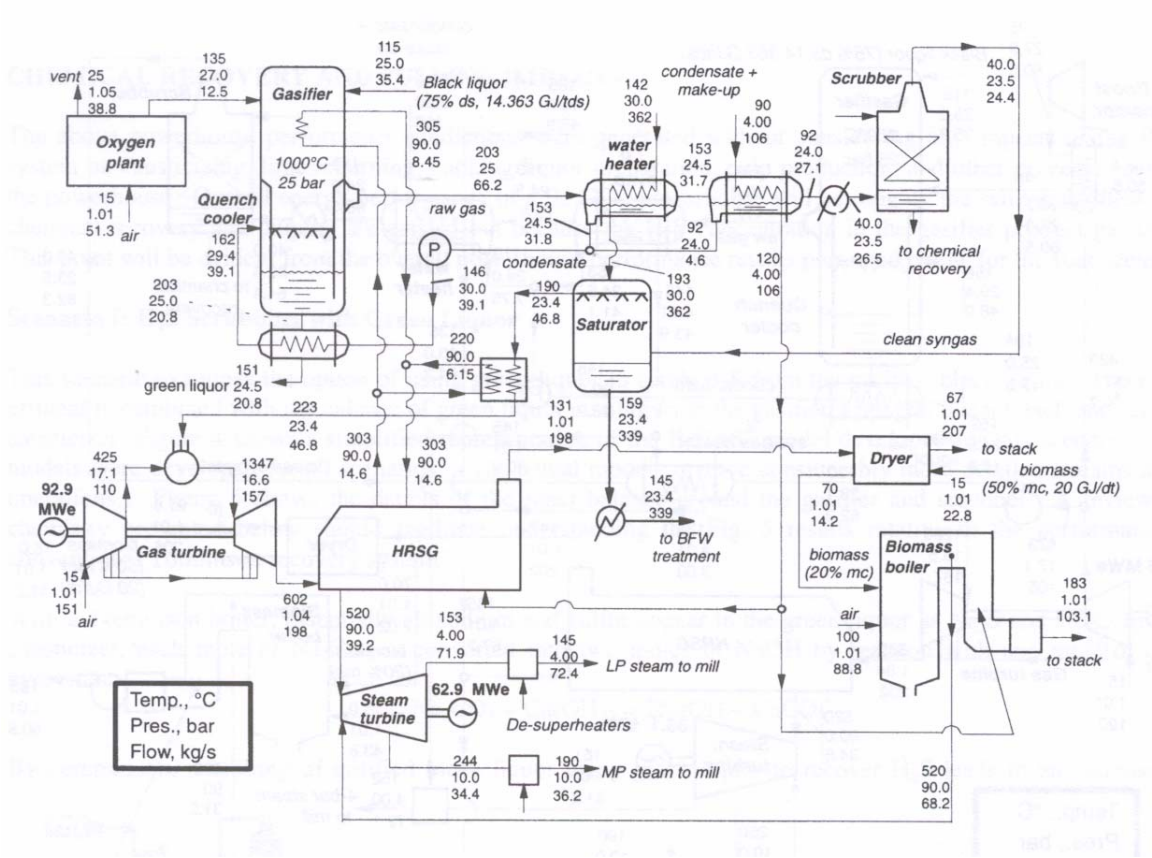

Figure 9: Heat and Mass Balance Schematic for Oxygen-Blown Combined Cycle High-Temperature Black Liquor Gasifier [20]

In the study done by Larson, et al, they found that the capital costs for installing a 1327 oven-dried metric ton per day (odmtpd) gasifier/combined cycle system are comparable to those of a Tomlinson furnace [20]. The 100% to 175% increase in electrical power generation that comes from the gasifier/combined cycle system, however, ends up with a large amount of operating credits each year. Table 1 compares the installed capital costs for the main units of interest in the recovery process. The air-blown gasifier with recycled hydrogen sulfide (H_2S) has the least expensive capital costs at $20 million less than the Tomlinson recovery boiler and still generates $11.6 million annually in operating credits as well [20].

Table 1: Cost Comparison for Tomlinson Recovery Boiler and Different Black Liquor Gasification Scenarios [20]

(million $)		BLGCC			
		Scenario I	Scenario II	Scenario III	Scenario IV
	Conventional Tomlinson	Green liq. scrubbing	H_2S Gas recycle	PS/AQ pulping	Air-blown H_2S recyc.
Tomlinson Island	159.8	---	---	---	---
Gasification Island	---	54.1	54.1	54.1	43.3
Combined Cycle Island	---	69.7	69.7	69.7	62.8
Biomass Boiler Island	16.9	37.6	37.6	37.6	24.9
H_2S recovery/recycle	---	36.0	16.4	19.6	26.9
Total Overnight Capital	**176.7**	**197.5**	**177.9**	**181.1**	**157.9**
Interest during constr.[a]	13.7	15.3	13.8	14.0	12.2
Total Installed Capital	**190.4**	**212.8**	**191.7**	**195.1**	**170.1**
Capital Relative to Conventional		**+22.5**	**+1.3**	**+4.7**	**-20.3**

(a) Interest during construction, assuming a 10% annual interest rate and equal expenditures (¼ of the total capital cost each) every 6 months during a 2-year construction period.

The cost assessment that was performed by Larson, et al proposes that the benefits of commercial application would be substantial [20]. This considerable change in cost is due primarily to the significant increase in power production that occurs with BLGCC. A BLGCC system will generate net operating savings of $12-$17 million per year (assuming the excess power generated by the gasification system is valued at $0.04/kWh) while having approximately the same capital cost as a conventional Tomlinson recovery furnace [20].

The four major processes that are involved in the high temperature gasification process are gasification itself, gas cooling and green liquor production, gas scrubbing, and gas firing. A schematic of the black liquor gasifier that was implemented in New Bern is shown in Figure 10 [8].

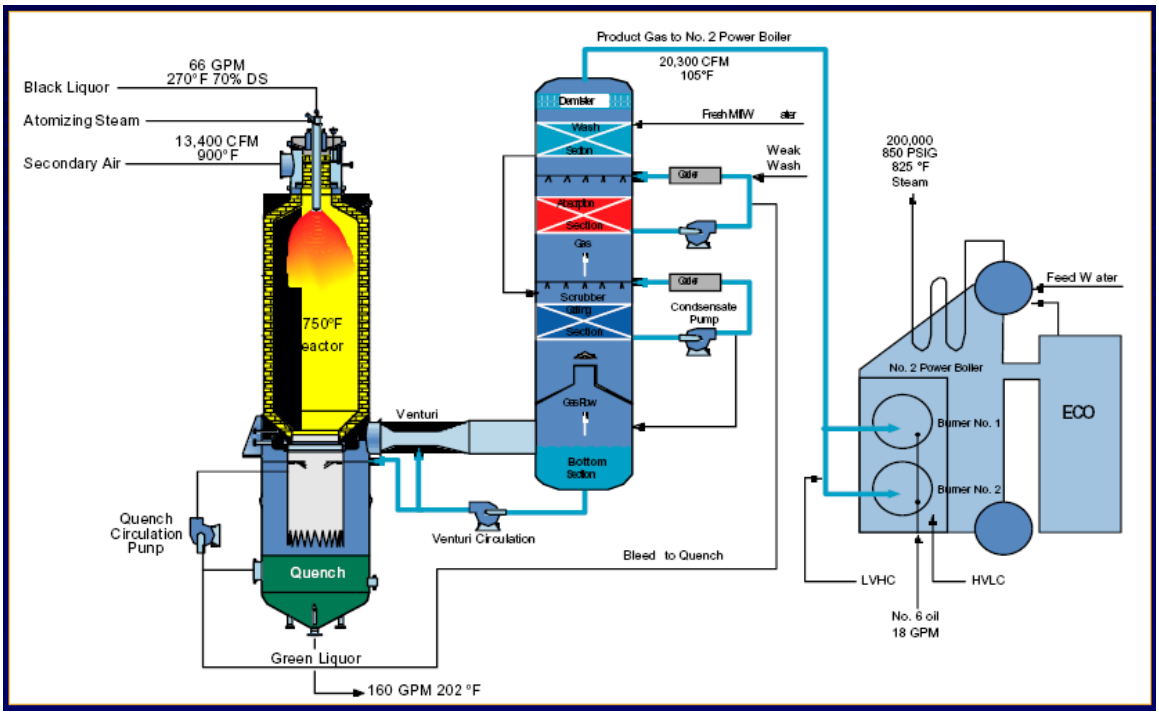

Figure 10: Schematic of the Gasification System Installed at Weyerhaeuser's New Bern Facility [8]

Atomized drops of black liquor pumped in at 500°C are mixed with air and partially combusted at 950°C inside the gasifier. This process occurs inside a refractory-lined reactor and produces combustible gas and smelt drops which consist of mainly sodium carbonate and sodium sulfide. Some of the smelt droplets that are formed hit the reactor wall and form a thin liquid film of smelt flowing to the reactor outlet. The gases that are formed inside the reactor are carbon monoxide, carbon dioxide, methane, hydrogen, nitrogen, water vapor, and a small amount of hydrogen sulfide. A spray quench is used to cool both the gas and smelt immediately after they exit the refractory lined area. A dissolver at the bottom of the reactor is used to collect raw green liquor that is formed from smelt droplets and excess condensate from the spray quench. The product gas is released from the reactor into a high-pressure drop venturi which removes the alkali

particulates in the gas. The product gas is further cooled and the majority of the remaining hydrogen sulfide is absorbed in weak wash via a combined tray and packed scrubber column. Green liquor is combined with any excess weak wash in the quench dissolver. Once the gas reaches the final scrubber stage, it is passed through a sieve tray and a demister array. Any excess condensate that comes from the bottom and cooling sections of the scrubber gets recycled back into the quench and venturi sprays. Finally, the gas that has been cooled and had the sulfur removed is burned [24].

During the first year of operation for the commercial scale high-temperature black liquor gasifier at Weyerhaeuser's New Bern facility, the availability of the system was at only 47% [8]. Some problems that needed to be overcome initially included black liquor delivery pump issues, power boiler issues, the condensing heat exchange issues, alkali carryover to the power boiler, venturi spray circuit pluggage, and excess H_2S stripping [8]. All of those problems have since been resolved. An additional and major problem was, and still is, the integrity of the refractory material lining the gasifier [8]. Figure 11 shows the production rates and downtime at the New Bern mill for 1997. The overall production rate was very low and even at the highest rates, did not reach the design rate. The production rates for 1998 are shown in Figure 12 and at about 85% capacity are notably higher than those from 1997. The problem, however, is still the amount of downtime at the mill. As of 1999, the in-service lifetime of the refractory lining of the gasifier was less than a year [8]. There is a lengthy amount of downtime necessary to replace the refractory lining and, consequently, alleviation of the need to replace it at least once a year will also help improve production rates.

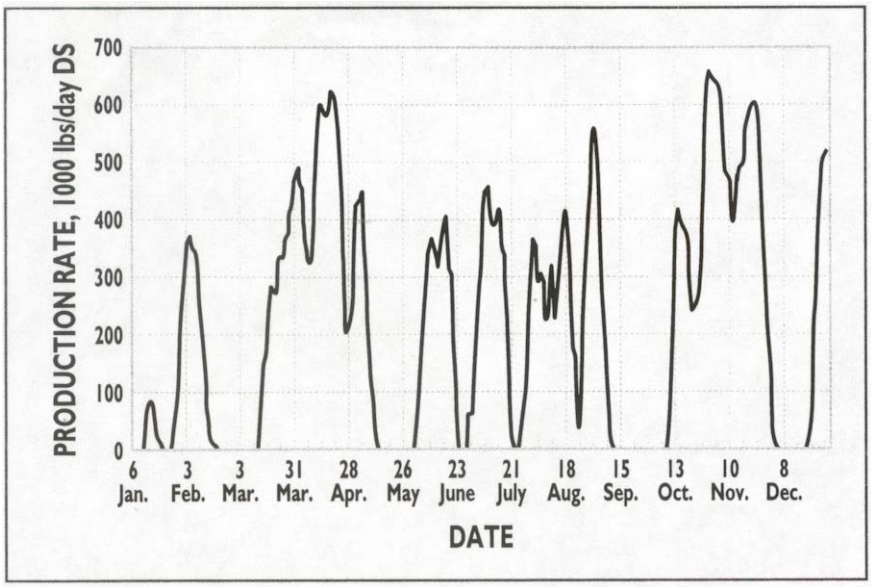

Figure 11: 1997 Production Rates at Weyerhaeuser's New Bern Mill with a High-Temperature Black Liquor Gasifier in Use [8]

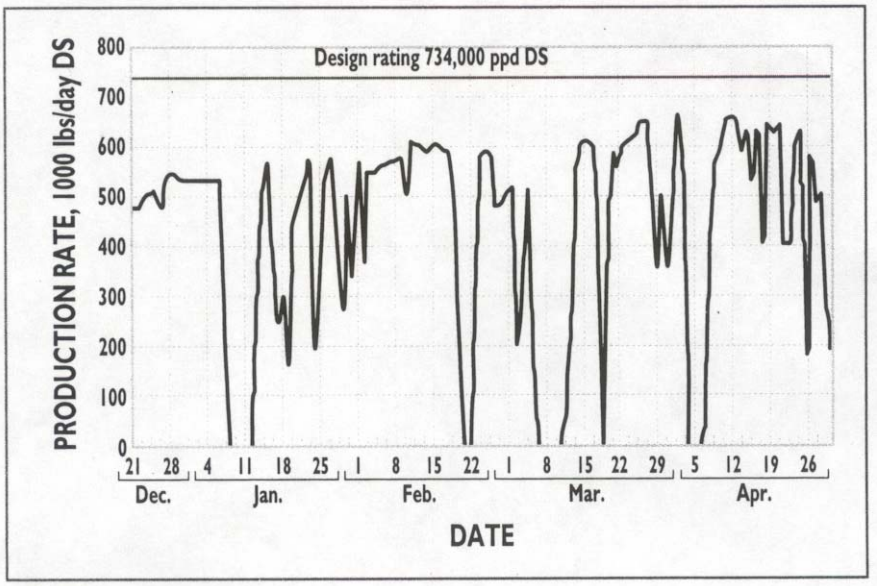

Figure 12: 1998 Production Rates at Weyerhaeuser's New Bern Mill with a High-Temperature Black Liquor Gasifier in Use [8]

2.2.2 Low Temperature Black Liquor Gasification

Gasifiers operating below the melting point of smelt are also an option in gasification of black liquor. This low temperature (about 700°C) process gives sodium carbonate (Na_2CO_3) in solid form and reduced gas with all sulfur in the form H_2S [5]. While this gasification technology does eliminate the problem of corrosion by molten smelt, it is not without problems of its own. Some problems that are encountered in low-temperature black liquor gasification systems are carbon conversion, bed agglomeration, and the formation of tars [25]. The MTCI gasification process, in the United States, and the ABB gasification process, in Sweden, processes are both examples of low temperature black liquor gasification [5]. A schematic of a typical low temperature black liquor gasifier is shown in Figure 13:

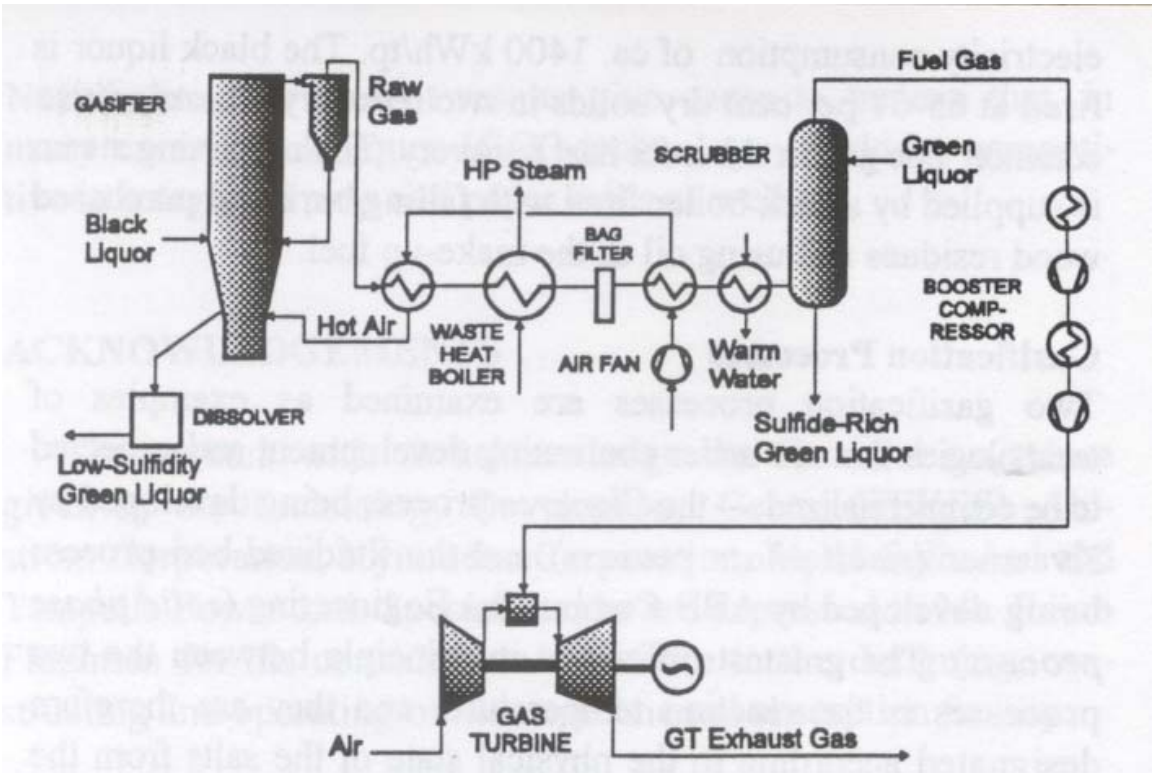

Figure 13: Schematic of a Low-Temperature Black Liquor Gasifier [26]

The gas exiting the reactor can be used to generate high-pressure steam and to preheat air to 350°C due to the fact that it leaves at the temperature of the gasifier [26]. This negates the need for gas quenching, which is necessary in high temperature black liquor gasification, and is consequently advantageous for power generation [26].

Temperature is not the only difference between these two gasification options. Instead of an entrained flow reactor, low temperature black liquor gasification uses a fluidized bed [6]. The MTCI technology uses steam gasification in indirect heated fluidized beds and the ABB gasifiers are partial combustion in long residence time fluidized beds [4]. Also, because of the reduced temperatures, it may not be necessary to used refractory lined vessels [15].

MTCI low-temperature gasification involves black liquor being gasified in a bubbling fluidized bed of Na_2CO_3 particles from the gasification operating at 600-650°C. The fluidizing media used by the MTCI process is made of steam or recycled process gas may also be used. In order to maintain proper operating temperature, heat exchangers, which are powered by some of the burned product gas, are immersed in the fluidized bed. Steam is generated from a waste heat boiler where the hot combustion gases are sent from the heat exchangers. The cyclone is used to remove particulate matter from the fluidized bed exit gas. The particulates are returned to the fluidized bed and the gas is cooled in a waste heat boiler and feedwater preheater, then quenched and scrubbed [4].

ABB modeled their gasification system off of the diagram shown in Figure 14 [15]. The bed of the ABB process would be made of Na_2CO_3 and Na_2S particles from the gasified black liquor and would operate at 700°C. It would operate by using partially combusted black liquor in a circulating fluidized bed gasifier with a cyclone. The fluidizing media and temperature control would be preheated compressed air. The gas from the reactor would be sent to a gas cooler then to a bag house to have more solids removed from the gas, and finally to the H_2S scrubber. The solids would be removed at the bottom of the gasifier [4].

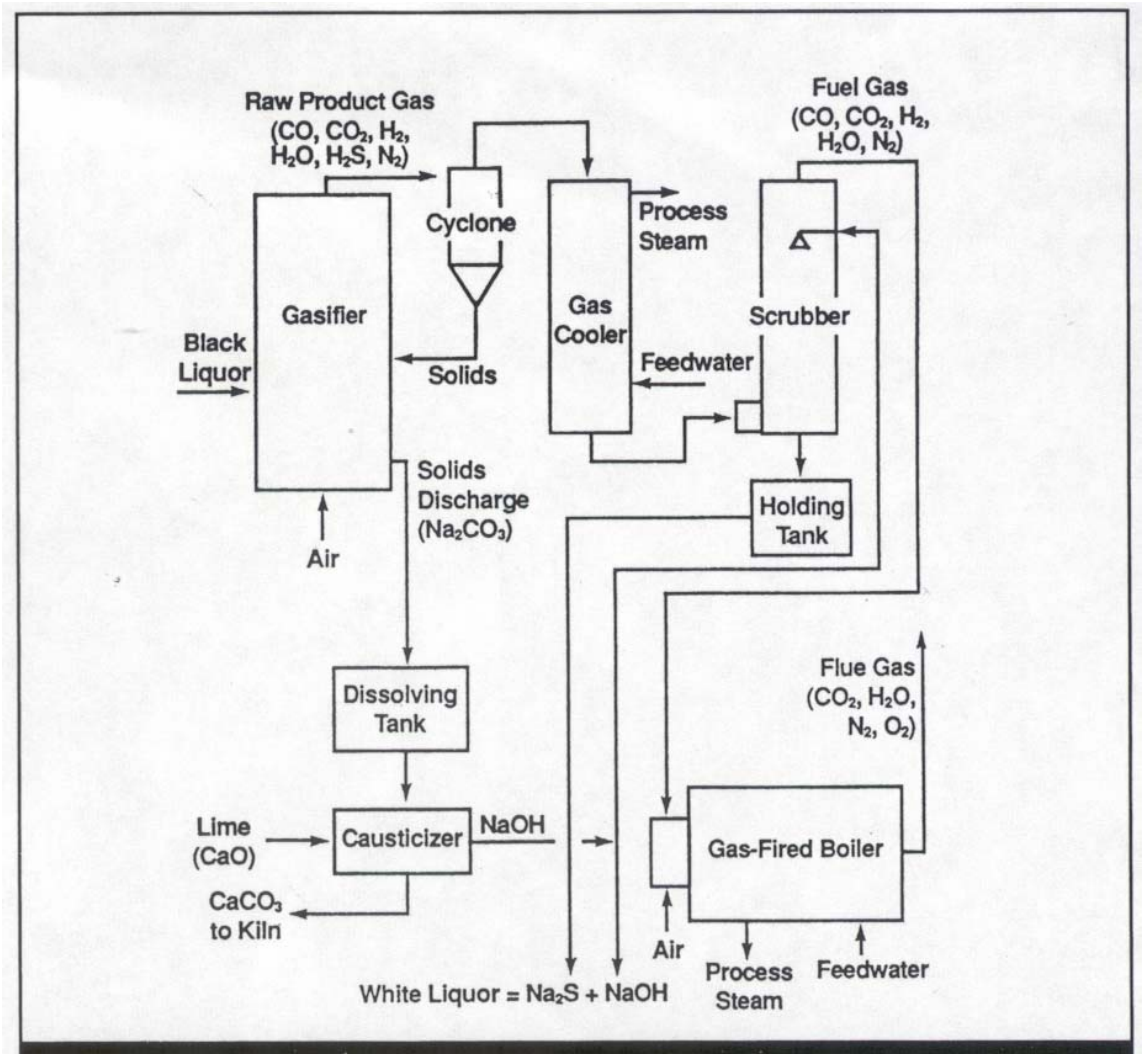

Figure 14: Diagram used to Design the Gasification System from ABB [15]

The ABB-Combustion Engineering fluidized bed low-temperature black liquor gasifier was compared to Kvaerner Pulping's CHEMREC™ process to determine which process provided more energy generation. While it was found that the low-temperature gasifier generated more electricity, the high-temperature gasifier actually had a higher overall efficiency [26]. The higher efficiency of the CHEMREC™ unit is due to the high pressure in the gasification plant coupled with lower amount of lost flue gas from the heat recovery steam generator. Also, most of the water from the gas can be condensed to produce low-pressure steam.

2.3 Refractory Materials

Refractory materials, by definition, are supposed to have high melting points. These materials may be exposed to different degrees of mechanical stress and strain, thermal stress and strain, corrosion/erosion from solids, liquids, and gases, gas diffusion, and mechanical abrasion at various temperatures [27]. Refractory linings are also used as insulation for processes to control the amount of heat lost and thus increase efficiency. Hence, it is necessary to investigate the tolerance of the refractory material for thermal expansion stresses (strain-controlled loads) [28]. Due to its many desired applications, refractories are created with varying properties and implemented so that the characteristics of the refractory material chosen will most closely match the needs of the process in which they will be used. With this in mind, it is obvious that the property requirements of refractories vary significantly according to their application and use in different processes even though about 70% of refractories are used in basic metal industries [27]. Abrasion and heat resistance as well as resistance to the impact and splashing of molten iron and slag is important in iron making, tolerance for mechanical

impingement and arcing due to electrical current create a need for good mechanical strength, high refractoriness, and basic slag resistance in electric arc furnaces, while the refractory material should have a non-wetting characteristic to molten aluminum in the aluminum industry, and abrasion resistance is key due to the flow of high velocity particles along with a necessary range of thermal conductivity in petrochemical refining [27].

Refractories are broken down into two broad categories, shaped (bricks and cast shapes) and unshaped (monolithic) and are then further distinguished using three more defined topics, physical, thermal and chemical properties [27]. The physical properties used to characterize refractory material are density, porosity, strength, and abrasion. The thermal properties are thermal shock, thermal conductivity, and thermal diffusivity and the chemical property is corrosion/erosion. The main requirements of shaped refractories are density, porosity, and dimensional tolerance [27].

Innovations with alumina-silica bricks were unequivocally driven by the ever increasing demands in the iron and steel industries for better refractory products to combat more severe service conditions [29]. As such, all other industries using alumina-silica bricks were able to benefit from the advancements. Alumina-silica bricks are not only relatively inexpensive in comparison to most basic brick, but can also be used in situations where castable refractories have definite disadvantages [29].

A simple definition of refractoriness is that the material will not melt or deform (shrink) under prolonged service in the furnace environment. Some of the problems that almost always occur due to excessive shrinkage are the opening of joints in a furnace, cracking, increased susceptibility to thermal shock, and any number of other problems. As such it is important to try and reduce the amount of shrinkage or melting that would occur in an in-service furnace environment [29].

Scientific principles, no longer trial and error, guided the development of fireclay brick after the advent of phase diagrams after about 1920 [29]. To this day, the most important binary system in refractory technology is the alumina-silica system [30]. The phase equilibrium diagram for the alumina-silica system, which is used to explain the technology of the alumina-silica refractories, is shown in Figure 15 [31]. In the Al_2O_3-SiO_2 system at normal atmospheric pressure, mullite, a material of major importance in ceramic technology, is the only stabile crystalline compound that exists [30]. Mullite ($3Al_2O_3 \cdot 2SiO_2$) is a refractory compound having a melting point of 1850°C, consequently, the higher the mullite content is in the refractory as the composition of the refractory approaches 72wt% alumina (which is equal to about 60mol%, the theoretical composition of mullite), the greater the refractoriness. Also, greater mullite content increases spalling resistance and greater glass content decreases spalling resistance. As can be seen from the phase diagram, refractories containing less than 60mol% alumina would be useless at temperatures above 1595°C due to the fact that they would begin to liquefy or melt whereas those refractory materials containing more that 60mol% to just slightly less than 100mol% alumina would not begin to melt until 1840°C. Pure alumina,

or corundum, has a melting point of about 2050°C [29]. Because of this, higher alumina content refractories can be used in a greater number of high-temperature applications. Another important period for the production of alumina-silica bricks was during World War II when it became important for those in North America to develop refractories based on bauxite instead of the basic refractories that had come from Europe and were now no longer available. The Bayer process also allowed for generation of a new line of "high-alumina" brick via the manufacture of calcined (burned) and tabular (sintered) alumina. Tabular alumina aggregates and calcined alumina are used in products in either the 90% or 99% alumina classes of refractory brick [29]. These high-alumina refractories are not only one of the most important refractory materials they are also the most diverse. Excellent resistance to corrosion by acidic slag material at high temperature, improved resistance to abrasion, spalling, and impact/load, and high refractoriness are characteristics of high-alumina refractories that exemplify why they are so widely applicable [30].

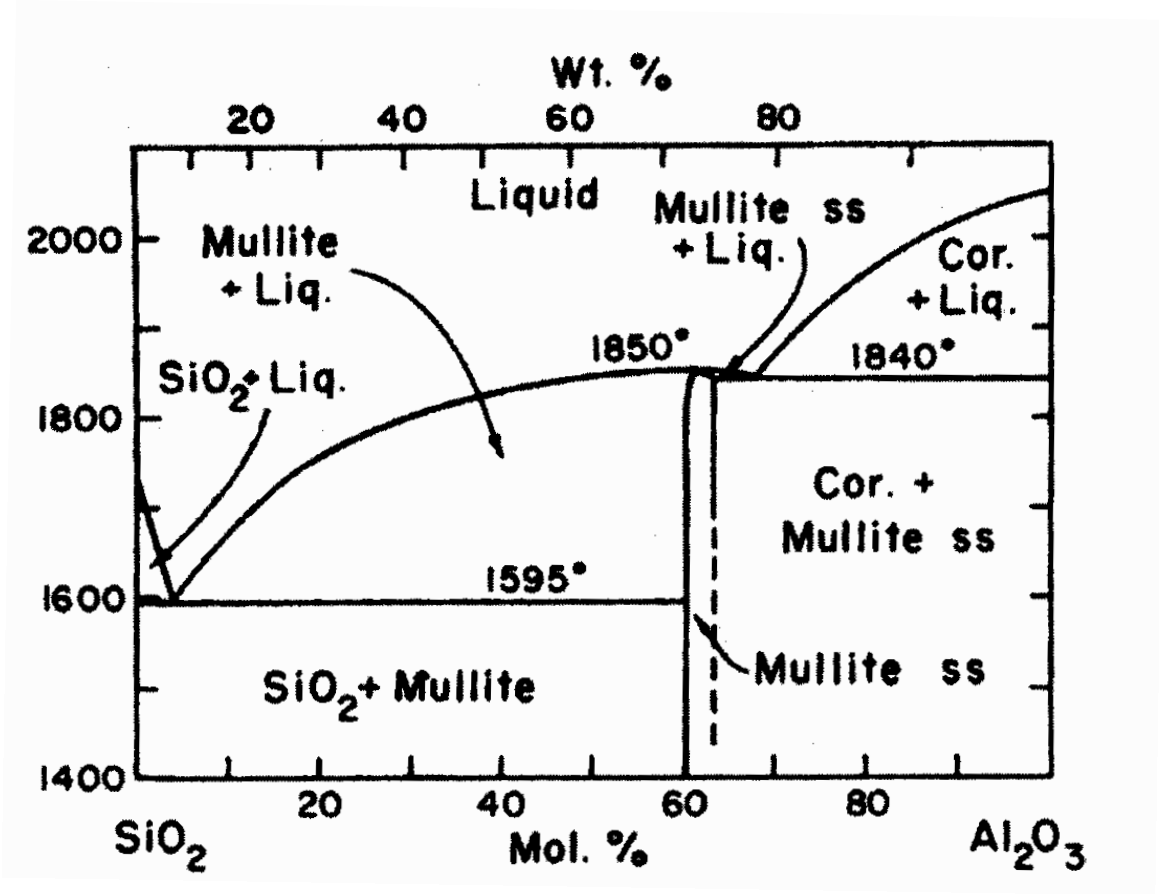

Figure 15: Phase Diagram of Al_2O_3 and SiO_2 [31]

Fluxing oxides exist in the raw materials used to create refractories and consequently their effects on the properties of the refractory need to be taken into account [29]. It has long been understood that the addition of small amounts of admixtures influences the quality and or quantity of the fired product. The effects of these impurities alter the quantitative phase diagram of a product [30]. Alkalis can be present in the form of sodium oxide (Na_2O) or potassium oxide (K_2O) along with other fluxes such as calcium oxide (CaO), iron oxide (FeO or Fe_2O_3), and titanium oxide (TiO_2). The greater flux content in the refractory, generally the more glass (vitrified state) will exist in the fired refractory. Since a lower glass content leads to higher shrinkage resistance upon

prolonged exposure to high temperatures and, consequently, less cracking and susceptibility to thermal shock, the refractory may show better service performance with a lower flux content [29].

Pore size and structure are important in determining the fracture toughness and thermal shock resistance of a refractory brick. The higher the apparent porosity of the refractory, the more resistance it will have to degradation by thermal shock. Also, the more interconnected the pores, the greater the insulation and thermal shock resistance provided by the refractory. High-alumina bricks are manufactured using a dry-pressing method which allows for a lower apparent porosity than those bricks made using extrusion [29]. In order to extrude the brick, there must be a higher water content in the mixture to obtain plasticity which ultimately leads to a higher apparent porosity. The dry-pressing method tends to produce finer pore sizes and structure in the fired product in comparison to those that have been extruded. Due to the fact that these bricks tend to ultimately be used at elevated temperatures, they are more sensitive to contamination [29]. Consequently, newer high-alumina brick manufacturing plants are designed in an attempt to reduce contamination and particle size segregation to provide smaller variations in the finished product. The main attributes to consider in a refractory plant are raw material storage, particle sizing and sized material storage, mixing, conveyance, presses, and kilns [29].

Some strength properties of the refractory materials improve as bulk density increases, however, thermal shock resistance decreases; therefore the chance for decreased spalling resistance exists. Fireclay bricks are susceptible to alkali attacks primarily in the form of

vapor-phase permeation through the hot face. There are two important consequences of this permeation, fluxing of the surface and formation of new phases resulting in expansion of the refractory [29]. Spalling and damage that occurs due to thermal shock are always important concerns for furnace designers and operators. The lower the thermal expansion coefficient of the refractory material, the more improved the thermal shock resistance. Even a slightly reduced alkali content in the refractory apparently affects subsidence under load and decreases spalling. Looking at 50% and 60% alumina class refractory bricks (such as Ufala®), it can be seen that they show an increased refractoriness over the fireclay bricks. Table 2 shows the composition and properties of 50% and 60% alumina class refractories. Refractory bricks that fall into the classification of 90% and 99% alumina (such as Jargal®M) are among the highest strength and erosion resistant refractories [29]. Table 3 gives the composition and properties of the refractory bricks in the 90% alumina class. The practical limit for alumina content in refractories for use in highest-temperature applications is about 96% Al_2O_3 (and 3.7% SiO_2) due to the fact that a higher alumina content would prohibit sintering in conventional kilns so as to allow good density and permanent linear change (PLC) properties [29].

Table 2: Composition and Properties of 50% and 60% Alumina Class Refractories [29]

	50% Al_2O_3 clay base	50% Al_2O_3 bauxite base	60% Al_2O_3 clay base	60% Al_2O_3 bauxite base	60% Al_2O_3 andalusite base
Chemical analysis					
Al_2O_3	50.5	49.5	58.1	62.1	58
SiO_2	44.5	49.5	38.2	32.5	39
Fe_2O_3	1.3	1.3	1.2	1.2	1.5
TiO_2	2.3	2.5	2.2	2.6	0.2
Alkalis	0.8	0.7	0.1	0.8	≤0.3
Physical properties					
Bulk density, g/cm^3	2.38–2.45	2.37	2.52	2.50–2.59	2.55
Apparent porosity, %	11–16	17.5	14.3	17–20	≤15
Modulus of rupture, Mpa	13.8–20.7	7.6–12.4	18.2	10.3–15.2	
Crushing strength, Mpa	48–69	28–55	58	34.5–62	≥60
PLC, 5 hr. @ 1600°C	+0.5 to +1.5	−1.0 to +1.0	−0.1	+2 to +4	
Panel spalling loss, %, 1650°C, preheat	<5	3–8	<2	3–5	

Table 3: Composition and Properties of 90% Alumina Class Refractories [29]

	Fused alumina-mullite matrix	Tabular alumina-corundum matrix	Alumina chrome	Alumina chrome spall resistant
Chemical analysis				
Al_2O_3	91.4	90.1	89.7	83.0
SiO_2	8.1	9.5	0.5	2.0
Fe_2O_3	0.3	0.1	0.2	0.1
Cr_2O_3	0.0	0.0	9.0	11.2
TiO_2	Trace	Trace	0.1	Trace
Alkalis	0.2	0.2	0.1	0.2
Physical properties				
Bulk density, g/cm^3	2.72–2.82	2.98	3.17	3.20
Apparent porosity, %	15–18	16	17.8	17.5
Modulus of rupture, MPa	11.7–17.2	16.1	31	11
Modulus of rupture @ 1482°C, MPa	≤5.2	9.1	13	10
Crushing strength, MPa	48.2–68.9	78.2	86	84
PLC %, 5 hr. @ 1705°C	0 to +1.5	−0.2		
PLC %, 5 hr. @ 1816°C			+0.7	−0.1
Panel spalling loss, %, 1650°C, preheat	0–5	0–2	0–2	0

The selection of the best refractory material for an application to increase service life, decrease down-time, and make the process more cost-effective is now more important than ever due to an extremely competitive environment. The pros and cons of different types of refractories must be assessed to ensure the best fit for the application and environment in which they will be used [32].

Due to the fact that black liquor gasification is a relatively new technology, very few commercial scale black liquor gasifiers exist. Molten smelt is extremely corrosive, so identifying an appropriate refractory material for use inside of the gasifier is important but rather difficult. Using the knowledge of acid-base reactions, logic would say that the best refractory for this application should be basic due to the fact that molten smelt is a basic solution. This accounts for simple acid-base chemical reactions where the acids and bases would otherwise react in order to neutralize the solution. In the glass-making process, the refractories are in constant contact with the molten glass creating a need for the refractories to be nonporous. As such, fused refractories are used in the molten glass contact areas [27]. A similar need is presented in the black liquor gasifier due to the refractory material's constant contact with molten smelt. Alumina is thought to be one of the best protective oxide coatings for use in high temperature environments. As such, alumina coatings are often used to protect base materials due to its wear and corrosion resistance and for its applicability as films on electronic devices [33]. In 1993 alumina was presented as the most promising refractory material for use in high-temperature black liquor gasifiers [6]. There was a lack of a better, more suitable alternative refractory material as of 2004 [9]. This is true even though alumina-silica bricks are neutral to

slightly acidic [29]. Because the high-alumina bricks such as Jargal®M are fired when they are made, the ceramic reaction and bonds have already been instituted by high-temperature firing and consequently do no exhibit any further change upon exposure to a high-temperature environment [27].

2.4 Refractory Corrosion

Refractories are used at elevated temperatures for structural purposes, and they are used in many cases to contain a high-temperature corrosive environment. The corrosive environment usually contains liquid phases that may participate in chemical reactions with the refractory at elevated temperatures resulting refractory consumption or wear. "Corrosion of refractories is refractory wear by loss of thickness and mass from the exposed face of the refractory as a consequence of chemical attack by a corroding fluid in a process in which the refractory and the corroding fluid react, approaching chemical equilibrium in the zone of contact between the refractory and the fluid [34]." Corrosion reactions proceed in the direction of localized equilibrium such that phase diagrams can be used to analyze corrosion situations and predict chemical strategies to minimize corrosion and wear rates. Some examples of the multiple types of refractory systems include fusion cast and/or bonded brick in a "working" lining placed in front of a backup or "safety" lining (or placed against a "shell) which have been used in high temperature black liquor gasification applications, thick-wall applications of concretes and other monolithics, and thin-wall applications of monolithics [34]. The gasifier lining at Weyerhaeuser's New Bern facility has been changed since its inception to reflect this multiple refractory system using high-alumina refractory such as Jargal®M as the "working" lining and a less expensive refractory like Ufala® as the "safety" lining.

While many different types of corrosion situations and refractory applications exist, there are a few fundamental principles that can be used in determining the appropriate refractory to be used in a given instance. Looking at the Lewis Theory of acid/base chemistry, it is easy to understand why the resistance of acid-based refractories to acidic solutions is better than their resistance to basic solutions and vice versa. At room temperature an acid in solution is simply defined as having an excess of hydrogen ions over hydroxyl ions such that it contributes hydrogen ions to the solution [34]. Using the Lewis Theory, acids are defined as electron acceptors in a reaction and bases are electron donors. Corrosion chemistry at elevated temperatures however dictates that an acidic material contains an excess of silica over basic materials like lime (CaO). Neutrality in a refractory reaction with slag is therefore defined as basic material to silica ratio of 1.0. An acidic material contains excess silica and therefore is one that contributes silica to the corrosion reaction. Ions flow from locations of high concentration to areas with low concentration. Hence, if the refractory material is compatible with the slag, there is a decreased need for reaction between material and solution in an attempt to reach equilibrium. This is why basic refractories incur less corrosion loss than acidic refractory materials in basic solutions. Corrosion reactions are an attempt by the system to achieve compatibility by progressing toward equilibrium. Although microscopically refractories are rarely at chemical equilibrium, the localized volumes at the corrosion interface may be at or close to equilibrium [34].

The porosity of the refractory material is another concern when researching refractories for use in corrosive environments because most contain void space or porosity. There are two classifications of porosity, that which involves open pores which are connected, open at the surface, and can be penetrated by fluid media and that which has closed porosity such that the fluid media is unable to penetrate the refractory material. In the case of closed porosity the corrosion area is restricted to the hot face, the surface of the material which is exposed to the corrosive material; however, with open porosity, corrosion can occur beyond the hot face due to the ability of the corrosive media to enter into the pores and penetrate the refractory [34]. There have been numerous studies that have shown the correlation between the nature and extent of the porosity of a refractory and the slag-corrosion resistance of that material. It is known that the more dense a refractory is, the more degradation resistant it is in comparison to more porous samples [35]. It has been seen that the corrosion rate of slag exposed refractory increases linearly with apparent porosity between the range of 12-16% apparent porosity. This estimation may not hold true at porosities above 20% [34]. Consequently, higher density refractories tend to resist corrosion better and exhibit lower wear rates due to their lower apparent porosity. However, low porosity refractories may also experience greater effects of spalling leading to higher wear rates due to their lower thermal shock resistance [34].

Increased porosity also allows the slag to diffuse more readily throughout the refractory material. Because a concentration gradient will cause mass transport via diffusion, it is not necessary to have an electric field to produce it [36]. Diffusion in a material is the movement of atoms, ions, or molecules relative to their neighbors. It is desirable to find

the pathway (i.e. mechanism of diffusion and the kinetics of migration) used by these particles to penetrate the material [30]. In order for diffusion to occur through a closely packed, less porous material, movement via vacancies in the lattice structure is advantageous. Where no vacancy exists, the slag can still penetrate using interstitial movement or an exchange mechanism, however, it is more difficult for either of these mechanisms to occur in a dense material. With interstitial movement, it is problematic for the molecules to fit through the small openings within the lattice structure. Since the activation energy required to exchange places with the nearest neighbor is very high along and concern about possible deformation of the material exists, exchange mechanisms are also not favorable. As such, vacancy movement allows the easiest pathway for the solution to penetrate the solid [37]. Because diffusion rates increase and viscosity of liquid solutions decrease with increasing temperature, the fact that high-temperature black liquor gasifiers (HTBLG) operate at around 1000°C also serves to increase the rate at which the molten smelt is able to penetrate through the refractory material.

A cross-sectional graphic to assist in describing the process by which corrosion occurs in refractory materials is shown in Figure 16 [34]. The reactive component or slag is interfaced with the refractory's exposed surface, also known as a hot face, at a high temperature. A temperature gradient exists within the refractory material with the temperature of the refractory decreasing from the hot face towards the back, unexposed side of the material. The slag reacts with the refractory at the hot face as well as within the pores to form new phases in the refractory. The slag is able to penetrate through the

pores of the refractory until it reaches a point in the material where the temperature is low enough to cause the slag to solidify. This point is referred to as the freeze plane. The less deep the slag has to penetrate in order to reach the freeze plane, the less area will be exposed to the corrosive material causing the corrosion to basically be restricted to the slag-refractory interface. This means that when the refractories have a very steep temperature gradient, they will exhibit lower corrosion rates due to less slag penetration. Steep temperature gradients can be seen with thin-walled refractories when water or steam is used as a cooling fluid in the furnace shell. In situation with thicker refractory walls, there are two stages of corrosion. Stage I is represented in Figure 17 and occurs in corrosion of both thick and thin walled applications [34]. In Stage I corrosion, the penetration depth of the slag attack is minimal and the reactions occur mainly at the surface. Stage II, as shown in Figure 18, only follows Stage I in thick walls due to the allowance for further penetration of the corrosive media by the broader temperature gradient. Stage II is characterized by full penetration of the refractory and extensive disruption by corrosion of the hot face region [34].

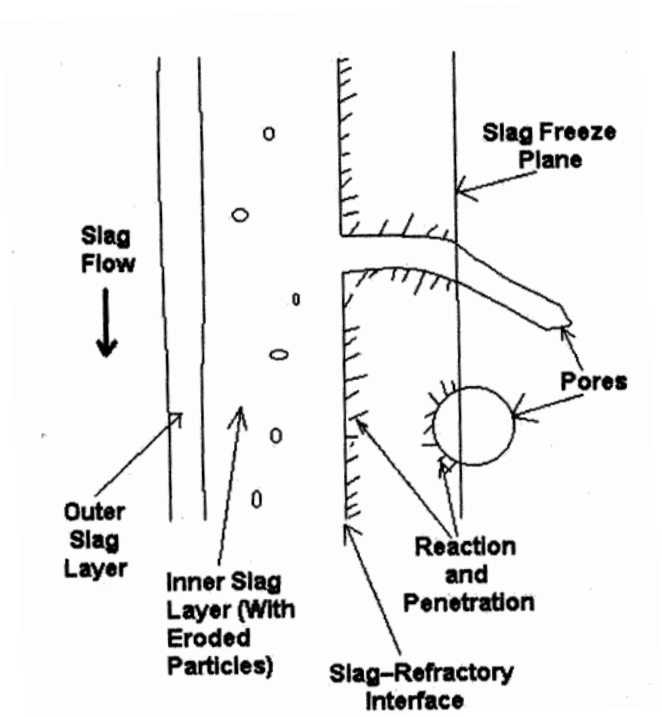

Figure 16: Cross Section of Refractory to Show Corrosion Mechanism [34]

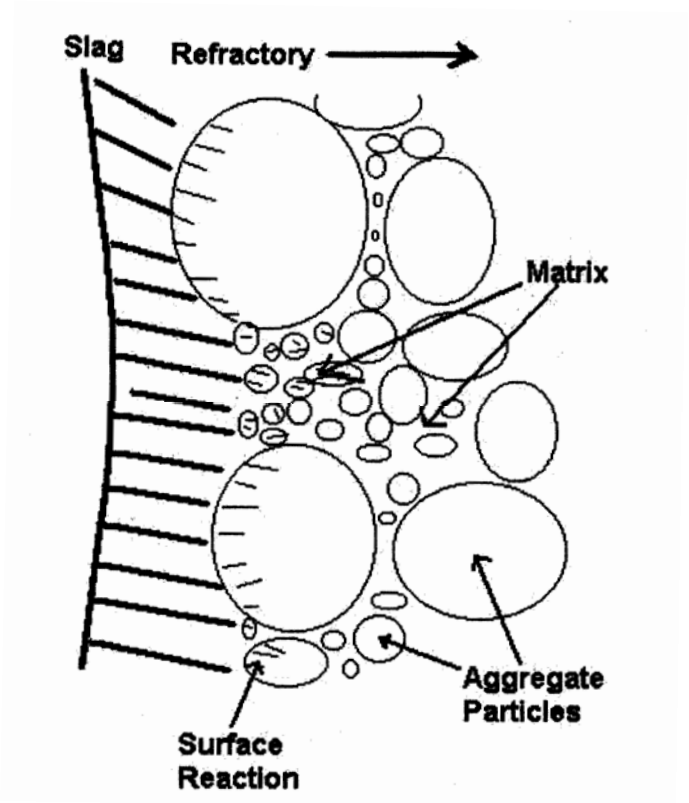

Figure 17: Stage I of Corrosion Mechanism where the Reaction Occurs Mainly at the Surface [34]

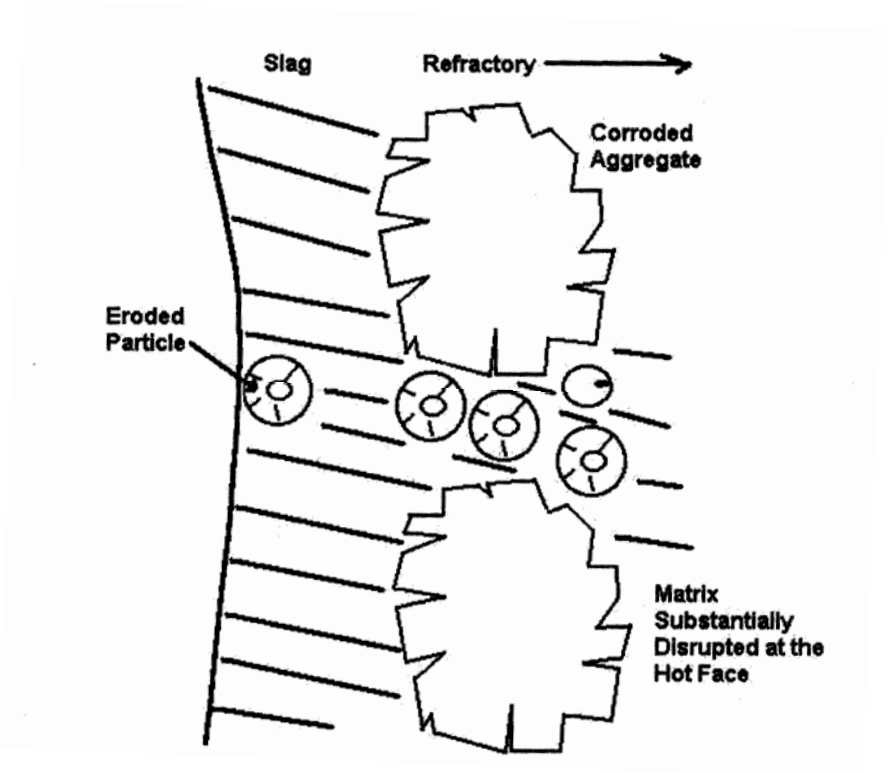

Figure 18: Stage II of Corrosion Mechanism where the Molten Slag Penetrates Deeper into the Refractory and Disrupts the Hot Face Region via Corrosion [34]

"Models for the corrosion process point to the fact that hot face temperature is the most important variable in controlling refractory life. To reduce corrosion loss, the usual approach is to employ higher-purity refractories or lower porosity refractories (such as fusion cast brick) because precise limits on hot face temperature are not practical given process goals [34]."

Refractory corrosion occurring in HTBLG environments begins with the reaction of the refractory with sodium salts from the molten smelt. The reaction pathways to convert α-alumina into β-alumina, β-alumina into β"-alumina, and β"-alumina into sodium aluminate are shown in Equations 6, 7, and 8, respectively [38]. The phase diagrams for

Na_2O with Al_2O_3 and Na_2O with SiO_2 are shown in Figures 19 and 20 [39, 40]. The phase diagram Na_2O-Al_2O_3-SiO_2 is shown in Figure 21 [41]. Each new product that is formed is larger in size than the reactant causing the refractory to expand. A complete conversion from α-alumina to sodium aluminate should cause a 133% volume increase [23]. The volume increase associated with each product formation is shown in Table 4 [23]. It is this volume change beneath the refractory surface that causes expansion and subsequent spalling because of the additional stresses applied to the material.

$$Na_2CO_3 + 11Al_2O_3 \rightarrow (Na_2O \times 11Al_2O_3) + CO_2 \quad (6)$$

$$5Na_2CO_3 + 6(Na_2O \times 11Al_2O_3) \rightarrow 11(Na_2O \times 6Al_2O_3) + 5CO_2 \quad (7)$$

$$5Na_2CO_3 + (Na_2O \times 6Al_2O_3) \rightarrow 12NaAlO_2 + 5CO_2 \quad (8)$$

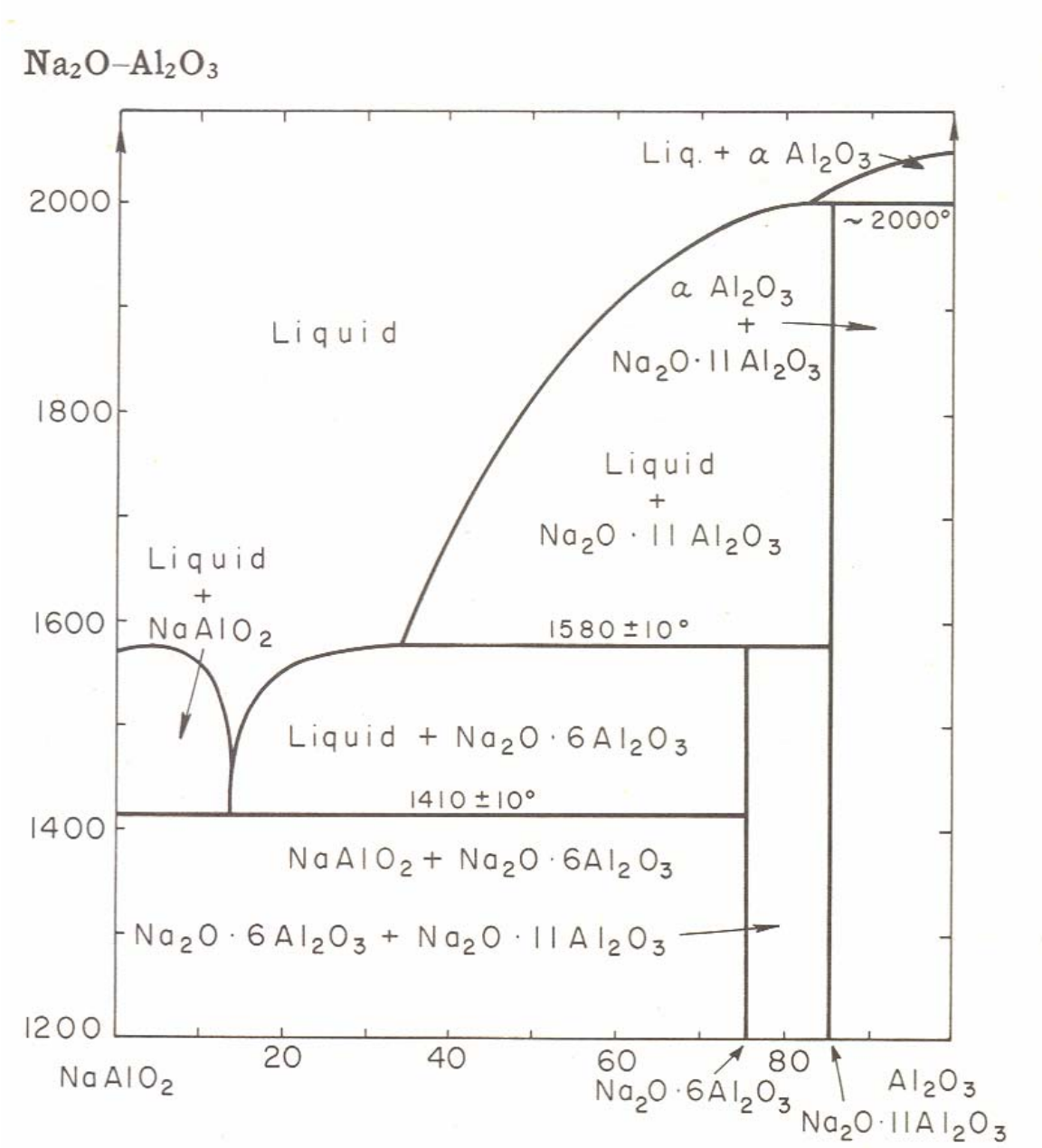

Figure 19: Phase Diagram of Na_2O and Al_2O_3 [39]

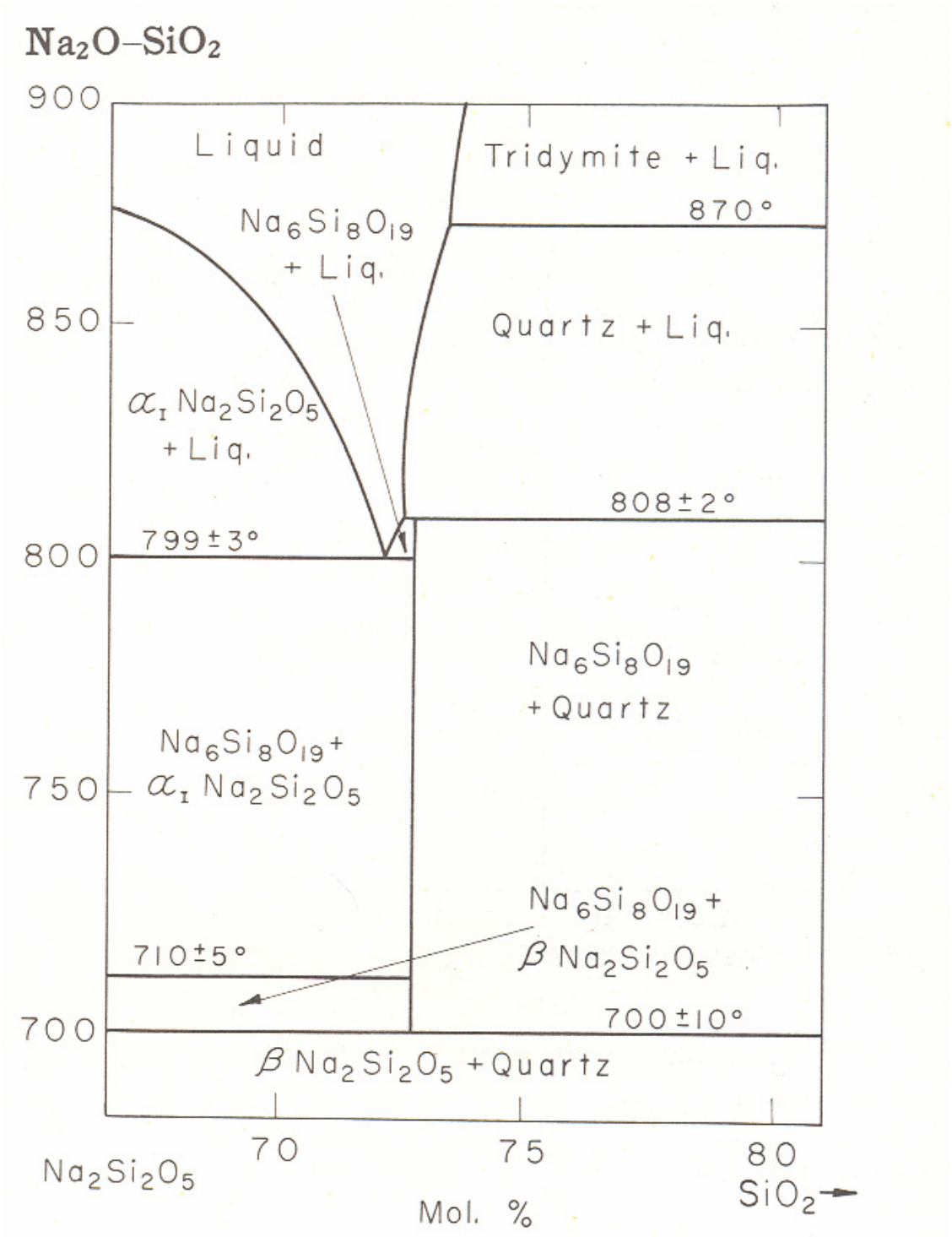

Figure 20: Phase Diagram of Na_2O and SiO_2 [40]

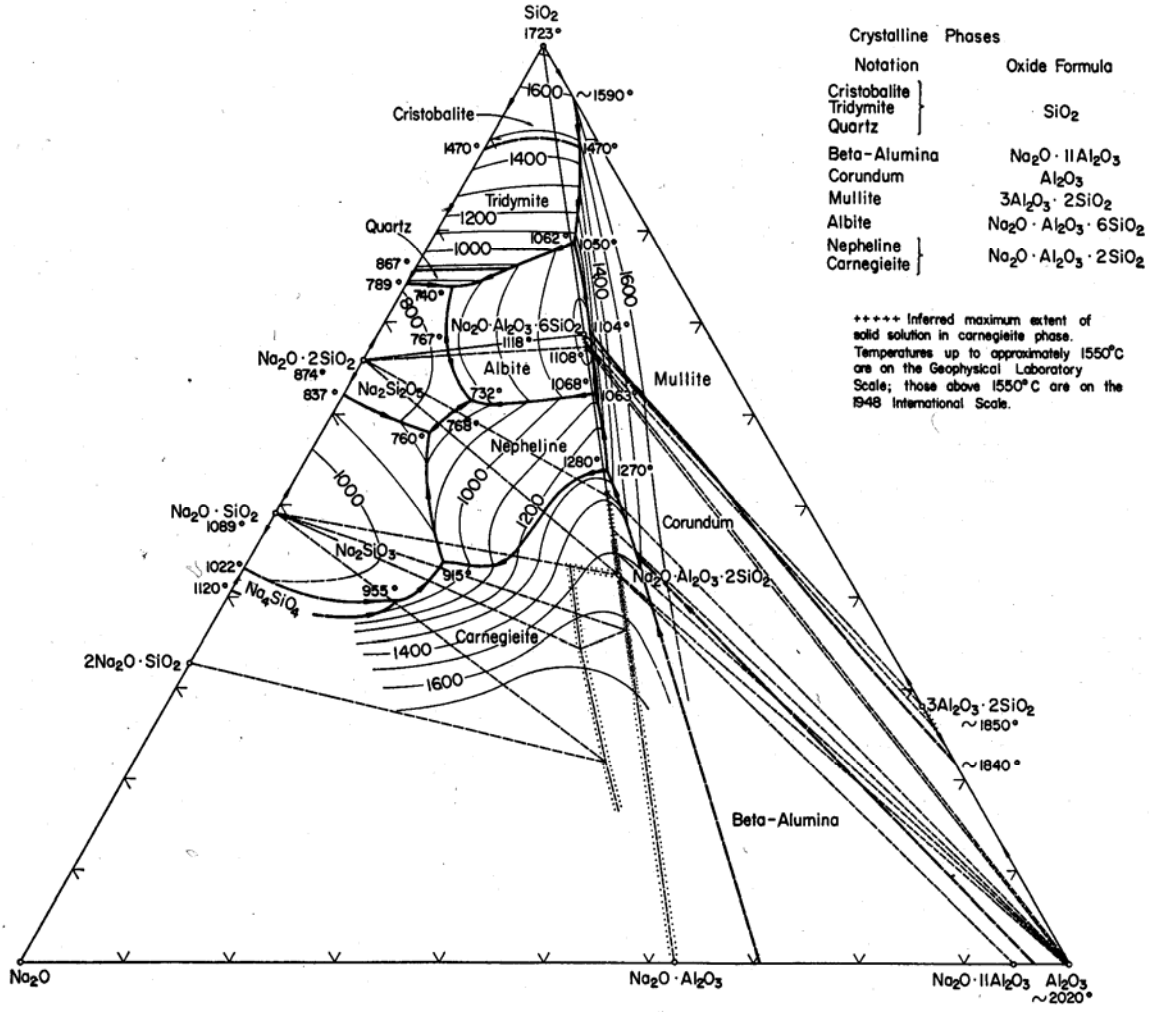

Figure 21: Phase Diagram of Na_2O-Al_2O_3-SiO_2 [41]

Table 4: Volume Changes Experienced by Alumina upon Reaction with Na_2O [23]

Material	Volume Expansion (% Compared to Al_2O_3)
Al_2O_3	-
β-Al_2O_3	31
β'-Al_2O_3	32
$NaAlO_2$	133

Expansion due to new product formation is not the only concern when working at high temperatures. When looking to install refractory material into an application such as a HTBLG, it is also necessary to take into consideration the thermal expansion that will occur as well. Thermal expansion is a measure of how temperature affects the specific volume of a material and is quantified in terms of a thermal expansion coefficient. This is especially important when considering coating applications because if the coating does not expand at the same or similar rate as the substrate material, additional stress may be placed on the material causing reduced strength or spalling of the material while in service earlier than anticipated [42]. The thermal expansion coefficients for Al_2O_3, CeO_2, Cr_2O_3, and ZrO_2 are given in Table 5. The substrate refractory and the coating materials used in these experiments have similar coefficients of thermal expansion and as such should not experience any major stresses or problems caused by expansion and shrinkage.

Table 5: Thermal Expansion Coefficients [43]

Material	Thermal Expansion Coefficient at 1300K (K^{-1}) x 10^{-5}
Al_2O_3	0.99
SiO_2	1.60
CeO_2	1.41
Cr_2O_3	0.76
ZrO_2	1.05

2.5 Molten Salts

Molten salts are "liquids having as structural units ions that have considerable freedom of movement under the influence of an electrical field, leading therefore to very high electrical conductance" [44]. Salt melts are versatile solvents in that they can dissolve a variety of different substances such as water, organics, metals, non-metals, and other salts [44]. Unfortunately, this is where the biggest problem in implementing high-temperature black liquor gasifiers occurs. Since molten salts are such effective solvents, it becomes exceedingly difficult to identify a material capable of containing molten salts for an extended period of time without being subjected to a significant amount of corrosion. This is best stated by Bloom when he says "the excellent solvent properties of molten salts give rise to their main industrial uses but at the same time are the cause of the corrosive action that makes for difficulties in their application" and "the lack of convenient refractory materials often leads to experimental difficulty in high temperature chemistry. Molten salts and vapors are often extremely corrosive and their solvent properties depend on composition and temperature…"[44] The same sentiment is reiterated by Lovering and Gale when they write "some [properties of molten salts] are actually less than desirable. Although the opportunity to operate in an ionic nonaqueous environment with fast reaction rates is attractive in many instances, the corrosive and

hygroscopic nature of many melts, as well as the elevated temperature often required, can cause intractable problems and limitations [45]." As defined by the Lewis Acid/Base Theory, acids are electron acceptors in a reaction and bases are electron donors. This theory can be used to note the differences between acidic and basic salt melts. A high thermodynamic activity of Na_2O also defines a basic molten salt whereas a molten salt having low Na_2O activity would be deemed acidic [46]. Salts containing high amounts of sodium carbonate (Na_2CO_3) are an example of a basic salt whereas high amounts of sodium sulfate (Na_2SO_4) would make the salt acidic in nature. Noble metals have a satisfactory resistance to corrosion by neutral and acidic melts and consequently platinum and gold tend to be used in construction of laboratory apparatuses yet they react relatively severely in basic melts [47]. Even so called inert materials such as platinum are soluble to some extent in molten salts [44]. A table containing typical properties of molten salts is shown in Table 6 [45].

Table 6: Physical and Chemical Properties of Molten Salts [45]

Physical	Chemical/electrochemical
High thermal conductivity	Wide range of thermochemical stability
High thermal capacity	Good solvents
Low density	High reaction rates
Moderate viscosity	Good electrochemical stability
Optically transparent (pure)	Low gas solubilities (except by chemical interactions)
High electrical conductivity	Low dielectric constants
Mutual miscibility	Adjustable acid-base properties
High surface energy, good wetting with low contact angles	Nonaqueous environment
Newtonian fluids	Standard potentials depend on system and differ from aqueous scale
Low vapor pressures	Corrosive
	Hygroscopic

Molten salts are good solvents for metals and as such this is another obstacle in identifying usable materials for industrial implementation; however, oxides are only soluble to a certain extent. Specifically, more than 50 mole % of metal can be dissolved by many molten sulfides (a component of smelt) and have the ability to form completely miscible solutions at high enough temperatures. There is also a noticeable increase in reaction rate, and thus a decrease in reaction time to only a few seconds, when the temperature of the salt melt is higher [44]. A list of materials that are typically used when dealing with molten salts and their temperature range and limitations is shown in Table 7 [45].

Table 7: Materials for Use in Molten Salts [45]

Material	Temperature range[a]	Uses	Limitations
Borosilicate glass	<450°C	Containment, insulator	Devitrification, poor seals to noble metals
P.t.f.e. (Teflon)	<300°C	Containment, insulator, fabrication	Opaque, low temperatures
Special glasses and silica	<700°C	Containment, optics	Cost, fabrication problems
Oxide ceramics (Al_2O_3, ZrO_2, etc.)	<1500°C	Containment, insulators	Fabrication restricted, soluble in some melts
Refractories, minerals (BN, SiC, pyrophyllite, diamond, etc.)	Very high	Containment, insulators	Expensive, limited fabrication, variable composition
Noble and refractory metals	Various	Containment, conductors, furnace shields	Expensive, reactive or soluble in some melts
Vitreous carbon	<1500°C	Containment, conductors	Fabrication restricted, variable properties according to source
Graphite/pyrolytic graphite	<1500°C	Containment, conductors, furnace shields	Porous/anisotropic, unsuitable for oxidizing conditions

[a] Normal range of operation

The non-electrolyte properties of molten salts such as refractive index, viscosity, and surface tension are similar to those of room temperature liquids and the thermal

conductivity of molten salts is only slightly higher despite the large difference in temperature. Molten salts are by far the best class of ionic conductors, and as such, the electrical conductivity of molten salts is extremely greater than room temperature liquids [44].

Alumina or magnesia capillaries have been used advantageously in higher temperature melting of very corrosive salts in order to determine electrical conductance [44]. As such, both of those refractory materials would present possible options for use in high temperature black liquor gasifiers.

2.6 Surface Treatment Options

"Methods that would reduce the penetration, wetting, and corrosive chemistry would significantly improve refractory performance…" [48] Due to the fact that refractory materials are such an integral part of industrial applications, it is important to continuously improve on their in-service performance. Surface treatments are extremely useful in that the base material can be chosen for its bulk properties and surface treatments applied to provide the desired surface properties such as corrosion resistance. This versatility makes these treatments very important to the engineering of machine components and tools. There are numerous options for the method in which these surface treatments are applied such as glazing and painting, gas carburizing, infrared heating, and dip-coating to name a few. As the demand for improved high performance materials grows, the market for surface treatments increases. This is especially true due to the fact that the properties of the surface can be just as important, especially for corrosion or environmental degradation of material, as those of the base material [10].

Barrier coatings exist to improve, protect, or preserve the substrate on which the coating is applied from damage or wear by its surrounding environment. There are many different coating applications that exist. Many of these coating and treatment options are specific to the type of substrate to which they are being applied such as electrodeposition and plasma nitriding for metals. Other coating options for possible use on ceramics include sputter deposition, chemical vapor deposition, spin coating, conventional brush coating, and dip coating. All coating methods use technology for the purpose of improving the base materials by adding layers of high performance materials to enhance the surface [49]. Conversely, methods such as ion implantation, high density infrared heating, and laser hardening are surface treatments that do not add a protective layer but instead modify the existing surface using heat or chemical treatments [10].

Coatings are applied to a base material to be resistant to corrosion or environmental degradation, provide a thermal barrier against high temperatures, or for other reasons. Whatever the motive, the vast majority of coatings are applied for a specific purpose and in order for those goals to be met, the coatings must be correctly bonded to the substrate material [50]. In keeping with this need, whenever a coating is applied to any object, the coating must be applied in the fluid state so that all interstices are sufficiently covered. Since it is impossible to apply a continuous coating by applying beads of solids to the base material, the coating materials are then limited to those materials that can exist in a liquid state under conditions that are not damaging to the material to which they will be applied. Also, when applying a coating, it is essential to ensure proper adhesion between

the coating and the substrate since lack of adhesion can lead to separation or to the penetration of reactants or pollutants along the surface of the base material [51]. It is also important for the coating and the base material to have similar coefficients of thermal expansion. If the two materials have vastly different size reactions to drastic changes in temperature, which often occurs in applications using refractory materials, there will be undue stress applied to the materials. This stress, tensile, shear, or compressive, may cause cracks within the coating and weakens the bond between substrate and coating and subsequently increases the likelihood of the protective coating spalling earlier then it otherwise would [42]. The properties of the applied coatings are dependent on which of the various methods were used in the application process [50].

- The spin coating technique involves applying an excess amount of coating solution (mixture of desired coating material and organic binder) to a substrate which is attached to a stage. The stage is then started into motion so that it spins at a pre-determined speed causing the excess coating solution to fly off. The centrifugal force forms an even coat on the surface of the material where the solvent used to make the coating slurry is allowed to evaporate [52].
- Random shaped powder is melted and quenched on the base material when the powder is dropped perpendicularly to a CO_2 laser beam when using the laser spray technique [53].
- Conventional brush coating is a method where liquid coatings are applied in using a coating applicator and then dried.

- Slurry or dip-coating involves immersing the base material in a coating bath (slurry) and slowly removing it at a constant speed. Assuming the slurry is of an appropriate consistency, this process should allow a sufficient amount of coating to remain on and coat the substrate material while the excess material returns to the bath. The more quickly the material is removed from the slurry, the thicker the coating will be. The thickness of the applied coat is dependent on up to six different effects [54]:
    1) Viscous drag upward on the liquid by the moving substrate
    2) Force of gravity
    3) Resultant force of surface tension in the concavely shaped meniscus
    4) Inertial force of the boundary layer liquid arriving at the deposition region
    5) Surface tension gradient
    6) The disjoining (or conjoining) pressure

Dip-coating and brush coating are both known as wetting processes where the coating material is applied in liquid form and only becomes solid upon cooling or solvent evaporation [55]. A liquid's ability to adhere to a given surface is known as wetting [56] Coating mechanisms such as dip-coating and conventional brush coating are inexpensive due to their minimal need for equipment and can conform to any shape substrate [54]. They are also relatively easy to apply in different situations allowing for in-situ application. In a study by Li, Li, and Stott [57] coatings were applied using a hybrid laser-flame spraying technique. The goal of this surface coating/treatment technique was to create a corrosion resistant coating for industrial use at high-temperatures and in molten slag. The hybrid technique combined coating application with additional surface treatment to make the added coating more dense and free of pores [57].

Surface treatments that alter the existing surface of the substrate material are also possible for use on ceramic refractory materials. A xenon arc lamp, high density infrared (HDI) heating, and combined laser sources are all methods that have been used in an attempt to create a dense, non-porous surface without applying any additional layers to the existing substrate. All three of the aforementioned surface treatments have been applied to high-alumina refractory in an attempt at decreasing corrosion rates at high temperatures or in molten slags. Melting and reforming a homogeneous, less porous surface without altering the chemical composition of the bulk material or the surface is the method by which these surface treatments attempt corrosion resistance. Upon HDI treatment of the castable alumina and aluminosilicate refractory tested, a marked decrease in penetration depth of molten copper was observed [48]. This decrease was attributed to the approximately 500μm deep pore-free surface that was created using HDI heating [48]. One of the main problems that had shown up while using laser treatments was cracking of the newly formed surface upon cooling because of the extremely steep temperature gradient within the material [58]. Upon pre-heating of the alumina-based refractory, there was no longer a steep thermal gradient and as such those negative effects were offset [58]. Some cracks that appear and are oriented perpendicular to the treated surface can be considered beneficial in that they increase thermal shock resistance [35], although that asset can be counteracted by the increased allowance for slag penetration through the material. Cracks that are parallel to the refractory face, however, are harmful to the material and may cause spalling of the treated surface [35]. A picture showing the difference in surface characteristics before and after laser treatment is shown in Figure 22

[58]. As can be seen, the porosity has been drastically reduced after laser treatment. Similar results regarding decreased porosity were seen after xenon arc lamp heat treatment was applied to the refractory surface as well [35].

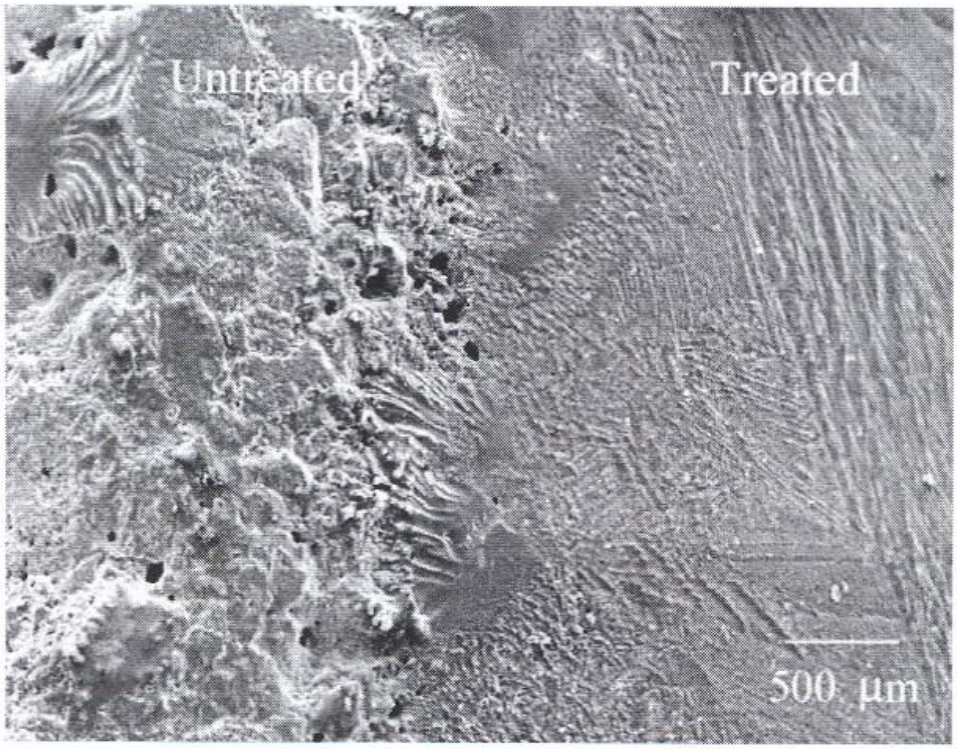

Figure 22: High-Alumina Refractory Sample where only the Right Half of the Sample has been Laser Treated to Close Surface Pores to Slow Molten Copper Penetration into the Sample whereas the Left Half of the Sample is Still Visibly Porous [58]

2.7 Previous Research

The degradation of refractory lining inside of a commercial scale high-temperature black liquor gasifier was occurring at a much faster rate than was predicted from smaller scale systems [7]. As such, it was necessary to determine a way in which to accurately model the corrosion occurring within a high-temperature black liquor gasifier. A laboratory test system was used and found to more accurately predict corrosion rates at a commercial

level [7]. As such, it can be assumed that the method used to replicate the high-temperature black liquor gasification environment in this experiment would provide an accurate assessment of the ability of the coatings to reduce refractory degradation.

Corrosion of high-performance ceramics under many conditions was studied by Gogotsi and Lavrenko [59]. They noted that "high-alumina ceramics are probably the most resistant oxide material, but even they are heavily attacked by melts of Na_2O, $Na_2S_2O_7$, Na_2O_2, and KOH" [59]. Of most relevance, alumina and yttria-stabilized zirconia were tested and it was found that alumina was resistant to NaCl, Na_2CO_3 up to 900°C, Na_2SO_4 up to 1000°C, and NaOH up to only 538°C. Alumina showed some reaction with KOH at 500°C with more severe corrosion at higher temperatures and some reaction in basic slags [59]. While one of the most thermodynamically stable ceramics is zirconia, which is also more refractory than alumina, it does undergo a phase transformation on cooling from firing temperature [59]. As such, it is necessary to stabilize the zirconia into the tetragonal form rather than allowing it to transform into the less corrosion resistant monoclinic form [59]. Normally CaO, MgO, or Y_2O_3 are added in small quantities to stabilize the zirconia. Li, Hirschfeld, and Brown [60] did suggest that scandia-stabilized zirconia may be more effective in slowing corrosion rates than the yttria-stabilized form. The yttria-stabilized zirconia as tested by Gogotsi and Lavrenko was resistant to basic slag attack, Na_2SO_4 up to 1000°C, and NaOH up to only 538°C. Moderate reaction was seen by the stabilized zirconia with KOH at 500°C and significant corrosion was noted at 900°C by Na_2CO_3 [59].

The corrosive effect of molten salts on mullite ($3Al_2O_3 \cdot 2SiO_2$) was studied by Jacobson, Lee, and Yoshio [46]. More acidic molten salts were determined to have low thermal Na_2O activities whereas high thermal Na_2O activities correspond to basic molten salts. Jacobson, Lee, and Yoshio predicted that sodium β-alumina and sodium aluminate will form when mullite is exposed to solutions with higher Na_2O thermal activities (basic molten salts). Sodium aluminosilicates were more likely to be formed when mullite was exposed to acidic molten salts. It was found that the acidic molten salts formed small amounts of Al_2O_3 and the basic molten salts formed different Na_2O-Al_2O_3-SiO_2 compounds [46] Generally speaking, the Na_2O will react with the silica within a refractory before reacting with the alumina components. The results of a study by Näfe and Kale [61] also confirm that there are higher Na_2O thermal activities under basic conditions and lower activities under acidic conditions. A diagram plotting the logarithm of Na_2O activity as a function of temperature to determine phase equilibria is shown in Figure 23. This diagram can be used to predict the prominent sodium/aluminum species that would occur in a melt if the Na_2O is known.

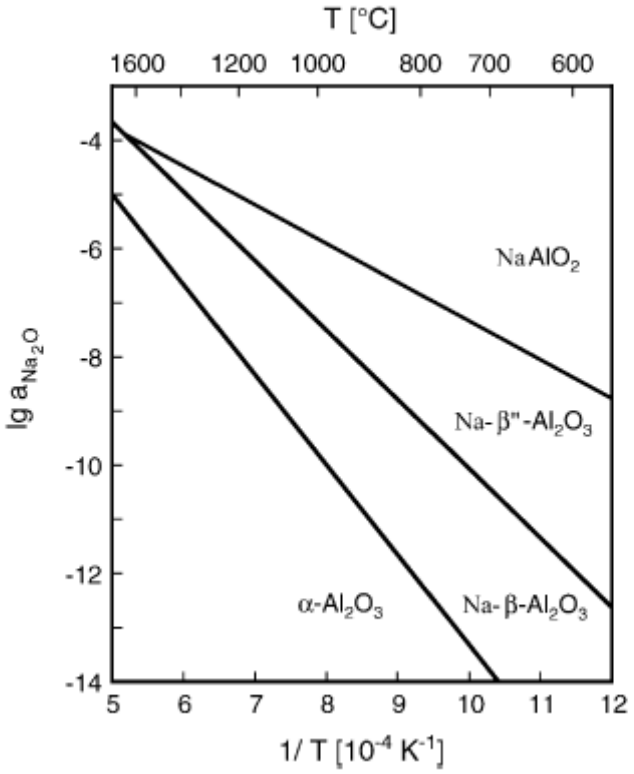

Figure 23: Dependence of Sodium/Aluminum Species Equilibria on Sodium Oxide Activity (Acidic or Basic Conditions) and Temperature [61]

Blachere and Pettit [62] noted that wetting of the surface of alumina by a salt melt was better under basic conditions at 1000°C than in acidic conditions. Impurities in the alumina also increased the amount of surface wetting that occurred. Because wetting of a material is also an indication of the reaction tendency the solution will have with the substrate, good wetting results in higher surface area contact and increased corrosion [62]. Blachere and Pettit also found that the corrosion that occurred was focused mainly at the grain boundaries in the sample and was worse under basic conditions [62]. Hirata, Akiyama, and Yamamoto [63] studied the hot corrosion resistance of sintered Cr_2O_3-Al_2O_3 ceramic in V_2O_5-Na_2SO_4 molten salt. It was hypothesized that the addition of chromia into the alumina ceramic would decrease the corrosion rate because of decreased

solubility and increased viscosity of the molten oxides and decreased diffusion rate of the salts through the ceramic [63]. Hirata, Akiyama, and Yamamoto agreed with Blachere and Pettit [62] that the molten salt penetrated at the grain boundaries increasing corrosion at those points [63]. The thickness of the corrosion layer of the 50mol%Cr_2O_3-Al_2O_3 was proportion to the ½ power of the holding time in the molten salts where the thickness was directly proportional to the holding time for the pure Al_2O_3 [63]. This suggests that the addition of chromia to the ceramic helped to slow the corrosion rate. It was also found that the density of the ceramic increased with higher sintering temperatures with a relative density over 95% at a sintering temperature of 1500°C. The sintering was found to increase grain size which could also serve to decrease the corrosion rate [63].

Lawson, Pettit, and Blachere [64] studied the hot corrosion of various purities of alumina ceramics by a sodium sulfate melt at 1000°C under basic conditions. They found that contact with even the slightest of impurities in the refractory material (0.11% SiO_2 in 99.8% Al_2O_3 refractory) caused the formation of sodium aluminum silicate products, primarily along the grain boundaries [64]. They found that generally there was an increase in corrosion with increasing impurity in polycrystalline aluminas. Hence, corrosion of industrial ceramics, which are generally less pure, by basic melts will lead to loss of refractory integrity and removal of alumina grains [64]. Hirata, Ota, and Morimoto [65] also examined the effect that impurities have on alumina corrosion by molten salts. The system they studied, however, was that of Al_2O_3 with molten V_2O_5-Na_2SO_4 at 900°C. They found that the thickness of the corrosion zone on the alumina ceramic varied linearly with holding time whereas the ceramic with low purity had a

damage zone that depended on the square root of the holding time [65]. It was also noted that SiO_2 impurities especially increased the rate of corrosion.

Mullite and fused-cast α-/β-alumina samples were taken from existing black liquor gasifiers and examined by Peascoe, Keiser, Hubbard, et al [7]. New mullite and fused-cast α-/β-alumina samples were exposed in a laboratory smelt test system and the results were compared to those found from the commercial scale gasifiers [7]. The mullite that was taken from the in-service gasifiers had considerable degradation and spalling. The surface that was in direct contact with the molten smelt experienced a color change and a 1-3 cm thick bubble was formed. The mullite that was tested in the small scale laboratory setting underwent such a sizable volumetric expansion that cracks were noted along the length of the sample [7]. They also found that the reaction depth of the sample exposed for 100 hours was nearly twice as deep as the corresponding 50 hour sample suggesting a linear penetration depth with respect to time. A color change along with some spalling and bowing was also noted in the in-service fused-cast α-/β-alumina. The expansion of the fused-cast α-/β-alumina was a significant, yet much smaller than that of the mullite at 0.7% after 100 hours of exposure in the laboratory smelt test system [7]. The fused-cast α-/β-alumina refractory is preferable to mullite for application in high-temperature black liquor gasifiers due to the loss of structural integrity and high rate of spallation of the mullite refractory. Higher purity α-alumina, however, appears to be the most corrosion resistant refractory at this time. Mencke [38] tested the effect of different coating types, number of coats, and coating environment on high alumina Jargal®M ceramic refractory in a molten synthetic smelt atmosphere. She tested coatings of yttria-

stabilized zirconia with the addition of chromia and ceria, no, one and three layer coatings, and coatings applied under atmospheric pressure and under vacuum. The number of coatings and coating environment did not have any significant effect on the corrosion resistance of the coatings [38]. The zirconia/chromia coatings did show some added protection against corrosion, however, did not significantly impede the corrosion reactions. As such, from the research done by Mencke, it cannot be concluded that either the zirconia/chromia or ceria coatings in any number of layers or under any coating environment are sufficient to slow corrosion rates of high alumina refractory by molten synthetic smelt.

Surface coatings and modifications have also been of interest in an attempt to slow corrosion rates. Tiegs, Kiggans, Montgomery, Harper, and Blue [48] performed surface modifications using high density infrared (HDI) heating on high alumina castable refractory and aluminosilicate refractory samples. The primary emphasis of the HDI technique was to reduce porosity providing an increased corrosion resistance. One of the benefits of HDI over laser melting techniques is that HDI is the ability to successfully treat large areas in a reasonable amount of time [48]. The mitigation of molten copper penetration into the refractory was measured after HDI treatments on both types of refractory. After the application of the HDI surface treatments, there was very little to no penetration of molten copper into the high alumina castable refractory. The surface of the HDI treated aluminosilicate refractory was not even wetted by the molten copper such that the molten copper actually fell off of the refractory surface after sample removal [48]. Li, Hirschfeld, and Brown [60] examined four coating types applied to Si_3N_4

ceramics using sol-gel and dip coating methods. Mullite, alumina, zirconia, and CMZP [$(Ca_{0.6}, Mg_{0.4})Zr_4(PO_4)_6$] coatings were applied in an attempt to prevent or slow corrosion by basic molten salts (Na_2CO_3) at 1000°C. All of the coated samples experienced a smaller weight loss then the uncoated samples. The zirconia coatings had the worst resistance to thermal shock testing due most likely to the large discrepancy between the thermal expansion coefficients of the coating and substrate materials [60]. While the alumina and mullite coatings did serve to decrease the weight loss that occurred upon Na_2CO_3 molten salt exposure, there was a sizeable decrease in flexure strength. The zirconia and CMZP coated samples, however, also lessened the weight loss of the samples but also had a higher flexure strength after corrosion and as such performed the best of the four tested coatings [60].

Chapter 3

Hypotheses

- The degradation of the alumina or alumina/silica refractory in molten sodium salts occurs as a result of the volume expansion due to formation of subsurface reaction products and subsequent spalling.
- The diffusion rate of the molten smelt through the sample can be slowed by closing the surface pores via surface coatings or other methods. As such, the corrosion rate of refractory materials can be decreased.

Chapter 4

EXPERIMENTAL PROCEDURE

4.1 Refractory Sample Preparation

The ceramic refractory materials, Jargal®M and Ufala®, were obtained from Oak Ridge National Laboratory in Oak Ridge, Tennessee. The chemical compositions for Jargal®M and Ufala® are listed in Table 8. Micrographs of Jargal®M and Ufala® refractory obtained using scanning electron microscopy are shown in Figures 24 and 25, respectively. Both types of refractory were cut using Buehler's Isomet 1000 Precision Cut Diamond Saw with 1 part Isocut Plus solution to 9 parts water as cutting fluid. The Jargal®M refractory was cut into approximately 1" x ½" x ½" blocks and 3½" x ½" x ½" sticks while the Ufala® was cut into both 1" x ½" x ½" blocks and 4" x ½" x ½" sticks as shown in Figures 26 and 27.

Table 8: Chemical Composition of Jargal®M and Ufala® Refractory

Specimen	Formula	Percentage of Total Weight in Jargal®M	Percentage of Total Weight in Ufala®
Alumina	(Al_2O_3)	>95.0%	58.1%
Silica	(SiO_2)	4.0%	38.2%
Titania	(TiO_2)	≈ 0%	2.2%
Iron Oxide	(Fe_2O_3)	≈ 0%	1.2%
Lime	(CaO)	≈ 0%	0.1%
Magnesia	(MgO)	≈ 0%	0.1%
Alkalies	(Na_2O + K_2O)	≈ 0.5%	0.1%

(a) (b)

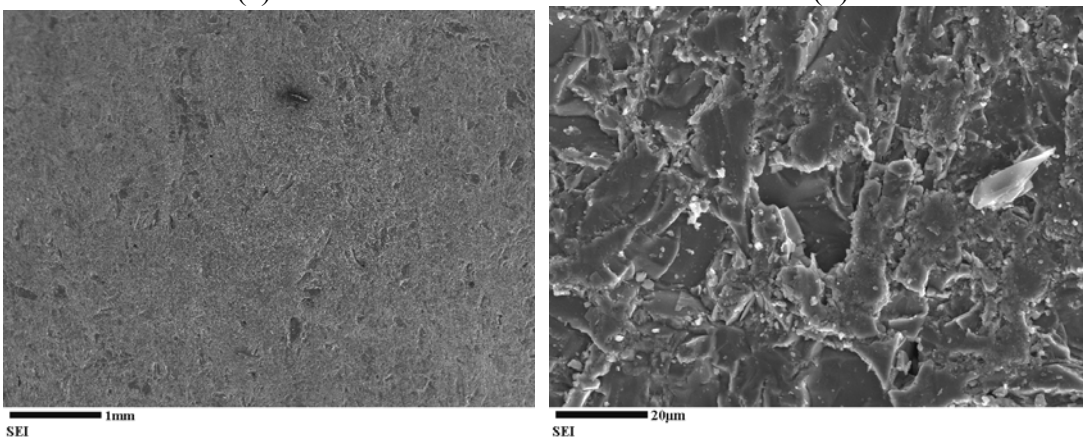

Figure 24: Micrograph of Jargal®M Refractory Showing Uniformity, Lack of Macropores, and Existence of Micropores at (a) 20x Magnification and (b) 1000x Magnification

(a) (b)

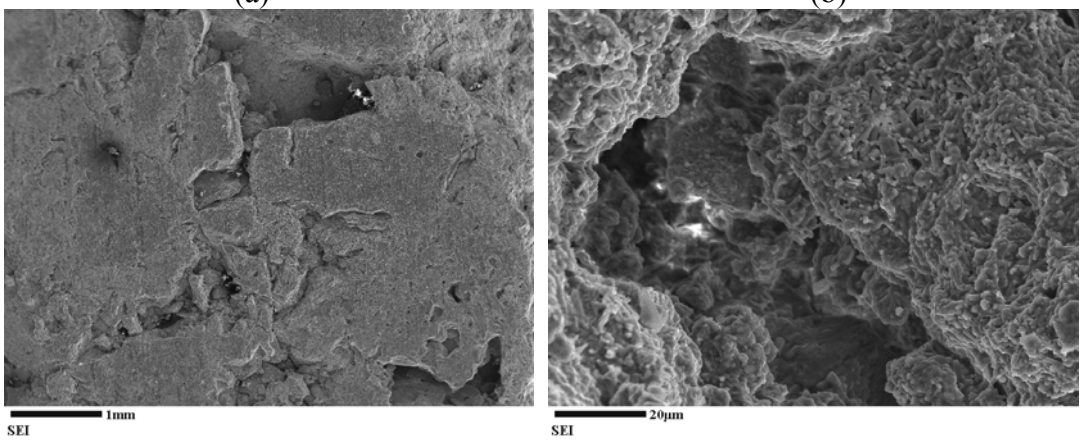

Figure 25: Micrograph of Ufala® Refractory Showing Depth and Number of Macropores and Micropores at (a) 20x Magnification and (b) 1000x Magnification

(a) (b)

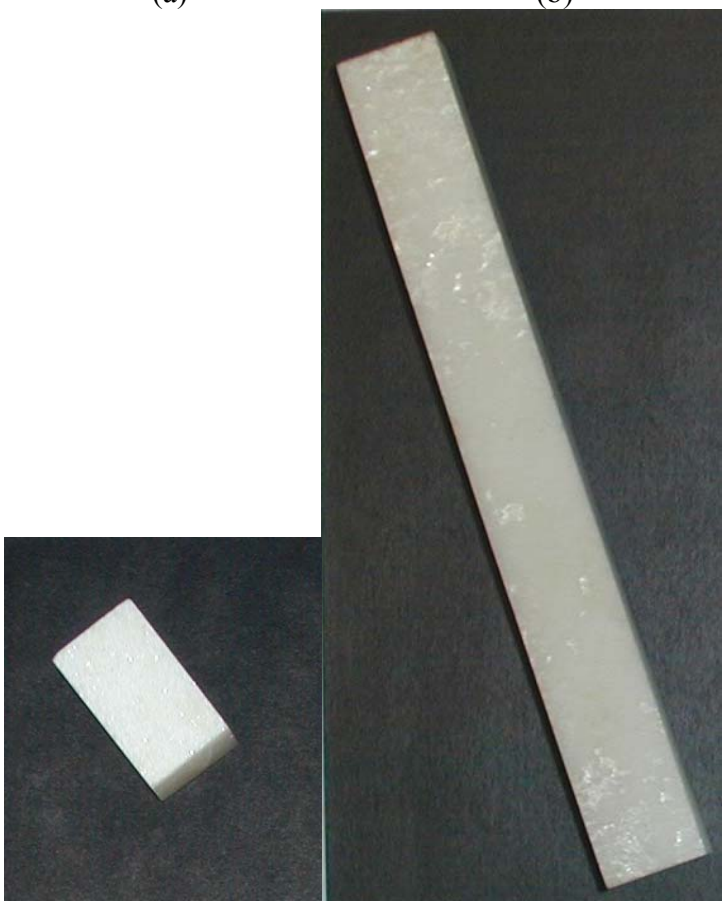

Figure 26: (a) Small Block and (b) Long Stick Samples of Jargal®M Refractory Before Molten Smelt Exposure as Sectioned for Testing

(a) (b)

Figure 27: (a) Small Block and (b) Long Stick Samples of Ufala® Refractory Before Molten Smelt Exposure as Sectioned for Testing

Once cut, the samples were immersed in acetone and put into the Sonicor Ultrasonic Cleaner for 15 minutes to remove the remaining cutting fluid from the pieces. Because of the greater porosity of the Ufala®, the cutting fluid was able to penetrate deeper into the piece and was not easily removed with just acetone and the Ultrasonic Cleaner. Consequently, the Ufala® samples then needed to be placed into the Fischer Scientific Isotemp Programmable Muffle Furnace at 500°C for 2 hours to burn off any remaining cutting fluid in the piece.

4.2 Coating Application

Five different metal oxides and combinations were chosen to be tested as barrier coatings for use in black liquor gasifiers. This homogeneous layer of metal oxides was applied using two different methods. One of the methods used to apply the coatings was a commercial C^3™ method whereas the other method was developed in this study to apply oxide coatings to the ceramic refractories in the laboratory. Three of those coating types, yttria-stabilized zirconia, ceria, and chromia, were applied using both techniques while the other two coating types, sodium cerium oxide and ceria plus powder, were only applied using commercial method.

The samples that were coated by C^3™ International Technologies were submerged in a metal oxide slurry for 24 hours before being withdrawn. The samples were then cured at 450°C for about 15 minutes. The additional metal oxide coating applied by C^3™ International Technologies was sodium cerium oxide which was created by layering sodium oxide and cerium oxide on the refractory surface.

A method to apply metal oxide powders was developed through this study. In order to create a slurry that would adhere to the refractory sample after the coating process, yet allow for easy removal of the organic binder while leaving the metal oxide behind, polyvinyl alcohol (PVA) was used as the base. The viscosity of five different solutions of polyvinyl alcohol was measured using a Grace Instruments 3500 viscometer to determine the correlation between viscosity and a functional coating base to disperse metal oxide evenly. Compositions of 5.66 wt%, 6.83 wt%, 7.41 wt%, 10 wt%, and 20 wt% PVA were all mixed and the viscosities were measured. The effect of time exposed

to the environment, to account for possible evaporation, and temperature on viscosity were also examined. It was determined that a 6.83 wt% solution of PVA in distilled water resulted in an optimum base to disperse metal oxide powders for surface application. The viscosity changes with respect to time were minimal as long as the mixtures were kept in a sealed container. The solutions were made by heating and stirring the mixture of PVA and water on a hotplate for approximately 3 hours until all of the PVA was dissolved. At that time, the appropriate amount of metal oxide powder was added and stirred until all of the powder was evenly dispersed throughout the solution. The viscosity of each 6.83 wt% PVA solution with the different type of metal oxide powders added was also measured after they were thoroughly mixed. The effect of varying amounts of metal oxide powder was also considered by adding the metal oxide powders in increments and measuring the viscosities after each addition. The metal oxide powders used were cerium oxide (CeO_2), yttria-stabilized zirconium oxide (Y_2O_3-ZrO_2), and chromium oxide (Cr_2O_3). All three of the metal oxide powders used to create the laboratory coatings were nanopowders with an average particle size of less than 100 nm. A coating applicator was used to apply an even layer of slurry to each sample. The samples were then placed in the drybox to allow the coatings to dry and set. Once dry, a visual analysis of the coating was done and a second layer was applied paying close attention to any locations where the first coat did not completely adhere. After a continuous barrier had been formed, the samples were placed into the Fischer Scientific Isotemp Programmable Muffle Furnace at 500°C for ½ hour to cure. Again, a visual assessment was done to ensure that a continuous layer of metal oxide has been applied to the sample. If the coating cracked during the curing process, an additional layer was

added and the process was repeated. Any cracks or voids in the coating will allow the molten smelt to penetrate the refractory quickly at those locations and thus essentially negate any benefits that would have come from the barrier coating. In order to sinter the coatings, the some coated refractory samples were also exposed to an infrared light at 1300°C for 2 hours. The refractory samples with IR sintered coatings were not suitable for testing due to their visibly cracked coating layer.

4.3 Black Liquor Gasifier Smelt Preparation

A smelt sample was taken directly from the Weyerhaeuser black liquor gasifier in New Bern, NC and analyzed in early 2002 for a previous study. Table 9 shows the composition of those smelt samples. The potassium and chloride content is shown in the table as only potassium chloride (KCl). Those chemicals may occur as not only potassium chloride but also as sodium chloride (NaCl) and potassium carbonate (K_2CO_3). The same sample was then analyzed again slightly more than a year later, again for a previous study. The composition of the year old smelt is shown in Table 10. As can be seen from the tables, it was found that the sodium sulfide (Na_2S) in the smelt oxidized while exposed to the environment allowing only small amounts of Na_2S to remain and react after time. Consequently, the corrosivity of the smelt could change thereby causing an improper replication of the environment inside a black liquor gasifier. Because of this, it was necessary to make and use a new batch of synthetic smelt for every set of experiments that were run to reduce the effect of oxidation on refractory exposure test results. This would ensure that the laboratory experiment would simulate the black liquor gasifier as closely as possible and will also be reproducible. Table 11 shows the amount of each chemical used, along with its weight percent, in the preparation of synthetic smelt

for all of the experiments with the exception of those meant to determine the effects of changing alkalinity and sulfidity. The composition used was based on the chemical makeup found in the initial analysis of the Weyerhaeuser smelt, shown in Table 9.

Table 9: Initial Analysis of Weyerhaeuser Smelt

Sample ID	Na_2CO_3 (Wt %)	Na_2S (mg/kg)	$Na_2S_2O_3$ (mg/kg)	Na_2SO_3 (mg/kg)	NaOH (mg/kg)	Na_2SO_4 (mg/kg)	KCl (mg/kg)
Smelt #2a	72.40	20.40	3.10	4.37	0.70	2.59	1.01
Smelt #2b	72.10	20.20	3.26	4.60	0.63	2.75	1.05
Smelt #3a	73.90	20.10	3.70	5.22	0.47	3.03	1.16
Smelt #3b	74.10	19.60	3.72	5.25	0.55	3.12	1.21
Composite	73.13	20.08	3.45	4.86	0.59	2.87	1.11
Scaled	68.94	18.93	3.25	4.58	0.55	2.71	1.04
Weigh Out (g)	414	114	19	27	3	16	6
Weight %	69	19	3	5	1	3	1

Table 10: Analysis of Weyerhaeuser Smelt After 1 Year

Sample ID	Na_2CO_3 (Wt%)	Na_2S (Wt%)	$Na_2S_2O_3$ (Wt%)	Na_2SO_3 (Wt%)	NaOH (Wt%)	Na_2SO_4 (Wt%)	KCl (Wt%)
Powder Smelt	42.80	0.13	4.25	13.60	23.50	2.51	0.66
Powder Duplicate	42.30	0.27	4.55	13.30	23.40	2.69	0.70
Chunk Smelt	41.20	0.07	2.54	16.20	24.50	2.58	0.69
Chunk Duplicate	41.10	0.26			24.30		

Table 11: Composition for 65/15 Carbonate to Sulfide Ratio Synthetic Smelt

Chemical Species	Chemical Formula	Amount (g)	Weight %
Sodium Hydroxide	NaOH	1.67	1.19
Sodium Sulfide	$Na_2S•9H_2O$	65.04	15.06
Sodium Sulfate	$Na_2SO_4•10H_2O$	12.86	4.04
Sodium Thiosulfate	$Na_2S_2O_3$	9.12	6.49
Sodium Sulfite	Na_2SO_3	3.59	2.56
Potassium Chloride	KCl	2.92	2.08
Potassium Carbonate	K_2CO_3	3.81	2.71
Sodium Carbonate	Na_2CO_3	92.47	65.87

4.4 Exposure of Refractories to Molten Smelt

Each of the chemicals used to create the synthetic smelt were weighed out to the fourth decimal place using the Mettler AE200 balance and mixed together. One long refractory sample was placed into each high purity α-alumina (99.8%) crucible before nearly 100 grams of synthetic smelt added to each crucible. If desired, one short refractory sample was then placed on top of the initial portion of smelt mixture and covered with the remaining amount of synthetic smelt for that crucible. Every smelt mixture was made separately for each crucible to ensure exact composition in each crucible.

To determine the extent of sodium sulfide's corrosive effects, both Jargal®M and Ufala® were exposed to five different compositions of molten smelt. Jargal®M samples were exposed to the molten smelts for 7 days whereas the Ufala® samples were exposed for only 36 hours. The ratios of weight percent of sodium carbonate to sodium sulfide were set to 65/15, 65/20, 65/25, 65/30, 65/35, respectively while the other chemical amounts were adjusted accordingly. The composition for the 65/15 carbonate to sulfide ratio mixture is listed above in Table 11 while the compositions for the remaining ratios are listed in Tables 12 – 15, respectively. After exposure, the samples were then analyzed and any significant differences were noted. For the remainder of the tests, the 65% sodium carbonate/15% sodium sulfide mixture was used due to the fact that it was a good replication of the smelt in a commercial black liquor gasification environment and the difference in corrosive effects caused buy the different compositions was not significant.

Table 12: Composition for 65/20 Carbonate to Sulfide Ratio Synthetic Smelt

Chemical Species	Chemical Formula	Amount (g)	Weight %
Sodium Hydroxide	NaOH	0.51	0.37
Sodium Sulfide	$Na_2S•9H_2O$	84.52	20.00
Sodium Sulfate	$Na_2SO_4•10H_2O$	10.01	3.21
Sodium Thiosulfate	$Na_2S_2O_3$	7.80	5.68
Sodium Sulfite	Na_2SO_3	2.38	1.73
Potassium Chloride	KCl	1.72	1.25
Potassium Carbonate	K_2CO_3	2.59	1.89
Sodium Carbonate	Na_2CO_3	90.48	65.87

Table 13: Composition for 65/25 Carbonate to Sulfide Ratio Synthetic Smelt

Chemical Species	Chemical Formula	Amount (g)	Weight %
Sodium Hydroxide	NaOH	0.249	0.189
Sodium Sulfide	$Na_2S•9H_2O$	101.32	24.97
Sodium Sulfate	$Na_2SO_4•10H_2O$	6.74	2.25
Sodium Thiosulfate	$Na_2S_2O_3$	6.21	4.71
Sodium Sulfite	Na_2SO_3	1.06	0.80
Potassium Chloride	KCl	0.387	0.293
Potassium Carbonate	K_2CO_3	1.21	0.915
Sodium Carbonate	Na_2CO_3	86.88	65.87

Table 14: Composition for 65/30 Carbonate to Sulfide Ratio Synthetic Smelt

Chemical Species	Chemical Formula	Amount (g)	Weight %
Sodium Hydroxide	NaOH	0.0580	0.0475
Sodium Sulfide	$Na_2S•9H_2O$	112.63	30.00
Sodium Sulfate	$Na_2SO_4•10H_2O$	3.50	1.26
Sodium Thiosulfate	$Na_2S_2O_3$	3.07	2.51
Sodium Sulfite	Na_2SO_3	0.118	0.097
Potassium Chloride	KCl	0.081	0.067
Potassium Carbonate	K_2CO_3	0.169	0.139
Sodium Carbonate	Na_2CO_3	80.38	65.87

Table 15: Composition for 65/35 Carbonate to Sulfide Ratio Synthetic Smelt

Chemical Species	Chemical Formula	Amount (g)	Weight %
Sodium Hydroxide	NaOH	0.00	0.00
Sodium Sulfide	$Na_2S•9H_2O$	122.90	34.13
Sodium Sulfate	$Na_2SO_4•10H_2O$	0.00	0.00
Sodium Thiosulfate	$Na_2S_2O_3$	0.00	0.00
Sodium Sulfite	Na_2SO_3	0.00	0.00
Potassium Chloride	KCl	0.00	0.00
Potassium Carbonate	K_2CO_3	0.00	0.00
Sodium Carbonate	Na_2CO_3	77.10	65.87

All of the crucibles containing only the smaller refractory blocks were covered with graphite lids that fit snuggly into the opening of the crucible. The crucibles containing the longer sticks of refractory were unable to be covered due to the fact that the refractory was longer than the crucible was deep. The graphite covers were used to react with any oxygen potentially remaining in the furnace atmosphere, although there should have been no oxygen left after having turned on the nitrogen purge system and allowing it to run for 1 hour prior to furnace start-up. A maximum of 9 crucibles were then placed into a stainless steel pan containing approximately 2" of sand in the bottom. The sand was used to absorb any molten smelt spilled during the tests to avoid damage to the heating coils of the furnace since it was both time consuming and expensive to repair the furnace. The locations of the samples within the crucibles in the pan were recorded to ensure that there would be no confusion as to which samples where which once they were removed from the oven. The pan containing the crucibles was placed into the Fisher-Scientific Isotemp Programmable Muffle Furnace located in a fume hood and the nitrogen purge system was set to $100\frac{cm^3}{\min}$ and allowed to run for one full hour before the oven was turned on and set to 1000°C. The nitrogen purge was run throughout the entirety of the experiment to keep

an oxygen-deficient environment within the furnace. The start time of the experiment was not recorded until the actual temperature inside the furnace reached the necessary 1000°C, approximately 2.5 hours. Most of the tests performed on Ufala® were then typically run for 36 hours whereas the vast majority of the tests performed on Jargal®M were run for 7 days due to Jargal®M's increased resistance to corrosion. In order to make a kinetic reaction determination, samples of Ufala® were also exposed to molten smelt for 12, 36, 72, 120, and 168 hours.

At the end of the testing period, the crucibles were removed using crucible tongs and extreme caution one at a time from the furnace. In order to ensure that the smelt within the crucibles remaining in the oven stayed in a molten phase, the furnace door was closed after each crucible was removed. The molten smelt was immediately poured out of the crucible into another stainless steel pan containing about 2" of sand, taking care not to allow the sample to fall out of the crucible along with the molten smelt. Long tweezers were used to retrieve the sample from the crucible and place it on a steel drying rack to cool, again recording the sample type in conjunction with its location. The crucibles were placed on ceramic plates to cool. Once cool, the crucibles were washed, dried, and examined for cracks to determine the viability of using them in future experiments.

4.5 Analytical Procedure

Prior to any molten smelt exposure, the coating mixtures were created for application onto the refractory materials. To determine the appropriate consistency of the solution, a viscometer was used to measure the viscosity of the mixtures. Once the samples were

removed from the molten smelt, it was necessary to perform a variety of analyses on the refractory to determine the depth and severity of corrosion and whether or not the barrier coatings tested provide a viable solution to this problem. In order to assess the level and effect of corrosion on the refractory, five different analytical techniques were used:

1) Gravimetric and Dimensional Analysis to measure weight and volume changes
2) Microhardness to ascertain the change in surface hardness due to reaction product formation
3) X-ray Diffraction (XRD) to identify the reaction products on the surface
4) Scanning Electron Microscopy (SEM) to evaluate the condition of the sample surface
5) Energy Dispersive X-Ray Spectroscopy (EDS) to determine reaction depth

4.5.1 Viscometry

To determine the viscosity of each mixture of polyvinyl alcohol and polyvinyl alcohol with metal oxide powder, the Grace Instruments M3500pH rotational viscometer was used. Once all of the equipment was turned on, it was necessary to allow the viscometer to perform a self-calibration before submerging the bob into any fluid. After the calibration was complete and the PVA was completely dissolved into solution, the sample could be loaded. The stage was lowered to access the sample holder before the mixture was poured into the cup. The sample cup was filled to the noted location, without overfilling, to obtain appropriate viscosity results. After ensuring that the sample holder was fit properly into the heating element and the heating element was correctly aligned with the stage, the stage was raised back to its original location. The Grace Instruments M3500pH software Gracedaq was used to obtain the viscosity measurements. Due to viscosity changes with temperature, it was necessary to have the same temperature setpoint of 75°F for each solution. Viscosity measurements were taken

for polyvinyl alcohol mixtures of 5.66, 6.83, 7.41, and 10 wt% without any addition of metal oxide powders. A sample at 20 wt% PVA was made, however, the solution was too viscous to obtain accurate viscosity readings. Since water evaporation could have an affect on the viscosity, the effects of allowing the mixture to be exposed to the environment uncovered for 24, 48, and 72 hours were examined. The viscosities for solutions that were maintained for 24, 48, and 72 hours in sealed containers were measured and recorded as well. Having decided on the 6.83 wt% PVA as the organic binder for the dip-coatings, metal oxide powder was added in small increments. Measurements were recorded after each addition of powder. Chromia, ceria, and 3% yttria-stabilized zirconia (YSZ) metal oxide powders were added in 1.5 gram intervals up to 15.0 grams for chromia and YSZ and up to 10.5 grams for ceria. Additional metal oxide powder was added at 5.0 gram increments up to 30.0 grams for chromia and ceria and 20.0 grams for YSZ. Powder additions and measurements were continued until the solution appeared saturated without having an extremely high viscosity. The equation for viscosity is shown in Equation 9 [66]

$$\eta = \frac{\tau}{D} \qquad (9)$$

where η is viscosity in poise, τ (shear stress) = F (force)/A (area) (dynes/cm^2) and D (shear rate) = v/x (s^{-1}). In this case v represents the velocity of the liquid and x is the liquid thickness [66].

4.5.2 Gravimetric and Dimensional Analysis

The weight, height, width, and length of all refractory samples were measured prior to and after molten smelt exposure. Since the blocks were not all uniform, their dimensions

were measured at a few different locations and the smallest value was recorded in order to ensure consistency. The weight was measured in grams to the fourth decimal place using the Mettler AE200 balance and the dimensions of the samples were measured in inches to the fourth decimal place using the Starett No. 721 digital caliper. From these measurements, it was possible to assess the volume changes and weight changes as it related to the corrosion resistance of the surface barrier coatings.

4.5.3 Microhardness

The microhardness test was performed before and after molten smelt exposure to determine the surface hardness of the refractory pieces using the Buehler hardness tester #1600-6125. The microhardness was measured three times, each on a flat portion of a different side, for every piece of refractory to calculate an average microhardness value. Using an average microhardness value gives a more accurate value than simply taking one measurement, due to the porous nature of ceramic refractory. When performing the microhardness tests, if an open pore exists under the test spot which you are testing, the microhardness reading was found to be lower than the actual microhardness of the sample. To test the unexposed pieces, 2000 grams of force (gf) were applied to a specific location for 15 seconds. This pressure left a diamond indentation on the surface in the form of a right pyramid with a square base having a 136° angle between the opposite faces. The diagonals of the diamond imprint were measured in micrometers (μm), recorded, and used to determine the surface area and subsequently the hardness of the refractory. The microhardness (HV) found using the Vickers hardness method is calculated according to Equation 10 using the test load at the time when the surface of the sample is indented when the test load is measured in Newtons [67]. To convert the test

load from kilograms of force (kgf), Equation 11 is used to calculate HV [67]. The shorter the diagonal, the higher the HV, and consequently the harder the surface of the tested sample, and vice versa. Due to fact that the refractory surface was generally softer post-exposure, the force applied to the sample was reduced to 1000gf for 15 seconds. Also, it was important to make sure that the area being tested, post-exposure, did not have any smelt remaining on the surface which could affect the reading. Upon exposure to molten smelt, the Ufala® refractory underwent severe surface deformation and it was extremely difficult and in some cases impossible to find a relatively flat location on which to measure the VHN. As such, the Vickers hardness number was not measured for any Ufala® samples.

$$HV = 0.102 \frac{F}{S} = 0.102 \frac{2F \sin \frac{\theta}{2}}{d^2} = 0.1891 \frac{F}{d^2} \qquad (10)$$

HV: Vickers hardness
F: Test load (N)
S: Surface area of indentation (mm^2)
d: Mean value of the diagonals of the indentation (mm)
θ: Angle between the opposite faces at the vertex of the diamond indenter

$$HV = \frac{F}{S} = \frac{2F \sin \frac{\theta}{2}}{d^2} = 1.854 \frac{F}{d^2} \qquad (11)$$

F: Test load (kgf)

4.5.4 X-Ray Diffraction

There are two different methods of X-ray diffraction that can be used, both of which have their advantages and disadvantages. The difference between single crystal and powder X-ray diffraction is that powder diffraction samples involve many small crystals with many different orientations versus a single crystal placed in front of the beam. Using the

single crystal method, you have the ability to record the angle and intensity of the reflections for any orientation of the sample allowing you to learn a great deal about the structure. However, there are constraints with this method such as difficulty in obtaining and orienting a single crystal, and the length of time it takes. Powder diffraction method, which was used in this experiment, is more advantageous for this application in that it takes an average over the different orientations and measures the scattered intensity so all of the reflections are guaranteed to be seen. Although, the problem is that it is more difficult to invert the measured intensities from the powder diffraction.

The x-ray diffraction patterns for solid powders have well defined diffraction lines whose spacing is related through the Bragg equation to the distance between the different crystal planes allowing determination of crystal size and chemical composition of crystalline compounds [44].

To be able to characterize the reaction products that formed on the surface of the refractory, X-ray diffraction (XRD) tests were done using the Philips APD3720 vertical goniometer in conjunction with the Philips XRG3100 X-ray generator. A modified sample holder was used to allow the entire sample to fit into the machine in a proper orientation. Pictures of the original sample holder in the X-ray diffractometer, the modified sample holder, how the sample fit into the additional sample holder, and how the modified sample holder fit into the original are shown in Figure 28. The X-ray diffractometer was connected to a computer where a program within PCAPD software version 3.6h (970115) by Philips was run that measured and recorded data at 0.010°

intervals of 2θ per second from 10° to 70°. A database containing powder diffraction files (PDF) was used to identify the diffraction peaks and determine the composition of the refractory and reaction products at the refractory surface. X'Pert HighScore Plus and PCPDFWIN computer programs were used in conjunction with the PDF files to identify the XRD peaks.

(a)

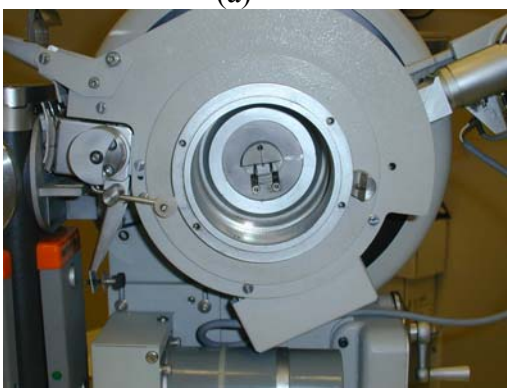

(b)

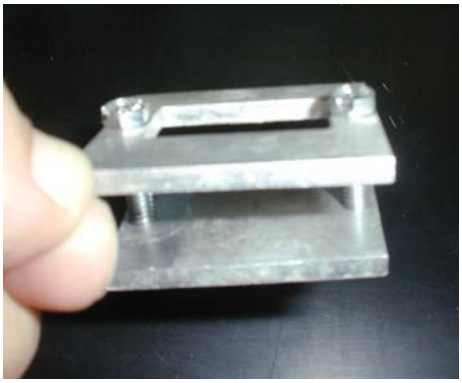

(c)

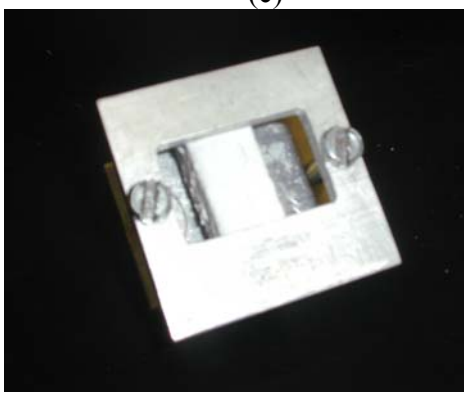

(d)

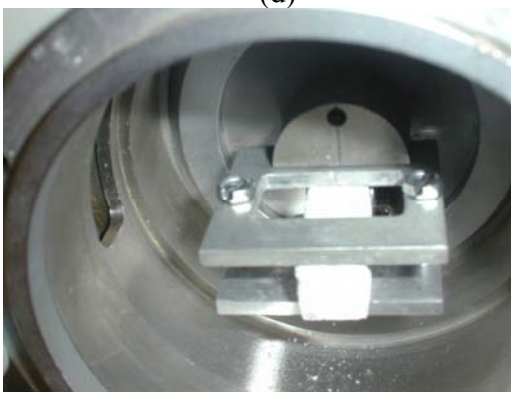

(e)

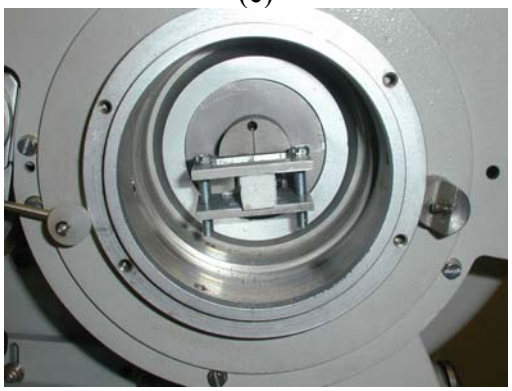

Figure 28: Pictures of the X-Ray Diffractometer (a) Original Sample Holder (b) Modified Sample Holder (c) Sample in Modified Sample Holder Independent of X-Ray Diffractometer (d) Modified Sample Holder Containing Sample in X-Ray Diffractometer (e) 2nd View of Modified Sample Holder with Sample in X-Ray Diffractometer

4.5.5 Scanning Electron Microscopy

The difference between scanning electron microscopes and conventional light microscopes is that the former uses electrons to create the magnified image whereas the latter uses the light waves with a series of glass lenses to create a magnified image. A scanning electron microscope also allows the images to be viewed in 3-dimensions at a much higher magnification then can be reached using a conventional light microscope. Due to the fact that the SEM uses electrons to magnify the image, the sample must either be made of a conductive material or coated with a thin layer of conductive material before examining the sample. Ceramics are generally not conducting materials, consequently the refractory samples had to be cut down, mounted, and coated with carbon or other conductive coatings such as gold or palladium before they can be analyzed using the scanning electron microscope (SEM). Since the reaction products on the refractory surface were water soluble, when cutting the samples using the Isomet 1000 diamond saw, kerosene was used as the cutting fluid instead of the water based Isocut Plus. This preserved the reaction products on the surface while still cooling and lubricating the diamond saw. The newly cut pieces were cleaned in the Sonicor Ultrasonic cleaner using methanol, another non-polar fluid, and dried on the drybox. Each section of the sample was then mounted on a carbon specimen mount stub using 12mm diameter double sided carbon adhesive tabs. The mounted samples were then carbon coated using the Denton DV-502A Hi-vap evaporator. The refractory samples were then analyzed using the JSM 6400 scanning microscope by JEOL. To begin the analysis, the sample was first placed into the vacuum column through an air-tight door. Once all of the air had been removed from the column via pumping, the sample was placed onto the holder where a beam of high energy electrons is released from an electron

gun at the top and sent through a series of magnetic lenses. Those magnetic lenses focus the electrons to a specific location where scanning coils near the bottom cause the focused beam to traverse the sample. Secondary electrons are knocked from the surface and x-rays are emitted when the electron beam hits the sample and jars an electron from the surface. Another electron from a higher shell then comes and fills the empty location that was left causing an x-ray to be released. X-ray is released in order to balance the energy difference between the two electrons. This can be used to determine chemical constituents in a local region with an EDS detector. A detector counts the secondary electrons that are emitted from each location on the surface of the sample by the bombardment of electrons and the signal is sent to an amplifier. The magnified image of the piece is then created using the number of electrons emitted from every spot on the sample and transmitted to the computer. Using the SEM, pictures of the surface as well as the cross section up to 1500x magnification were taken and digitized using the Geller dPict32 program on the computer.

4.5.6 Energy Dispersive X-ray Spectroscopy

After pictures were taken of the samples using the SEM, energy dispersive x-ray spectroscopy (EDS) via a line profile was used to determine the reaction depth on a sectioned sample. Using a line profile EDS enabled the comparison of elemental composition versus depth inside the exposed refractory. The EDS is a standard chemical microanalysis technique used to identify and measure elemental composition that tends to be used in tandem with scanning electron microscopy. The elemental composition of the analyzed sample volume is determined using the x-rays that are emitted from the sample during bombardment by the electrons. Since each element has a characteristic x-ray

energy, the x-ray detector from the EDS evaluates the number of x-rays that were discharged versus their energy at each point on the line. Hence, the spectrum that is formed by the EDS using a line profile has peaks for each element that provide the relative weight percent of that element found in the sample at that depth. Each spectrum that was obtained from this method was analyzed and used to determine the reaction profile on each sectioned sample. The EDS was done at low magnification to allow for the entire width of the sample to be scanned along a line from the edge of the sample towards the center using the DBSpirit program. Through the DBSpirit program 348 points were taken on each line across a time span of 300 seconds to obtain a more accurate reading. The EDS scan was used to determine the amounts (in weight percent) of sodium, aluminum, silica, sulfur, and any metal oxide used in the coating at each point in the sample. The reaction depth was identified from the location where concentration of sodium and sulfur was more than the base composition and that for aluminum was less than the unreacted layer.

Chapter 5

RESULTS AND DISCUSSION

This chapter discusses results from various experiments and analyses described in the previous chapter. The results will be divided into five sections: performance of uncoated refractory materials in molten smelt, coatings, microstructure, kinetics of refractory/smelt reaction, and surface properties. These results are intended to show the viability of using dip coatings or conventional brush coatings to slow corrosion rates of alumina-based ceramic refractory in high-temperature black liquor gasifiers. Due to the intrinsic and stark differences that exist between Ufala® and Jargal®M, the majority of the comparisons made will be done only within the same base refractory material type in order to derive more accurate correlations.

5.1 Performance of Uncoated Refractory Materials in Molten Smelt

Initial tests were carried out to understand the degradation of selected refractory materials in different smelts. Tests were performed in 99.80% pure dense α-alumina crucibles at 1000°C. The effect on refractory degradation of changing sulfidity in smelt was initially tested on only small Jargal®M block samples for seven days. The effects of increasing sulfide content on the Vickers Hardness Number (VHN), a measure of microhardness, volume, and weight on Jargal®M are shown in Figures 29-31. All raw data for microhardness, volume, and weight changes as effected by changing sulfidity, exposure time, and coating type are shown in Appendix A. The VHN measurements shown in the graph were obtained using the average of three values taken at different points on the

sample to compare microhardness changes at the surface after molten smelt exposure. Microhardness is a measure of surface hardness as measured on a microscopic scale. That ability to withstand the load is a measure of the microhardness of the sample the hardness value as given in Equation 11. As can be seen from Figure 29, all of the samples tested for microhardness experienced an extreme loss of surface hardness after exposure to molten smelt. The smallest decrease in the surface hardness was ~ 44% whereas the greatest decrease in surface hardness was nearly 75% lower compared to the unexposed Jargal®M refractory. There was no pattern to the changes in the hardness in different smelts tested. While there is no doubt that corrosion or deterioration due to reaction was occurring, the changes in surface hardness are a result of the reaction products that exist on the sample surface being less hard than the original refractory. Duplicate samples were tested to confirm reproducibility and confirm all initial test results. The original sample run at 30% sulfide was very much an anomaly and as such was not included in the results. Smelt had adhered to the surface and had to be carefully removed before measurements were taken which, in the case of the 65/30 smelt, could have resulted in the low weight reading and the subsequent inaccuracy in the measurements. The difference was immediately noticeable from a visual assessment of the sample upon removal from the crucible. Although measurements were still taken for this sample, the results were not included on graphs used to determine the effect of increasing sulfidity on refractory degradation. Pictures of the anomalous sample and a typical sample prior to exposure and upon removal from the mixture are shown in Figure 32. From the graphs below, it can be seen that there is no observable trend in the deterioration rate of Jargal®M as a function of smelt components. Using these results,

there appears to be no significant effect in changing the sulfide content in the smelt. As such, the effect of local composition changes in the molten smelt in black liquor gasifiers will not affect the performance of ceramic refractories significantly.

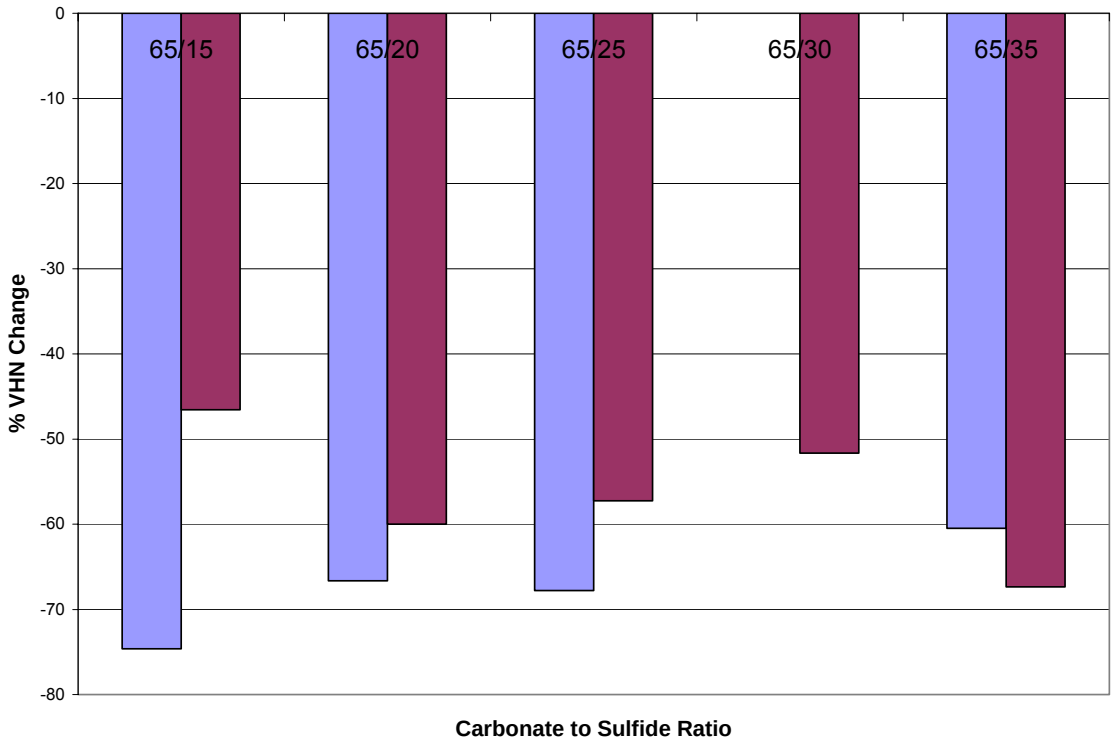

Figure 29: Results from Duplicate Jargal®M Refractory Samples Showing Changes in Microhardness Due to Exposure to Molten Smelt with Different Carbonate/Sulfide Ratios (shown in graph) at 1000°C for 7 days

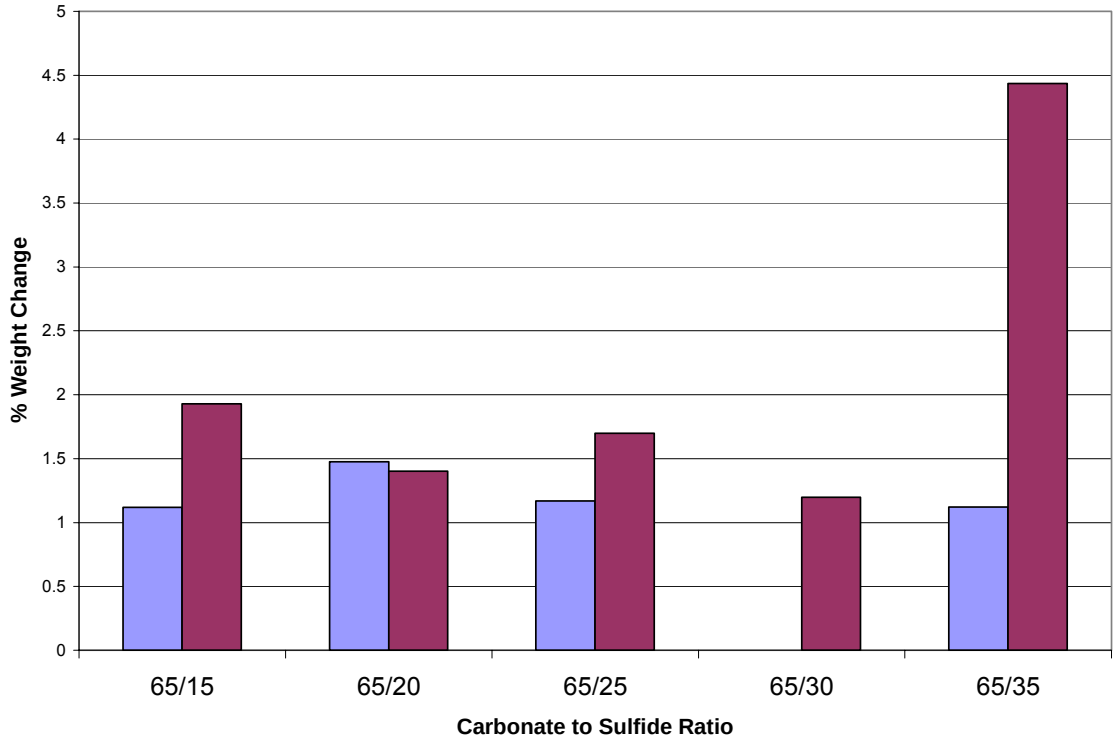

Figure 30: Results from Duplicate Jargal®M Refractory Samples Showing Changes in Weight Due to Exposure to Molten Smelt with Different Carbonate/Sulfide Ratios (shown in graph) at 1000°C for 7 days

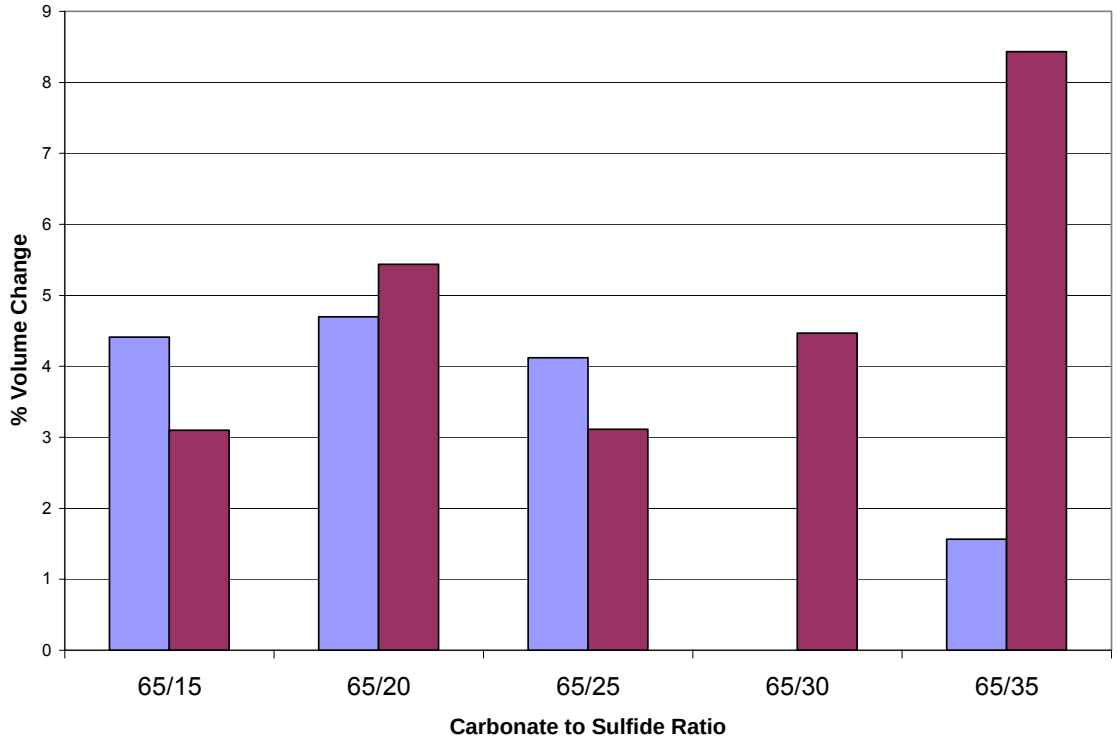

Figure 31: Results from Duplicate Jargal®M Refractory Samples Showing Changes in Volume Due to Exposure to Molten Smelt with Different Carbonate/Sulfide Ratios (shown in graph) at 1000°C for 7 days

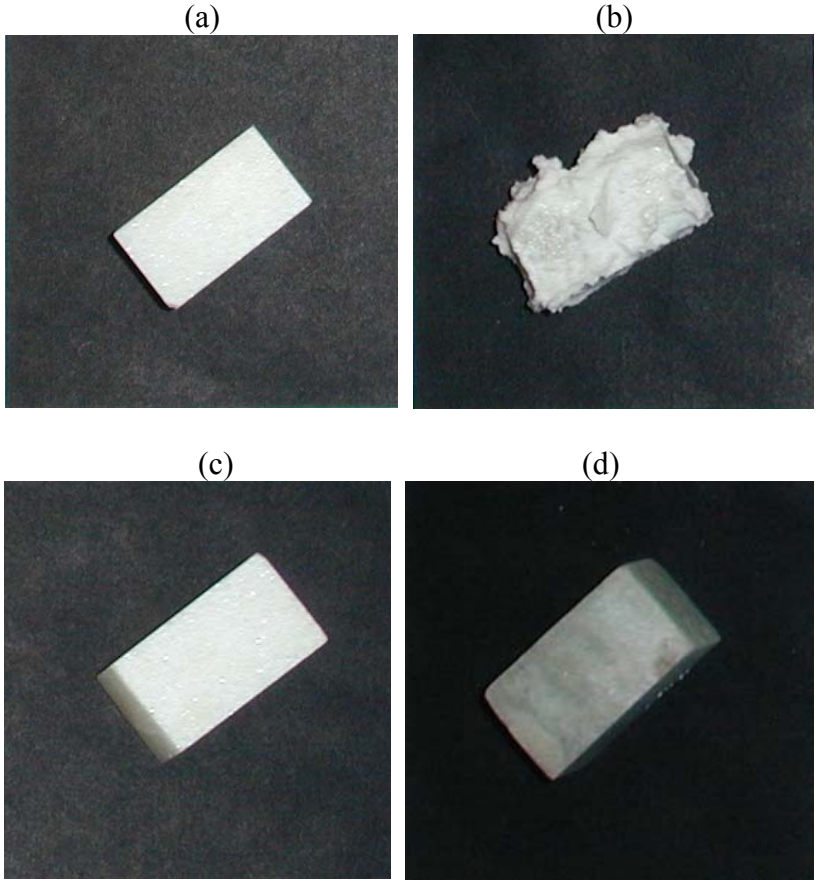

Figure 32: (a) Jargal®M Sample Before Exposure to Molten Smelt of Carbonate/Sulfide Ratio of 65/30 (b) Anomaly Jargal®M Sample After Exposure to Molten Smelt of Carbonate/Sulfide Ratio of 65/30 (c) Duplicate Jargal®M Sample Before Exposure to Molten Smelt of Carbonate/Sulfide Ratio of 65/30 (d) Typical Appearance of Jargal®M Sample After Exposure to Molten Smelt of Carbonate/Sulfide Ratio of 65/30

Although changes were seen on Jargal®M refractory after 7-day exposure to smelt at 1000°C, the changes were rather small. The Jargal®M samples were intact after molten smelt exposure without spalling. The second refractory used in this study, Ufala®, has mullite phases and contains much higher concentrations of silica than Jargal®M. Ufala® samples were tested in molten smelts with changing sulfide compositions as well. Although molten smelts are aggressive environments in the high-temperature black liquor gasifiers, the vapor phase from the molten alkali salts can also react with the refractory

material degrading its structural properties. To include the effect of corrosive vapors in the experiment and evaluate the refractory and coatings performance, long, partially submerged samples in addition to the short, completely submerged block samples were included in further tests. Consequently, two long stick samples and one short block sample of Ufala® were exposed to smelt of varying carbonate to sulfide ratios for 36 hours. After the samples were removed from the smelt and the measurements were made, the volume and weight changes (by percent) were plotted against their carbonate to sulfide ratio and compared. The graphs showing the dimensional and gravimetric changes of the Ufala® samples with changing sulfidity are shown in Figures 33 and 34, respectively. Due to the severity of the corrosion that occurs when Ufala® is exposed to molten smelt, microhardness readings cannot be easily obtained and as such are not used in the evaluation for Ufala®. X-ray diffraction was used to analyze the reaction products found on the surface of each of the samples. While not all peaks were positively identified, a summary of the XRD results for each sample are shown in Table 16. All of the samples tested showed the presence of β-alumina and sodium aluminate. The only sample on which sodium aluminum silicate was not also identified was that of the 65/30 ratio of carbonate to sulfide. Because the 4" long sticks as well as the short block samples were used to test the Ufala® refractory, it was also necessary to describe how the measurements were quantified since the entire length of the stick is not submerged in the melt. Again, their was no trend in the effect of increasing sulfidity on the formation of surface products, with β-alumina being most prevalent on the 65/20 and 65/35 samples, sodium aluminate on the 65/15 and 65/30 pieces, and sodium aluminum silicate on the 65/25. The pictures in Figure 35 help to explain the categorization of the different

segments of the stick samples. The width and depth dimensional measurements were measured at both the submerged liquid exposure end and the vapor exposure end. Scanning electron microscopy and x-ray diffraction were additionally performed on the section at the vapor/liquid interface. Because of the nature of the length measurements on the long samples, they spanned from the liquid exposure side to the vapor exposure. The gravimetric analysis was not separated into vapor exposure and liquid exposure sides for measurement. Consequently, it is expected that the percent weight change for the long stick samples would be less than the corresponding block samples but still follow the same trend. Since the corrosive effect of the vapor was less severe than that of the liquid, the vapor exposure measurements were not used in determining the effect of sulfidity on corrosion rate. The graphs shown below not only show the effect of sulfidity on corrosion rate, but the comparison between Figures 30-31 above and Figures 33-34 below confirm the previously discussed difference in corrosion resistance between Jargal®M refractory and Ufala® refractory. This observation will be discussed in more detail later.

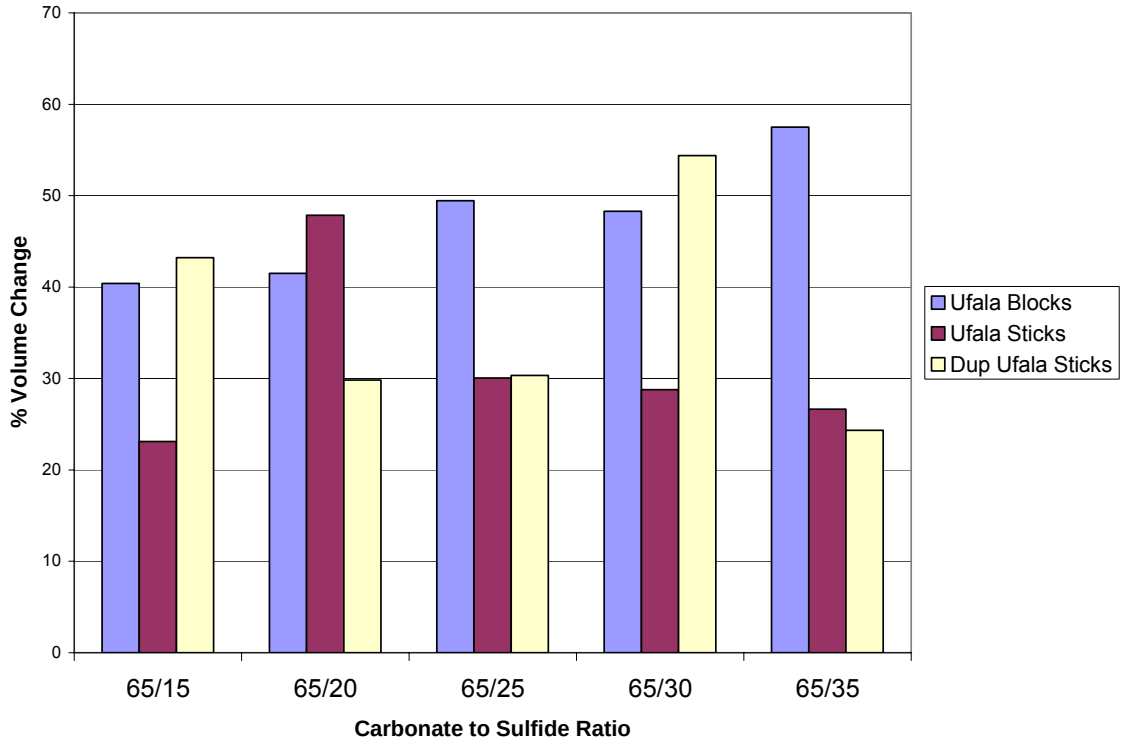

Figure 33: Results from Blocks and Duplicate Sticks of Ufala® Refractory Samples Showing Changes in Volume Due to Exposure to Molten Smelt with Different Carbonate/Sulfide Ratios (shown in graph) at 1000°C for 36 Hours

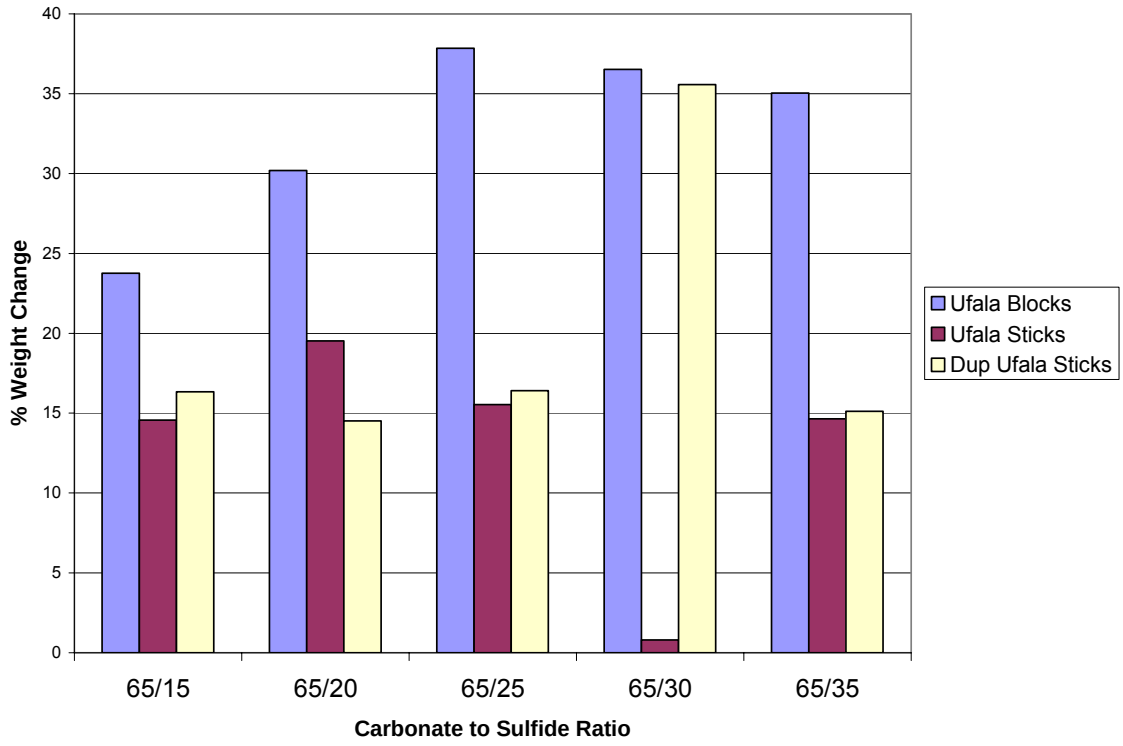

Figure 34: Results from Blocks and Duplicate Sticks of Ufala® Refractory Samples Showing Changes in Weight Due to Exposure to Molten Smelt with Different Carbonate/Sulfide Ratios (shown in graph) at 1000°C for 36 Hours

Table 16: Surface Products on Ufala® After Exposure to Molten Smelt for 36 Hours at 1000°C for Changing Sulfidity from XRD

Alkalinity/Sulfidity	Surface Products After 36-Hours Exposure
65/15	β-alumina, sodium aluminate, sodium aluminum silicate
65/20	β-alumina, sodium aluminate, sodium aluminum silicate
65/25	β-alumina, sodium aluminate, sodium aluminum silicate
65/30	β-alumina, sodium aluminate
65/35	β-alumina, sodium aluminate, sodium aluminum silicate

(a) (b)

(c)

Figure 35: Placement of Ufala® Stick Sample in Crucible for Testing (a) Length of the Stick Sample in an Empty Crucible (b) Same Stick Sample with the Unreacted Synthetic Smelt (c) Point to which Molten Smelt Submerges the Sample. The Portion of the Refractory Completely Covered by Molten Smelt After the Mixture has Liquefied will be Referred to as the Liquid Exposure (liq) End. The Segment of the Refractory at the Directly at the Vapor/Liquid Interface will be Noted as the Interface. The Remainder of the Sample Exposed to Mainly the Furnace Atmosphere and Some of the Corrosive Vapors will be Called the Vapor Exposure (vap) End

Although the gravimetric and dimensional data provide important information, the reaction depth data obtained using EDS is the most valuable. Using the reaction depth information from the EDS data, it can be established whether or not an increase in sulfide content in the smelt causes the reaction to proceed deeper into the sample. Penetration depth is also an important indicator in determining spalling. A graph showing the penetration depth as it changes with increasing sulfidity is shown in Figure 36. No pattern in the penetration depth could be found from these results. Penetration depth depends upon the probability of open porosity in a given sample, so with a limited number of samples, there is enough scatter to prevent determination of any conclusions on the effect of smelt composition on reaction depth.

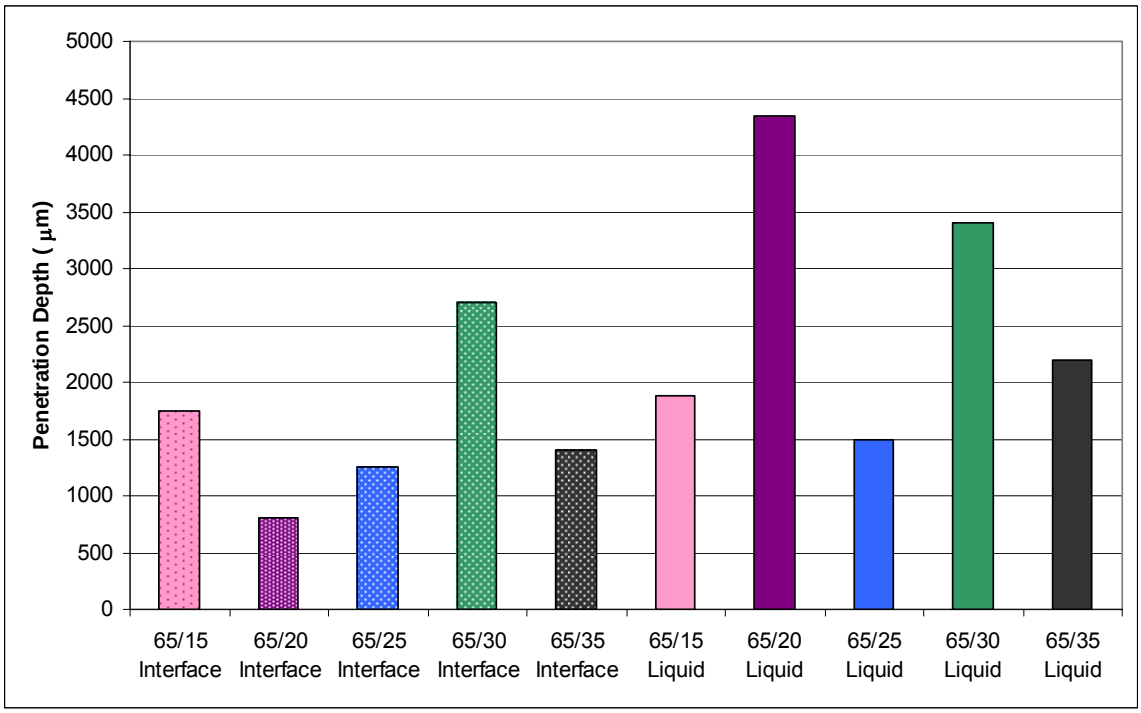

Figure 36: Results from Interface and Liquid Exposure Sections of Long Stick Samples of Ufala® Refractory Showing Changes in Penetration Depth Due to Exposure to Molten Smelt with Different Carbonate/Sulfide Ratios (shown in graph) at 1000°C for 36 Hours

The effect of sulfidity also did not show a definitive trend on the Ufala® samples. It was decided that all remaining experiments would be run using a carbonate to sulfide ratio of 65/15 because of the similarity to the environment commercial high temperature black liquor gasifiers.

5.2 Metal Oxide Coatings

The laboratory tests are performed in 99.80% pure α-alumina crucibles which exhibit little to no effects from corrosion even after exposing them to molten smelt for sometimes upwards of a hundred hours whereas the samples being tested experience some level of corrosion after only a few hours of exposure. The crucibles do not fail due to corrosion but because of cracking from thermal shock. This implies that the high purity alumina performs so well due to its high density and low porosity. Extremely high purity alumina is very expensive and not resistant to thermal shock and therefore not a feasible option for commercial installation. The use of a more thermal shock resistant base material with a dense, minimally porous surface coating would be beneficial for application in high-temperature black liquor gasifiers.

The main goal in testing different coating types and applications was to find an inexpensive and effective method of coating refractory materials that would have the ability to be applied in-situ. A surface treatment or coating that needed to be applied during fabrication was undesirable because of eventual replacement issues. It is extremely costly and undesirable to have to remove and entirely replace all of the refractory material in a high temperature black liquor gasifier. This would be the situation if the coatings are unable to be applied and cured after the refractory has been

installed which would also result in a longer down-time. Consequently, it would be preferable for the surface coating not to need a heat treatment; however, if one is necessary, it again should be limited to one that could be done in-situ. Infrared surface vitrification and coating sintering were both considered as possible treatment options, but on an industrial scale infrared treatment would be rather costly as such the use of infrared treatment was not a main focus. After infrared treatment, the coatings on the Ufala® were visibly discontinuous due to severe cracking and as such were never exposed to synthetic molten smelt. Pictures of all three samples with IR treated coatings are shown in Figure 37. To alleviate some of the thermal shock experienced by the refractory samples, and in an attempt to create viable coatings, heating the samples to moderately high temperatures to remove the organic binder and heat the sample before raising the temperature to the final curing temperature could be tried. Although costs would be increased, sintering the coatings could be an option that deserves more attention and experimentation. A potential problem with surface and/or coating sintering is similar to the trouble Jargal®M has with resistance to thermal shock due to lower porosity. Also, if the smelt were to penetrate through the sintered coating, the effects of spalling could be more severe due to larger segments spalling due to the cohesive nature of the surface.

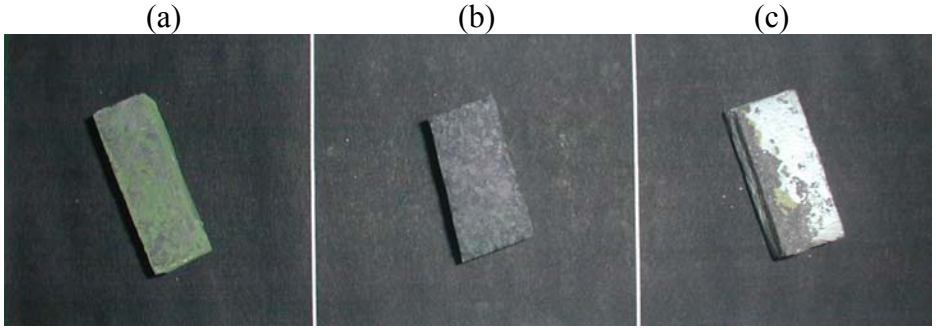

Figure 37: (a) Chromia (b) Ceria (c) YSZ Coatings After IR Treatment at 1300°C for Two Hours. The Coatings were Visibly Cracked and as such were not Exposed to Molten Smelt

Metal oxide coatings were developed through this project which will henceforth be referred to as KP coatings in this thesis. Literature research suggested that a simple and inexpensive way to apply the surface coatings was to use either a dip-coating or conventional brush coating method. Using either of these coating options would not require any new or additional equipment for the creation or application of the coatings. Because coatings cannot be applied in a solid phase, the metal oxide powders needed to be applied in liquid form using a solute that would not only be non-reactive with the base material, but one that could also be removed by simple heating and curing without disturbing the coatings. An organic binder with a low melting point, which could easily be burned off of the substrate, was used. Review of literature did not provide any information as to the viscosity or composition of the organic binder/water solution. The information that was found did however provide suggestions as to which organic binder to use. Polyvinyl alcohol seemed to be the most prevalent and as such was selected as the organic binder to be used in this experiment. Initial tests were done to first identify the consistency of the organic binder solution to which the metal oxide powder would be added. To determine to the proper composition, mixtures of the organic binder polyvinyl

alcohol (PVA) in water were made in five different ratios and the viscosities tested. The viscosity provides a measurement of the thickness of a solution which determines its flow characteristics. This information gave a good indication of the thickness of each individual layer applied to the substrate. If the solution consisting of only the organic binder and water is too viscous, the applied coatings may be too thick. The same logic holds that if the mixture is not viscous enough, it may not adhere well enough to the surface making the coating layer too thin. Temperature has a significant effect on the viscosity of a solution. To quantify this, a series of experiments were performed before any other viscosity tests were run. The viscosity was constantly measured as the mixture cooled from 140°F to 80°F. The results of changing viscosity with temperature of a 6.83 wt% PVA are shown in Figure 38. There is a decrease in viscosity with increasing temperature so it is extremely important for the viscosity measurements to be taken at the same temperature. These results can be used to change the viscosity of coating mixtures for laboratory or commercial applications.

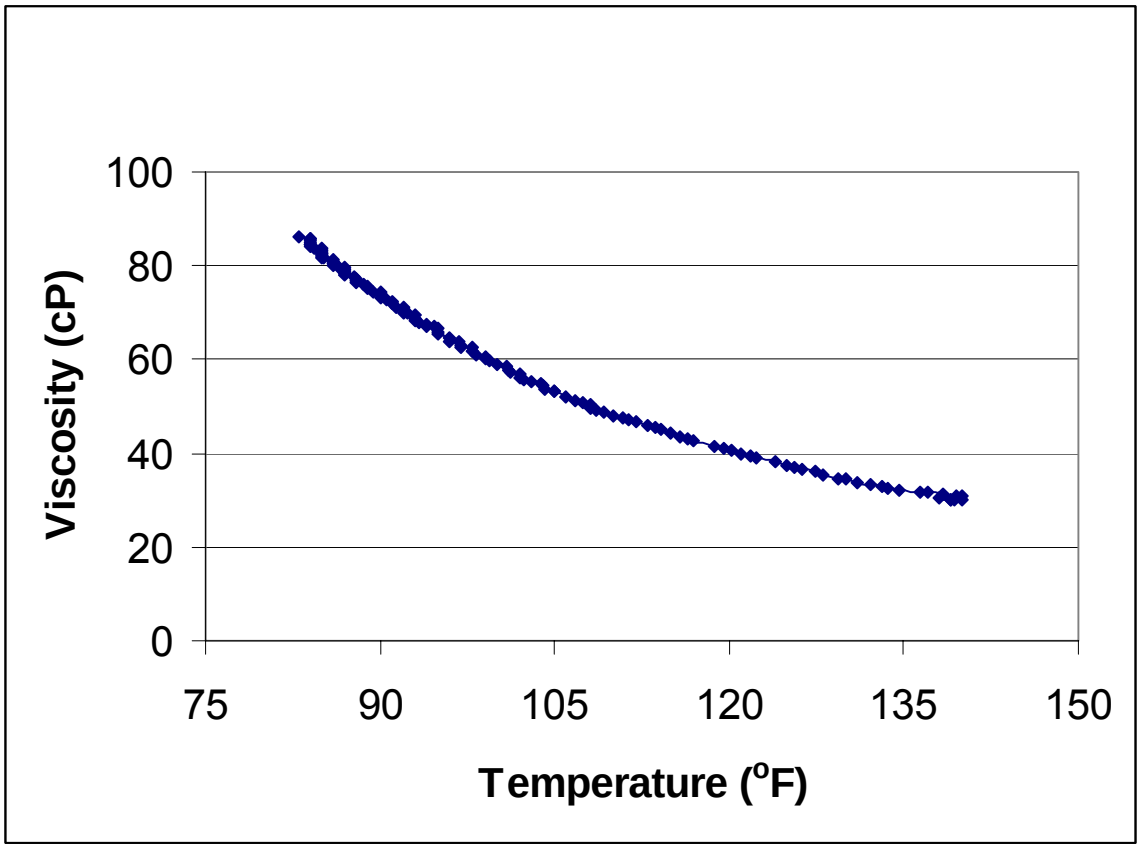

Figure 38: Results Showing the Effect of Temperature on Viscosity for a 6.83 wt% PVA in Water Solution from 80-140°F

Beginning with a 20 wt% PVA mixture, it was not only visually obvious that the solution was too viscous, but that observation was confirmed after attempting to determine the viscosity. Because of the thickness of the solution, the bob from the viscometer had a very difficult time rotating and was consequently stopped before any significant measurements were obtained. All of the graphs showing the viscosity results are shown in Appendix B. Figure 39 shows a graph of the viscosity measurements for each PVA mixture over time.

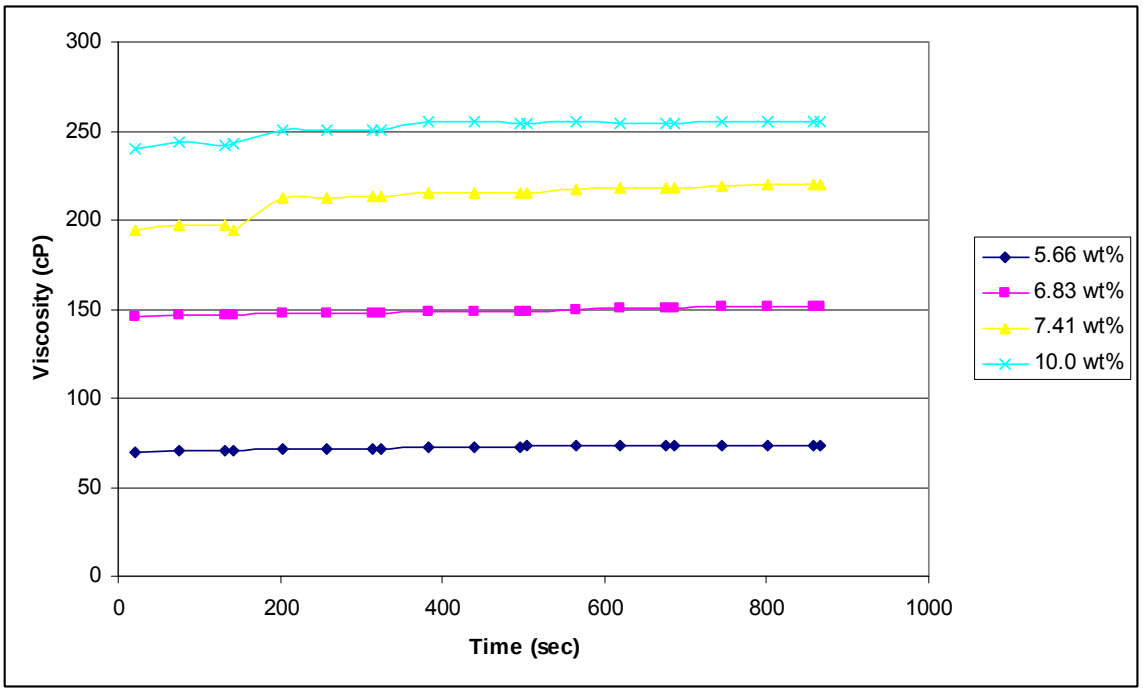

Figure 39: Viscosity Results of Each Mixture of Different Composition of PVA with Water Having No Metal Oxide Powder Added

As expected, the viscosity of the mixture increased with greater amounts of PVA in solution. Upon a combination of visual assessment after dip-coating one refractory sample with the each of the PVA mixtures and analysis of the viscosity data, it was decided that 6.83 wt% PVA would be the base solution for the coatings. This composition allowed for any thickening incurred by the addition of the metal oxide powders before becoming too viscous. To determine if coating mixtures would have to be made fresh each time coatings were to be applied, the effect of time on the PVA and water mixtures in open and completely sealed containers on viscosity was monitored. The viscosity of the solutions was initially recorded and the mixture was then left for 24 hours either uncovered or in a sealed container. The viscosity results for the mixture left open to the atmosphere are shown in Figure 40 and those for the mixture in a sealed container are shown in Figure 41. Data shows that, with an open container, the PVA and

water mixture increases by approximately 50% whereas for a sealed container the viscosity changes were not significant over a 24 hour time period. The minimal viscosity changes seen by the PVA in water mixture in a sealed container enable continued use of the same solution as long at it is kept sealed.

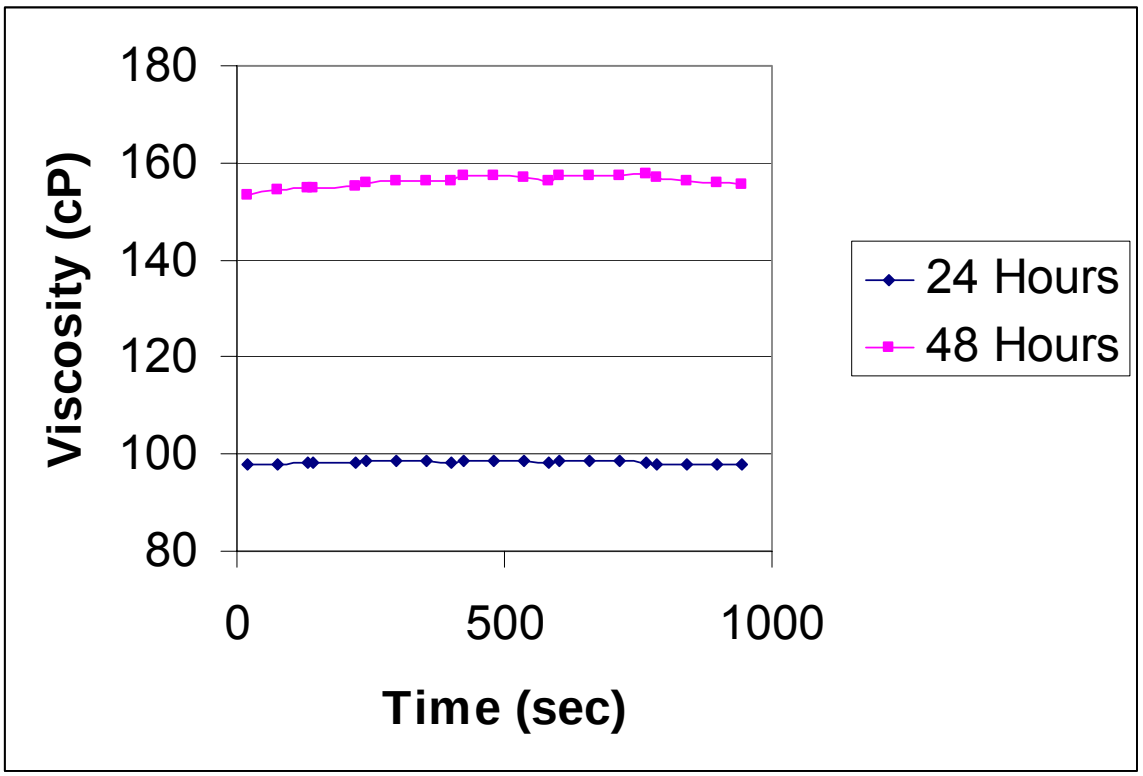

Figure 40: Graph of Viscosity Data of 5.66 wt% PVA in Water Mixture at 73°C After 24 and 48 Hours of Being Exposed to the Open Atmosphere

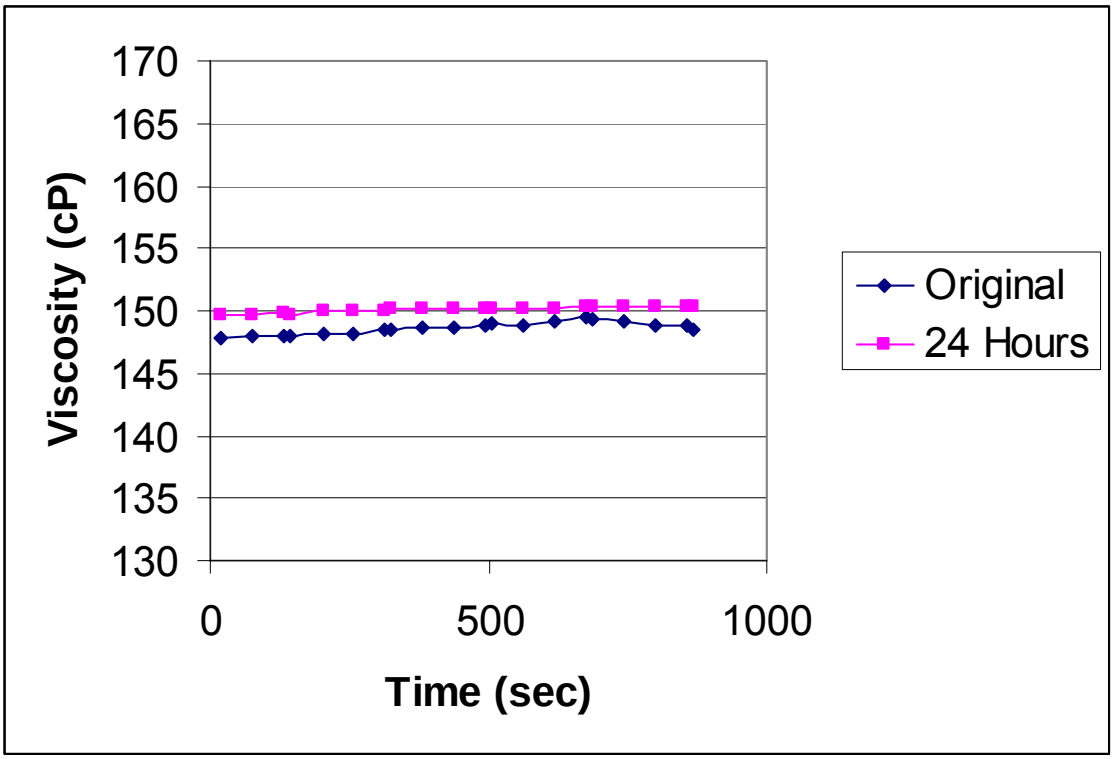

Figure 41: Graph of Viscosity Data at 76°C of 6.83 wt% PVA in Water Immediately After Preparation and After 24 Hours in a Sealed Container

Multiple methods of coating application were tried in an attempt to determine the best way to apply the metal oxide coating to the substrate. Tweezers were originally used to remove the refractory from the slurry, but once the sample was removed the options for drying were either to allow the sample to remain in the tweezers or to set it into a drybox. Either option caused the PVA to dry on the sample and stick to the drying apparatus as well. Upon separation, these coatings had large voids or inconsistencies which would render it essentially useless. Thin wire was tried by wrapping it around one end of the refractory sample, dipping it into the slurry, and slowly withdrawing the sample. The end of the wire that was not in contact with the sample was used to hang the samples while they dried. Due to gravity and the fluid nature of the coatings, the solution would flow to the lower end of the sample causing a large mass of material at the end and the coating

layer to be uneven. In another attempt, the same technique was used, however, upon removal from the bulk coating, an additional piece of thin wire was used to cradle the opposite end of the sample in the hopes that a more level surface would cause the solution to remain in place long enough to dry. Although the problem of uneven coating thickness was slightly relieved, once the coating had dried and the wire needed to be removed, the problem of separation from the substrate and well as inconsistencies arose. It became obvious that if the dip-coating method was to work, an apparatus that would hold the samples in place while only making contact in a small area and rotating the sample would be needed. Wanting to keep the application method as simple as possible, the conventional brushing method was examined as a possibility. The uncoated substrates were placed on the drybox rack such that one of the four longer sides was laying flat on the rack. At this time the drying fan was in the off position. Only the top surface of each material sample was coated before the drybox fan was started and allowed to run until the coatings had solidified. Each piece was then rotated so that an uncoated side adjacent to the recently coated one was now the top surface. Again, those surfaces were coated, allowed to dry, and rotated until four of the six sides were coated. The sample was then turned 90° such that one of the two shorter sides was laying flat on the rack. The same procedure was then used to coat both remaining ends of the material. Although it required a slightly longer period of time to apply and dry the coatings, those coatings that were applied using this process were continuous and much more uniform then those applied using the other techniques. In industrial application, either a brush or spray coating applicator could be used to achieve similar results.

Once the binder composition and application method were determined, the metal oxide powders were added incrementally and their viscosities were monitored. A graph of the viscosity with respect to time is shown in Figure 42 for each amount of CeO_2 powder added to the PVA mixture. The trend shows that an increase in the amount of metal oxide causes the solution to thicken. At higher metal oxide contents, the initial viscosity readings are inconsistent with the average reading. This could be caused by a lapse in time between when the bob begins to rotate and when it actually gets up to speed in the more viscous solutions. Enough powder needed to be added to the solution to ensure that once the organic binder was burned off during curing or sample exposure, a continuous layer of metal oxide powder remained as the coating. The main objective was to close open porosity in ceramic refractory and add a barrier coating to slow down molten smelt reaction with the base refractory. The addition of powder continued until there was enough metal oxide powder in the PVA solution for it to be saturated but before the coating became too thick. Even after the addition of the maximum amount of metal oxide powder, it was important that the viscosity still be low enough for an appropriate coating thickness. The amount of metal oxide powder within the solution was found to be important for the coating integrity. Coated samples were then cured at 500°C. During curing, the PVA burns off leaving only the metal oxide on the surface so if the coating slurry contained an insufficient amount of metal oxide powder, there would be voids and cracks in the coating. The other potential problem with the curing process was that while the binder was being evaporated, the possibility for the top layer of the coating to dry quickly causing the remaining PVA to crack the coating in order for gases to escape into the furnace atmosphere existed.

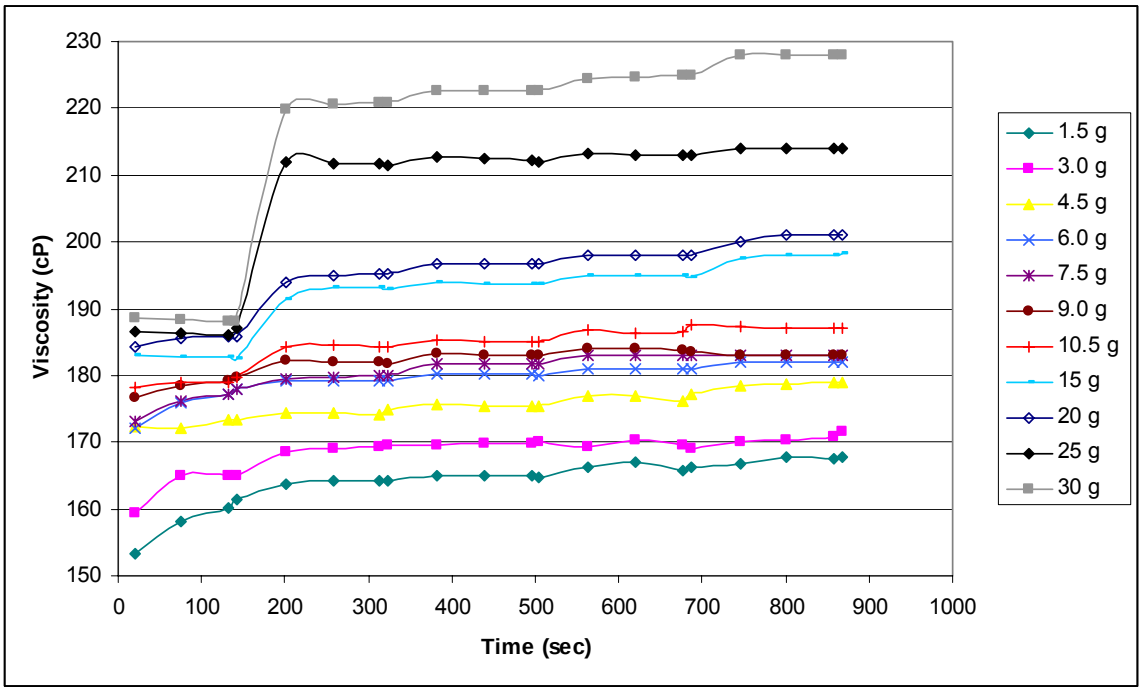

Figure 42: Results for Viscosity Changes Experienced by PVA with Water Mixture upon Addition of Ceria (CeO_2) Powder at 73°F

To remove the organic binder, the coated samples were cured for 30 minutes at 500°C. After curing and testing a number of coated samples, samples that had not been cured were also tested to determine if the uncured oxide coatings were able to better withstand the corrosive environment. The results comparing the cured and uncured coatings are shown in later sections.

The coatings applied by C^3™ International were applied using a patented process in which the coatings form a molecular bond several layers deep into the substrate. These industrial applied coatings are also applied in a specifically prepared liquid formula and heated to create the infusion and bonding reaction. Much like the KP coatings, either a traditional furnace or infrared (IR) light could be used to cure the coatings. It is claimed

that the coating penetration depth is 200-1000 angstroms into the substrate. Line-of-sight and dimensional issues are not problematic when using this technique. Due to the fact that the coatings applied by C^3™ are done via a dip-coating method, the costs for the industrially applied coatings are relatively low as well.

To ensure that the coating material was present on the refractory surface, x-ray diffraction (XRD) and energy dispersive x-ray spectroscopy (EDS) were performed on the C^3™ samples as well as on the cured and uncured KP samples prior to molten smelt exposure. The patterns obtained from XRD were compared with powder diffraction files to identify specific peaks. Each of the pure metal oxide powders used in the coatings was tested before being applied to the samples as well. The XRD graphs obtained from the pure powders were also used to help prove the existence of the metal oxide coatings on the refractory surface after coating. All of the XRD plots are shown in Appendix C. The results from all of the XRD and EDS experiments confirmed the existence of the selected coating materials. The main surface components identified were the desired metal oxides from the coatings and β-alumina. The KP uncured YSZ showed a small amount of α-alumina and the KP uncured chromia sample showed α-alumina as well as a minor amount of sodium aluminate prior to exposure.

5.3 Microstructure

Two different types of refractory base materials, Jargal®M and Ufala®, were used during testing throughout this study. The selected refractory materials have very different chemical composition and physical properties. Ufala® refractory is a mixture of alumina, silica, iron oxide, and other impurities whose microstructure contains different

phases. The apparent porosity of Ufala® is also much greater at 14.7% than that of the fused-cast alumina refractory, Jargal®M, providing much larger and easier pathways for molten smelt penetration into the material. As evidenced by Figure 43, a collection of scanning electron microscope pictures of Ufala®, there are both macropores and micropores on the surface of Ufala®. There is a stark contrast between the macrostructure and microstructure of the Jargal®M and Ufala® refractories. In comparison to the Ufala® material, the Jargal®M samples had a very uniform microstructure showing the presence of one phase. Micrographs of Jargal®M taken with the SEM are shown in Figure 44. The micrographs in Figure 44 show that even at a magnification of 500x, the surface of the Jargal®M sample was homogeneous. The Jargal®M was also lacking presence of macropores, however, micropores were visible at higher magnification.

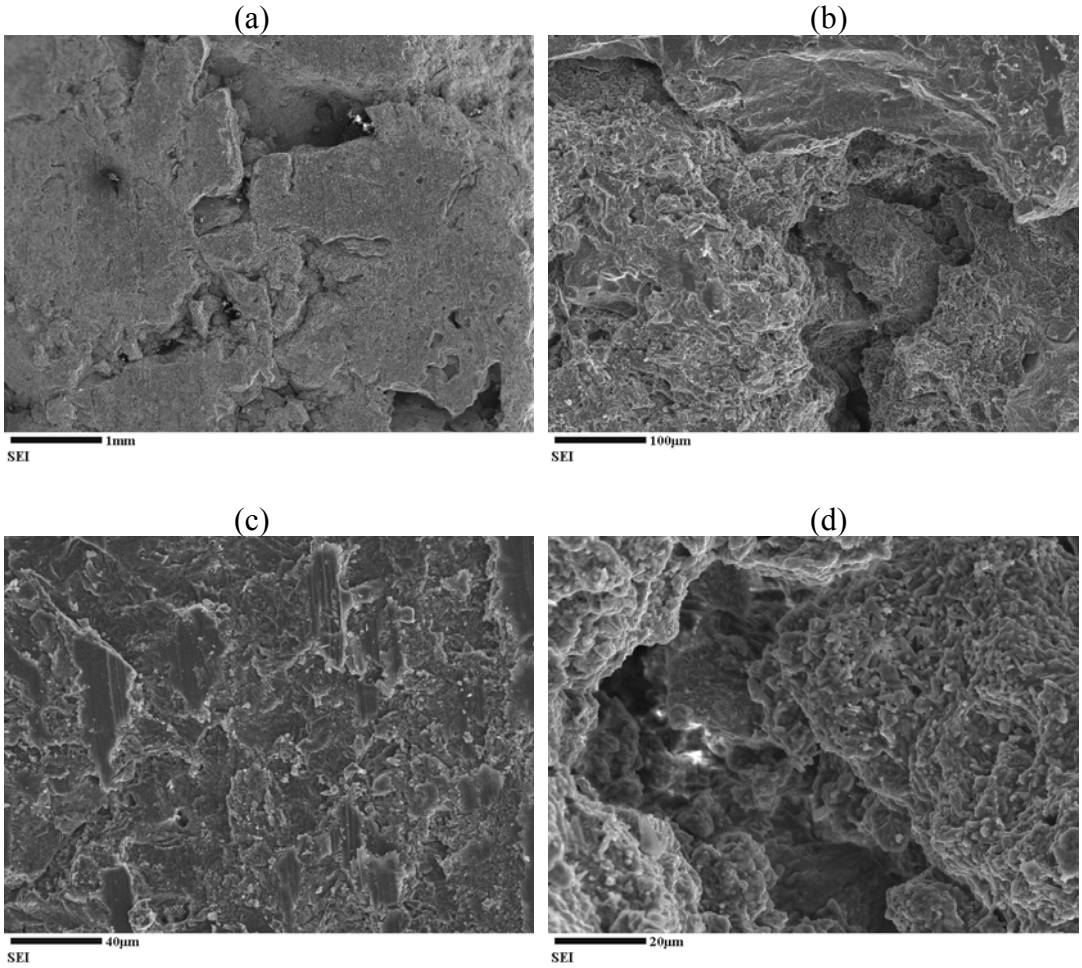

Figure 43: SEM Micrographs of Ufala® at (a) 20x (b) 200x (c) 500x and (d) 1000x Magnification

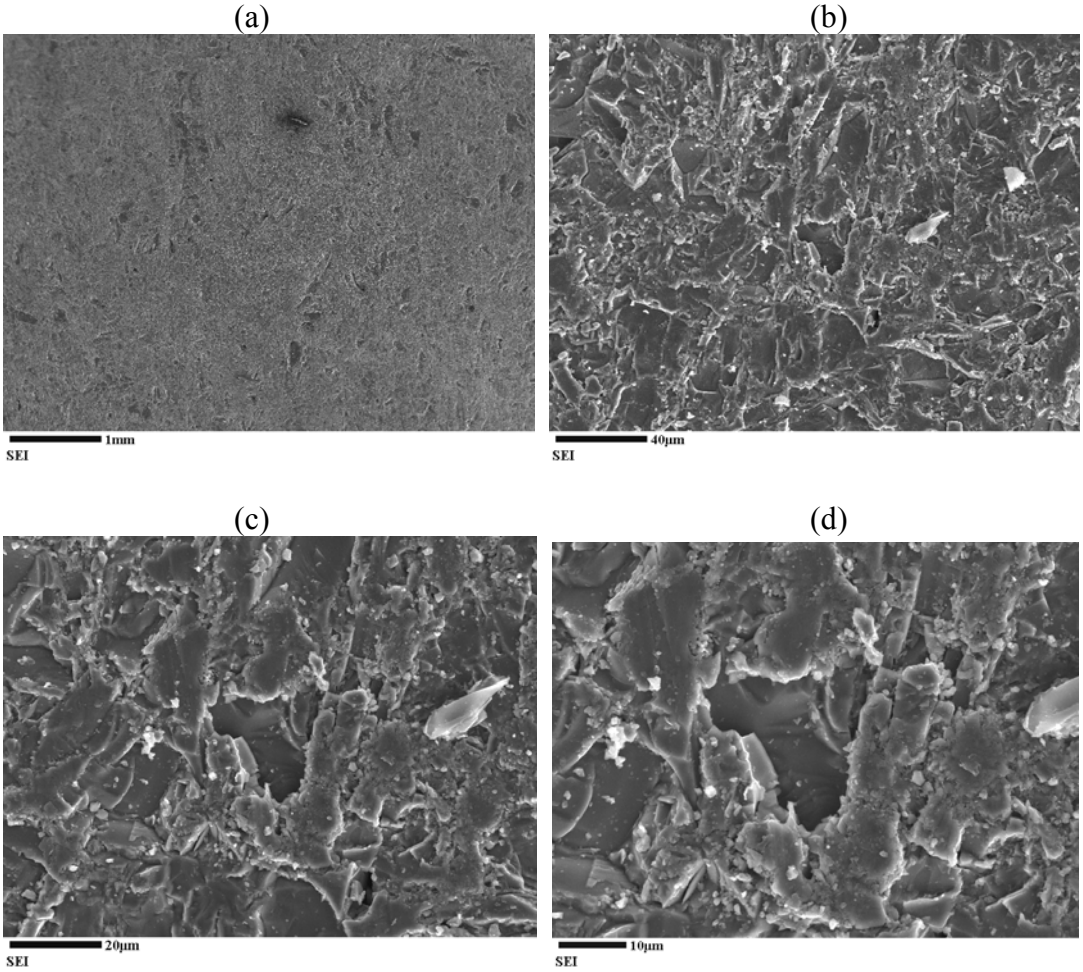

Figure 44: SEM Micrographs of Jargal®M at (a) 20x (b) 500x (c) 1000x and (d) 1500x Magnification

There are advantages and disadvantages to both types of refractory material in not only industrial applications. High porosity materials have much better resistance to thermal shock because the null space within the material allows for internal expansion without spalling unlike high-purity fused-cast alumina refractory such as Jargal®M. Also, the heat insulation properties of the refractory are enhanced with increasing porosity [58]. The converse of that however, is Ufala® is significantly more susceptible to corrosion due to that porosity. While Jargal®M is more resistant to corrosion, and as such performs much better uncoated than the lower purity Ufala® in service, it is less resistant

to thermal shock because of decreased porosity and consequently less void space within the sample. More porous, multi-phase (less pure) refractories such as Ufala® are also significantly less expensive then high purity refractory material. One of the goals of this project was to determine if one or more of the surface coatings would provide a corrosion resistant barrier between the molten smelt and the base refractory. The Ufala® was selected as the base refractory material for coating evaluation because of its low cost as well as the fact that volume increase and refractory degradation occurred upon shorter exposure and were apparent. This also made gravimetric and dimensional changes possible to study the effectiveness of coatings. Hence, if it is feasible to inexpensively modify the surface of the Ufala® in-situ and have results that are comparatively good with respect to corresponding results using Jargal®M, installation of Ufala® would considerably lower the capital costs of the gasifier. This is especially true because untreated Jargal®M does not perform particularly well in high temperature black liquor gasification environments and as such could also use a protective barrier coating applied to improve performance. Under the hypothesis that the reduction or elimination of pores on the refractory surface would decrease the rate of deterioration and effects of corrosion, the main goal of the coatings was to block the surface porosity to slow the penetration of molten smelt into the refractory.

5.4 Kinetics of Refractory/Smelt Reaction

Before exposing any coated pieces of refractory to the molten smelt, it was desirable to determine the effect of exposure time on the Ufala® samples. A Ufala® stick and block sample were tested at each different time interval and their weight and volume change, surface products, and reaction depth were recorded and analyzed. Figures 45 and 46

show the volume and weight change experienced by the samples after each time period. The volume and weight data from the Ufala® refractory samples exposed for 72, 120, and 168 hours is also plotted in Figure 47. A linear trendline for each set of points was added along with the corresponding R^2 value to show how well each trendline fit the given data. The linear trendline in each case fit to better than 99% showing that kinetics of the reaction were linear. As the reaction is allowed to proceed for longer periods of time, there should be a marked increase in the amount of sodium aluminate in the sample after exposure. The physical changes that take place upon molten smelt exposure indicate the occurrence of reactions with sodium oxide to convert α-alumina (Al_2O_3) and β-alumina (Na_2O x $11Al_2O_3$) into β'-alumina (Na_2O x $6Al_2O_3$) and sodium aluminate ($NaAlO_2$) via the reaction pathways shown below [38].

$$Na_2CO_3 + 11Al_2O_3 \rightarrow (Na_2O \times 11Al_2O_3) + CO_2 \quad (6)$$

$$5Na_2CO_3 + 6(Na_2O \times 11Al_2O_3) \rightarrow 11(Na_2O \times 6Al_2O_3) + 5CO_2 \quad (7)$$

$$5Na_2CO_3 + (Na_2O \times 6Al_2O_3) \rightarrow 12NaAlO_2 + 5CO_2 \quad (8)$$

Figures 19 and 21, as shown in a previous section, give phase diagrams of Na_2O-Al_2O_3 and Na_2O-Al_2O_3-SiO_2, respectively which also shows the changes that alumina and silica experience upon reaction with soda. The information obtained from the phase diagrams confirms the reactions of Na_2O with Al_2O_3 and SiO_2. Increasing the amount of sodium that is in the mixture decreases the purity of alumina changing it from corundum or mullite to compounds containing more sodium such as β-alumina, albite, carnegieite, nephaline, and, with a high enough percentage of sodium, sodium aluminate.

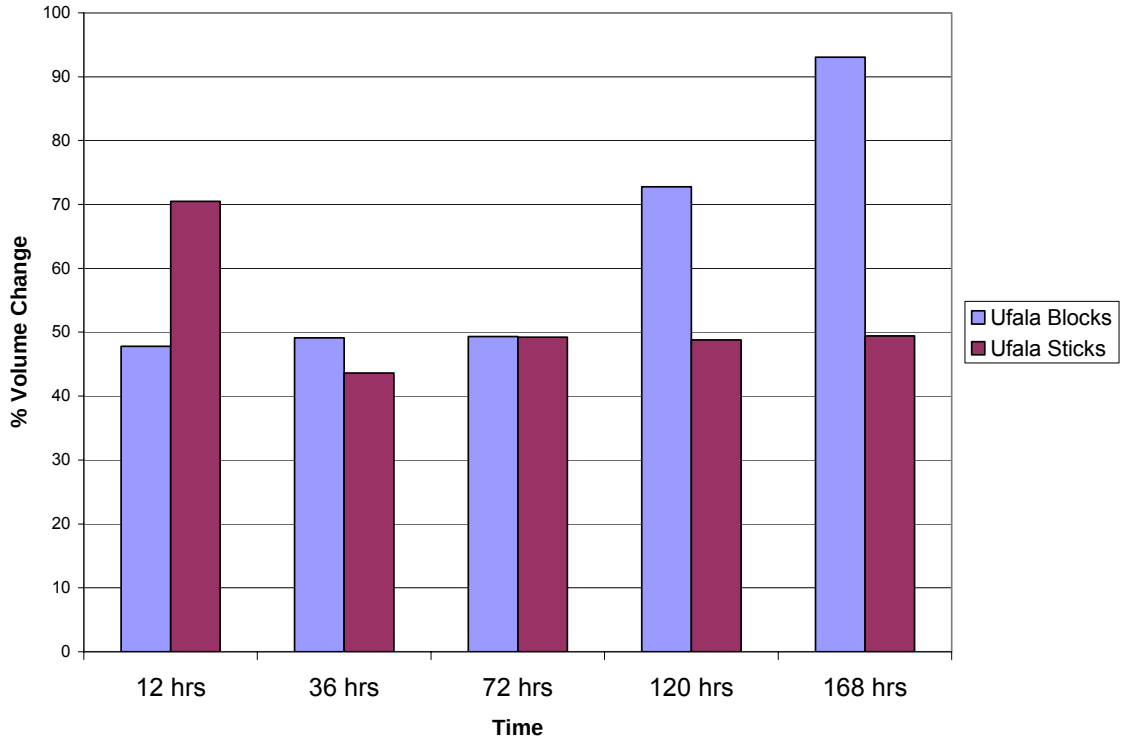

Figure 45: Results for Ufala® Refractory Samples Showing Changes in Volume Due to Exposure to Molten Smelt for Varying Time Periods (shown in graph) at 1000°C

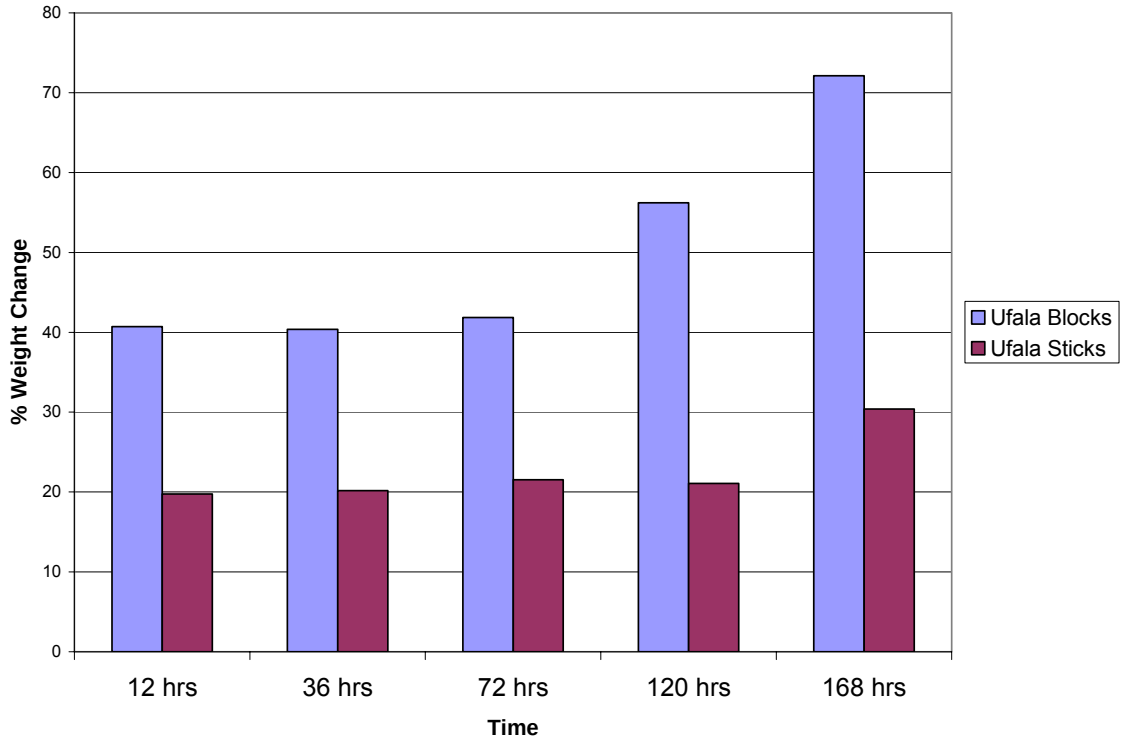

Figure 46: Results for Ufala® Refractory Samples Showing Changes in Weight Due to Exposure to Molten Smelt for Varying Time Periods (shown in graph) at 1000°C

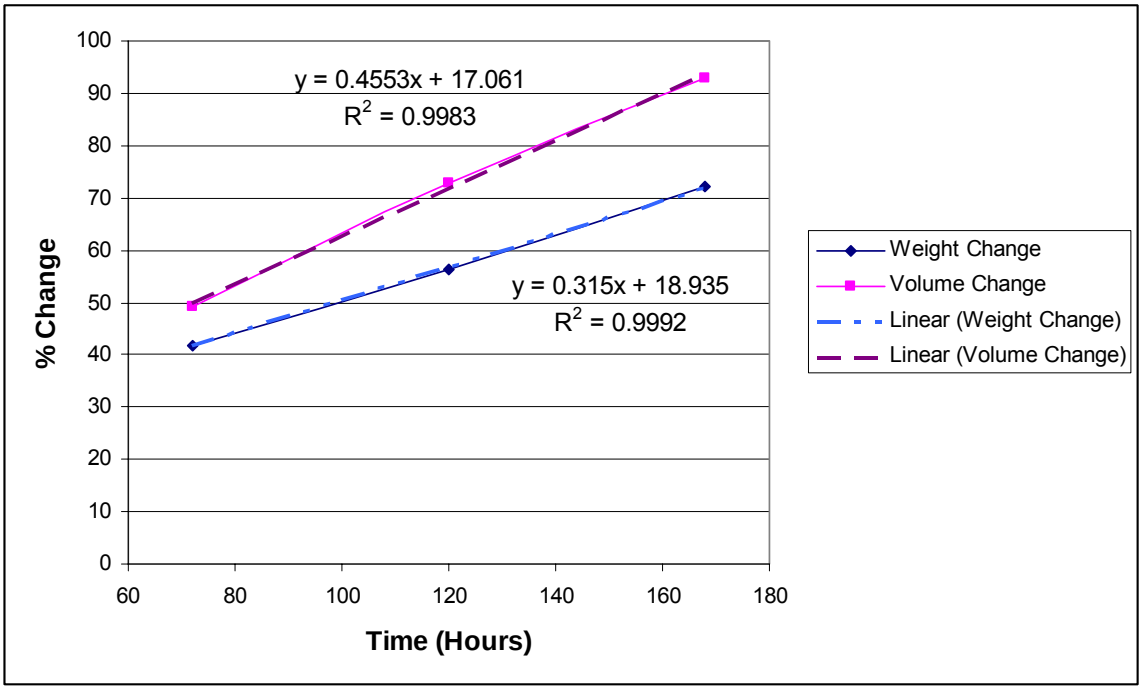

Figure 47: Results for Ufala® Refractory Samples Showing Changes in Volume and Weight Due to Exposure to Molten Smelt for Varying Time Periods (from 72-168 hours as shown in graph) at 1000°C. A Linear Trendline has been added to Show the Adherence of the Results to a Linear Relationship.

With the size of sodium aluminate being substantially larger (~133%) than the reactants in this situation, there should be a consistent increase in volume and weight changes of the samples. The trend of the results supports the theory that the samples will continue to increase in size until the entire sample has been converted to sodium aluminate if exposed for a long enough period of time. While none of the samples tested experienced a volume increase as large as 133%, the Ufala® block sample exposed for 168 hours had a more than 90% increase in volume and more than 70% increase in weight showing a significant shift towards sodium aluminate or sodium aluminum silicate. There were even sizable cracks visible on the 168-hours exposed Ufala® samples, as shown in Figure 49, attesting to the extremely corrosive nature of molten smelt and the notable volume increase experienced by the samples.

Figure 48: A Ufala® (a) Block and (b) Long Stick Sample Showing Cracks Down the Length of the Sample Due to Volume Expansion After Being Exposed to Molten Smelt for 168 Hours at 1000°C

Upon examination of volume and weight changes, the reaction proceeds at an approximately linear rate with increasing exposure time, especially if the focus is only on the 72, 120, and 168 hour short block samples. With the constant reaction rate, it could then be said that there is no formation of protective scales to slow the corrosion rate that occurs during the reaction between the refractory material and the molten smelt. Also, any pore closing effect that may be caused by the volume increase of the refractory is of no help and corrosion is able to continue unimpeded. As such, the corrosion mechanism that occurs should progressively degrade the material until, if allowed to proceed for a long enough duration, presumably no refractory material would remain.

This shift towards sodium aluminate and sodium aluminum silicate was confirmed using X-ray diffraction data. A summary of the surface products found after each time of exposure is shown in Table 17. From analysis of the XRD graphs it could be seen that after the 12-hour exposure period there was still a marginal amount of α-alumina able to be identified on the surface with the majority of the peaks being β-alumina. No a-alumina peaks were found on the 36-hour exposure graphs, with β-alumina still present and an increasing amount of sodium aluminate and sodium aluminum silicate. By the end of the 168-hour exposure the main products on the surface were sodium aluminate and sodium aluminum silicate with only a scant few peaks identifying β-alumina. This confirms the shift towards sodium aluminate thought to occur via the reaction pathways previously shown.

Table 17: Surface Products on Ufala® from XRD for Different Exposure Times to Molten Smelt at 1000°C

Time	Surface Products After Exposure
12 hr	α-alumina, β-alumina, sodium aluminate, sodium aluminum silicate
36 hr	β-alumina, sodium aluminate, sodium aluminum silicate
72 hr	β-alumina, sodium aluminate, sodium aluminum silicate
120 hr	β-alumina, sodium aluminate, sodium aluminum silicate
168 hr	β-alumina, sodium aluminate, sodium aluminum silicate

At this point, the effect of spalling that occurs on the refractory material and its effects on the gravimetric and dimensional information that was obtained must be considered. The weight and volume (or thickness) changes can be used in a determination of the amount of spalling that occurred. If desired, the thickness change can be calculated by simply taking the cube root of the volume change. Because spalling can cause layers of the refractory to completely corrode or separate from the surface, it can be difficult to determine the actual amount of refractory material lost to spalling and the amount of that volume loss that is being negated by product growth. This is especially true because the internal volume increase is one of the main factors behind spalling.

The graph in Figure 49 shows the penetration depth for each segment of the Ufala® samples as measured at each time exposure. All three of the areas of refractory stick

sample, liquid exposure, interface, and vapor exposure, exhibit scatter in their penetration depth data. The scatter that occurred in the penetration depth data for the liquid phase end of the sample matched the weight and volume trends experienced by the long stick samples. This trend is, however, different from the assessment of the block samples that was made from the volume and weight data which essentially showed a consistent increase in volume and weight with increasing time. Because spalling is a factor that must be considered in high temperature black liquor gasifiers, it is probable that the scatter is being caused by spallation and differences in surface porosity from sample to sample. Because of the direct contact with the molten smelt, the liquid exposure surface should spall more quickly then either of the other two sections. Immediately after spalling, the penetration depth would appear less due to the loss of a layer of surface material. It is difficult to accurately account for the loss of that material in this comparison because of corresponding volume increase.

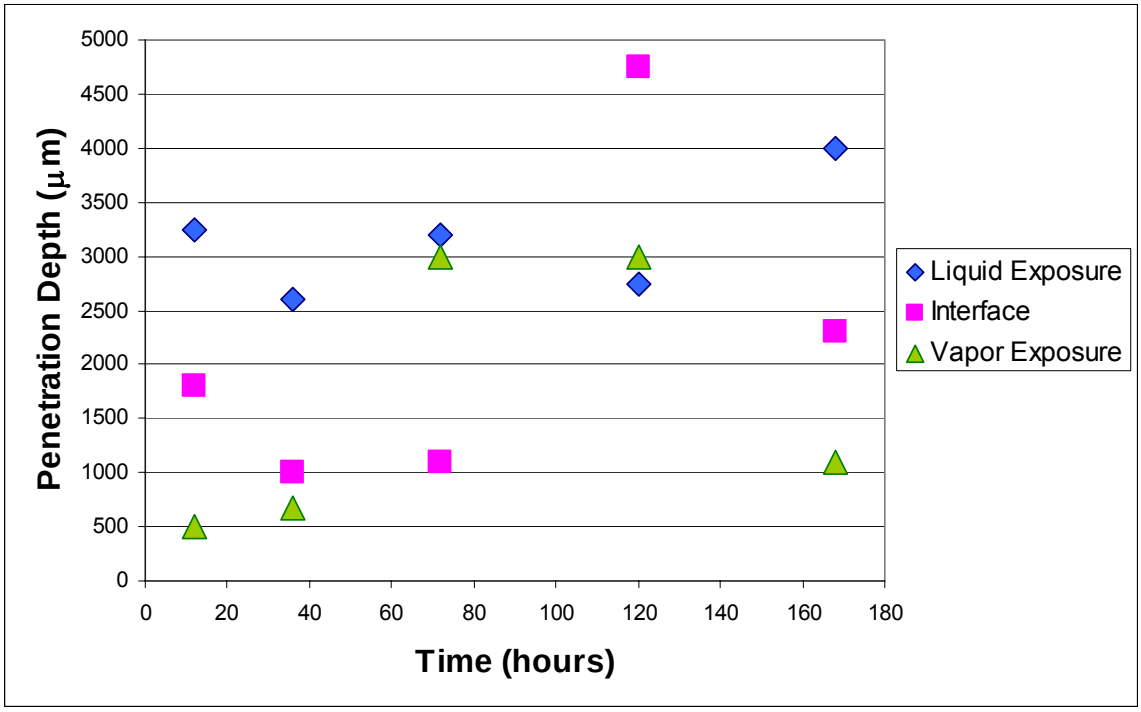

Figure 49: Results for Ufala® Refractory Samples Showing Changes in Penetration Depth Due to Exposure to Molten Smelt for Varying Amounts of Time (shown in graph) at 1000°C

Once all of the measurements and data were obtained for the uncoated samples of both refractories, Figures 50 and 51 were plotted to provide a comparison of the percentage weight and volume change, respectively, that occurred after 7 days for uncoated Jargal®M and Ufala® small block and long stick samples. This not only confirms the obvious difference in quality as measured by corrosion resistance between the two types of refractories, but it also provides a good baseline since the volume changes that occur at the vapor exposure end of the long stick samples should be minimal and this information, therefore, provides an approximation of the experimental error in the dimensional measurements. The average weight change of the uncoated Ufala® after being exposed for seven days was almost 67% for block samples and upwards of 26% for stick samples. The average volume change of Ufala® was nearly 87% for the block samples and more

than 46% for the stick samples. None of the Jargal®M samples that were exposed for same period of time had a volume increase of more than 2% or a weight gain of greater than 7% proving that the uncoated Jargal®M refractory material has better corrosion resistance than uncoated Ufala®.

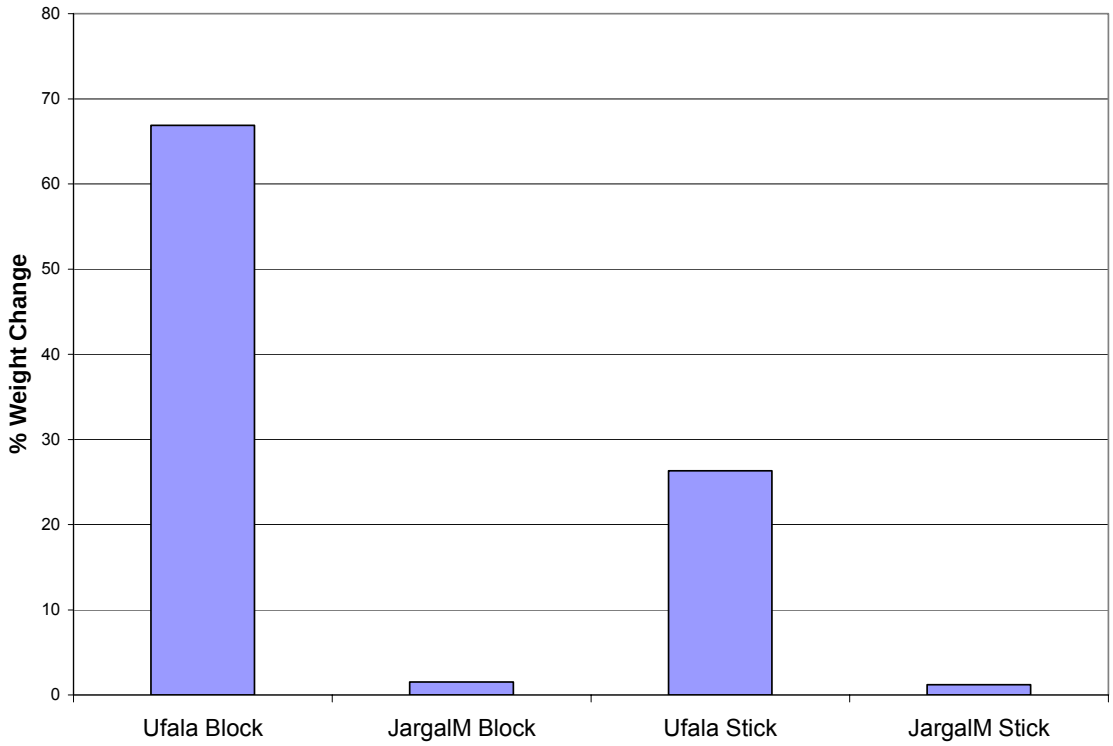

Figure 50: Results for Exposed Uncoated Ufala® and Jargal®M Refractory Samples Showing Changes in Weight Due to Exposure to Molten Smelt at 1000°C for 7 days

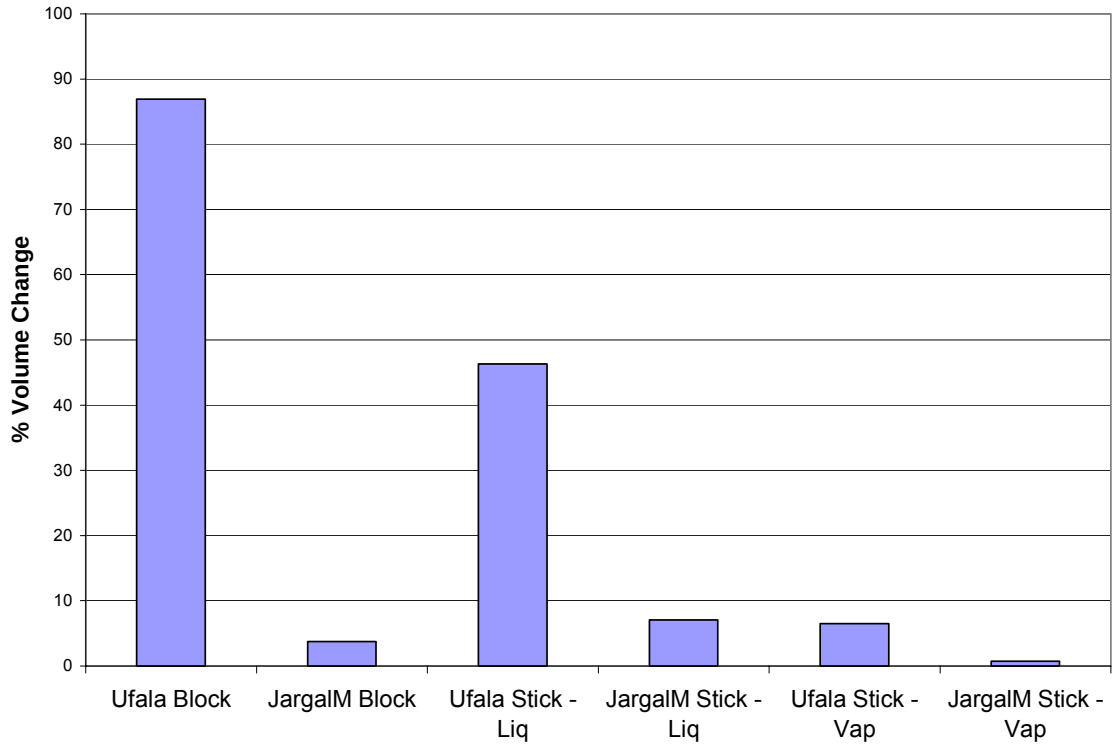

Figure 51: Results for Exposed Uncoated Ufala® and Jargal®M Refractory Samples Showing Changes in Volume Due to Exposure to Molten Smelt at 1000°C for 7 days

By applying the surface barrier coatings, it was hypothesized that the pore size and distribution would be reduced and consequently that the rate of corrosion would be decreased. After testing, the coated samples needed to be analyzed for not only the performance of each coating type in comparison to the uncoated baseline standard but also compared to each other to see if the industrially applied coatings performed noticeably differently than the KP coatings. Figures 52 and 53 show the weight changes for the block samples and stick samples for each KP and C^3™ coating type after 36-hour exposure to molten smelt at 1000°C. Figures 54 and 55 show the volume changes for the same block and stick samples.

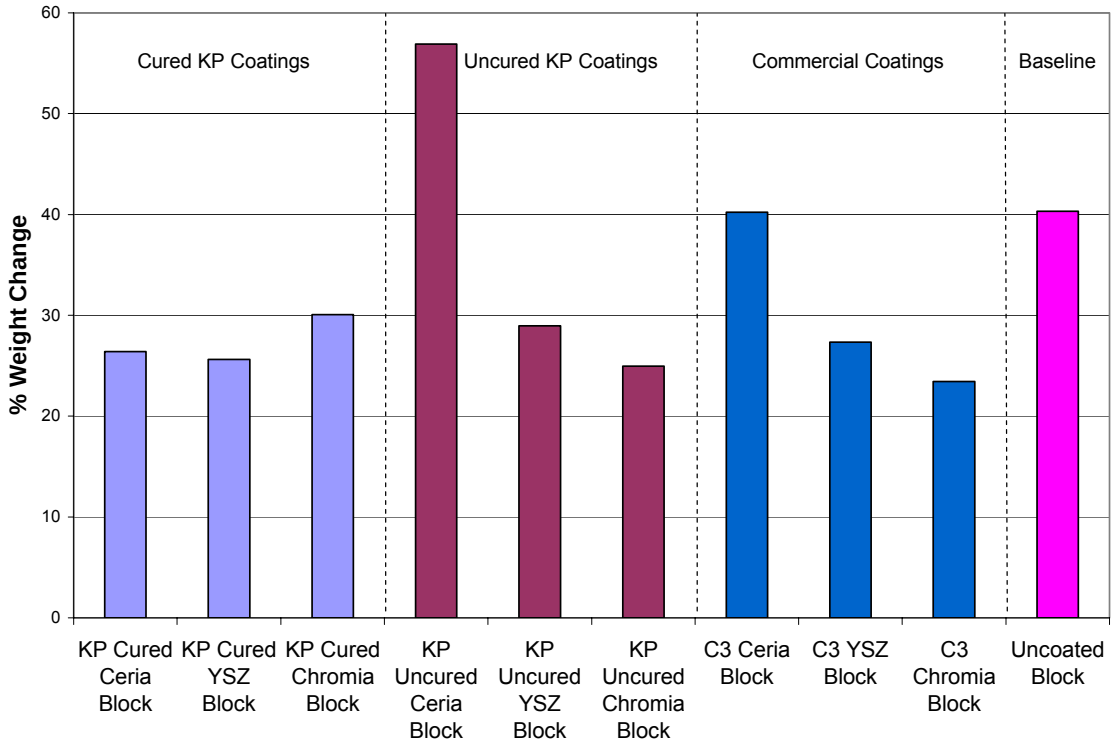

Figure 52: Results from Ufala® Refractory Block Samples with Different Coating Types (shown in graph) Showing Changes in Weight Due to Exposure to Molten Smelt at 1000°C for 36 hours to Determine Coating Viability for Use in HTBLG

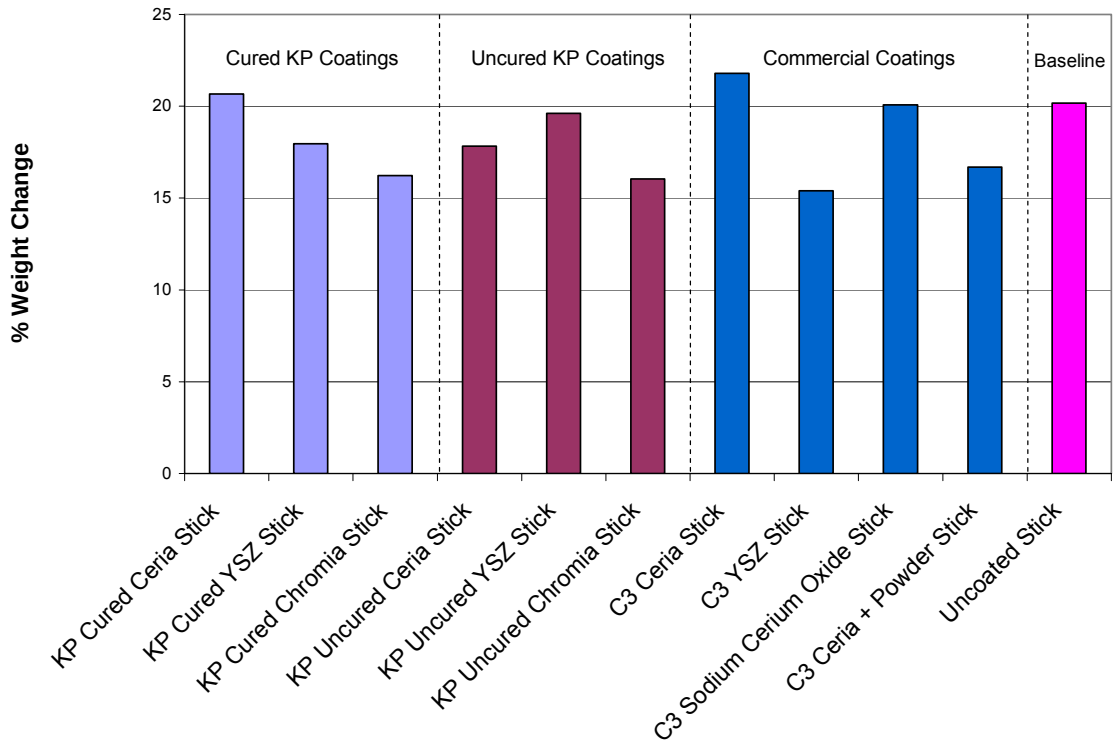

Figure 53: Results from Ufala® Refractory Long Stick Samples with Different Coating Types (shown in graph) Showing Changes in Weight Due to Exposure to Molten Smelt at 1000°C for 36 hours to Determine Coating Viability for Use in HTBLG

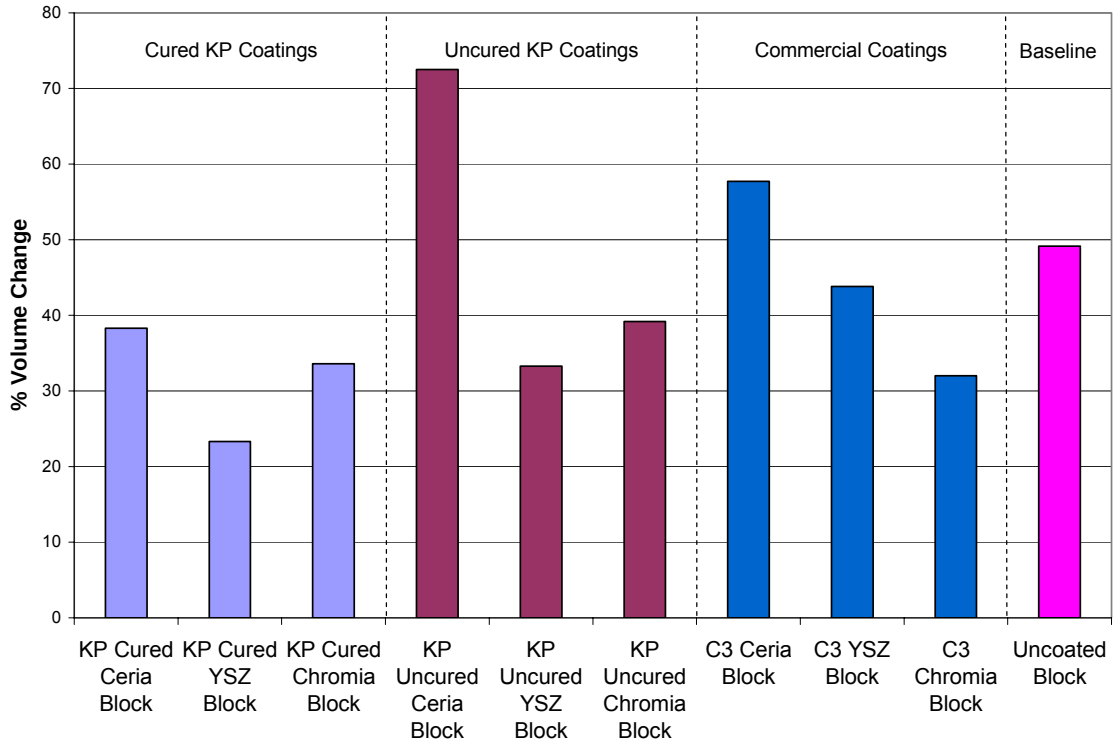

Figure 54: Results from Ufala® Refractory Block Samples with Different Coating Types (shown in graph) Showing Changes in Volume Due to Exposure to Molten Smelt at 1000°C for 36 hours to Determine Coating Viability for Use in HTBLG

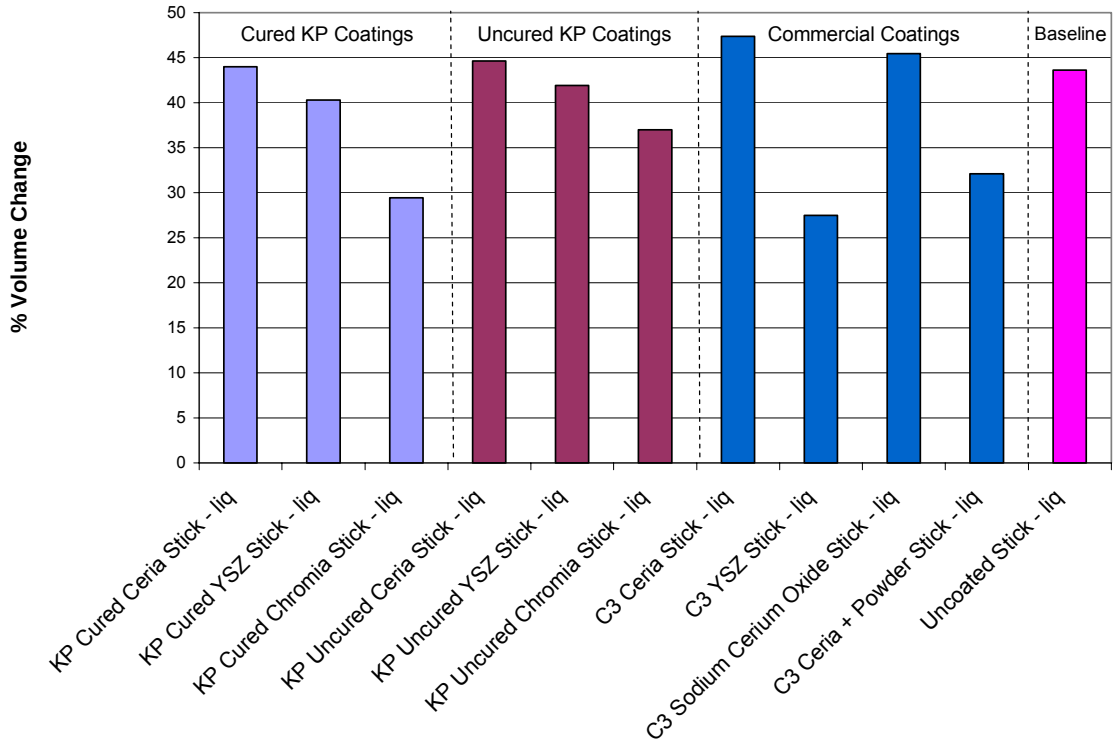

Figure 55: Results from the Liquid Exposure Section of Ufala® Refractory Long Stick Samples with Different Coating Types (shown in graph) Showing Changes in Volume Due to Exposure to Molten Smelt at 1000°C for 36 hours to Determine Coating Viability for Use in HTBLG

From the data given in Figures 52-55, it can be noted that all samples experience both volume and weight increases regardless of coating type. While analyzing the dimensional and gravimetric data an important factor to take into account is that, because of the porous nature of the Ufala® refractories, some salts may remain on the surface of the sample and dry after being removed from the molten smelt adding to the volume and weight measurements. KP cured YSZ and uncured chromia and C^3™ applied chromia on the Ufala® blocks all experienced roughly 34% less weight gain than the corresponding uncoated sample. C^3™ applied YSZ decreased weight gain by ~32% and

the KP cured chromia showed a 27% decrease in weight gain. The KP cured YSZ coated Ufala® block sample had nearly 53% less volume expansion than its uncoated counterpart. C^3™ applied chromia and KP cured chromia and uncured YSZ coated Ufala® block samples showed about 35% and 33% less volume increase than the uncoated sample, respectively. The KP cured chromia and C^3™ applied YSZ performed the best with respect to volume and weight increases and KP uncured chromia also performed well with respect to volume on the long Ufala® stick samples. The chromia and yttria-stabilized zirconia samples appear to match up similarly in both the volume and weight increases that the samples experienced. Those coating types consistently showed the smallest volume and weight increases in both sized samples. Overall, the cured coatings had a lower rate of degradation in terms of weight change or volume increase than their uncured counterparts although some uncured samples performed decently. While these results are encouraging, these coatings still do not perform as well as higher-purity alumina Jargal®M and consequently are not adequate at this point for use in a commercial scale high-temperature black liquor gasifier. Using the weight and volume changes of the blocks and sticks, it can be concluded that the ceria coatings were by far the least effective, seeing as those samples typically had the largest increase in volume and weight regardless of whether they were industrially applied or if they were or were not cured. The samples coated with sodium cerium oxide also incurred a significant weight gain and quite a large increase in volume, second only to the C^3™ ceria coated stick sample. This could in part be due to the fact that the coating itself contains the chemical species sodium which the coating is trying to prevent from penetrating the sample. The sodium on the surface may provide a possible mechanism to aide in

diffusion of Na_2O into sample. The sodium on the surface could also cause the reactions that convert alumina into sodium aluminate to begin before the samples have ever been exposed to the molten smelt. Another possible downfall of the sodium cerium oxide coating is that, since there was ceria present in the coatings, which have been shown to increase weight and volume gain above that of even the uncoated refractory, the integrity may have been compromised. Although it is difficult to obtain conclusive results using these details alone, this information is helpful in understanding the degradation rate of the refractory.

Data obtained from the energy dispersive x-ray spectroscopy (EDS) analysis is the information most indicative of the severity of the effects of corrosion and the effectiveness of the surface coatings that were applied. The lines on which the EDS scans were performed were drawn on the cross-sectional face perpendicular to the exposed face. These line scans provide important details about the depth to which the reactions occurred and as such tell how deep the molten smelt penetrated into the refractory. This determination is possible due to the fact that the composition of the refractory will change and there will be a notable increase in sodium as the reaction progresses into the refractory. Aluminum (Al), sodium (Na), silicon (Si), and sulfur (S) were scanned for in all of the EDS applications and the metals used in the coatings (yttrium (Y), zirconium (Zr), cerium (Ce), and chromium (Cr)) were scanned for in the corresponding samples. Determining the amount and depth of the metals used in the coatings remaining post-exposure, if any, helps to establish the effectiveness of the coatings. Also, scanning for the metals used in the coatings helps to get an idea of the

diffusion that occurs throughout the porous refractory, since the coating solution was only applied to the exterior of the samples. The line scans acquired using energy dispersive x-ray spectroscopy and the corresponding pictures of the samples to identify the location of the line scans can be seen in Appendix D. Visual measurements were also taken from the EDS line scans for each sample and used to aid in the analysis due to the possibility for sample contamination during sectioning of the samples. An example of an SEM/EDS picture is shown in Figure 56. The reaction depth estimated in this sample was about 1700 μm which corresponds well to the visual difference in the sample. The reaction depth of each sample was classified as the point at which the amount of Na in the samples dropped significantly and conversely the amount of Al increased sharply. The EDS scans could also be used to verify the significant difference in refractory purity by comparing the Ufala® and Jargal®M refractory scans. The scans on which the base material was uncoated, unexposed Jargal®M show very little silica and mostly alumina in the samples whereas the line scans on uncoated, unexposed Ufala® samples had a much higher silica content. Graphs of the reaction depth for the interface and liquid exposure sections of KP and C^3™ coated Ufala® refractory samples along with an uncoated baseline are shown in Figures 57 and 58, respectively. These results also confirm that the YSZ and chromia coatings perform the best of the tested metal oxide coatings in slowing corrosion by molten smelt at 1000°C.

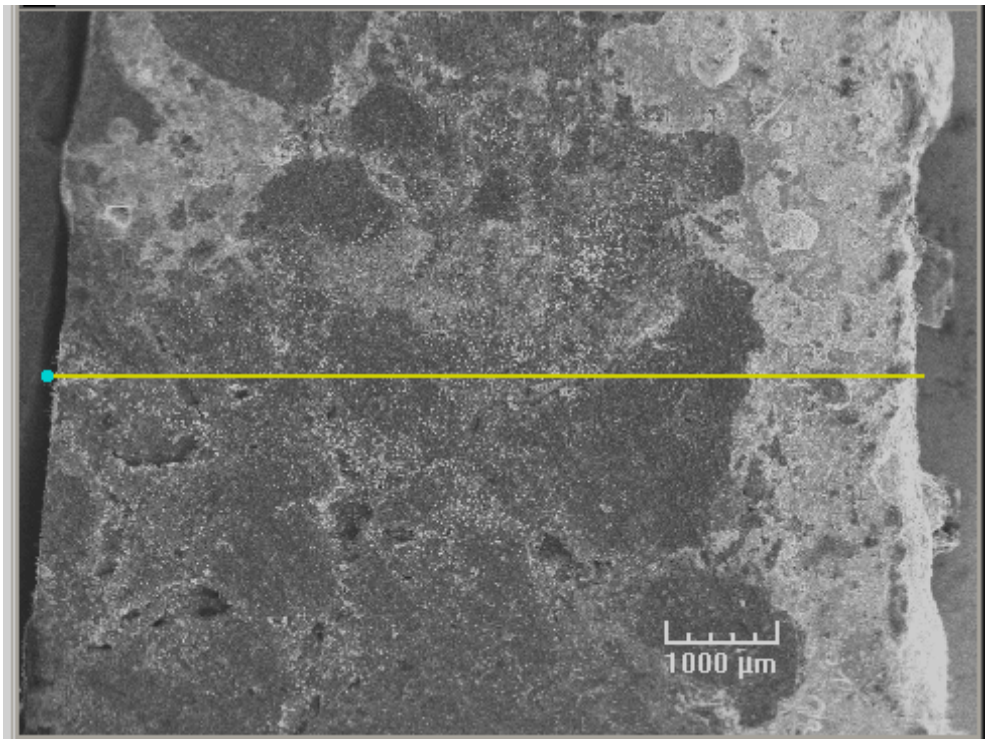

Figure 56: An SEM Micrograph of the Cross-section of the Liquid Exposure Section of an Uncoated Ufala® Long Stick Refractory Sample Exposed to Molten Synthetic Smelt with a 65/25 Carbonate to Sulfide Ratio for 36 Hours with the Location of the Line Scan Shown in Yellow. The Approximate Penetration Depth is Visible on the Picture where the Color Change can be Noted.

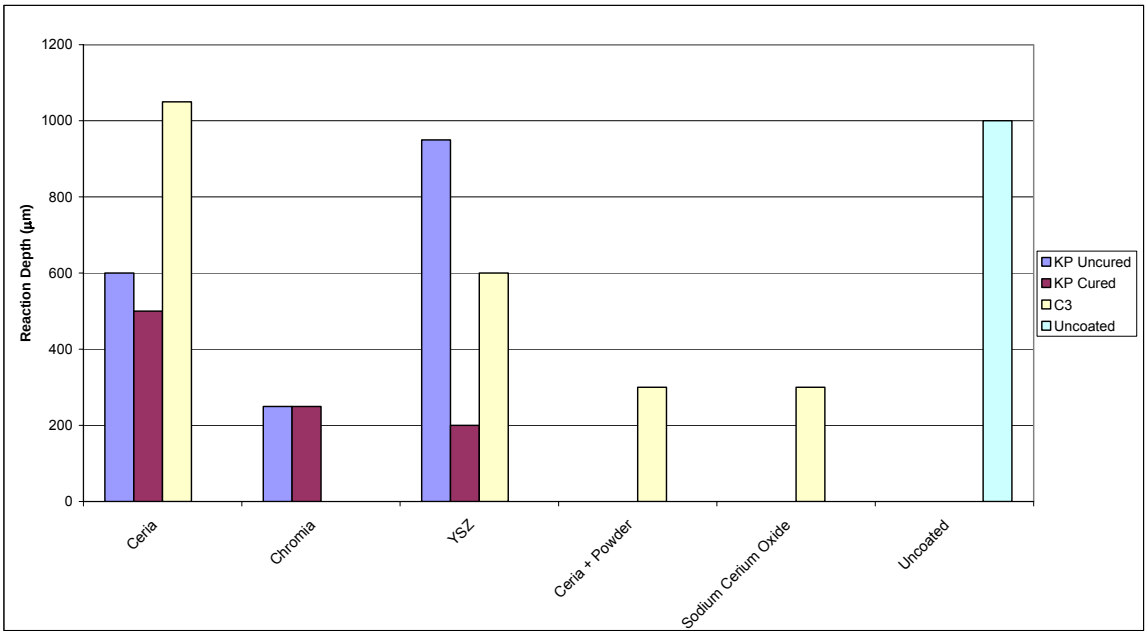

Figure 57: Results from Interface Sections of Ufala® Refractory Long Stick Samples with Different Coating Types (shown in graph) Showing Changes in Reaction Depth Due to Exposure to Molten Smelt at 1000°C for 36 hours to Determine Coating Viability for Use in HTBLG

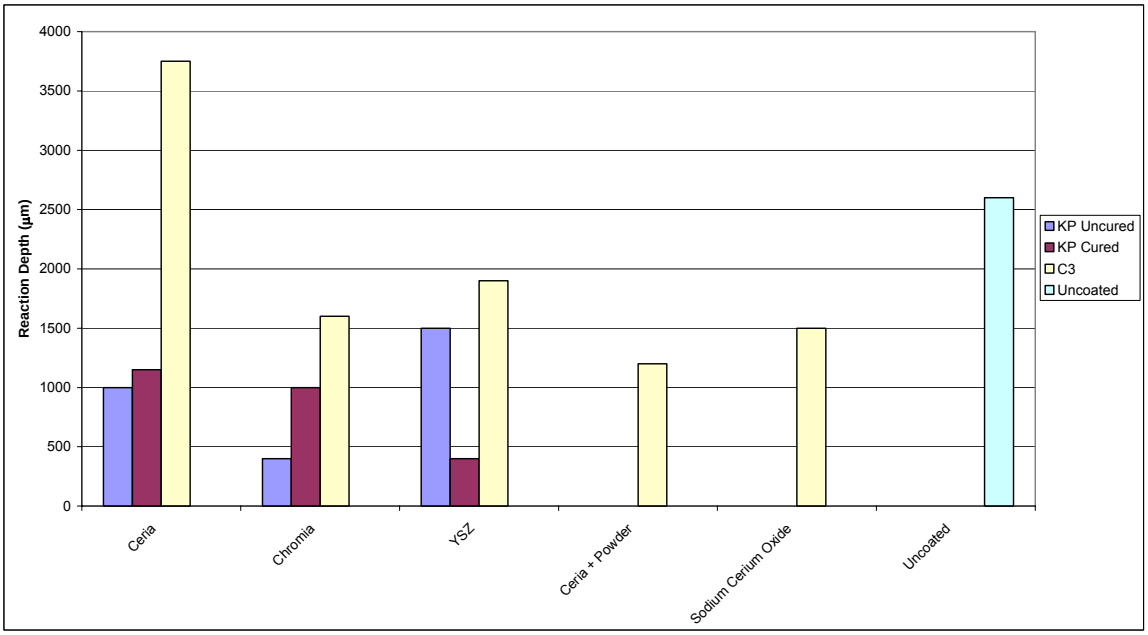

Figure 58: Results from Liquid Exposure Sections of Ufala® Refractory Long Stick Samples with Different Coating Types (shown in graph) Showing Changes in Reaction Depth Due to Exposure to Molten Smelt at 1000°C for 36 hours to Determine Coating Viability for Use in HTBLG.

5.5 Surface Properties

Pictures of all samples were taken prior to and after their exposure to molten smelt. These pictures were used for qualitative analysis of the samples. Pictures of a Jargal®M long stick sample and a Ufala® long stick sample exposed to molten smelt at 1000°C are shown in Figure 59. The visual differences between the two samples are extremely easy to observe. The fact that a reaction has even occurred on the Jargal®M is only barely noticeable with a slight color change from white to bluish green upon visual inspection. The changes in the Ufala® are not only the color difference, but also a conspicuous size increase and overall deformation of the sample can be seen. Shown in Figure 60 are the sectioned pieces of the exposed samples of both Jargal®M and Ufala® refractory. From the pictures and the visually observable change, it can be seen that the Ufala® refractory

is corroded much more quickly by the molten smelt and as a result has a deeper reaction depth.

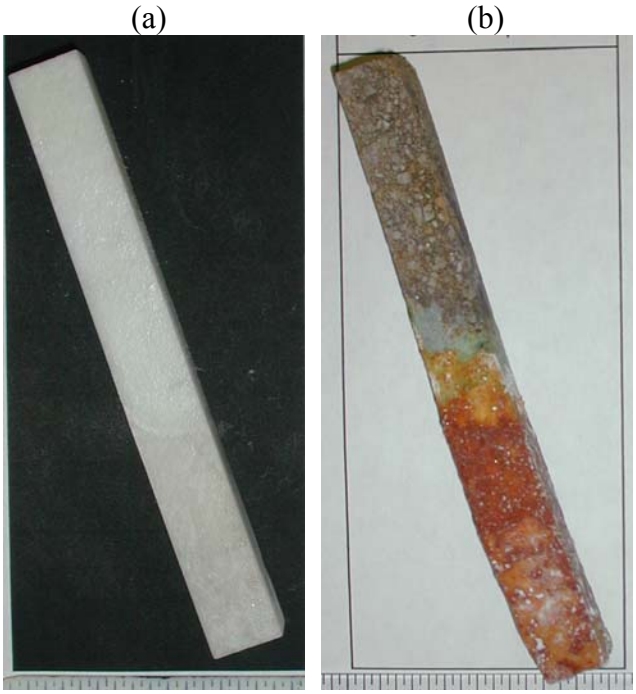

Figure 59: Exposed (a) Jargal®M and (b) Ufala® Long Stick Samples to Show the Visible Difference in Degradation Experienced by Each Refractory Type

(a)

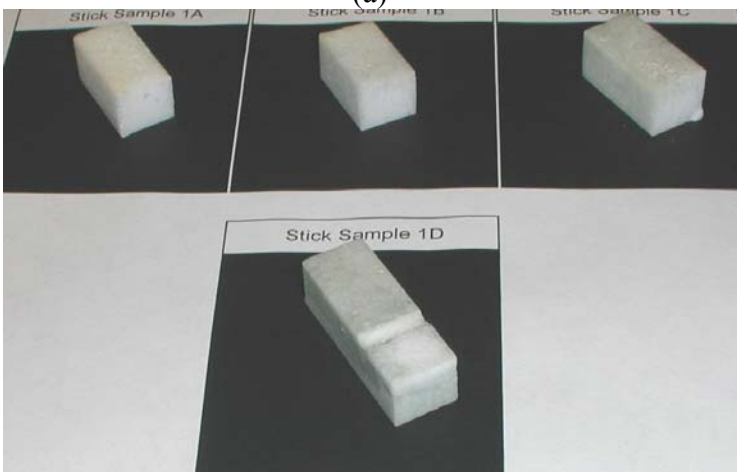

(b)

Figure 60: Exposed Sectioned Jargal®M and Ufala® Stick Samples to Show the Difference Between Liquid, Interface, and Vapor Exposure as well as the Color Change and Penetration Depth that can be Seen on the Sectioned Ufala® Samples

To determine what reaction products were formed on the surface of the samples after exposure, the surfaces of both types of refractory material with and without coatings were analyzed using x-ray diffraction. Although some of the peaks were unable to be positively identified and a few of the graphs contained significant noise making it difficult to categorize the peaks, a table showing the species that were on the surface prior to exposure to molten smelt, and after 36 hours of exposure is shown in Table 18. This comparison also notes that the KP coatings had essentially the same surface products after exposure as the C^3™ coatings.

Table 18: Surface Products as Detected by X-Ray Diffraction on Coated and Uncoated Ufala® Samples Before and After 36-Hour Exposure to Molten Smelt

Coating	No Exposure Surface Species	36-hour Surface Products
Uncoated	α-alumina, β-alumina, sodium aluminate, sodium aluminum silicate	β-alumina, sodium aluminate, sodium aluminum silicate
C^3™ YSZ	α-alumina, β-alumina, sodium aluminum silicate, zirconia	β-alumina, sodium aluminate, sodium aluminum silicate, zirconia
C^3™ Ceria	β-alumina, sodium aluminate, ceria	β-alumina, sodium aluminate, sodium aluminum silicate, ceria
C^3™ Chromia	α-alumina, β-alumina, sodium aluminate, sodium aluminum silicate, chromia	β-alumina, sodium aluminate, sodium aluminum silicate, chromia
C^3™ Ceria +Powder	α-alumina, β-alumina, sodium aluminum silicate, ceria	β-alumina, sodium aluminate, sodium aluminum silicate, ceria
C^3™ Na_2CeO_3	β-alumina, sodium aluminate, sodium aluminum silicate, ceria	β-alumina, sodium aluminate, sodium aluminum silicate, ceria
KP Uncured YSZ	α-alumina, β-alumina, zirconia	β-alumina, sodium aluminate, zirconia
KP Uncured Ceria	β-alumina, ceria	β-alumina, sodium aluminate, sodium aluminum silicate, ceria
KP Uncured Chromia	α-alumina, β-alumina, sodium aluminate, chromia	β-alumina, sodium aluminate, sodium aluminum silicate, chromia
KP Cured YSZ	β-alumina, zirconia	β-alumina, sodium aluminate, sodium aluminum silicate, zirconia
KP Cured Ceria	β-alumina, ceria	β-alumina, sodium aluminate, sodium aluminum silicate, ceria
KP Cured Chromia	β-alumina, chromia	β-alumina, sodium aluminate, sodium aluminum silicate, chromia

Although some tested metal oxide coatings definitely showed promising results, there was no one coating that provided a sufficient barrier to slow the penetration of molten smelt into the refractory and prevent significant corrosion damage. These results do prove that a barrier coating can decrease the degradation rates, however, surface porosity needs to be completely closed for any coating or surface modification to work effectively in harsh molten smelt environments. If a coating can be found that provides a sufficient protective barrier that could be applied and cured in-situ, it would be most effective and practical solution for high-temperature black liquor gasifiers.

Chapter 6

Conclusions

The important conclusions that may be drawn from these results are discussed in this section.

- High alumina Jargal®M with lower porosity performs significantly better than lower purity, higher porosity alumina/silica refractories such as Ufala® in molten synthetic smelt at 1000°C.
- The volume increase due to refractory/smelt reaction in molten smelts with sodium salts is the main reason for the spalling and corrosion of alumina containing refractories.
- Although dense alumina ceramics will also degrade in sodium salt smelts, accelerated corrosion of the refractory materials happens via diffusion of the molten salts through open pores in the ceramic.
- No protective scales are formed on the refractory surface nor does pore closure that may occur on the refractory surface due to volume expansion occur to slow corrosion. This leads to a linear rate of corrosion reaction.
- Changing sulfidity of the molten salt mixture does not have a significant effect on weight or volume change or penetration depth of alumina refractories tested.
- Metal oxide coatings that were developed in the laboratory in this study performed at the same level as the coatings applied commercially.

- Coating Ufala® with chromia or yttria-stabilized zirconia noticeably slowed the degradation that occurred due to molten smelt exposure. They did not, however, sufficiently impede the corrosion rate or spalling of the refractory for commercial use.
- Coating Ufala® with ceria or sodium cerium oxide did not slow the rate of corrosion that occurred to the samples.
- Curing of the laboratory coatings at 500°C was important as the cured samples provided improved corrosion resistance over the uncured coatings. This shows that further sintering by curing at a higher temperature will be beneficial.

Chapter 7

Recommendations for Future Work

While the method used to test a refractory's resistance to corrosion in a high-temperature black liquor gasification environment gives an accurate portrayal of the refractory performance, the untreated refractory and metal oxide coatings or in-situ treatment options are currently insufficient. Also, using the current method, it is difficult to know exactly when spalling of the sample occurred and how much of the sample was lost. In that regard, having the ability to monitor the weight changes of the sample during the exposure to molten smelt would be advantageous. The progressive weight increase of the sample would then be known and an accurate calculation could be made on the amount of refractory that was lost due to spalling and exactly when the spalling happened during exposure. Yttria-stabilized zirconia coatings tested in the laboratory runs performed best in decreasing the corrosion rate. Chromia also showed some promising corrosion protection, however, neither of these coatings performed adequately enough to be implemented commercially. The coating methods used in this research were not only relatively simple but also inexpensive making them a favorable option. More research should be continued in the field of yttria-stabilized zirconia and chromia coatings because the current results are promising. It may also be of interest to try scandia-stabilized zirconia coatings, sintering coatings, and surface treatments such as high-density infrared or combined laser sources. Scandia-stabilized zirconia has been suggested as a more corrosion resistant coating than its yttria-stabilized counterpart. Sintering of coatings was briefly attempted, however, the coatings did not adhere well to the base material across

the whole surface. Regardless of the coating type or whether it is heat treated or not, it is necessary to ensure that when the coatings are applied, they are continuous and adhere well to the substrate material. Without proper adhesion and adequate coating, the coatings are essentially useless. A method that would effectively close the surface pores should slow the diffusion of the molten salts through refractory. Because of the success seen using high density infrared treatments to slow corrosion of alumina based refractory in molten copper, the same technique should be of interest for use on refractory ceramics in high-temperature black liquor gasification environments. As such, methods should continue to be explored that would close or reduce surface porosity to increase corrosion resistance. After application of surface barrier coatings or other treatments, tests to determine the kinetics of the coated refractory/smelt reaction should be performed to compare the rates of reaction. Different options for gasifier lining materials should also be considered. Even though high-temperature black liquor gasification appears to be a beneficial and cost effective replacement for the traditional Tomlinson recovery boiler, without a lasting refractory material to line the gasifier, it can not effectively be implemented.

Appendix A

Microhardness, Volume, and Weight Change Data

Raw Data for Jargal®M Refractory Samples Prior to Molten Smelt Exposure for 7 Days at 1000°C. The Samples Highlighted in Pink were Block Samples Exposed to Smelt of Varying Carbonate/Sulfide Ratios (as Noted). Those Highlighted in Orange were Block Samples Coated with the Noted Metal Oxide Tested in Molten Smelt with Carbonate to Sulfide Ratio of 65/15. The Samples Highlighted in Yellow were the Vapor and Liquid Exposure Sections of a Stick Sample Tested in a Molten Smelt with Carbonate to Sulfide Ratio of 65/15.

	Pre-Exposure								
Sample	**Weight**	**Length**	**Height**	**Width**	**Volume**	**VHN**			**Avg VHN**
65/15	14.4493	0.9255	0.5165	0.5400	0.2581	312	298	332	314.0
65/20	13.4380	0.9750	0.5110	0.4685	0.2334	274	286	263	274.3
65/25	10.3141	0.9720	0.3260	0.5750	0.1822	530	412	375	439.0
65/30	13.8162	0.9565	0.5325	0.4860	0.2475	162	315	368	281.7
65/35	10.2128	0.7180	0.4610	0.5440	0.1801	363	349	381	364.3
65/15	8.7867	0.8000	0.3600	0.5380	0.1549	285	299	327	303.7
65/20	12.6190	0.8005	0.5420	0.5160	0.2239	344	395	361	366.7
65/25	12.2231	0.9400	0.4535	0.5085	0.2168	336	342	356	344.7
65/30	9.3008	0.8425	0.3785	0.5100	0.1626	159	401	352	304.0
65/35	7.8702	0.9575	0.3070	0.4755	0.1398	604	397	421	474.0
Na_2CeO_3	14.9168	0.9315	0.5495	0.5195	0.2659	546	666	578	596.7
CeO_2	13.1471	0.9425	0.4775	0.4970	0.2237	917	731	757	801.7
CeO_2 Dup	13.1599	0.9800	0.5185	0.4595	0.2335	790	686	715	730.3
Stick - Liq	53.4458	4.2290	0.4990	0.4790	1.0108				
Stick - Vap			0.5020	0.4720	1.0020				

Raw Data for Jargal®M Refractory Samples After Exposure to Molten Smelt for 7 Days at 1000°C. The Samples Highlighted in Pink were Block Samples Exposed to Smelt of Varying Carbonate/Sulfide Ratios (as Noted). Those Highlighted in Orange were Block Samples Coated with the Noted Metal Oxide Tested in Molten Smelt with Carbonate to Sulfide Ratio of 65/15. The Samples Highlighted in Yellow were the Liquid and Vapor Exposure Sections of a Stick Sample Tested in a Molten Smelt with Carbonate to Sulfide Ratio of 65/15.

	Post-Exposure								
Sample	**Weight**	**Length**	**Height**	**Width**	**Volume**	**VHN**			**Avg VHN**
65/15	14.6110	0.9355	0.5535	0.5205	0.2695	76.8	86.2	75.9	79.6
65/20	13.6364	0.9805	0.5275	0.4725	0.2444	98	96.6	80.1	91.6
65/25	10.4345	0.9785	0.5875	0.3300	0.1897	75.2	146	203	141.4
65/30	12.3268	0.9620	0.5345	0.4895	0.2517	184	163	123	156.7
65/35	10.3274	0.7230	0.5475	0.4620	0.1829	112	150	170	144.0
65/15	8.9563	0.8035	0.5410	0.3675	0.1597	156	175	156	162.3
65/20	12.7958	0.8215	0.5510	0.5215	0.2361	113	169	158	146.7
65/25	12.4307	0.9480	0.5120	0.4605	0.2235	170	137	135	147.3
65/30	9.4121	0.8530	0.5160	0.3860	0.1699	146	111	184	147.0
65/35	8.2192	0.9685	0.4815	0.3250	0.1516	141	116	207	154.7
Na_2CeO_3	15.1441	0.9475	0.5770	0.5370	0.2936	239	366	285	296.7
CeO_2	13.3983	0.9545	0.5015	0.4965	0.2377	79.7	65.1	70.9	71.9
CeO_2 Dup	13.4140	0.9875	0.5310	0.4690	0.2459	69.3	59	56.6	61.6
Stick - Liq	54.0755	4.2285	0.5175	0.4945	1.0821				
Stick - Vap			0.5030	0.4745	1.0092				

Volume, VHN, and Weight Change Data for Jargal®M Refractory Samples After Exposure to Molten Smelt for 7 Days at 1000°C. The Samples Highlighted in Pink were Block Samples Exposed to Smelt of Varying Carbonate/Sulfide Ratios (as Noted). Those Highlighted in Orange were Block Samples Coated with the Noted Metal Oxide Tested in Molten Smelt with Carbonate to Sulfide Ratio of 65/15. The Samples Highlighted in Yellow were the Liquid and Vapor Exposure Sections of a Stick Sample Tested in a Molten Smelt with Carbonate to Sulfide Ratio of 65/15.

Sample	Volume Change (% change)	VHN Change (% change)	Weight Change (% change)
65/15	4.41	-74.64	1.12
65/20	4.70	-66.62	1.48
65/25	4.12	-67.79	1.17
65/30	1.68	-44.38	-10.78
65/35	1.56	-60.48	1.12
65/15	3.10	-46.54	1.93
65/20	5.44	-60	1.40
65/25	3.11	-57.25	1.70
65/30	4.47	-51.64	1.20
65/35	8.43	-67.37	4.43
Na_2CeO_3	10.41	-50.28	1.52
CeO_2	6.26	-91.03	1.91
CeO_2 Dup	5.33	-91.56	1.93
Stick - Liq	7.05		1.18
Stick - Vap	0.72		

Raw Data for Ufala® Refractory Samples Prior to Molten Smelt of Carbonate to Sulfide Ratio of 65/15 Exposure for 36 Hours (Unless Otherwise Noted) at 1000°C. Coating Type for Each Sample (if Applicable) is Listed in the Table.

	Pre-Exposure				
Sample	**Weight**	**Length**	**Height**	**Width**	**Volume**
Uncoated 7 Day Block	8.5121	0.8675	0.4780	0.5300	0.2198
Uncoated 7 Day Block Dup	9.2337	0.9475	0.5210	0.4865	0.2402
Uncoated 7 Day Stick - Liq	45.6922	4.5520	0.4885	0.4580	1.0184
Uncoated 7 Day Stick - Vap			0.5590	0.4815	1.2252
Uncoated 7 Day Stick - Liq Dup	46.5643	4.5550	0.5140	0.4780	1.1191
Uncoated 7 Day Stick - Vap Dup			0.5400	0.4860	1.1954
KP Cured CeO2 Block	9.8763	0.9350	0.5690	0.4220	0.2245
KP Cured CeO2 Stick - Liq	47.2685	4.5375	0.5080	0.5285	1.2182
KP Cured CeO2 Stick - Vap			0.4765	0.4835	1.0454
KP Uncured CeO2 Block	6.1972	0.8615	0.5190	0.3480	0.1556
KP Uncured CeO2 Stick - Liq	41.0455	4.5540	0.4960	0.3800	0.8583
KP Uncured CeO2 Stick - Vap			0.5260	0.4760	1.1402
KP Cured YSZ Block	9.0669	1.0420	0.4780	0.4745	0.2363
KP Cured YSZ Stick - Liq	47.5972	4.4850	0.6010	0.5080	1.3693
KP Cured YSZ Stick - Vap			0.4815	0.4805	1.0377
KP Uncured YSZ Block	9.0109	1.0865	0.4700	0.4230	0.2160
KP Uncured YSZ Stick - Liq	28.9929	4.5755	0.4085	0.3470	0.6486
KP Uncured YSZ Stick - Vap			0.5020	0.3660	0.8407
KP Cured Chromia Block	8.6431	1.1535	0.4710	0.4105	0.2230

	Pre-Exposure				
Sample	**Weight**	**Length**	**Height**	**Width**	**Volume**
KP Cured Chromia Stick - Liq	29.7208	4.5650	0.4225	0.3895	0.7512
KP Cured Chromia Stick - Vap			0.5090	0.3775	0.8772
KP Uncured Chromia Block	7.6279	1.3145	0.4725	0.2985	0.1854
KP Uncured Chromia Stick - Liq	33.4546	3.9455	0.4845	0.4285	0.8191
KP Uncured Chromia Stick - Vap			0.5550	0.4095	0.8967
Uncoated Block	8.2933	1.1980	0.5270	0.3425	0.2162
Uncoated Stick - Liq	52.0082	4.5410	0.5275	0.4745	1.1366
Uncoated Stick - Vap			0.5645	0.5335	1.3676
C3 YSZ Block	10.1499	1.1360	0.5330	0.4205	0.2546
C3 YSZ Stick - Liq	40.7188	3.9180	0.4490	0.4375	0.7696
C3 YSZ Stick - Vap			0.5525	0.4554	0.9859
C3 Ceria Block	8.3915	1.1330	0.5150	0.3430	0.2001
C3 Ceria Stick - Liq	43.8859	4.5375	0.5050	0.4265	0.9773
C3 CeO2 Stick - Vap			0.5570	0.4415	1.1158
C3 Chromia Block	9.9840	1.1775	0.4725	0.4110	0.2287

	Pre-Exposure				
Sample	**Weight**	**Length**	**Height**	**Width**	**Volume**
C3 Na2CeO3 Stick - Vap			0.5060	0.4625	1.0612
C3 CeO2 + Powder Stick - Liq	44.2095	4.5325	0.5015	0.4745	1.0786
C3 CeO2 + Powder Stick - Vap			0.5805	0.4650	1.2235

Raw Data and Volume and Weight Change for Ufala® Refractory Samples After Exposure to Molten Smelt of Carbonate to Sulfide Ratio of 65/15 Exposure for 36 Hours (Unless Otherwise Noted) at 1000°C. Coating Type for Each Sample (if Applicable) is Listed in the Table.

	Post-Exposure					Volume Change	Weight Change
Sample	**Weight**	**Length**	**Height**	**Width**	**Volume**	**(% change)**	**(% change)**
Uncoated 7 Day Block	13.7604	1.0255	0.5805	0.6675	0.3974	80.81	61.66
Uncoated 7 Day Block Dup	15.8911	1.1305	0.6795	0.6035	0.4636	93.04	72.10
Uncoated 7 Day Stick - Liq	55.8647	4.6500	0.5675	0.5525	1.4580	43.16	22.26
Uncoated 7 Day Stick - Vap			0.5590	0.4815	1.2516	2.15	
Uncoated 7 Day Stick - Liq Dup	60.7276	4.7965	0.6075	0.5740	1.6726	49.45	30.42
Uncoated 7 Day Stick - Vap Dup			0.5365	0.5150	1.3253	10.86	
KP Cured CeO2 Block	12.4834	0.9990	0.6305	0.4930	0.3105	38.31	26.40
KP Cured CeO2 Stick - Liq	57.0340	4.6895	0.5900	0.6340	1.7542	43.99	20.66
KP Cured CeO2 Stick - Vap			0.4755	0.4865	1.0848	3.77	
KP Uncured CeO2 Block	9.7237	0.9935	0.6410	0.4215	0.2684	72.51	56.90

	Post-Exposure					Volume Change	Weight Change
Sample	**Weight**	**Length**	**Height**	**Width**	**Volume**	**(% change)**	**(% change)**
KP Uncured CeO2 Stick - Vap			0.5160	0.4680	1.1398	-0.034	
KP Cured YSZ Block	11.3900	1.0880	0.5305	0.5050	0.2915	23.33	25.62
KP Cured YSZ Stick - Liq	56.1416	4.5630	0.7100	0.5930	1.9212	40.30	17.95
KP Cured YSZ Stick - Vap			0.4825	0.4775	1.0513	1.31	
KP Uncured YSZ Block	11.6191	1.1410	0.5340	0.4725	0.2879	33.28	28.95
KP Uncured YSZ Stick - Liq	34.6791	4.7165	0.4855	0.4020	0.9205	41.93	19.61
KP Uncured YSZ Stick - Vap			0.4990	0.4650	1.0944	30.18	
KP Cured Chromia Block	11.2431	1.2385	0.5270	0.4565	0.2980	33.60	30.08
KP Cured Chromia Stick - Liq	34.5452	4.6440	0.4775	0.4385	0.9724	29.44	16.23
KP Cured Chromia Stick - Vap			0.4975	0.3625	0.8375	-4.52	
KP Uncured Chromia Block	9.5310	1.3780	0.5420	0.3455	0.2580	39.18	24.95

	Post-Exposure					Volume Change	Weight Change
Sample	**Weight**	**Length**	**Height**	**Width**	**Volume**	**(% change)**	**(% change)**
KP Uncured Chromia Stick - Vap			0.5405	0.4020	0.8751	-2.41	
Uncoated Block	11.6388	1.3080	0.6065	0.4065	0.3225	49.13	40.34
Uncoated Stick - Liq	62.5001	5.1930	0.5810	0.5410	1.6323	43.61	20.17
Uncoated Stick - Vap			0.5660	0.5365	1.5769	15.31	
C3 YSZ Block	12.9263	1.2225	0.6260	0.4785	0.3662	43.82	27.35
C3 YSZ Stick - Liq	46.9869	4.0000	0.4955	0.4950	0.9811	27.47	15.39
C3 YSZ Stick - Vap			0.5585	0.4590	1.0254	4.01	
C3 Ceria Block	11.7680	1.2730	0.6100	0.4065	0.3157	57.72	40.24
C3 Ceria Stick - Liq	53.4523	4.7635	0.5900	0.5125	1.4404	47.38	21.80
C3 CeO2 Stick - Vap			0.5600	0.4430	1.1817	5.90	
C3 Chromia Block	12.3240	1.2365	0.5145	0.4745	0.3019	32.01	23.44

	Post-Exposure					Volume Change	Weight Change
Sample	**Weight**	**Length**	**Height**	**Width**	**Volume**	**(% change)**	**(% change)**
C3 Na2CeO3 Stick - Vap			0.5050	0.4640	1.1035	3.99	
C3 CeO2 + Powder Stick - Liq	51.5881	4.6305	0.5595	0.5500	1.4249	32.11	16.69
C3 CeO2 + Powder Stick - Vap			0.5830	0.4665	1.2594	2.93	

Appendix B

Viscometry

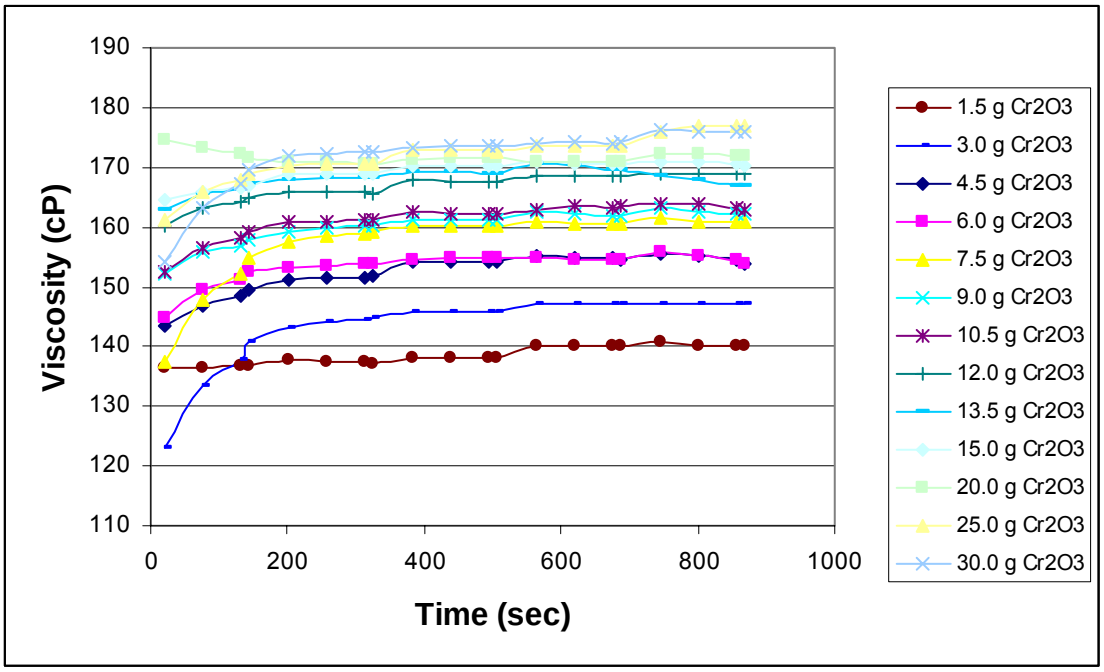

Results for Viscosity Changes Experienced by PVA with Water Mixture upon Addition of Chromia Powder at 73°F

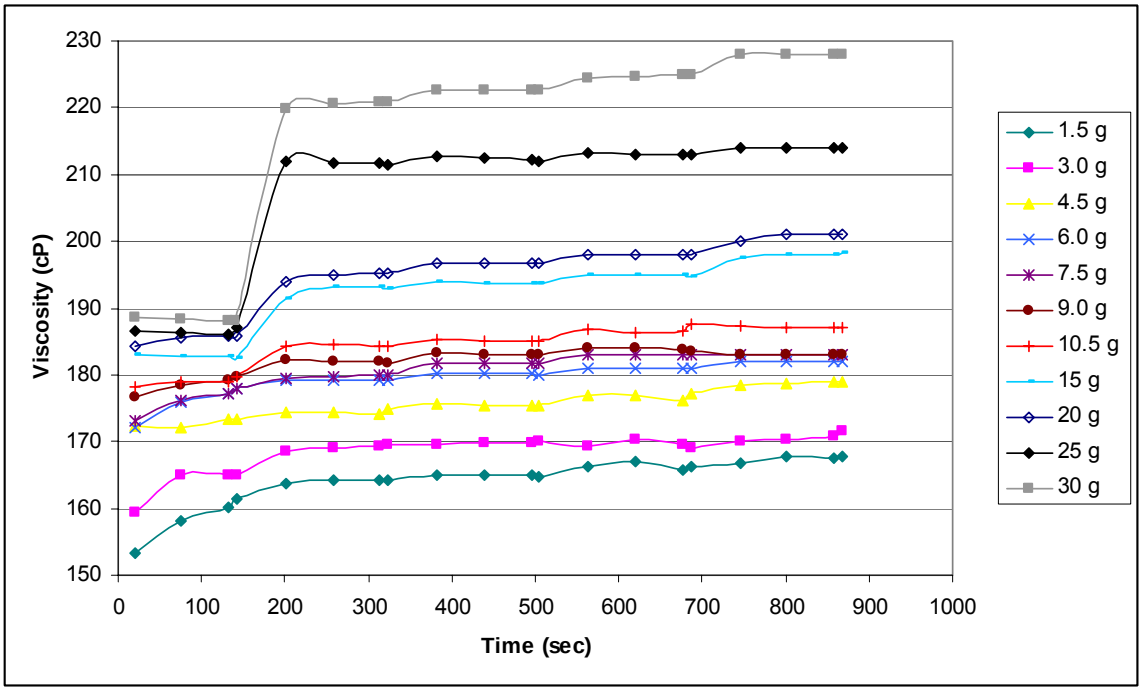

Results for Viscosity Changes Experienced by PVA with Water Mixture upon Addition of Ceria Powder at 73°F

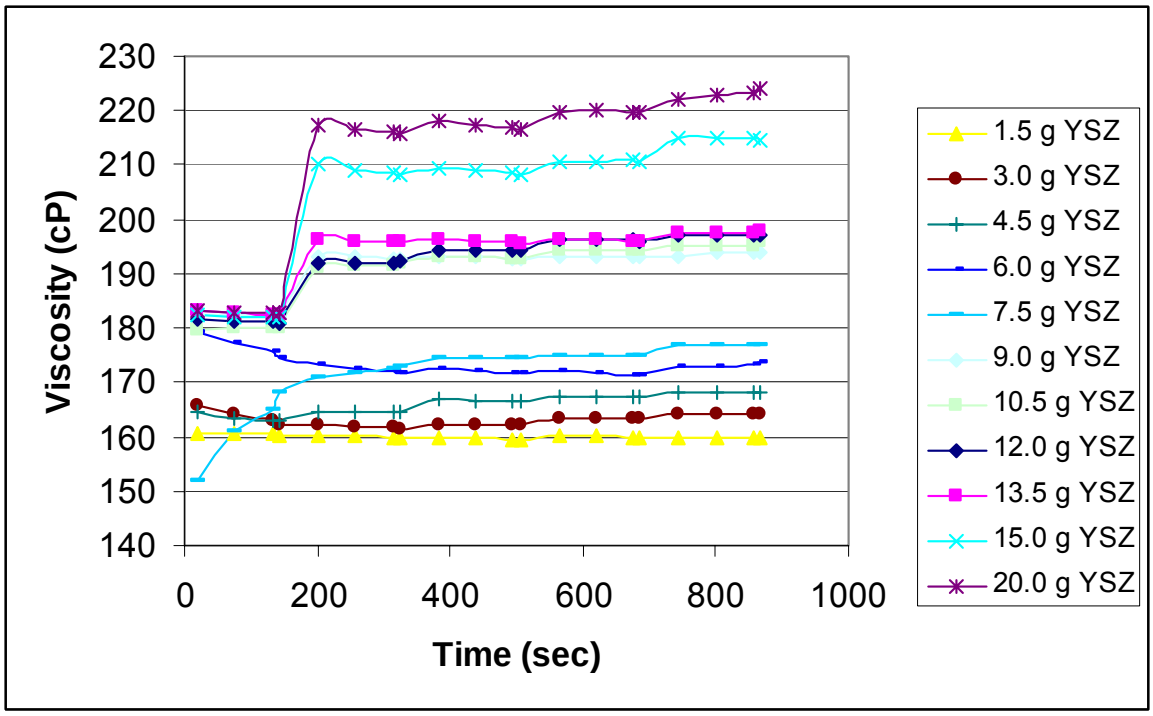

Results for Viscosity Changes Experienced by PVA with Water Mixture upon Addition of YSZ Powder at 73°F

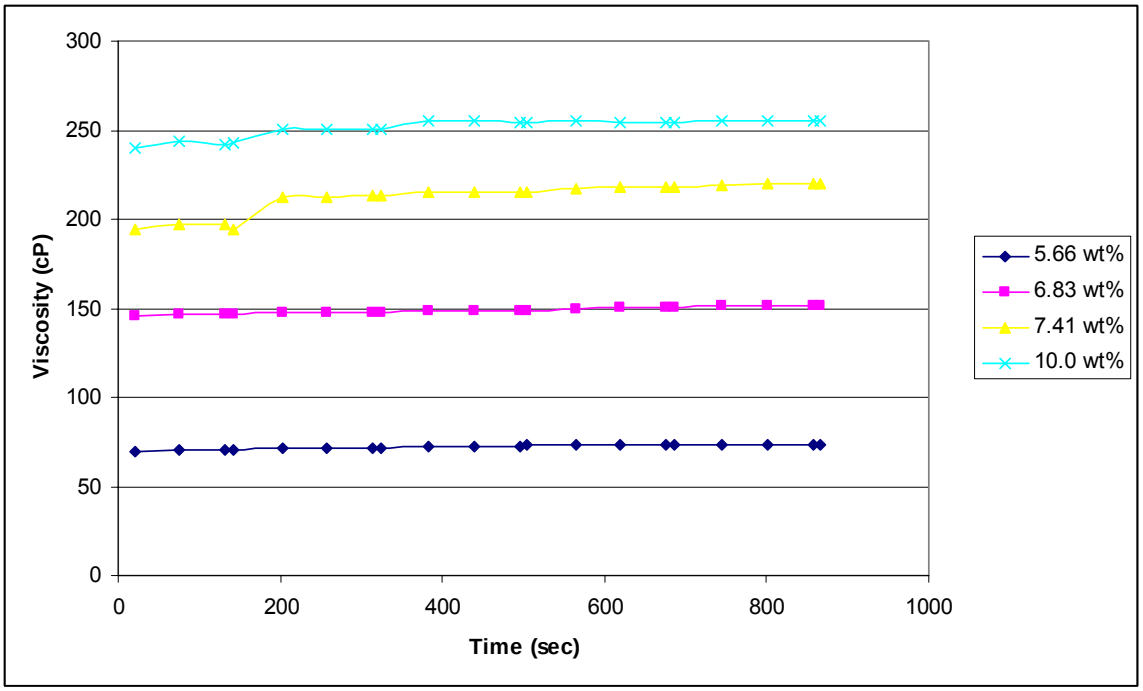

Results Showing the Effect of Increasing PVA Concentration in Water on Viscosity at 77°F

Appendix C

X-Ray Diffraction

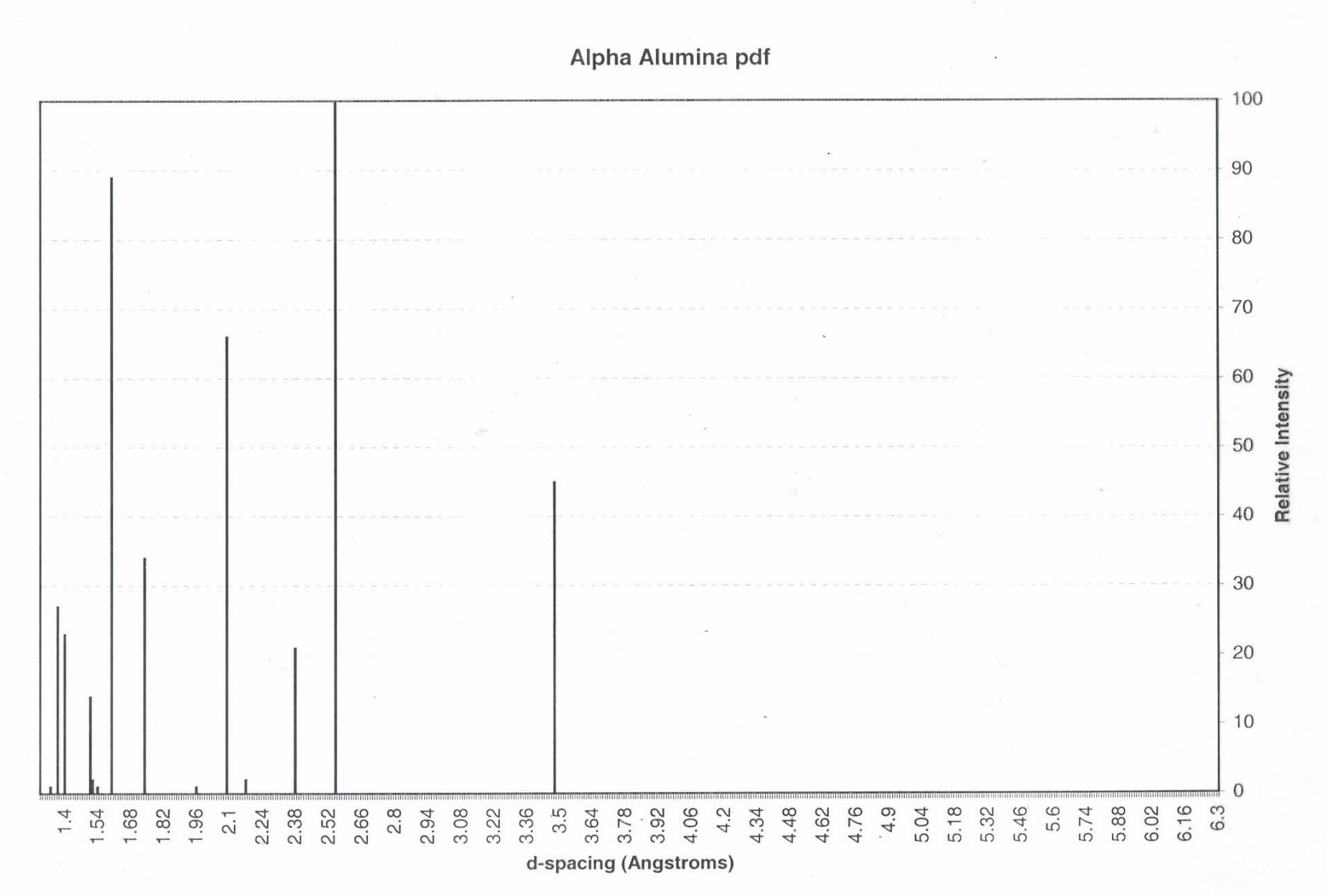
Alpha Alumina pdf
100
90
80
70
60
50
40
30
20
10
0
Relative Intensity
1.4
1.54
1.68
1.82
1.96
2.1
2.24
2.38
2.52
2.66
2.8
2.94
3.08
3.22
3.36
3.5
3.64
3.78
3.92
4.06
4.2
4.34
4.48
4.62
4.76
4.9
5.04
5.18
5.32
5.46
5.6
5.74
5.88
6.02
6.16
6.3
d-spacing (Angstroms)

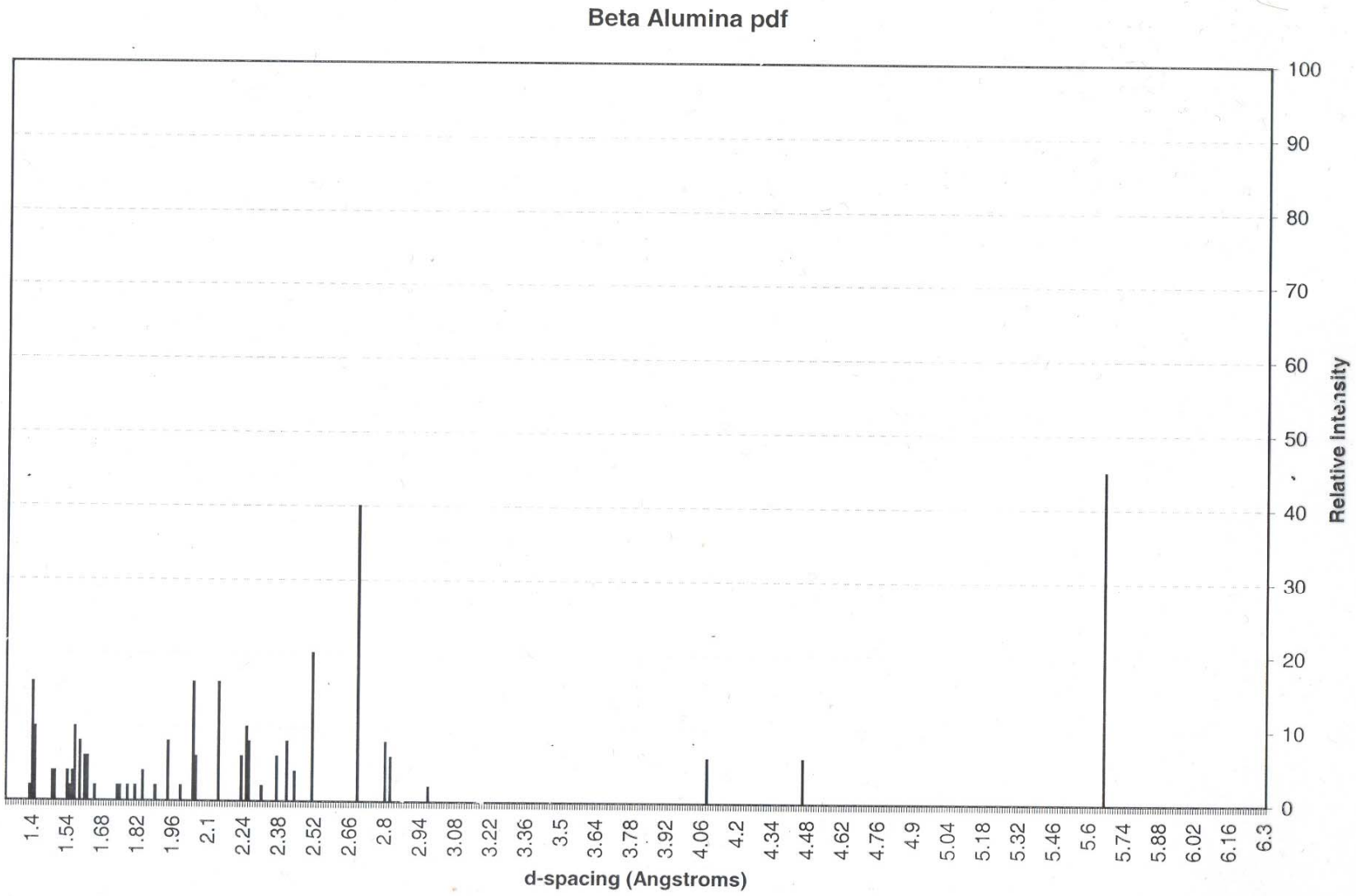
Beta Alumina pdf
100
90
80
70
60
50
40
30
20
10
0
Relative Intensity
1.4
1.54
1.68
1.82
1.96
2.1
2.24
2.38
2.52
2.66
2.8
2.94
3.08
3.22
3.36
3.5
3.64
3.78
3.92
4.06
4.2
4.34
4.48
4.62
4.76
4.9
5.04
5.18
5.32
5.46
5.6
5.74
5.88
6.02
6.16
6.3
d-spacing (Angstroms)

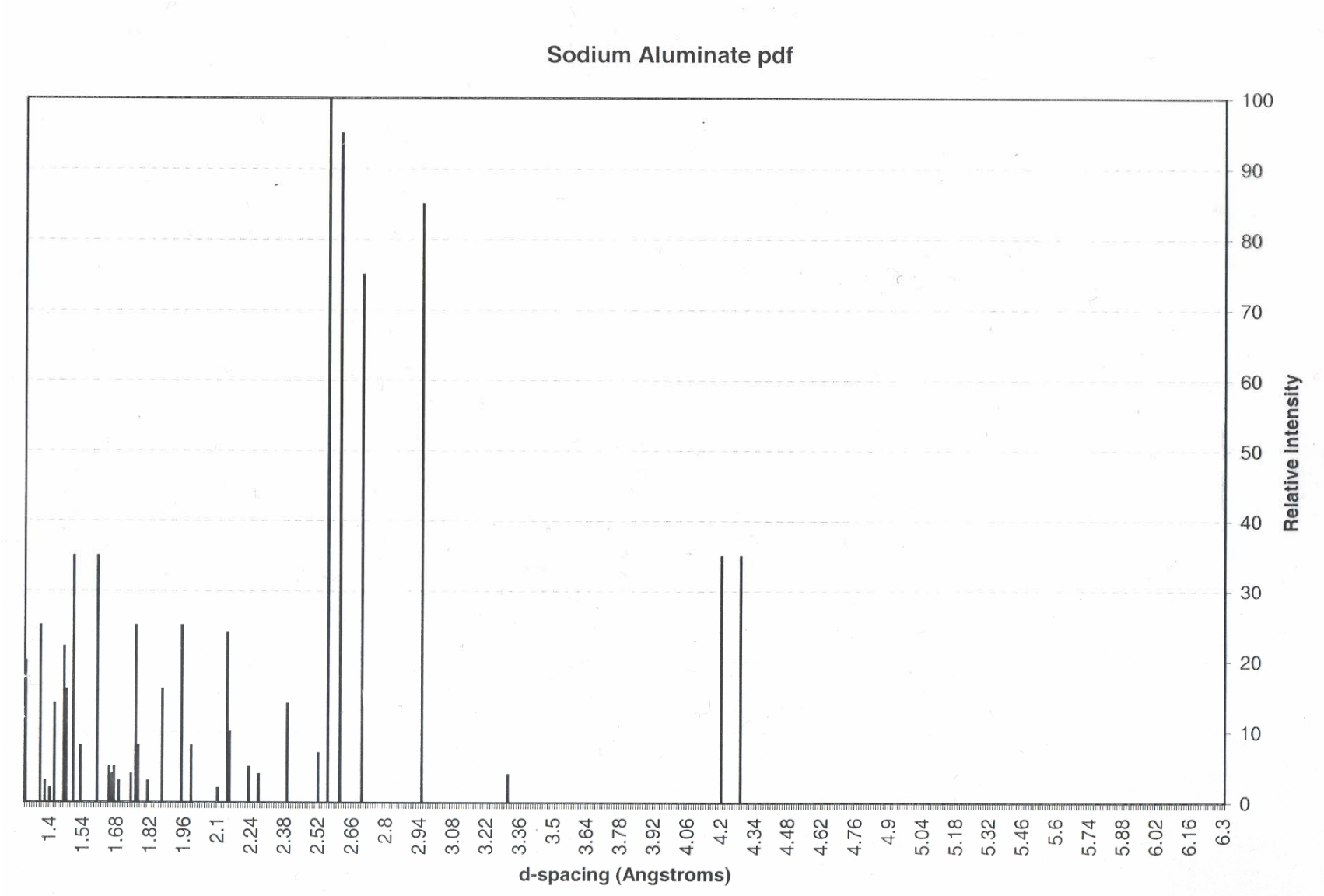
Sodium Aluminate pdf
100
90
80
70
60
50
40
30
20
10
0
Relative Intensity
1.4
1.54
1.68
1.82
1.96
2.1
2.24
2.38
2.52
2.66
2.8
2.94
3.08
3.22
3.36
3.5
3.64
3.78
3.92
4.06
4.2
4.34
4.48
4.62
4.76
4.9
5.04
5.18
5.32
5.46
5.6
5.74
5.88
6.02
6.16
6.3
d-spacing (Angstroms)

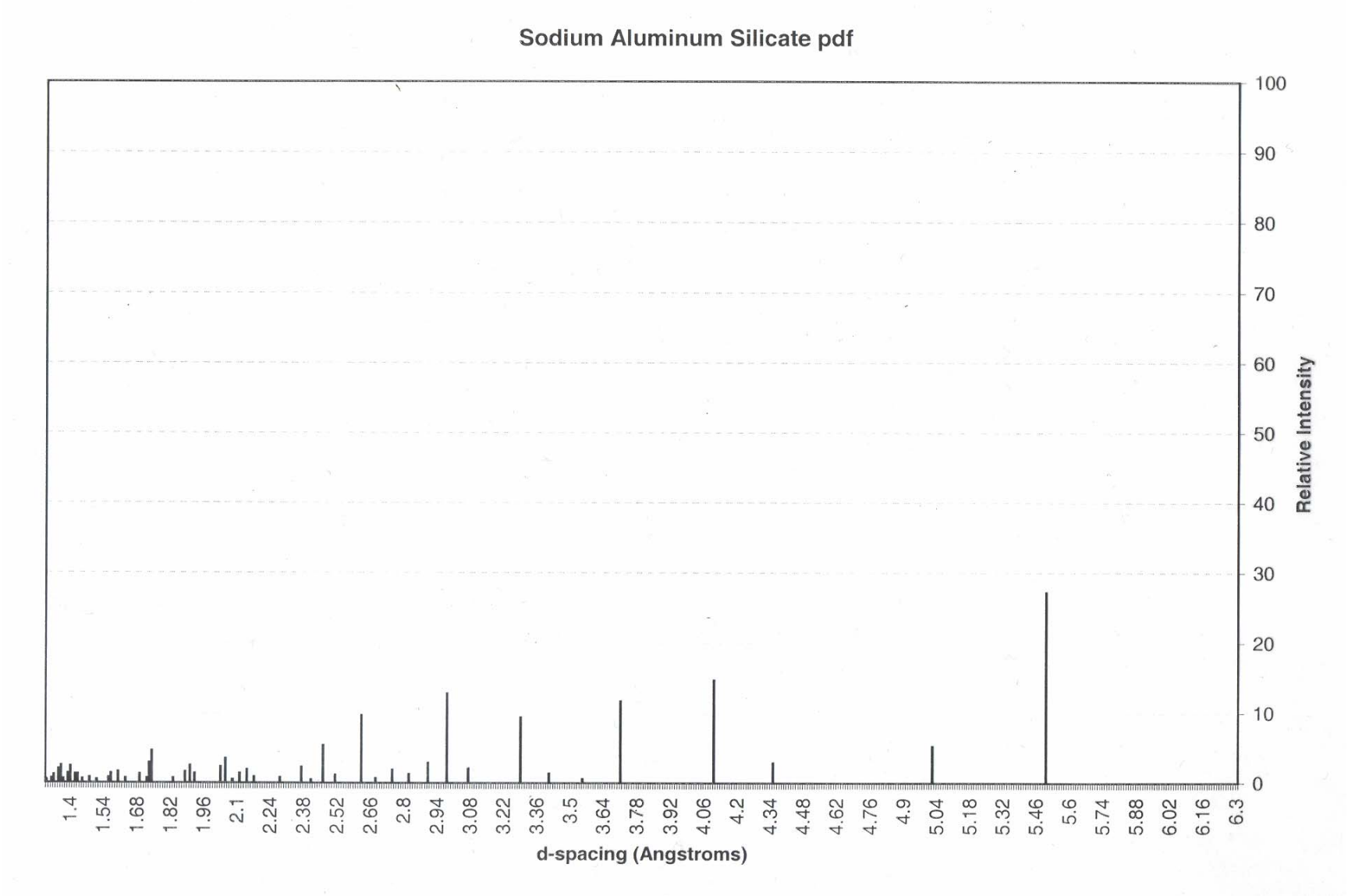
Sodium Aluminum Silicate pdf
100
90
80
70
60
50
40
30
20
10
0
Relative Intensity
1.4
1.54
1.68
1.82
1.96
2.1
2.24
2.38
2.52
2.66
2.8
2.94
3.08
3.22
3.36
3.5
3.64
3.78
3.92
4.06
4.2
4.34
4.48
4.62
4.76
4.9
5.04
5.18
5.32
5.46
5.6
5.74
5.88
6.02
6.16
6.3
d-spacing (Angstroms)

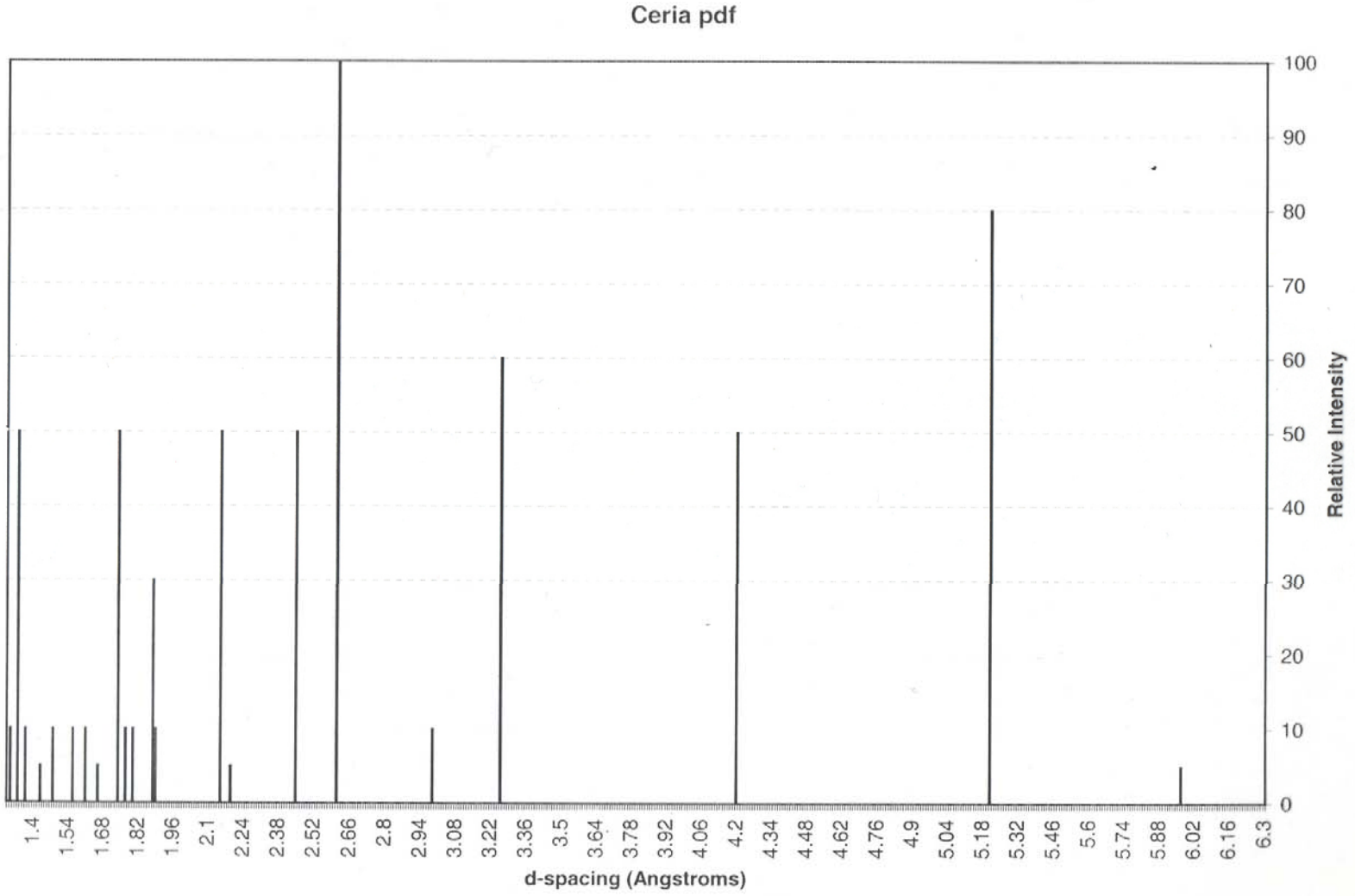
Ceria pdf
100
90
80
70
60
50
40
30
20
10
0
Relative Intensity
1.4
1.54
1.68
1.82
1.96
2.1
2.24
2.38
2.52
2.66
2.8
2.94
3.08
3.22
3.36
3.5
3.64
3.78
3.92
4.06
4.2
4.34
4.48
4.62
4.76
4.9
5.04
5.18
5.32
5.46
5.6
5.74
5.88
6.02
6.16
6.3
d-spacing (Angstroms)

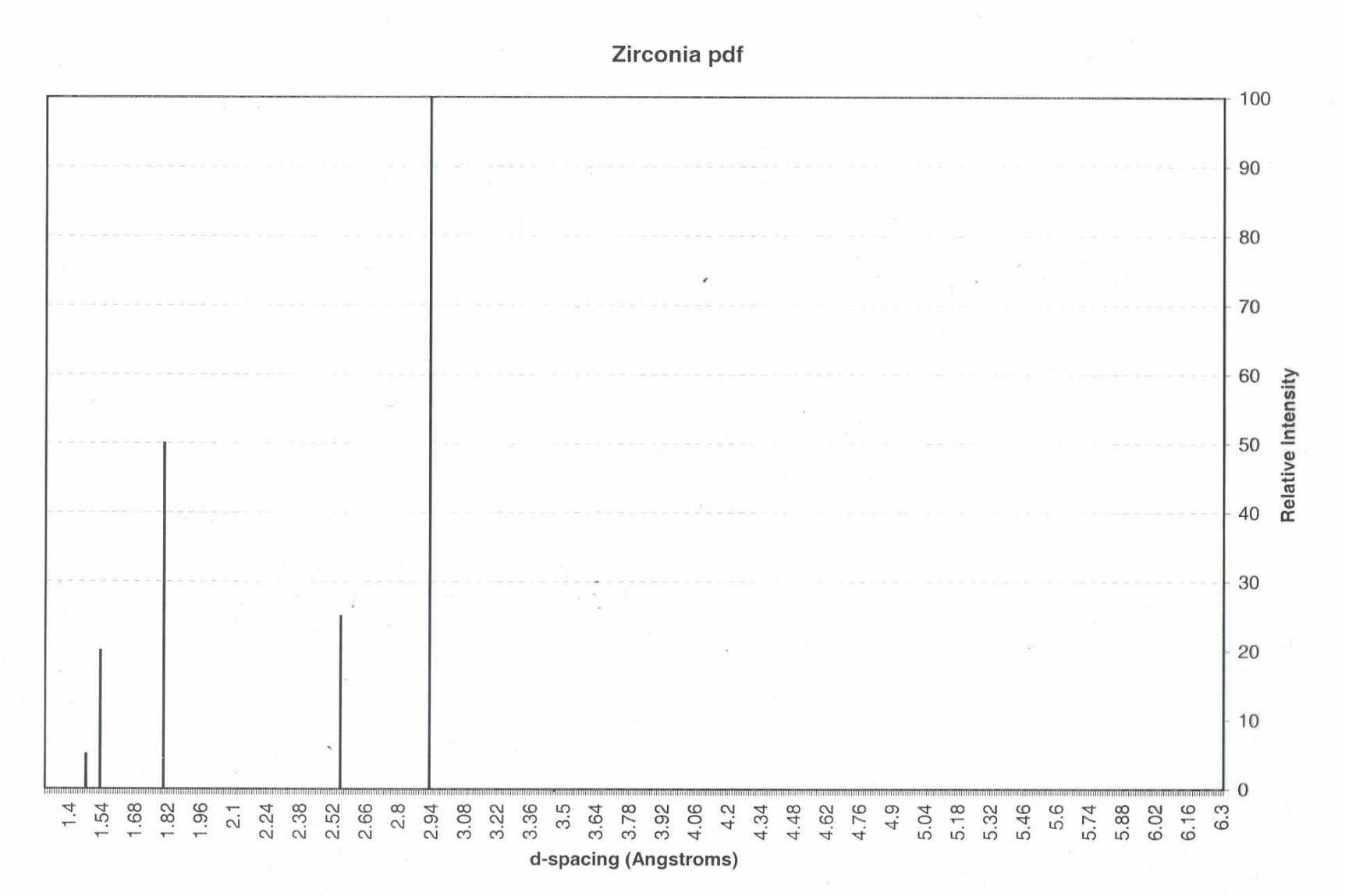
Zirconia pdf
100
90
80
70
60
50
40
30
20
10
0
Relative Intensity
1.4
1.54
1.68
1.82
1.96
2.1
2.24
2.38
2.52
2.66
2.8
2.94
3.08
3.22
3.36
3.5
3.64
3.78
3.92
4.06
4.2
4.34
4.48
4.62
4.76
4.9
5.04
5.18
5.32
5.46
5.6
5.74
5.88
6.02
6.16
6.3
d-spacing (Angstroms)

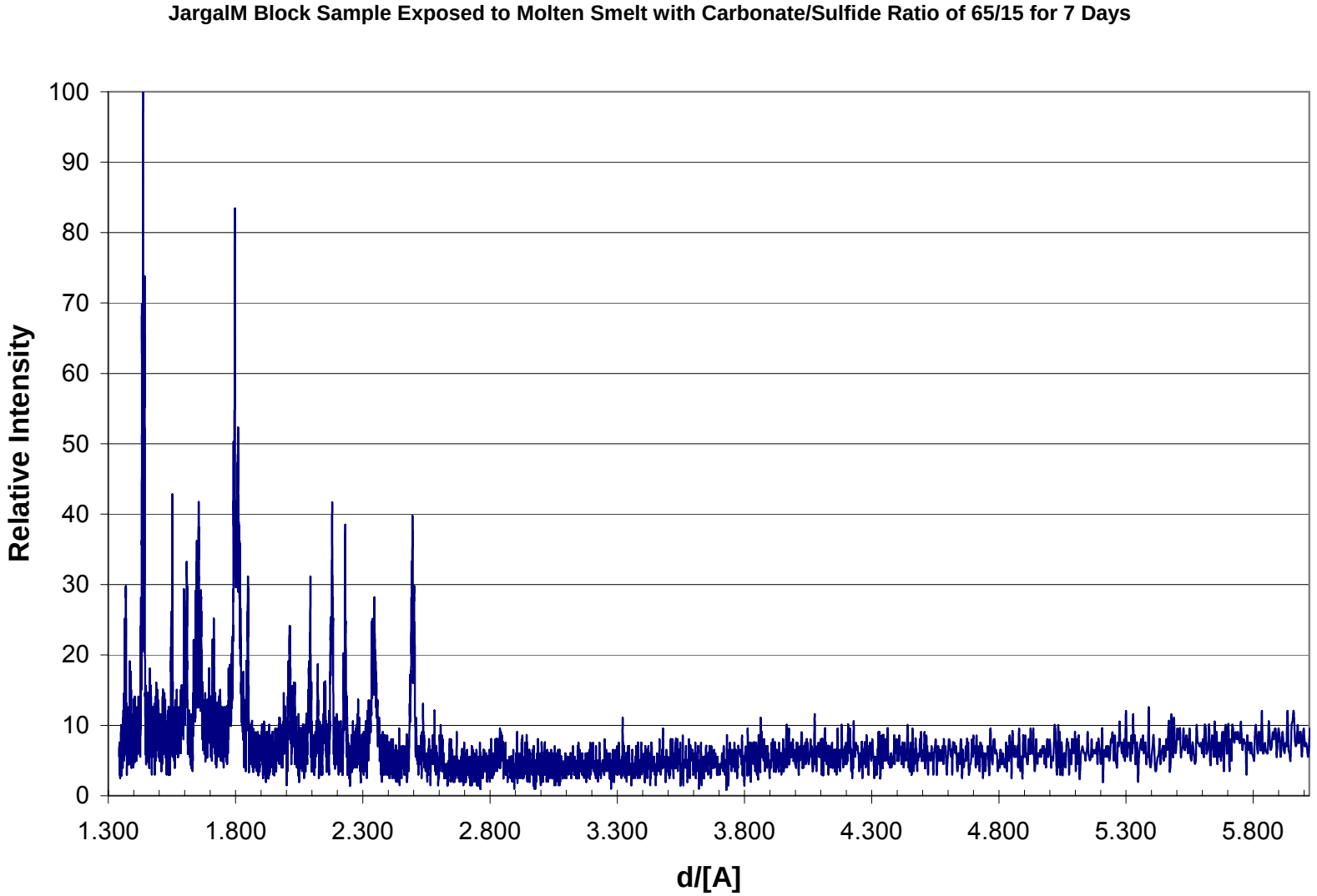
JargalM Block Sample Exposed to Molten Smelt with Carbonate/Sulfide Ratio of 65/15 for 7 Days
Relative Intensity
100
90
80
70
60
50
40
30
20
10
0
1.300
1.800
2.300
2.800
3.300
3.800
4.300
4.800
5.300
5.800
d/[A]

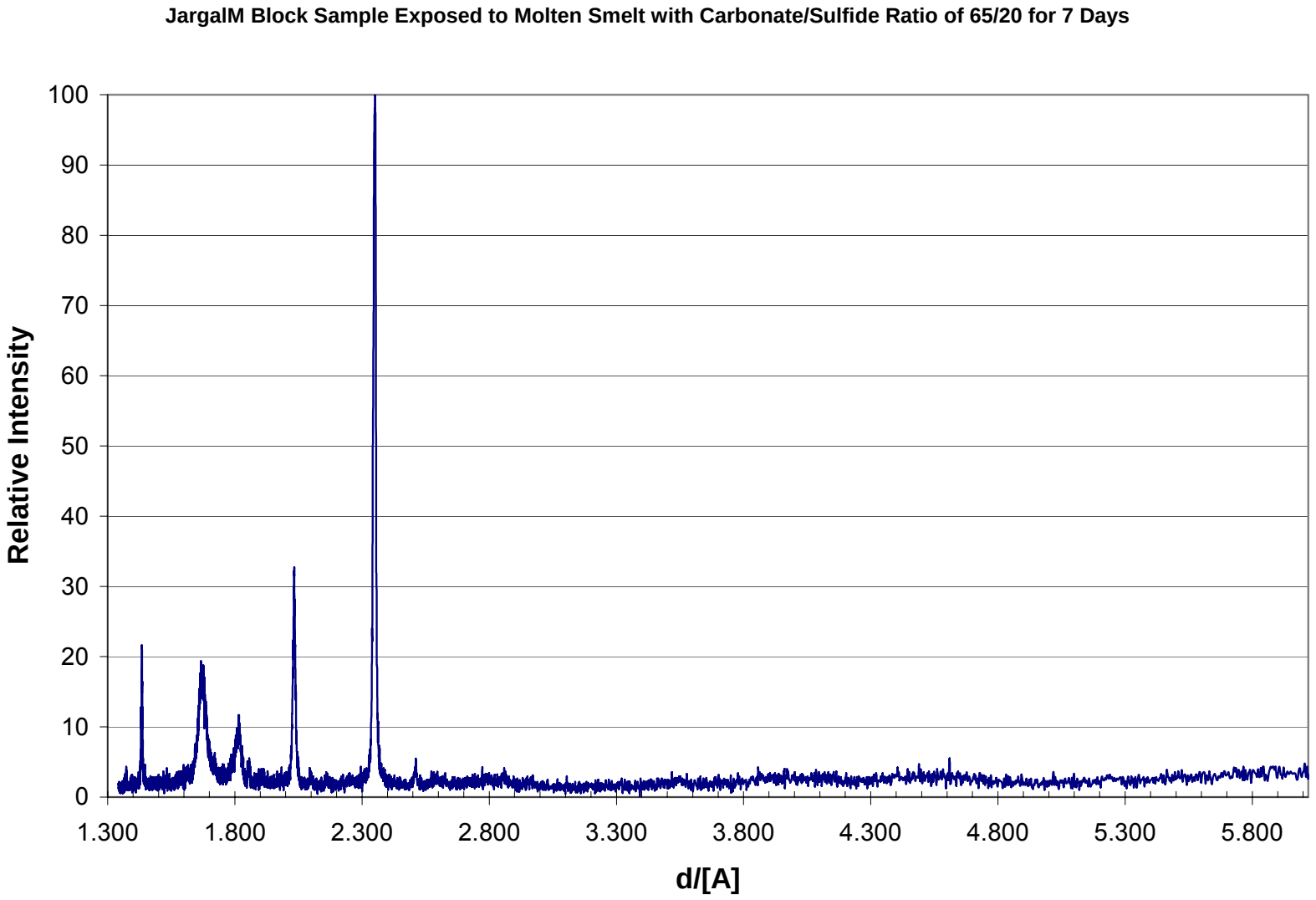
JargalM Block Sample Exposed to Molten Smelt with Carbonate/Sulfide Ratio of 65/20 for 7 Days
Relative Intensity
100
90
80
70
60
50
40
30
20
10
0
1.300
1.800
2.300
2.800
3.300
3.800
4.300
4.800
5.300
5.800
d/[A]

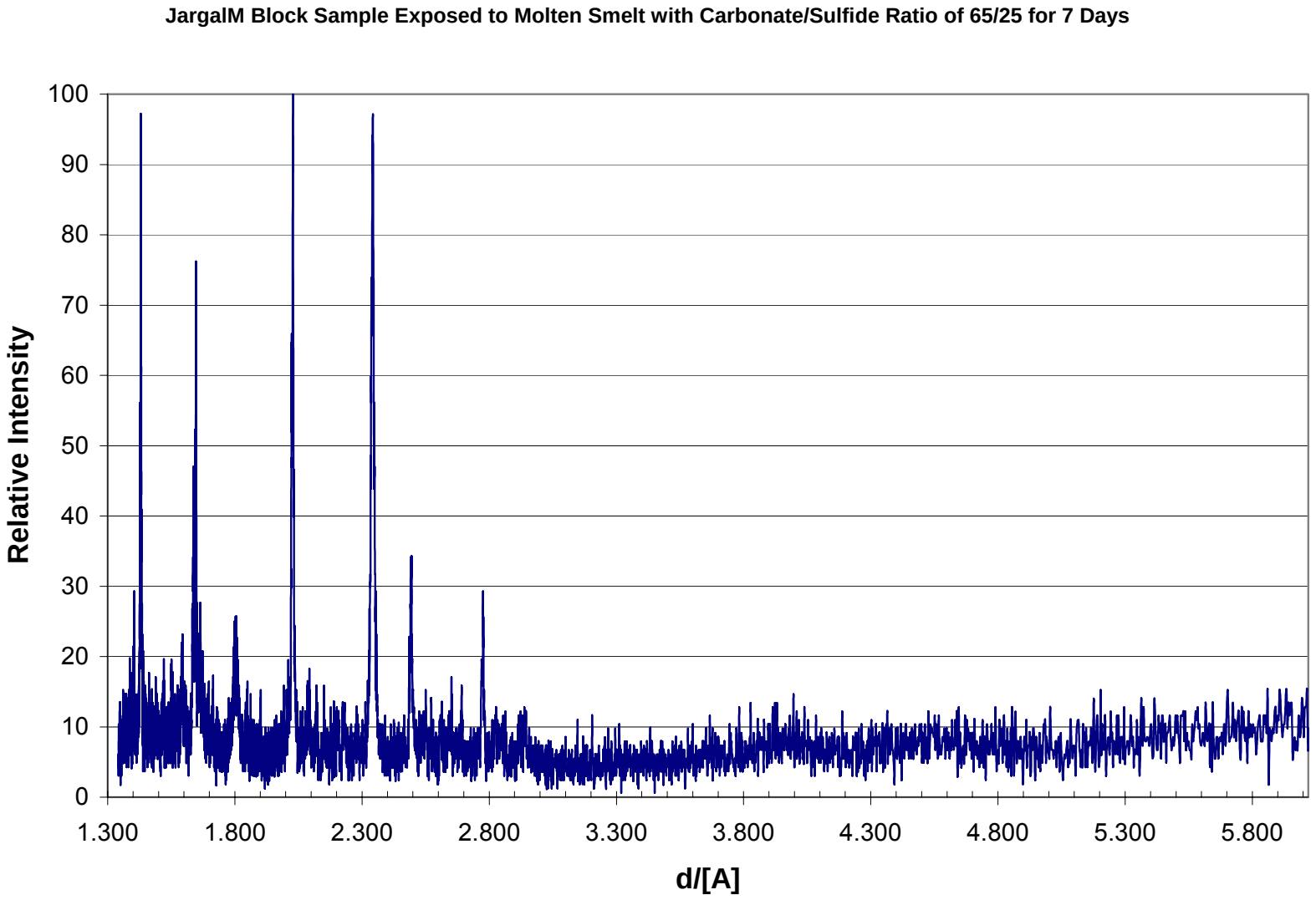
JargalM Block Sample Exposed to Molten Smelt with Carbonate/Sulfide Ratio of 65/25 for 7 Days
Relative Intensity
100
90
80
70
60
50
40
30
20
10
0
1.300
1.800
2.300
2.800
3.300
3.800
4.300
4.800
5.300
5.800
d/[A]

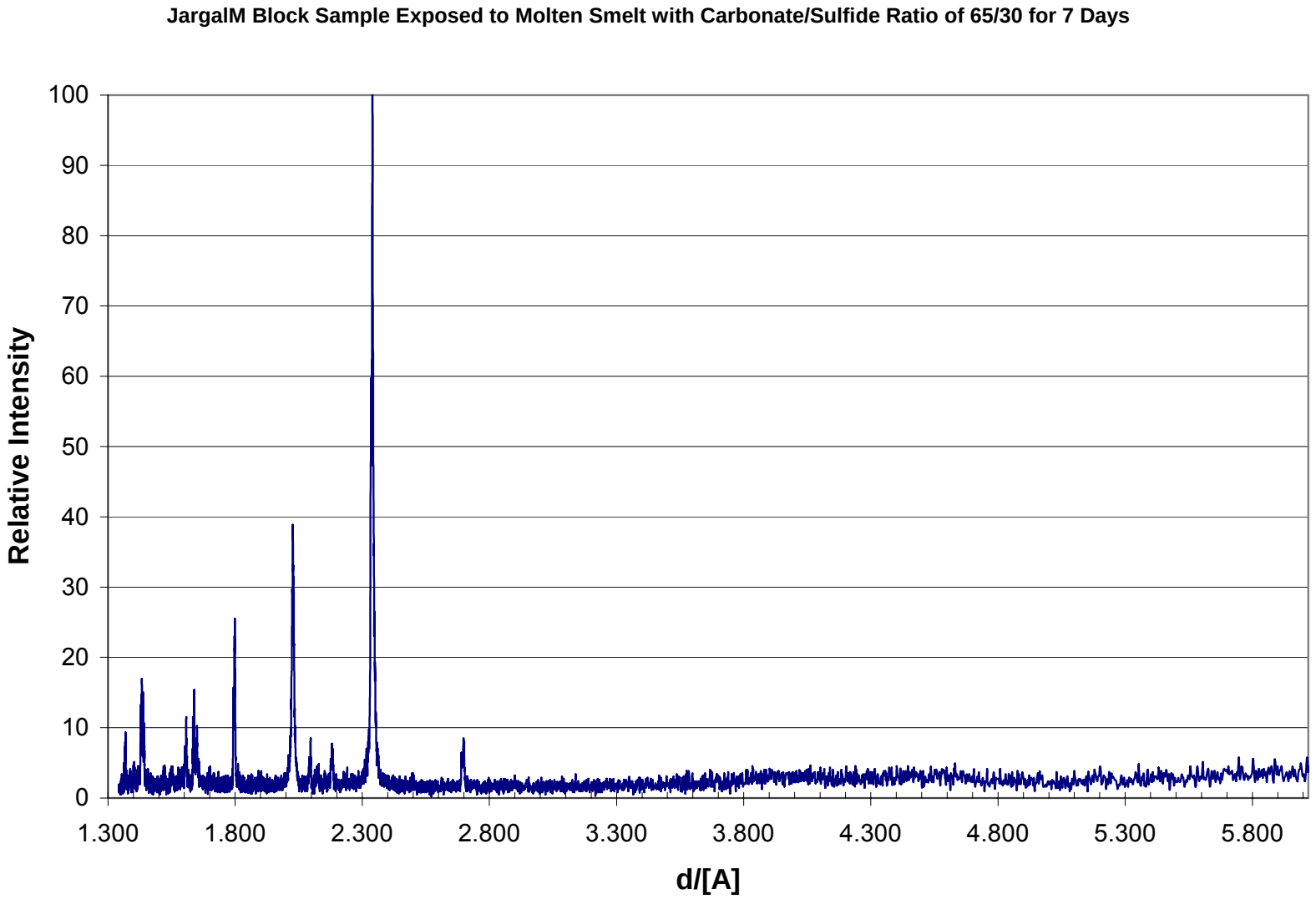
JargalM Block Sample Exposed to Molten Smelt with Carbonate/Sulfide Ratio of 65/30 for 7 Days
Relative Intensity
100
90
80
70
60
50
40
30
20
10
0
1.300
1.800
2.300
2.800
3.300
3.800
4.300
4.800
5.300
5.800
d/[A]

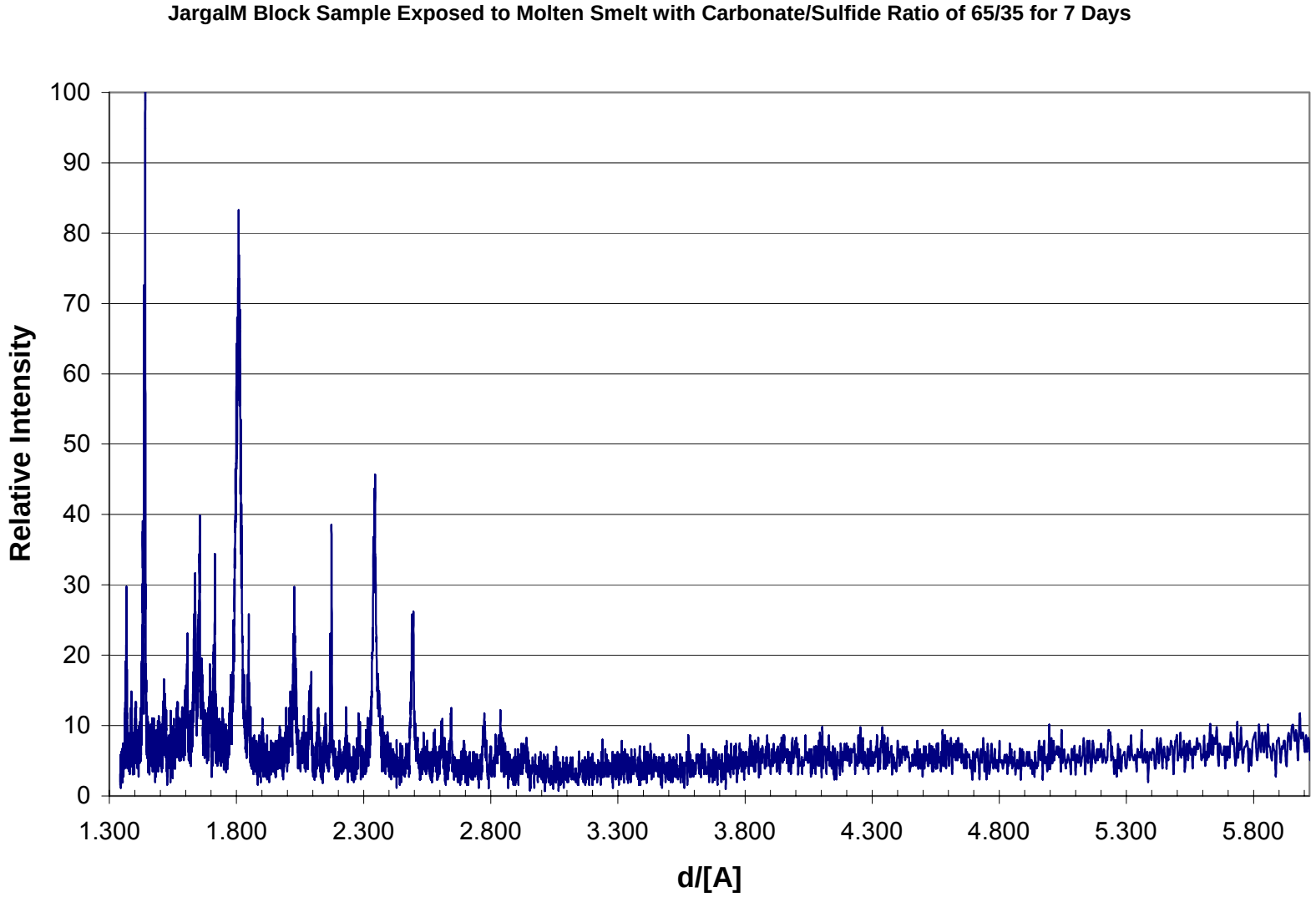
JargalM Block Sample Exposed to Molten Smelt with Carbonate/Sulfide Ratio of 65/35 for 7 Days
Relative Intensity
100
90
80
70
60
50
40
30
20
10
0
1.300
1.800
2.300
2.800
3.300
3.800
4.300
4.800
5.300
5.800
d/[A]

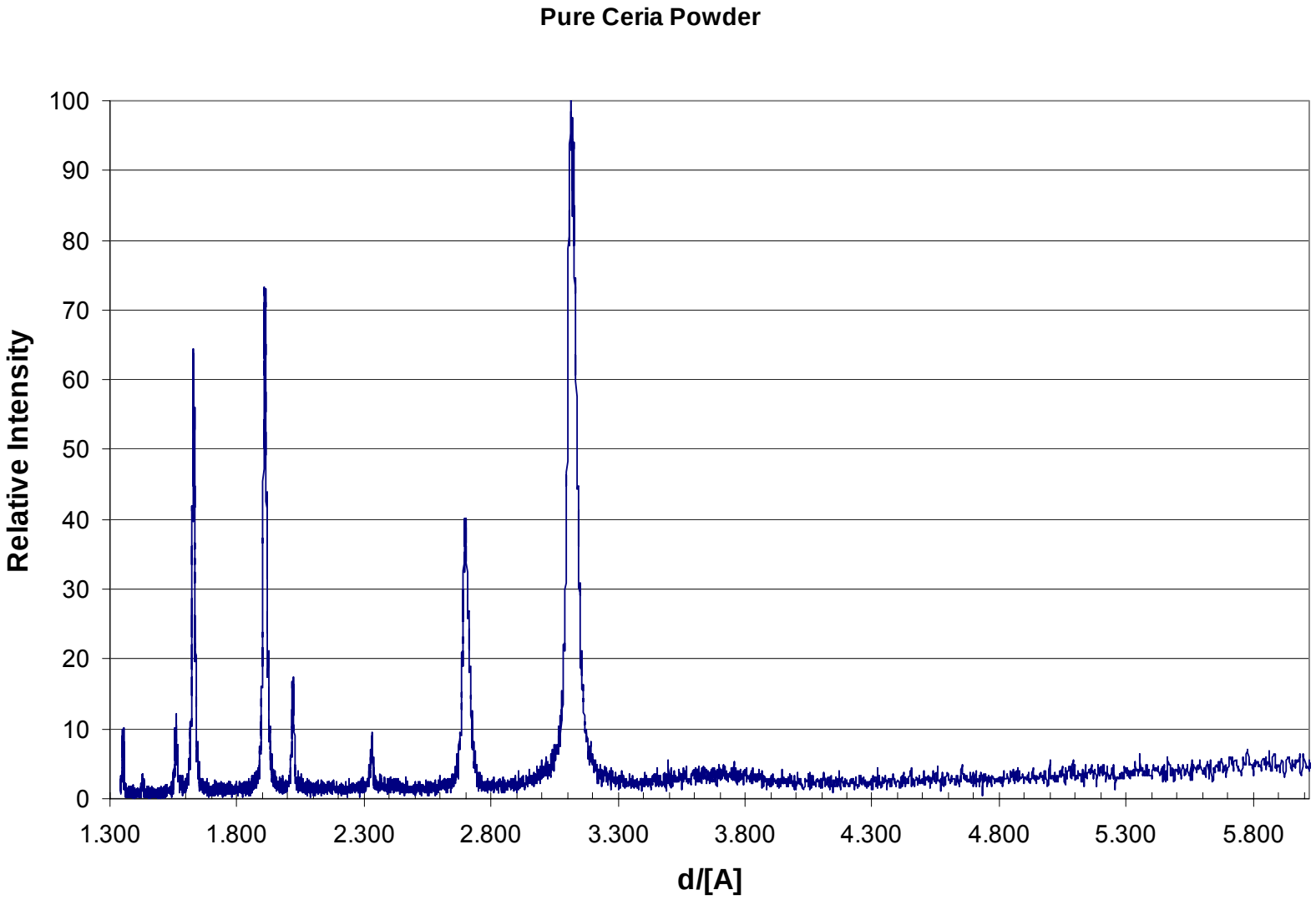
Pure Ceria Powder
Relative Intensity
100
90
80
70
60
50
40
30
20
10
0
1.300
1.800
2.300
2.800
3.300
3.800
4.300
4.800
5.300
5.800
d/[A]

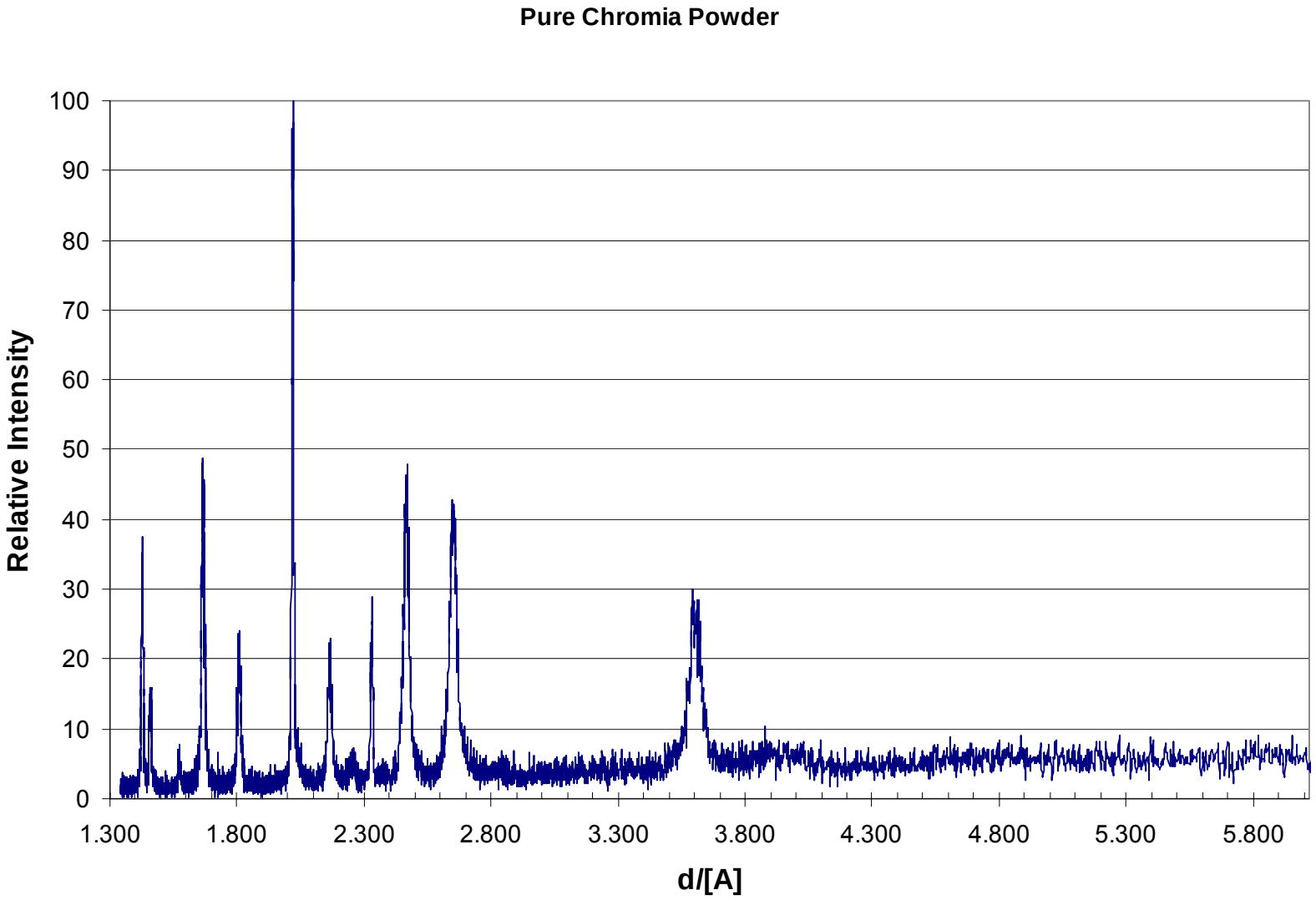
Pure Chromia Powder
Relative Intensity
100
90
80
70
60
50
40
30
20
10
0
1.300
1.800
2.300
2.800
3.300
3.800
4.300
4.800
5.300
5.800
d/[A]

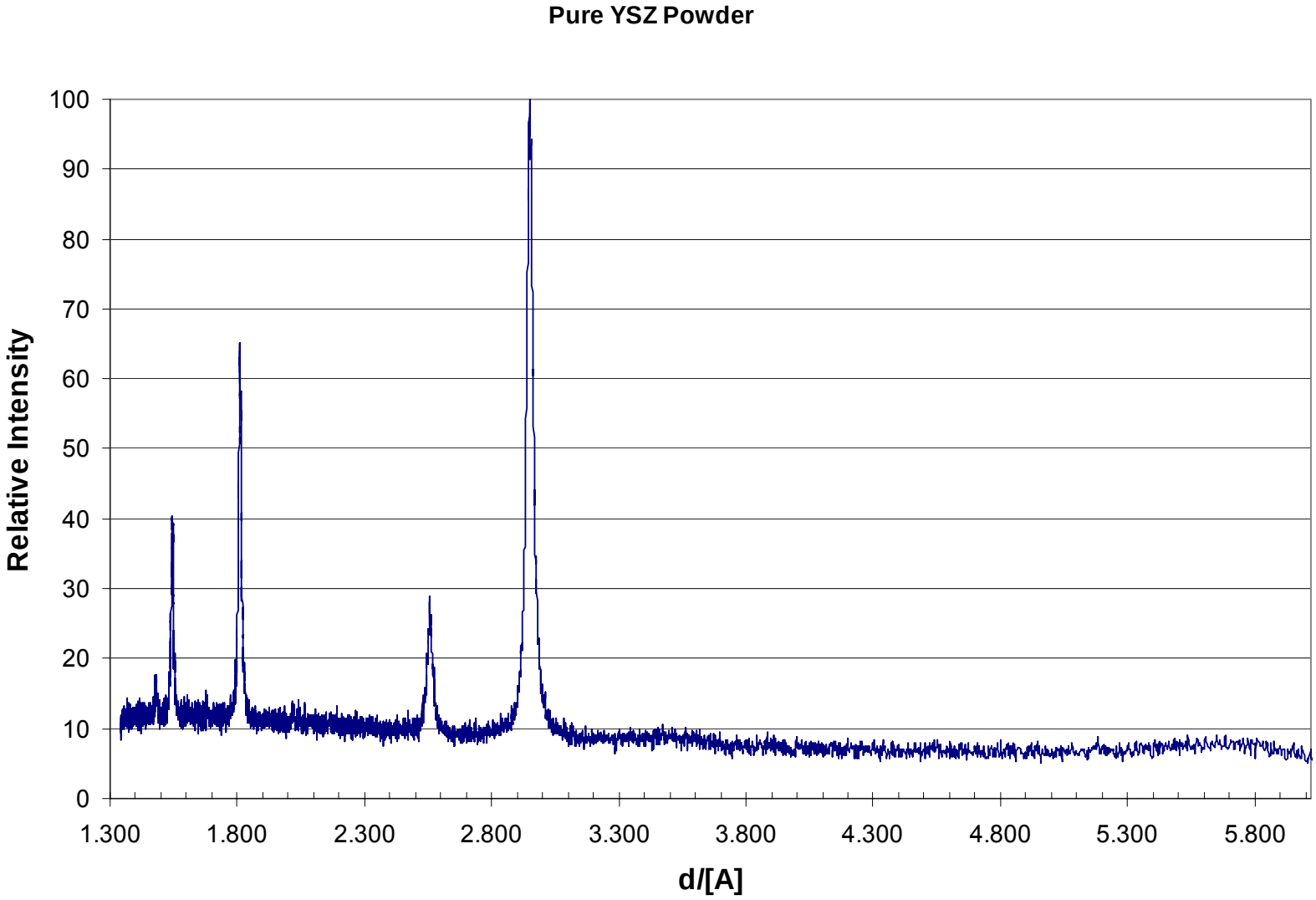
Pure YSZ Powder
Relative Intensity
100
90
80
70
60
50
40
30
20
10
0
1.300
1.800
2.300
2.800
3.300
3.800
4.300
4.800
5.300
5.800
d/[A]

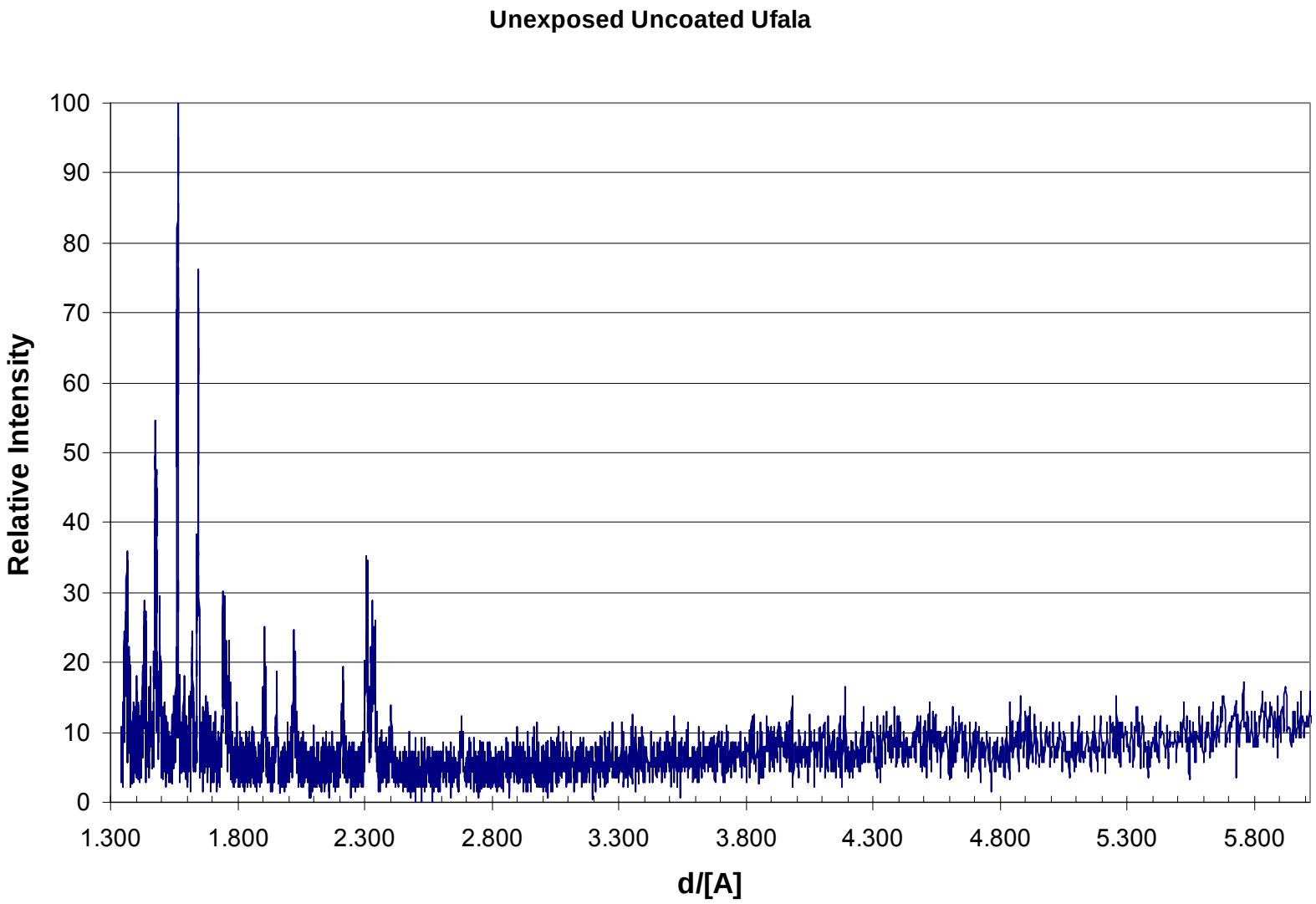
Unexposed Uncoated Ufala
Relative Intensity
100
90
80
70
60
50
40
30
20
10
0
1.300
1.800
2.300
2.800
3.300
3.800
4.300
4.800
5.300
5.800
d/[A]

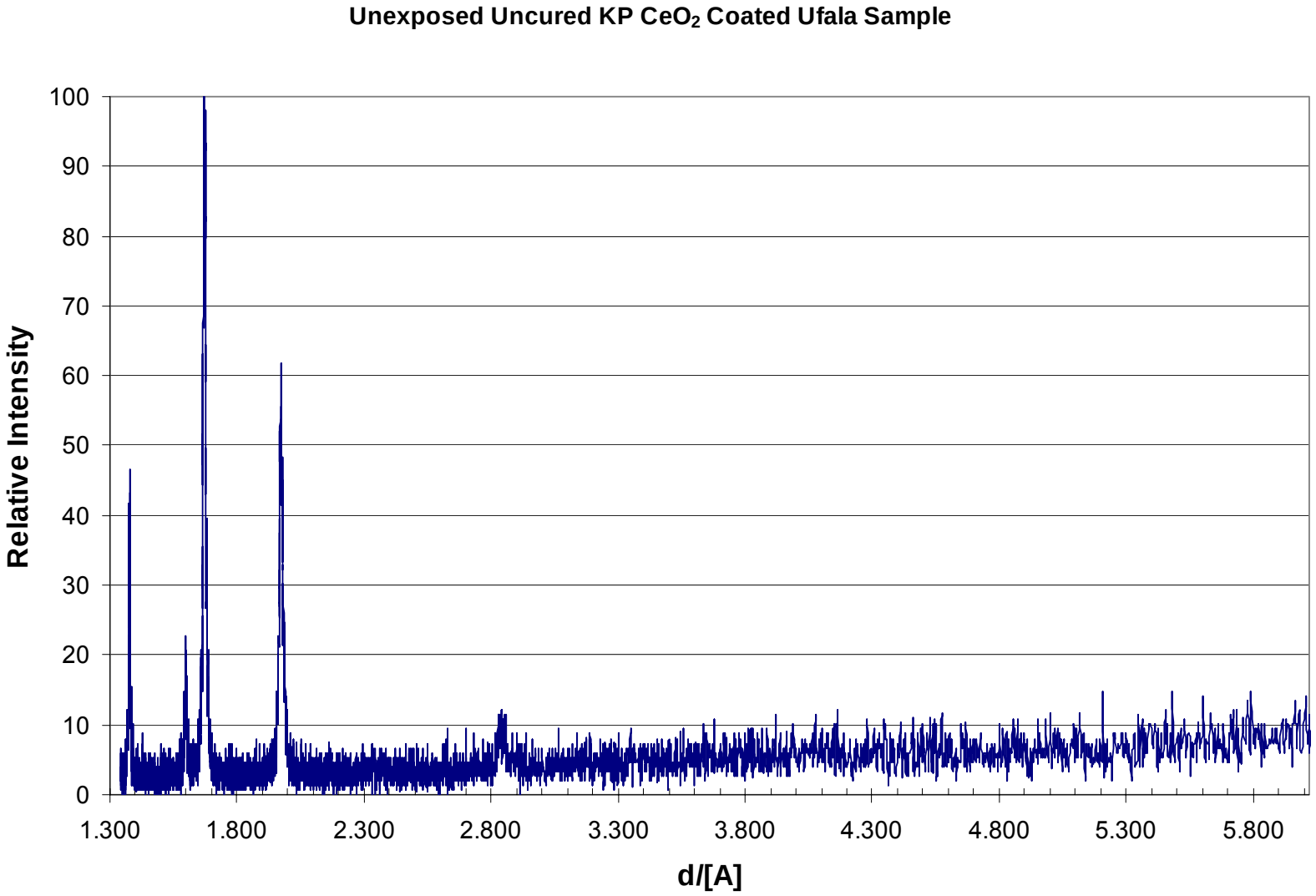
Unexposed Uncured KP CeO2 Coated Ufala Sample
Relative Intensity
100
90
80
70
60
50
40
30
20
10
0
1.300
1.800
2.300
2.800
3.300
3.800
4.300
4.800
5.300
5.800
d/[A]

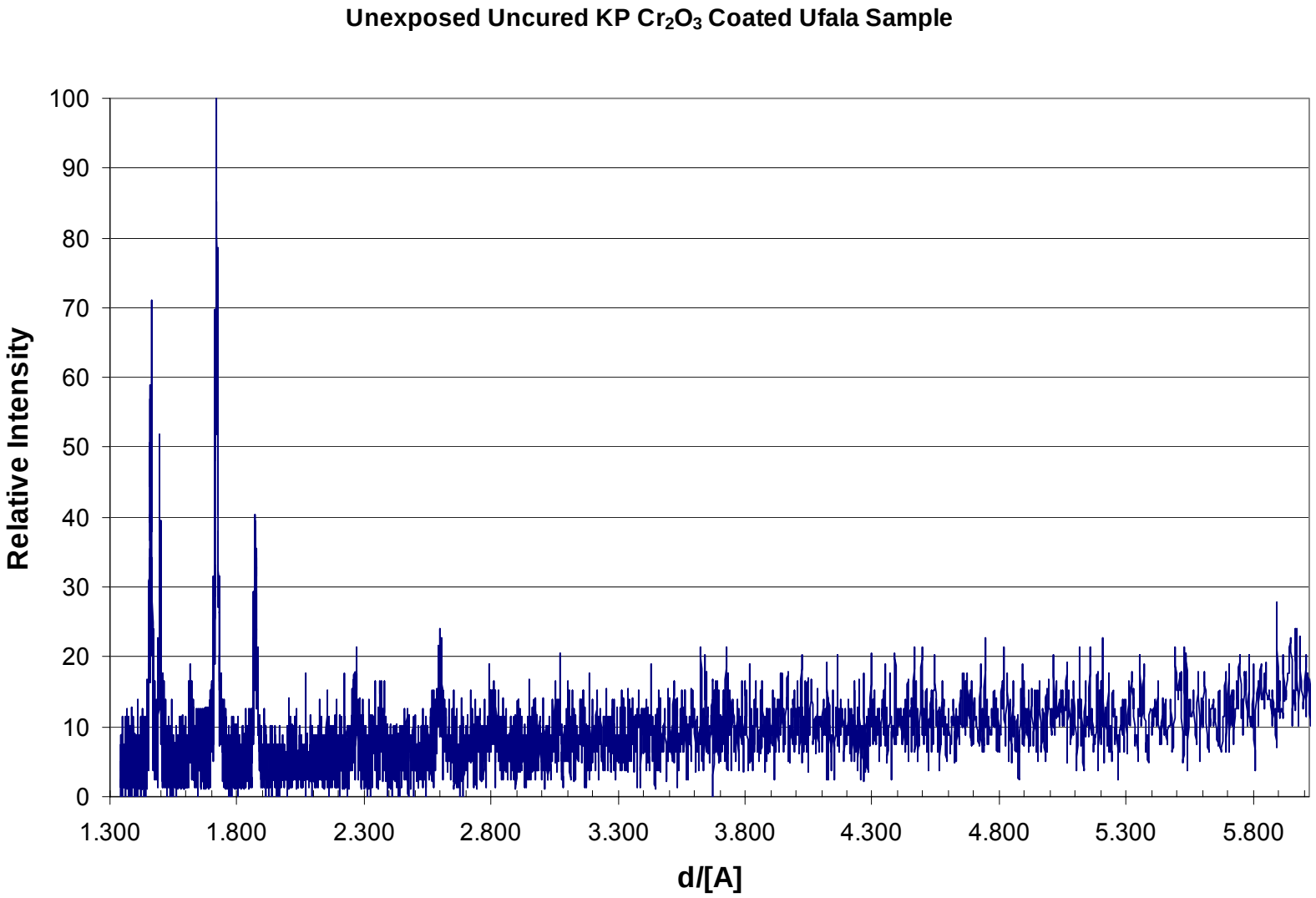
Unexposed Uncured KP Cr_2O_3 Coated Ufala Sample
Relative Intensity
100
90
80
70
60
50
40
30
20
10
0
1.300
1.800
2.300
2.800
3.300
3.800
4.300
4.800
5.300
5.800
d/[A]

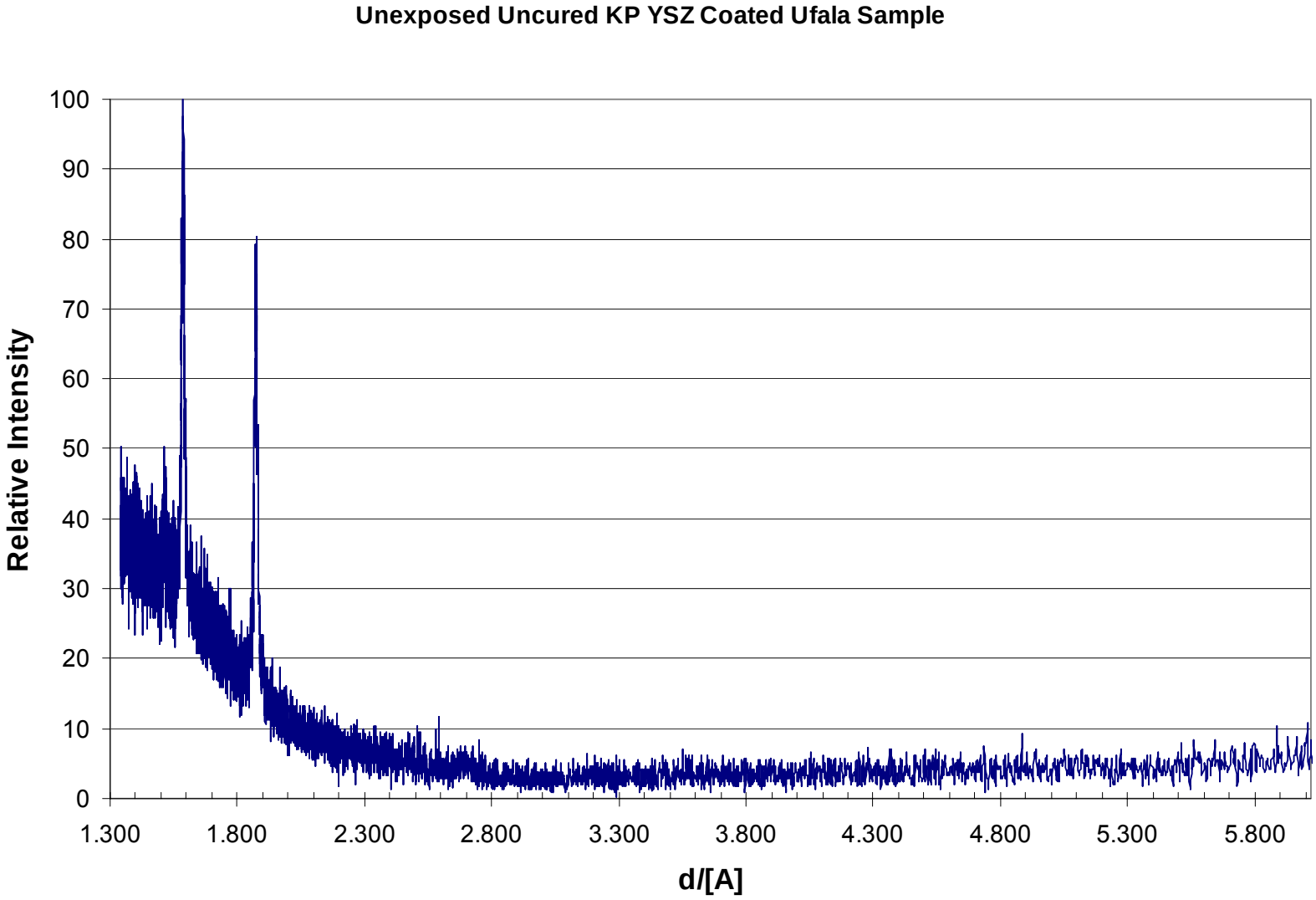
Unexposed Uncured KP YSZ Coated Ufala Sample
Relative Intensity
100
90
80
70
60
50
40
30
20
10
0
1.300
1.800
2.300
2.800
3.300
3.800
4.300
4.800
5.300
5.800
d/[A]

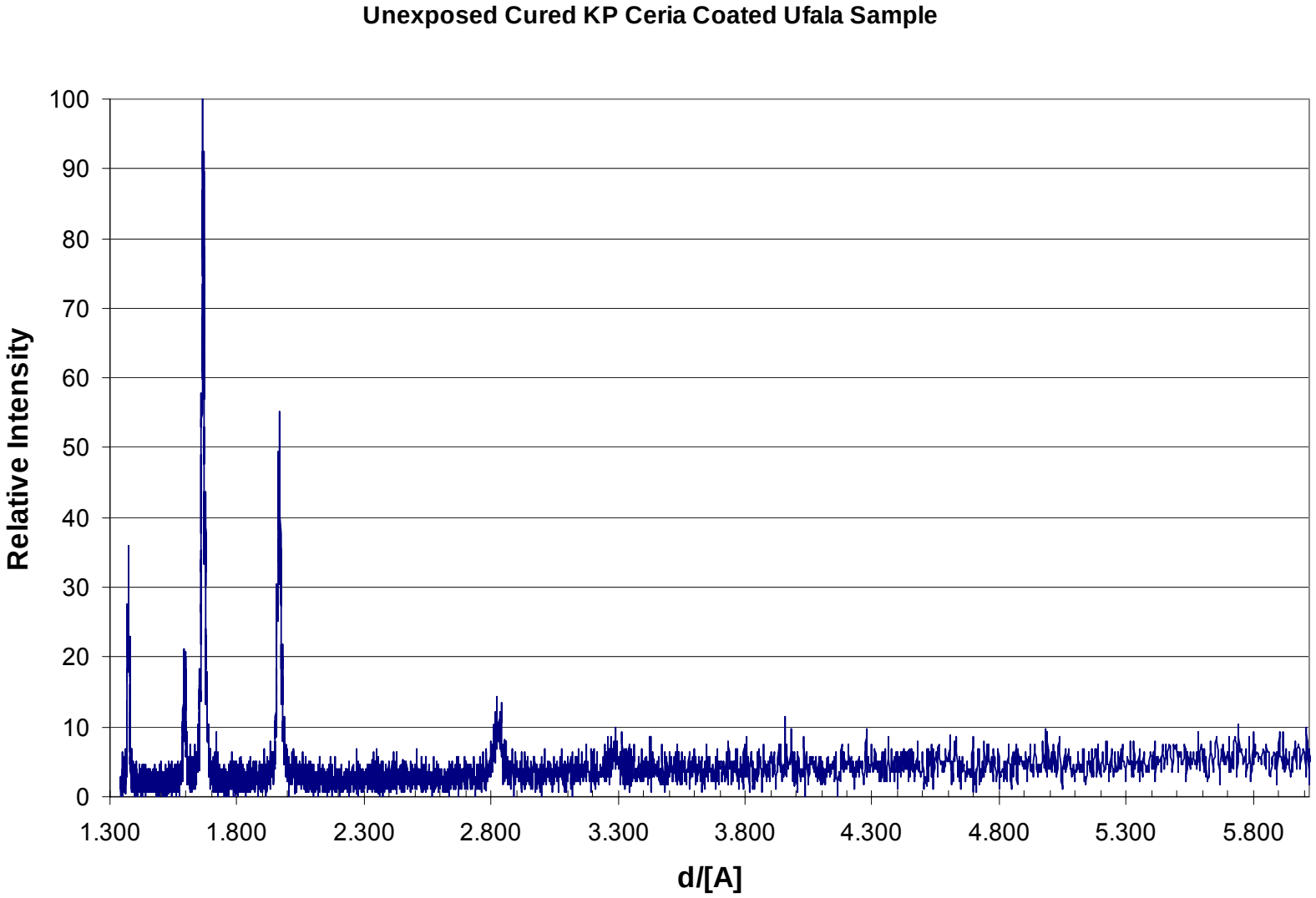
Unexposed Cured KP Ceria Coated Ufala Sample
Relative Intensity
100
90
80
70
60
50
40
30
20
10
0
1.300
1.800
2.300
2.800
3.300
3.800
4.300
4.800
5.300
5.800
d/[A]

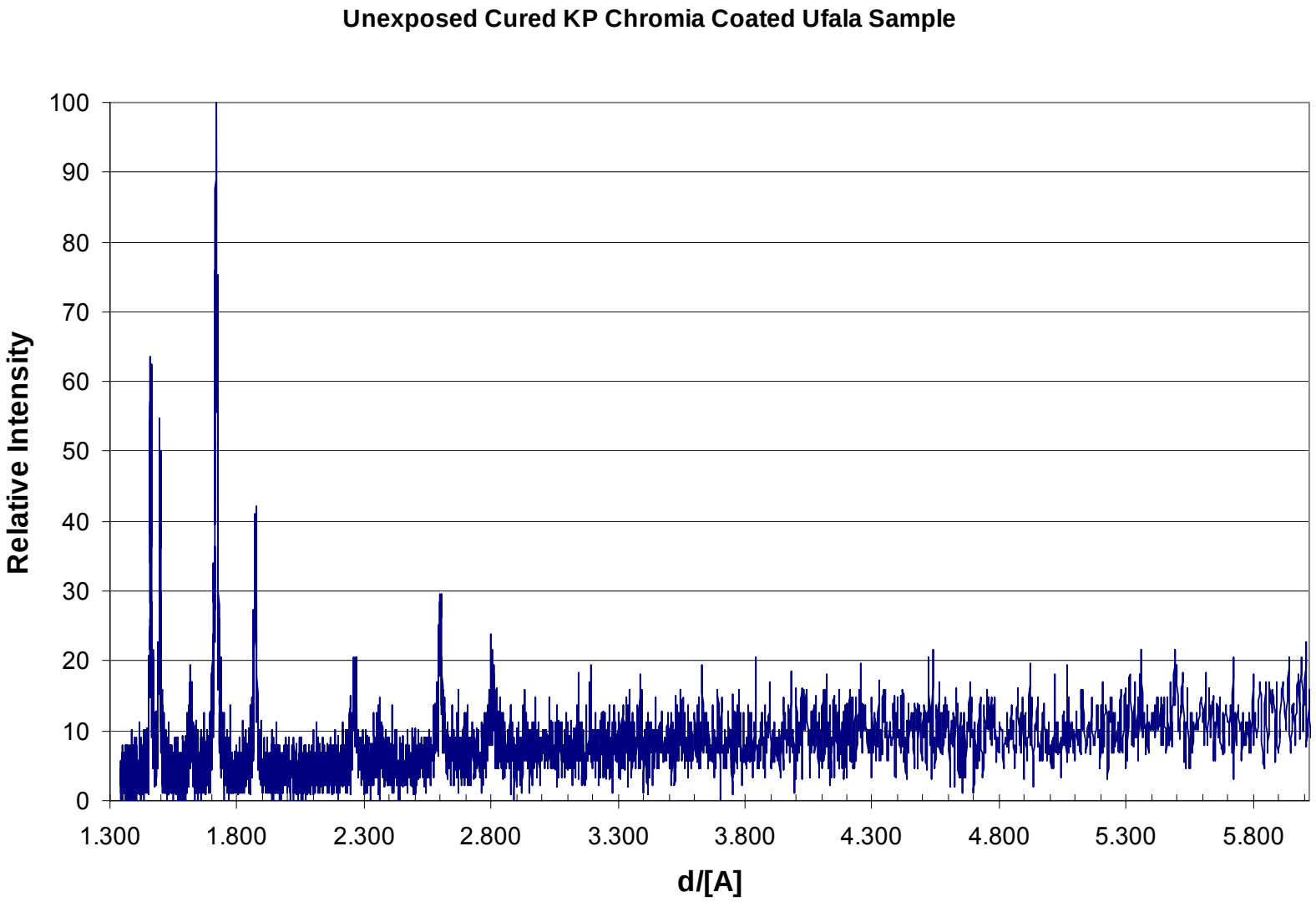
Unexposed Cured KP Chromia Coated Ufala Sample
Relative Intensity
100
90
80
70
60
50
40
30
20
10
0
1.300
1.800
2.300
2.800
3.300
3.800
4.300
4.800
5.300
5.800
d/[A]

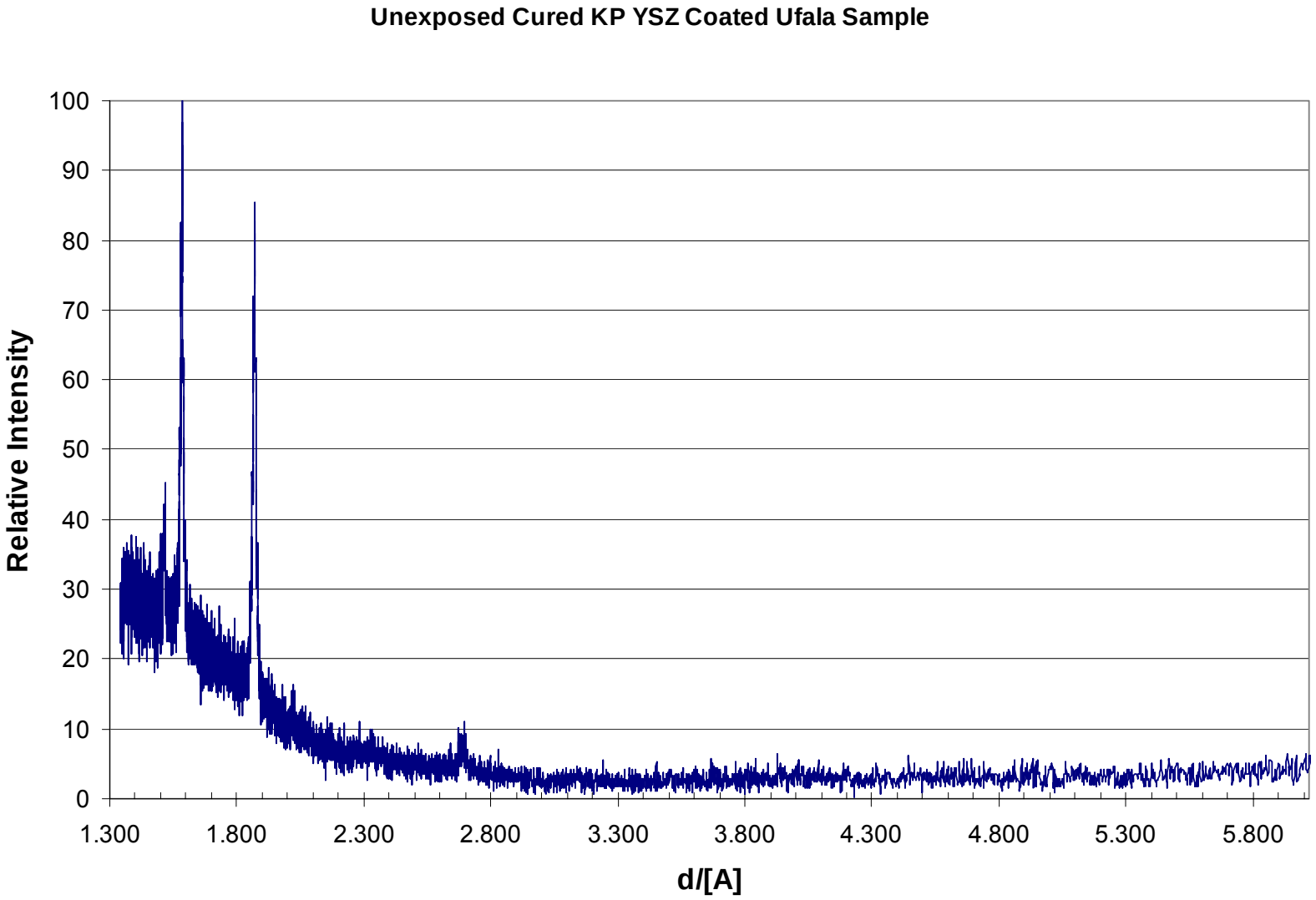
Unexposed Cured KP YSZ Coated Ufala Sample
Relative Intensity
100
90
80
70
60
50
40
30
20
10
0
1.300
1.800
2.300
2.800
3.300
3.800
4.300
4.800
5.300
5.800
d/[A]

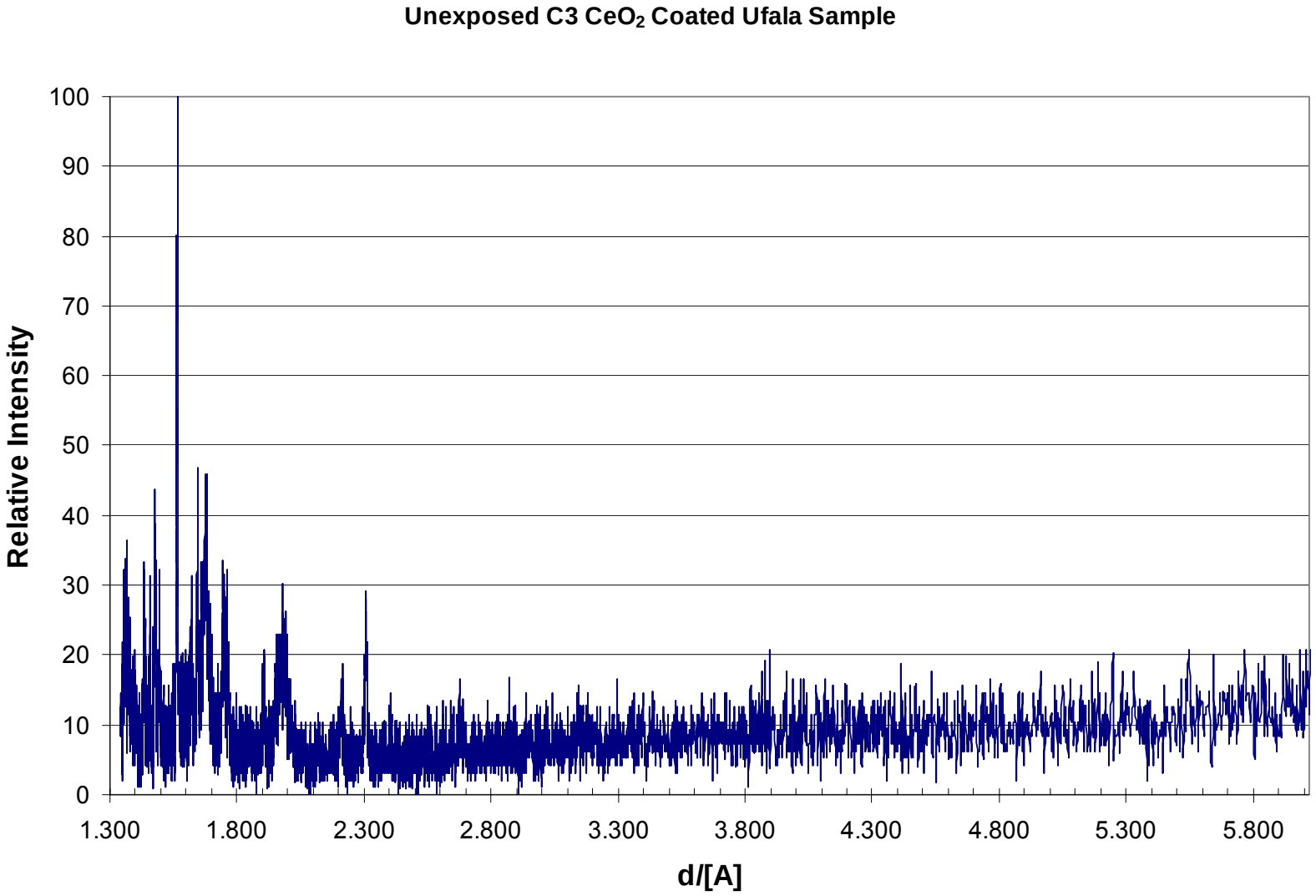
Unexposed C3 CeO2 Coated Ufala Sample
Relative Intensity
100
90
80
70
60
50
40
30
20
10
0
1.300
1.800
2.300
2.800
3.300
3.800
4.300
4.800
5.300
5.800
d/[A]

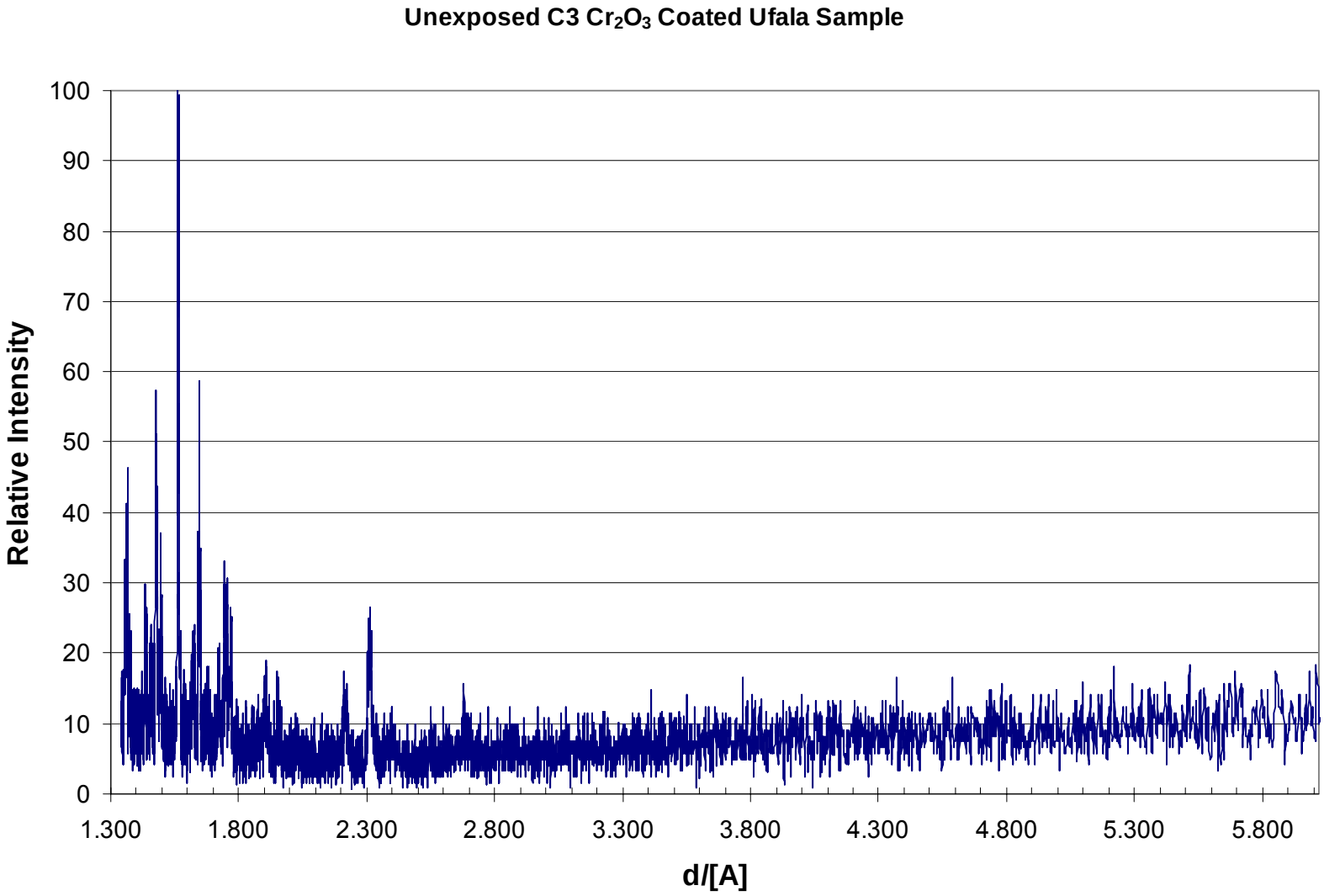
Unexposed C3 Cr_2O_3 Coated Ufala Sample
Relative Intensity
100
90
80
70
60
50
40
30
20
10
0
1.300
1.800
2.300
2.800
3.300
3.800
4.300
4.800
5.300
5.800
d/[A]

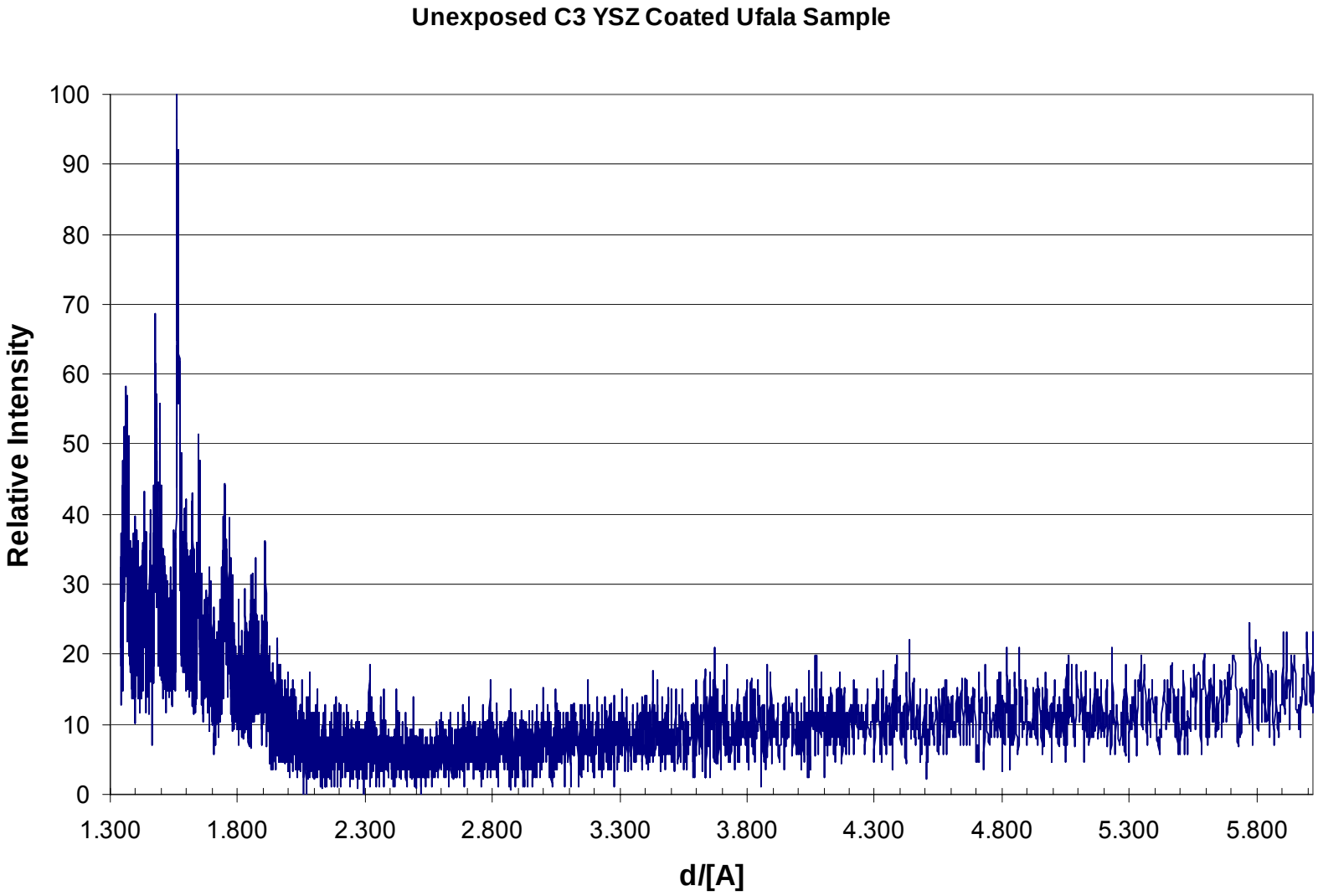
Unexposed C3 YSZ Coated Ufala Sample
Relative Intensity
100
90
80
70
60
50
40
30
20
10
0
1.300
1.800
2.300
2.800
3.300
3.800
4.300
4.800
5.300
5.800
d/[A]

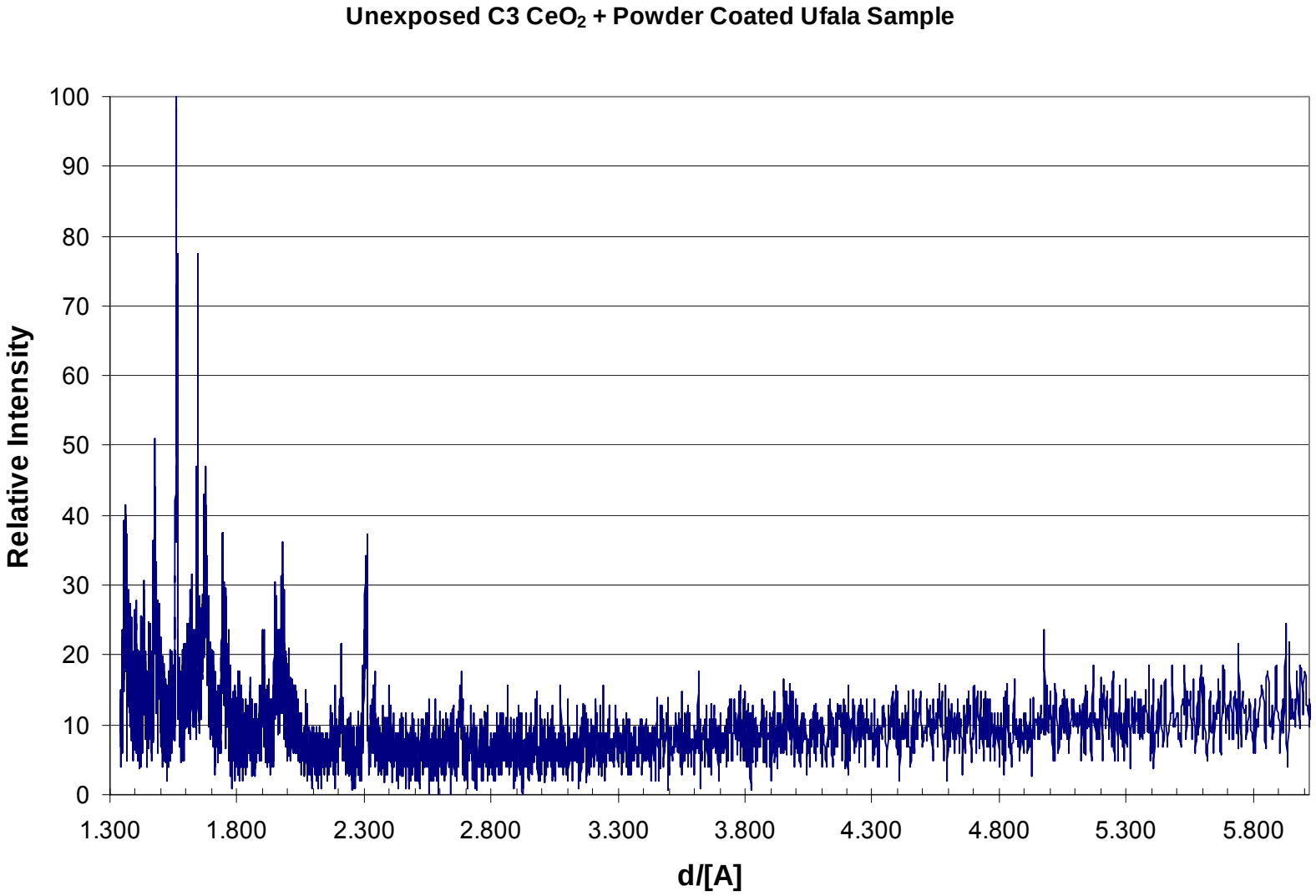
Unexposed C3 CeO2 + Powder Coated Ufala Sample
Relative Intensity
100
90
80
70
60
50
40
30
20
10
0
1.300
1.800
2.300
2.800
3.300
3.800
4.300
4.800
5.300
5.800
d/[A]

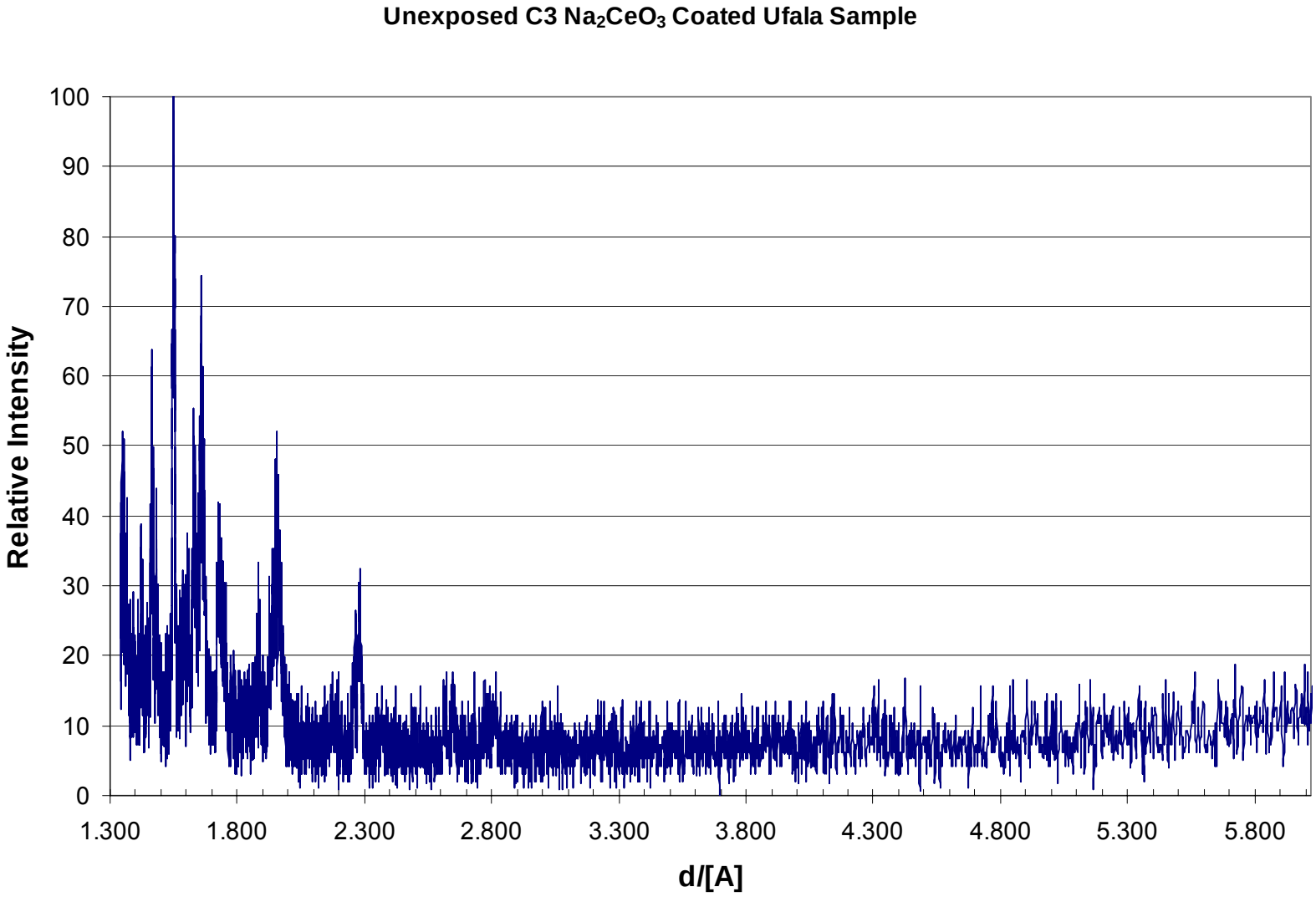
Unexposed C3 Na_2CeO_3 Coated Ufala Sample
Relative Intensity
100
90
80
70
60
50
40
30
20
10
0
1.300
1.800
2.300
2.800
3.300
3.800
4.300
4.800
5.300
5.800
d/[A]

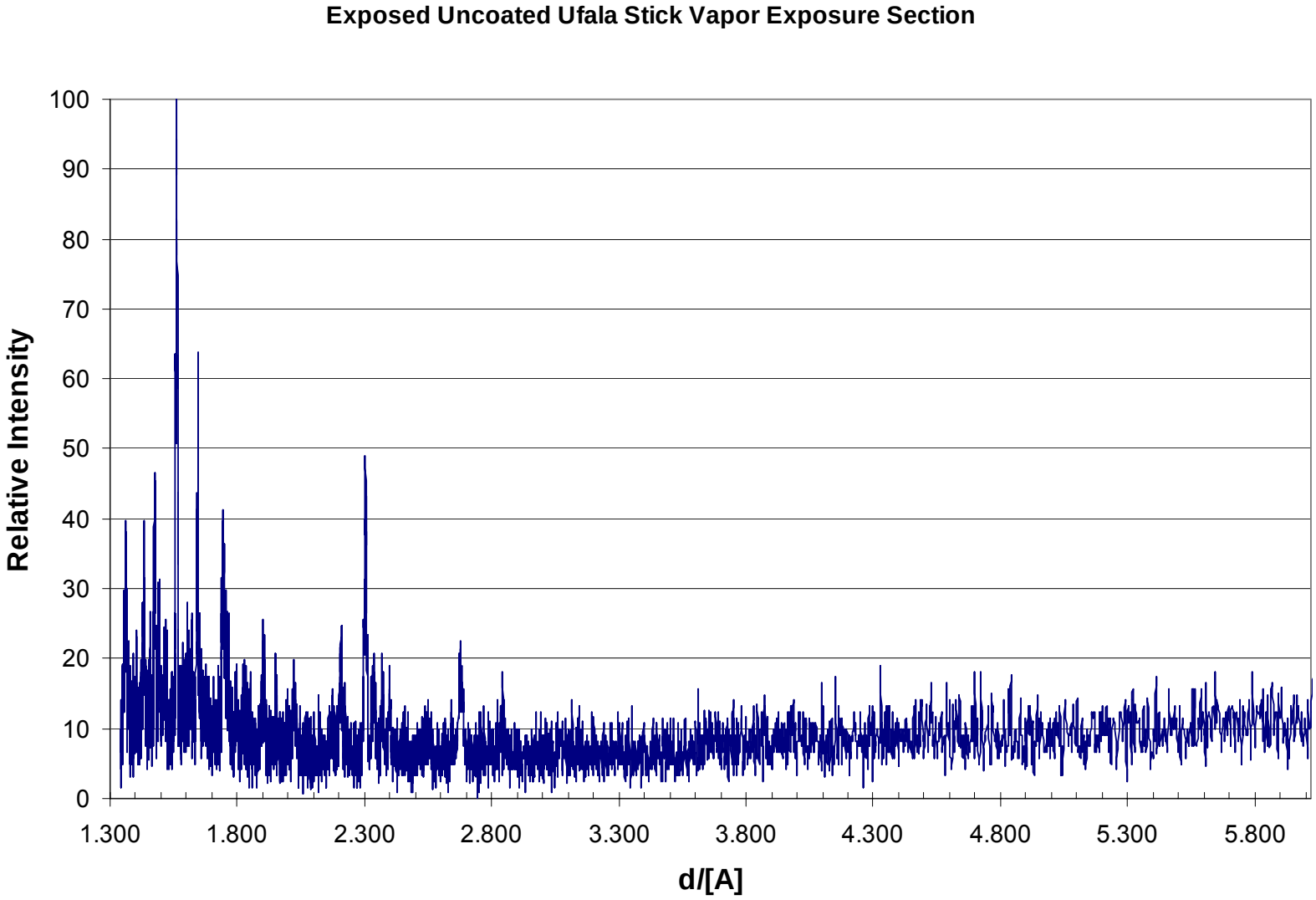
Exposed Uncoated Ufala Stick Vapor Exposure Section
Relative Intensity
100
90
80
70
60
50
40
30
20
10
0
1.300
1.800
2.300
2.800
3.300
3.800
4.300
4.800
5.300
5.800
d/[A]

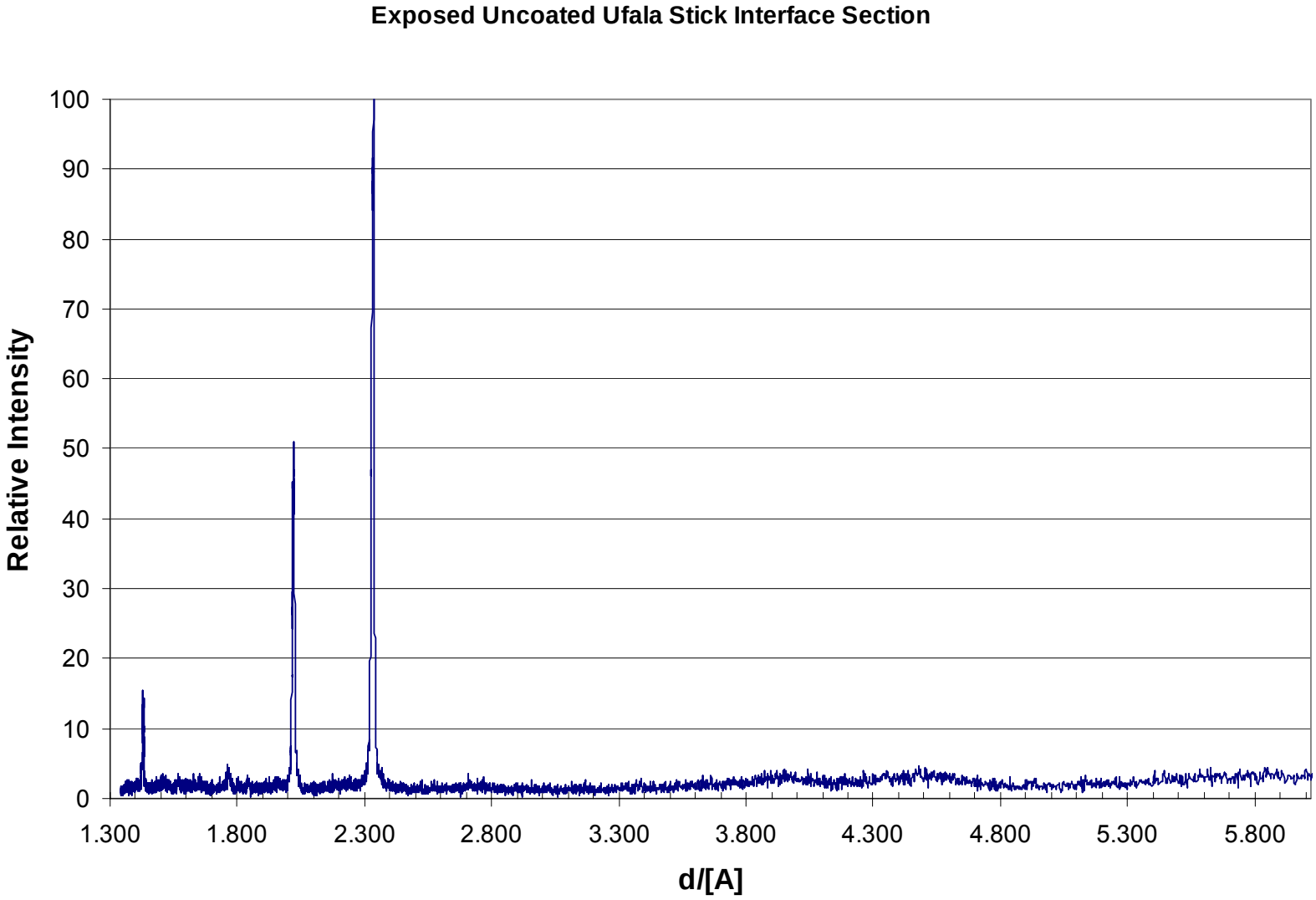
Exposed Uncoated Ufala Stick Interface Section
Relative Intensity
100
90
80
70
60
50
40
30
20
10
0
1.300
1.800
2.300
2.800
3.300
3.800
4.300
4.800
5.300
5.800
d/[A]

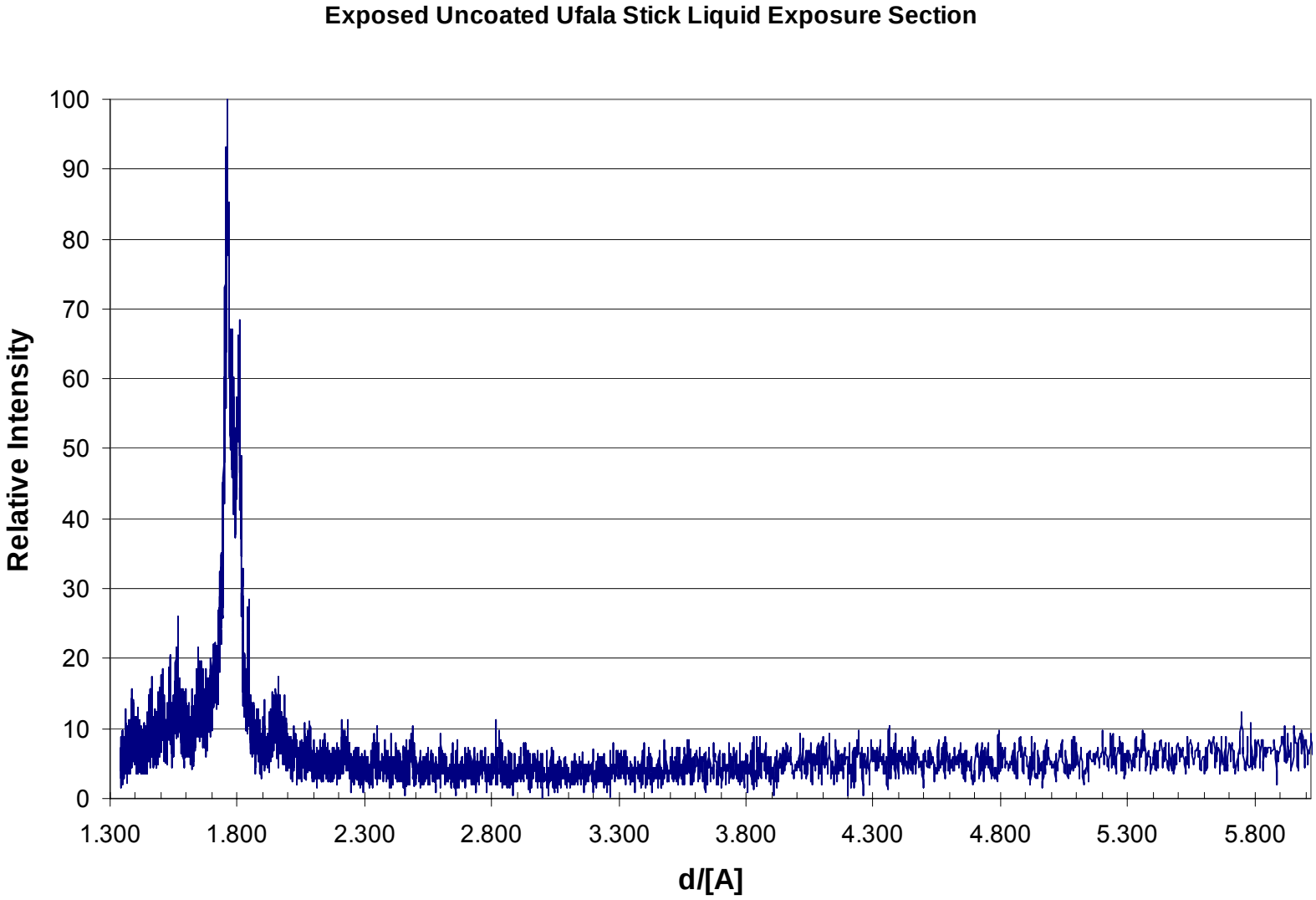
Exposed Uncoated Ufala Stick Liquid Exposure Section
Relative Intensity
100
90
80
70
60
50
40
30
20
10
0
1.300
1.800
2.300
2.800
3.300
3.800
4.300
4.800
5.300
5.800
d/[A]

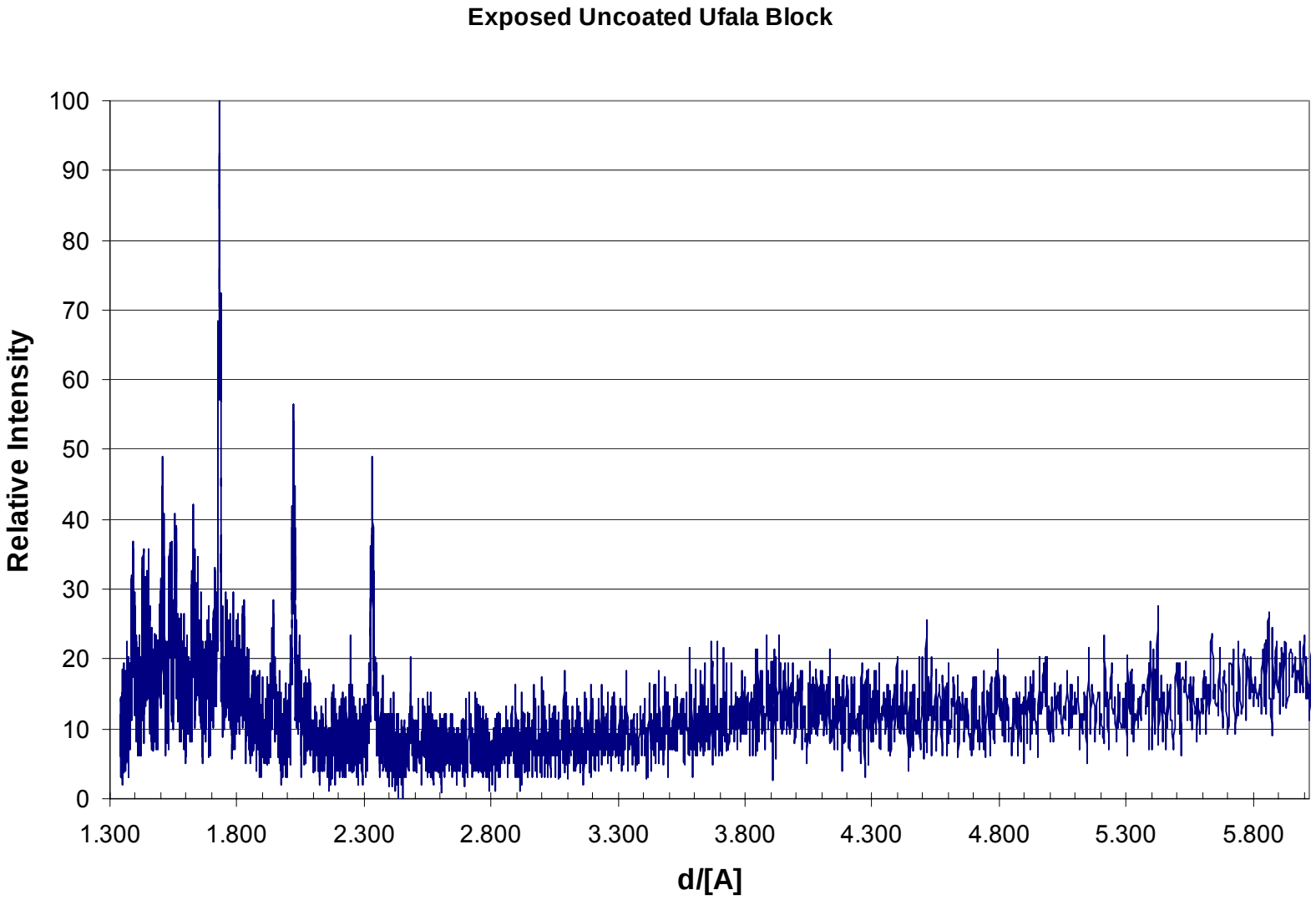
Exposed Uncoated Ufala Block
Relative Intensity
100
90
80
70
60
50
40
30
20
10
0
1.300
1.800
2.300
2.800
3.300
3.800
4.300
4.800
5.300
5.800
d/[A]

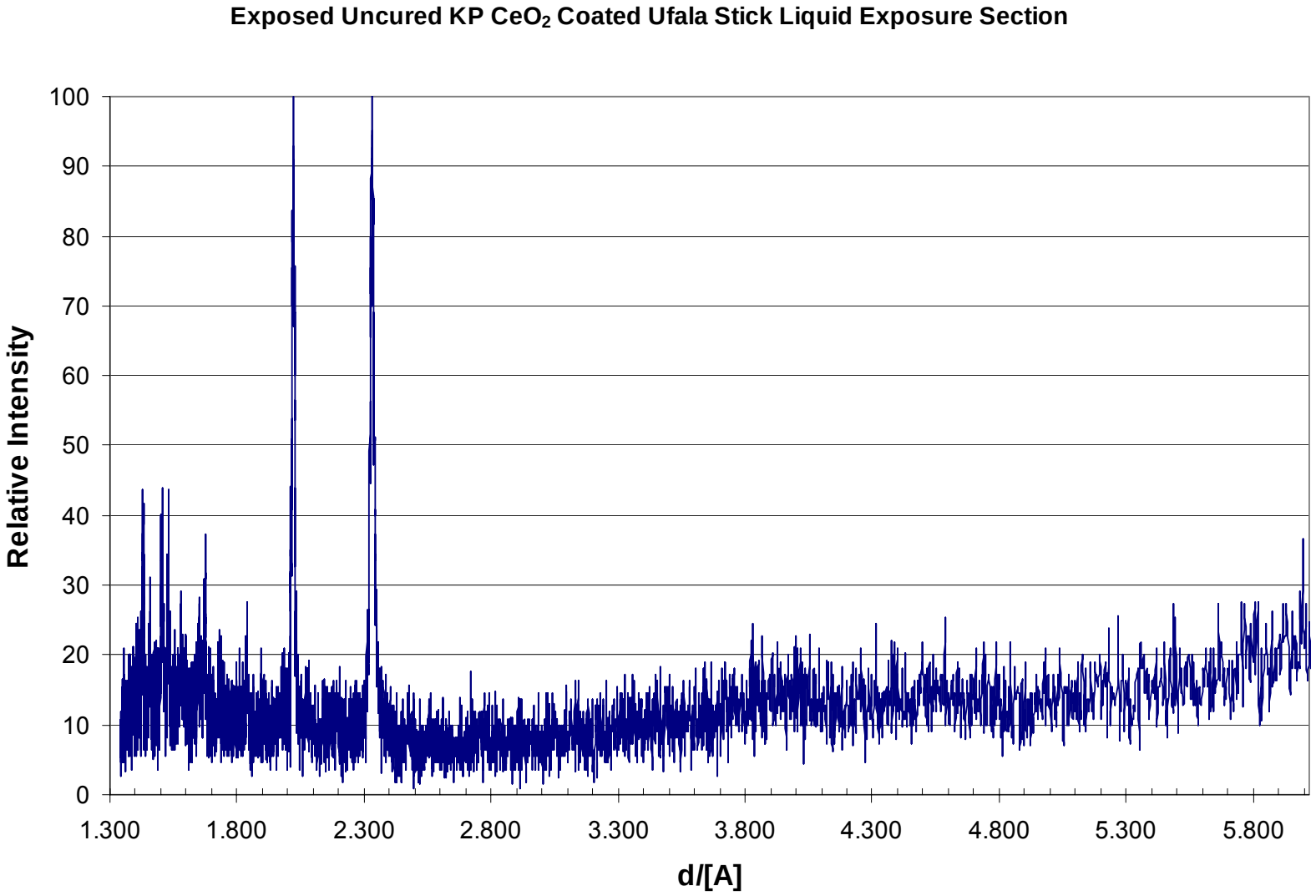
Exposed Uncured KP CeO2 Coated Ufala Stick Liquid Exposure Section
Relative Intensity
100
90
80
70
60
50
40
30
20
10
0
1.300
1.800
2.300
2.800
3.300
3.800
4.300
4.800
5.300
5.800
d/[A]

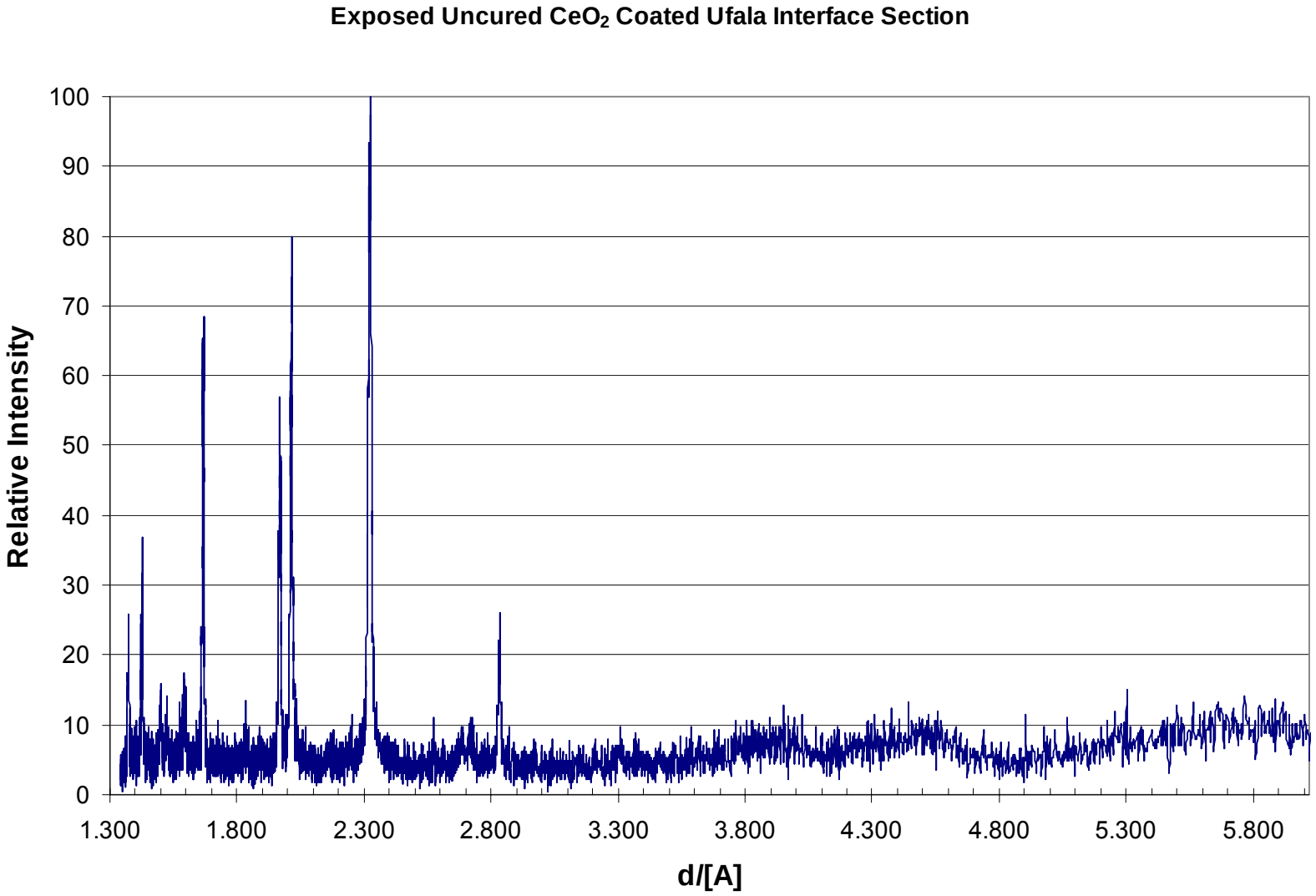
Exposed Uncured CeO2 Coated Ufala Interface Section
Relative Intensity
100
90
80
70
60
50
40
30
20
10
0
1.300
1.800
2.300
2.800
3.300
3.800
4.300
4.800
5.300
5.800
d/[A]

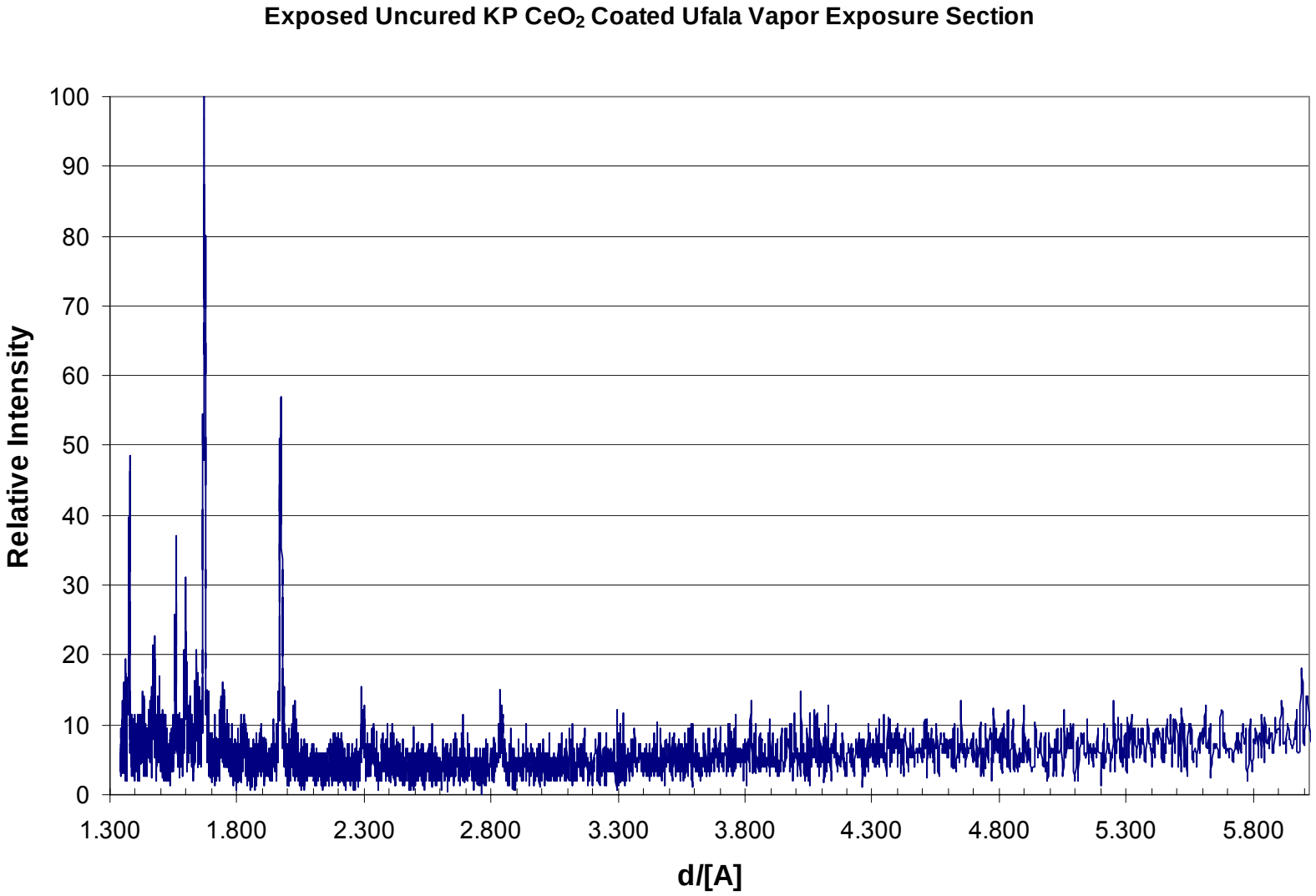
Exposed Uncured KP CeO2 Coated Ufala Vapor Exposure Section
Relative Intensity
100
90
80
70
60
50
40
30
20
10
0
1.300
1.800
2.300
2.800
3.300
3.800
4.300
4.800
5.300
5.800
d/[A]

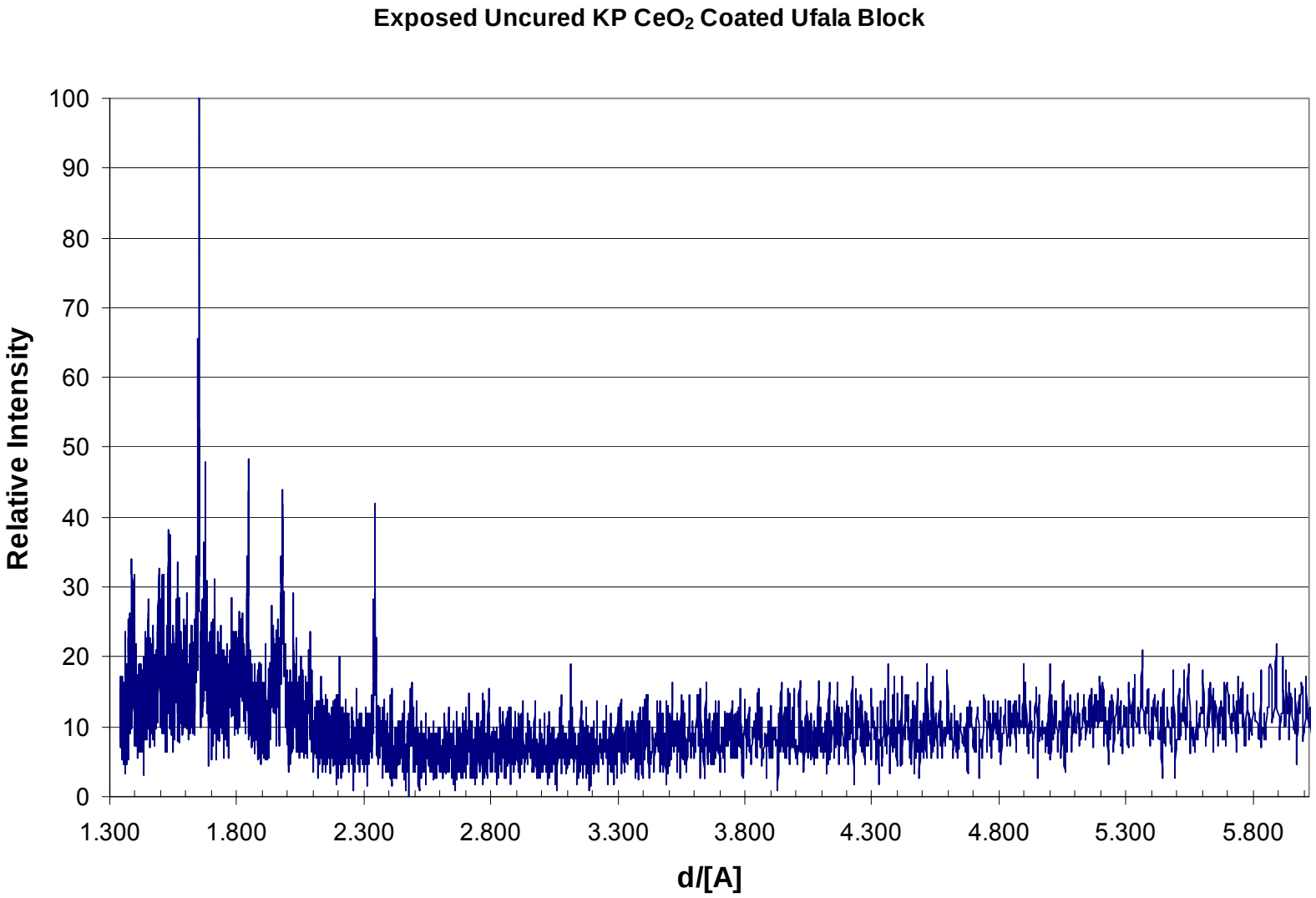
Exposed Uncured KP CeO_2 Coated Ufala Block
Relative Intensity
100
90
80
70
60
50
40
30
20
10
0
1.300
1.800
2.300
2.800
3.300
3.800
4.300
4.800
5.300
5.800
d/[A]

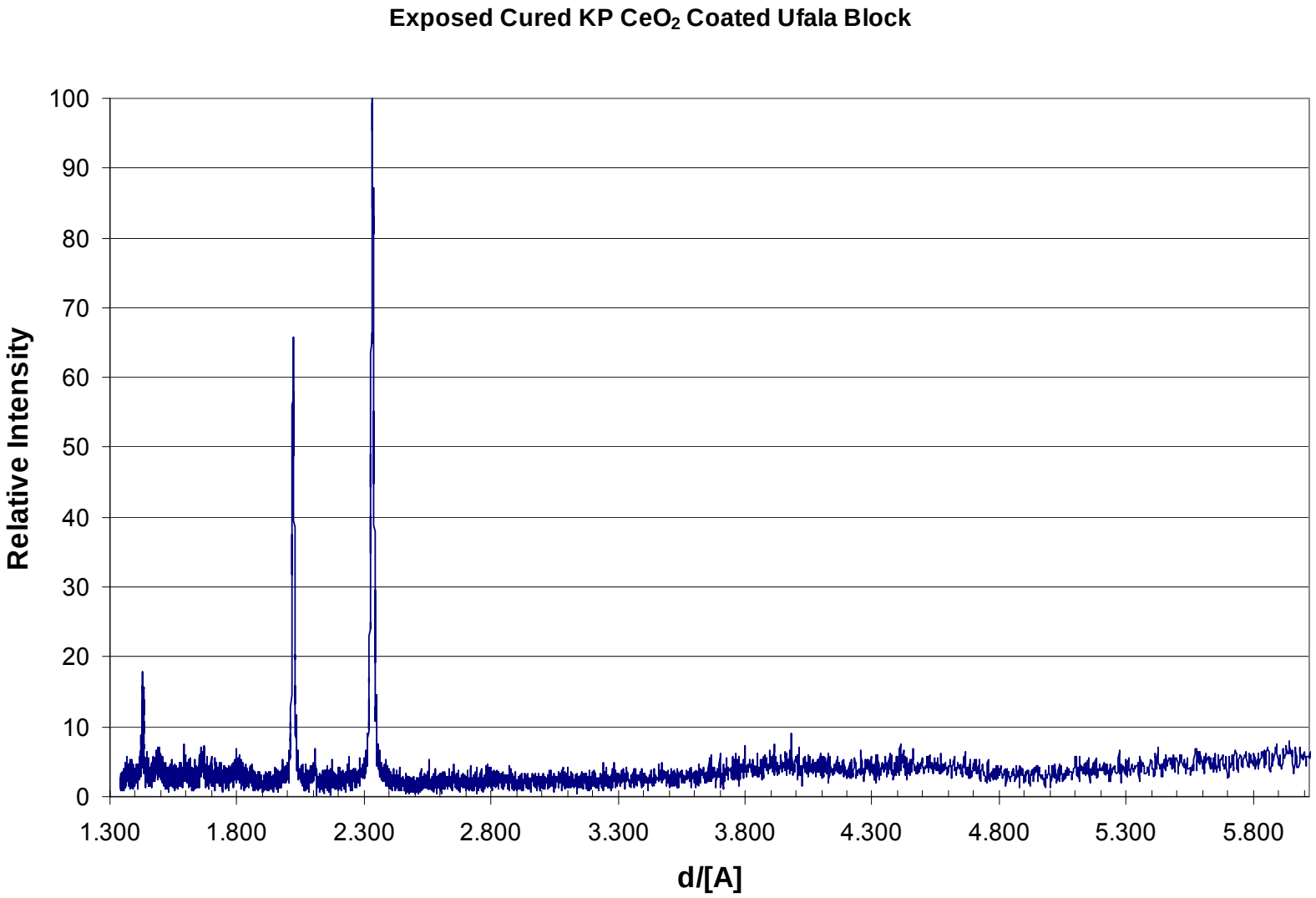
Exposed Cured KP CeO2 Coated Ufala Block
Relative Intensity
100
90
80
70
60
50
40
30
20
10
0
1.300
1.800
2.300
2.800
3.300
3.800
4.300
4.800
5.300
5.800
d/[A]

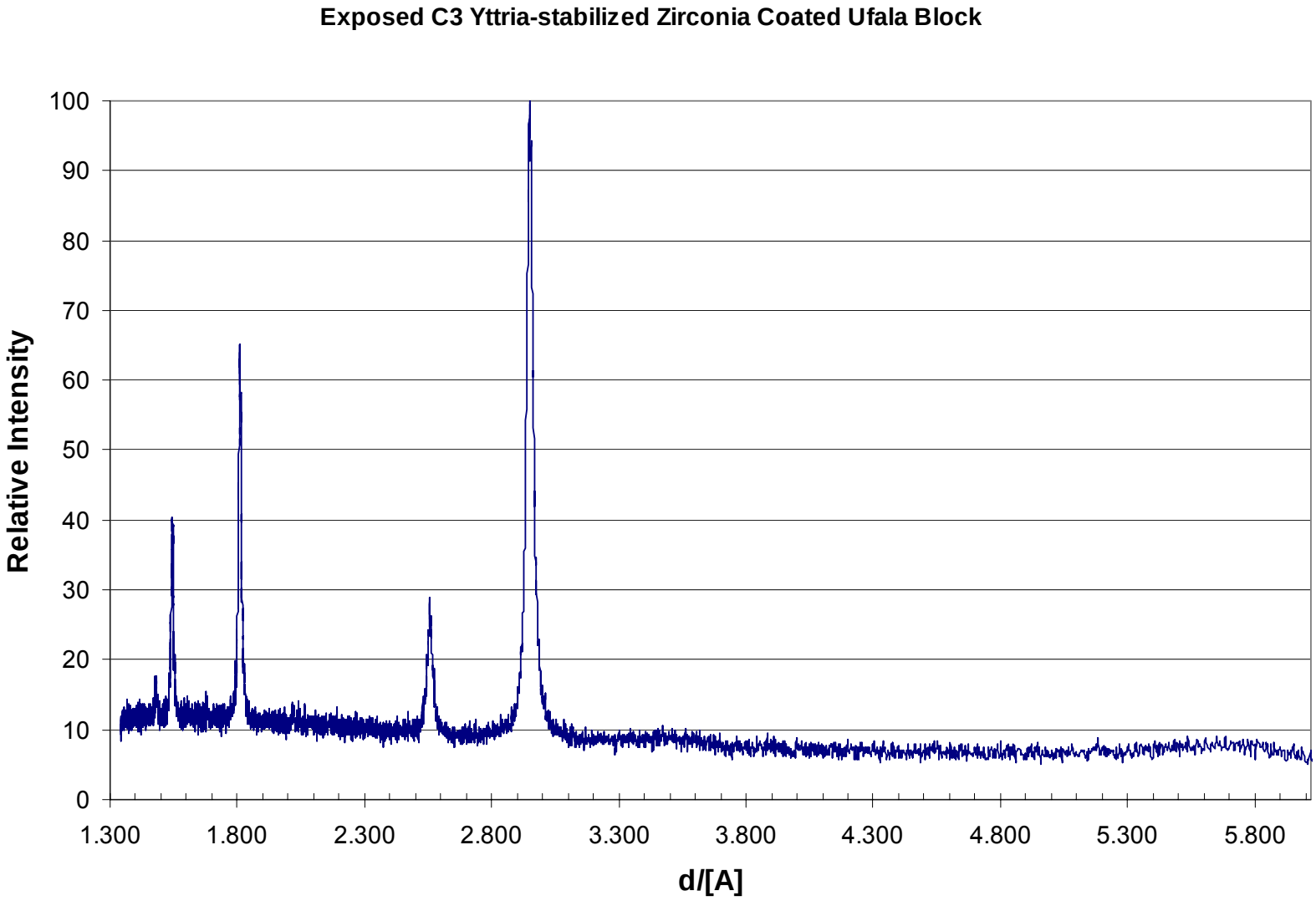
Exposed C3 Yttria-stabilized Zirconia Coated Ufala Block
Relative Intensity
100
90
80
70
60
50
40
30
20
10
0
1.300
1.800
2.300
2.800
3.300
3.800
4.300
4.800
5.300
5.800
d/[A]

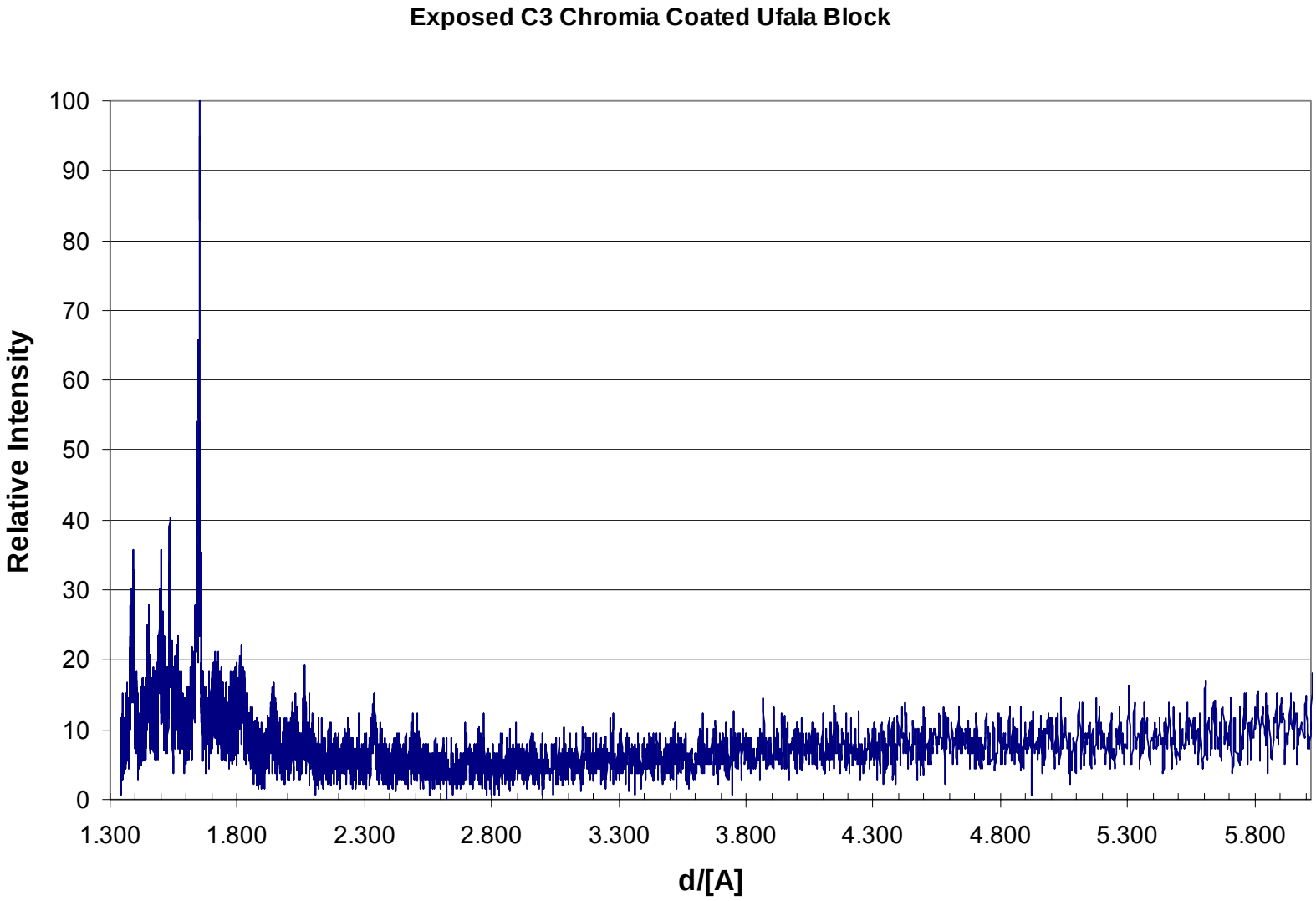
Exposed C3 Chromia Coated Ufala Block
Relative Intensity
100
90
80
70
60
50
40
30
20
10
0
1.300
1.800
2.300
2.800
3.300
3.800
4.300
4.800
5.300
5.800
d/[A]

Appendix D

SEM/EDS

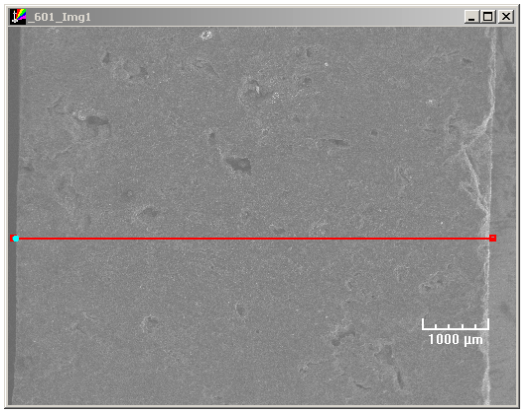

12 hour exposed Ufala® Stick - Vapor Exposure

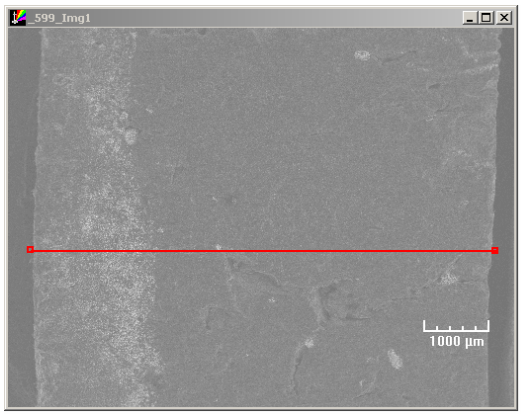

12 hour exposed Ufala® Stick - Interface

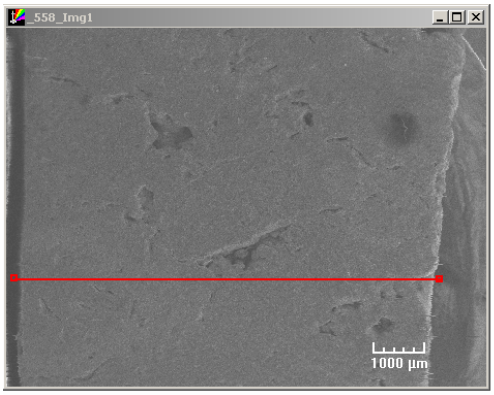

36 hour exposed Ufala® Stick - Vapor Exposure

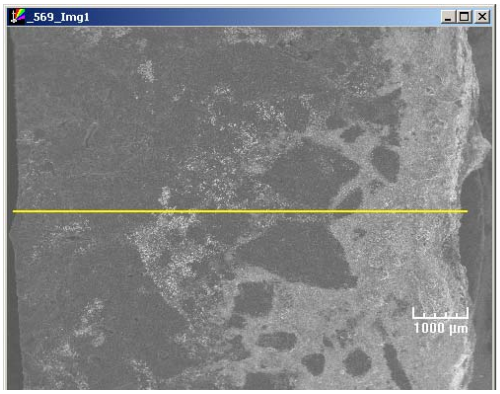

36 hour exposed Ufala® Stick - Liquid Exposure

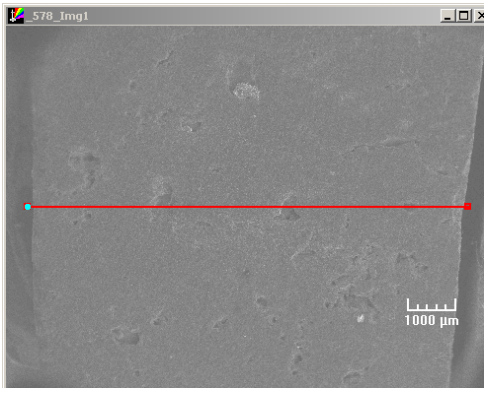

72 hour exposed Ufala® Stick - Vapor Exposure

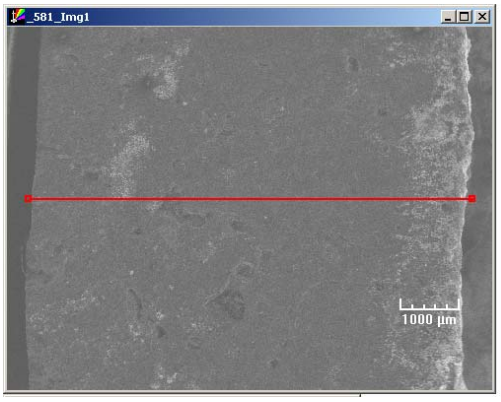

72 hour exposed Ufala® Stick - Interface

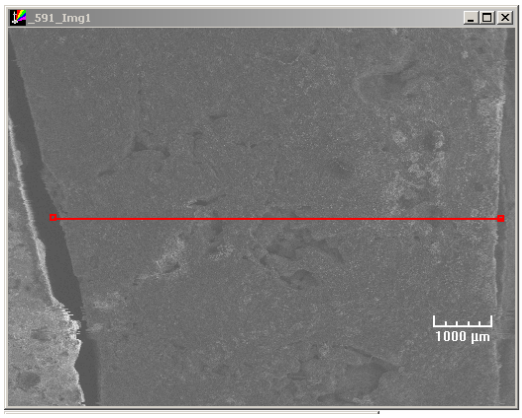

120 hour exposed Ufala® Stick - Vapor Exposure

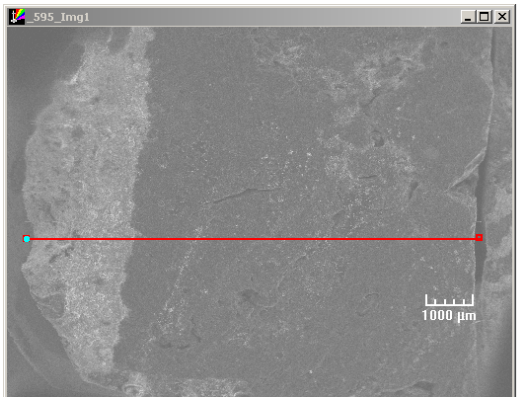

120 hour exposed Ufala® Stick – Interface

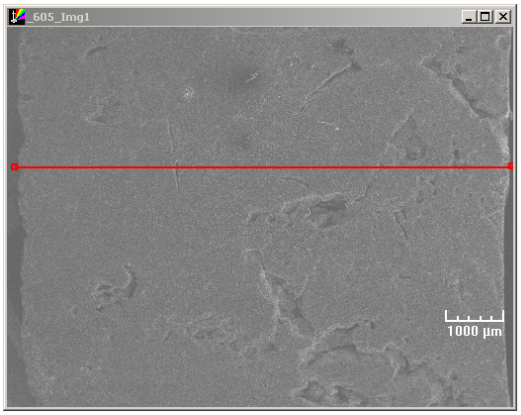

168 hour exposed Ufala® Stick - Vapor Exposure

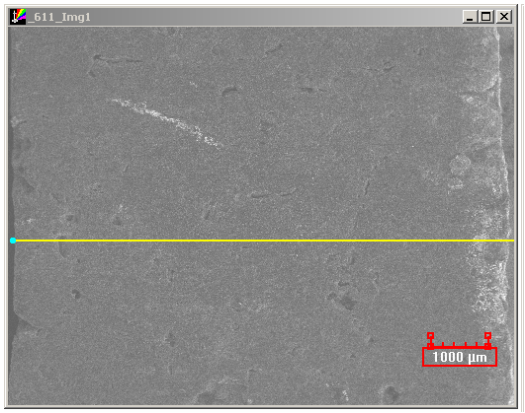

168 hour exposed Ufala® Stick – Interface

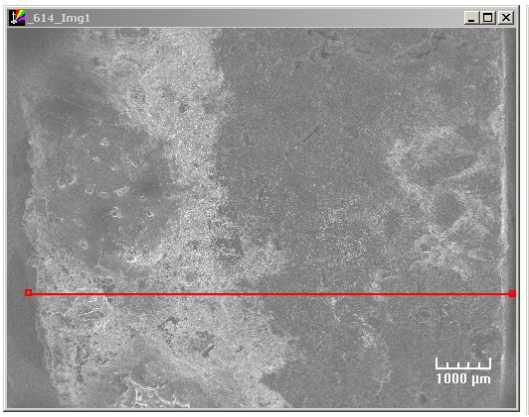

168 hour exposed Ufala® Stick - Liquid Exposure

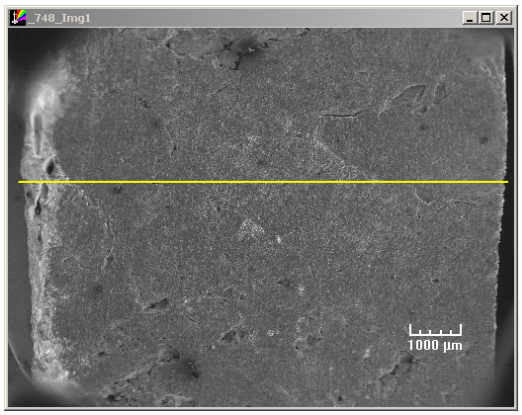

36 hour exposed C3 YSZ Coated Ufala® Stick - Interface

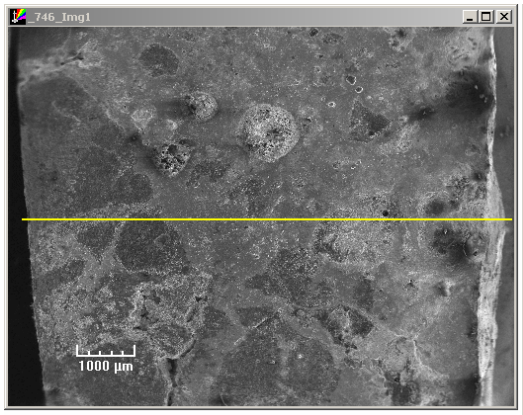

36 hour exposed C3 YSZ Coated Ufala® Stick - Liquid Exposure

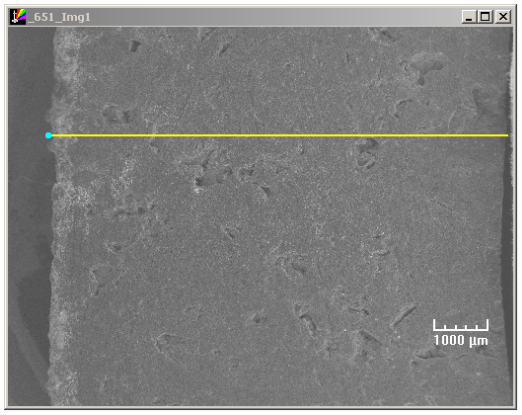

36 hour exposed C3 Na2CeO3 Coated Ufala® Stick - Interface

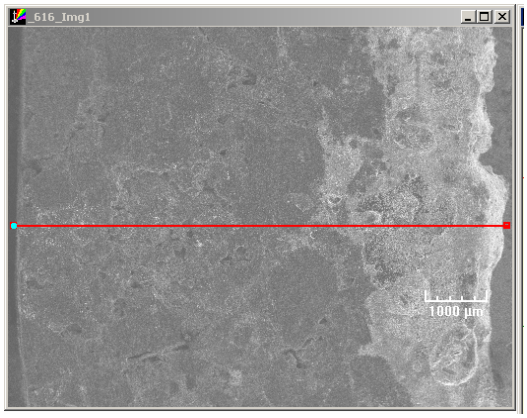

36 hour exposed C3 Cr2O3 Coated Ufala® Block

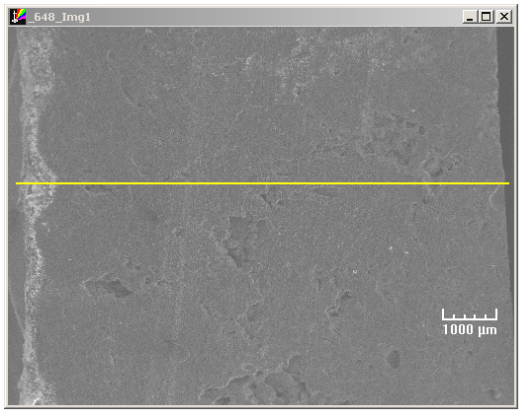

36 hour exposed C3 CeO2 + Powder Coated Ufala® Stick - Interface

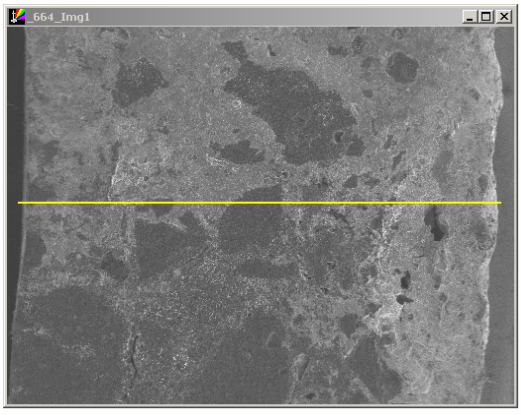

36 hour exposed C3 CeO2 Coated Ufala® Stick – Liquid Exposure

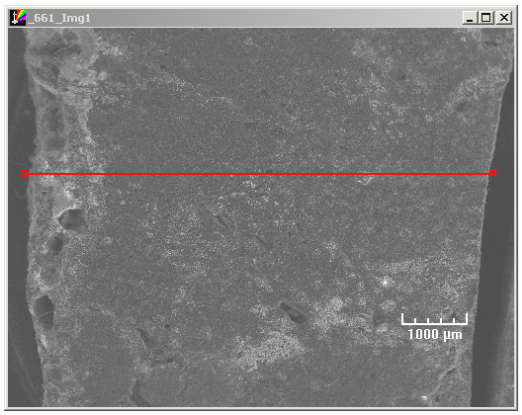

36 hour exposed C3 CeO2 Coated Ufala® Stick – Interface

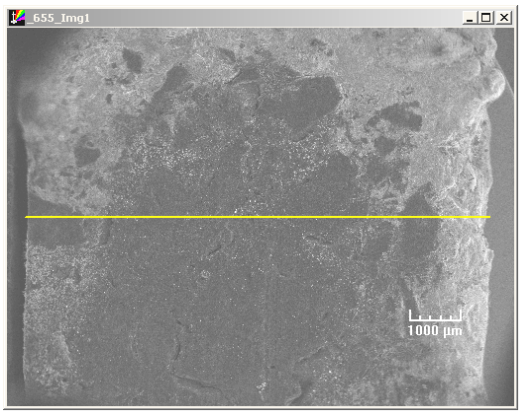

36 hour exposed KP Uncured CeO2 Coated Ufala® Stick – Liquid Exposure

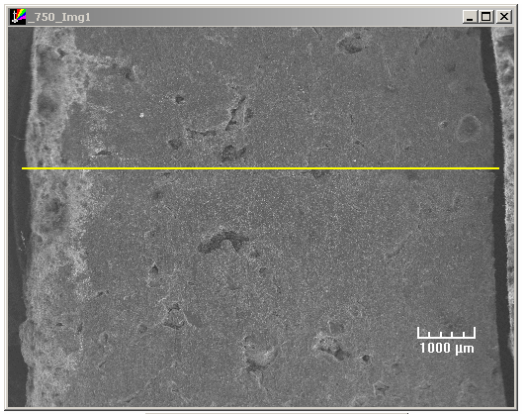

36 hour exposed KP Uncured YSZ Coated Ufala® Stick – Interface

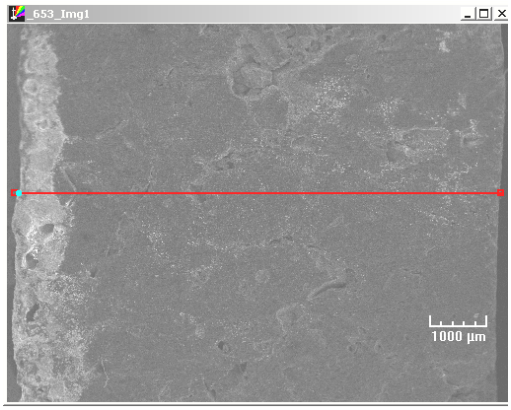

36 hour exposed KP Uncured CeO2 Coated Ufala® Stick – Interface

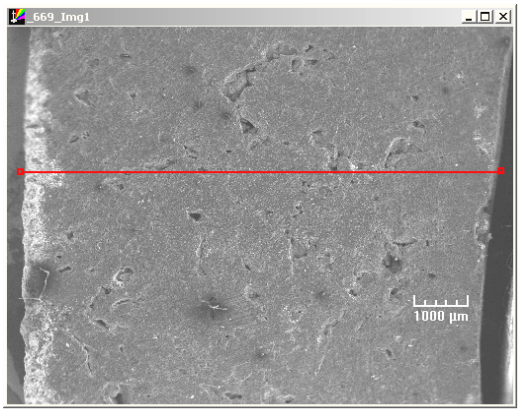

36 hour exposed KP Uncured Cr2O3 Coated Ufala® Stick – Interface

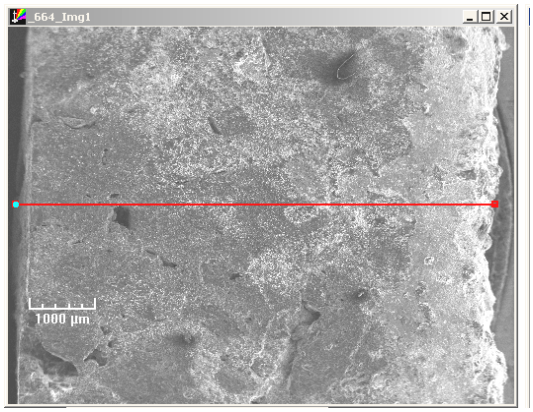

36 hour exposed KP Cured Cr2O3 Coated Ufala® Stick – Interface

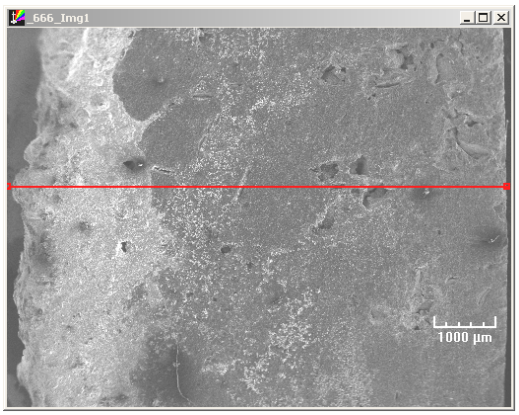

36 hour exposed KP Cured Cr2O3 Coated Ufala® Stick – Liquid Exposure

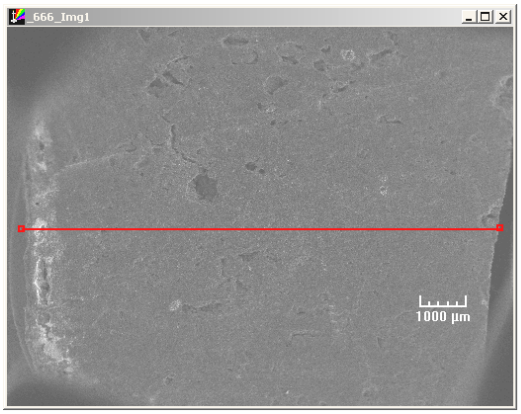

36 hour exposed KP Cured CeO2 Coated Ufala® Stick – Interface

36 hour exposed Uncoated Ufala® Stick – Interface – Carbonate to Sulfide Ratio 65/35

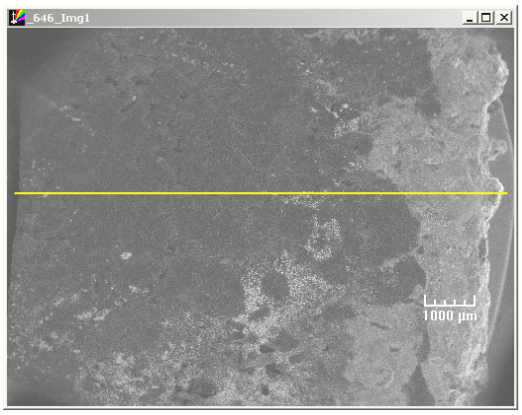

36 hour exposed Uncoated Ufala® Stick – Liquid Exposure – Carbonate to Sulfide Ratio 65/35

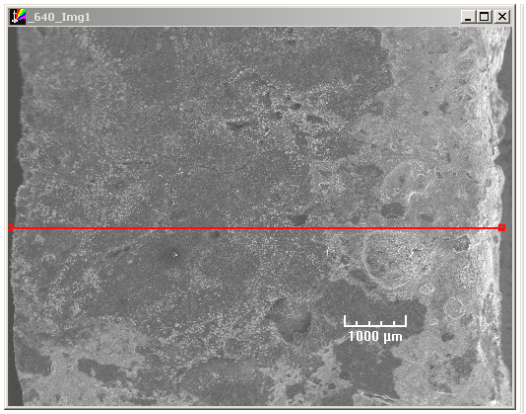

36 hour exposed Uncoated Ufala® Stick – Liquid Exposure – Carbonate to Sulfide Ratio 65/30

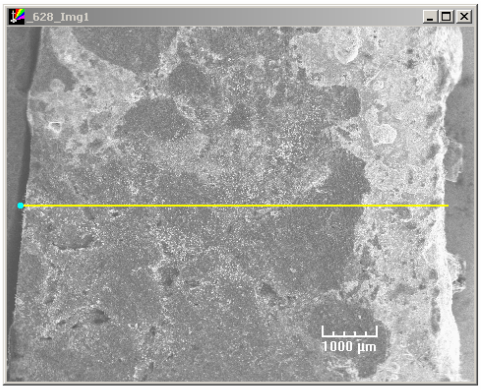

36 hour exposed Uncoated Ufala® Stick – Liquid Exposure – Carbonate to Sulfide Ratio 65/25

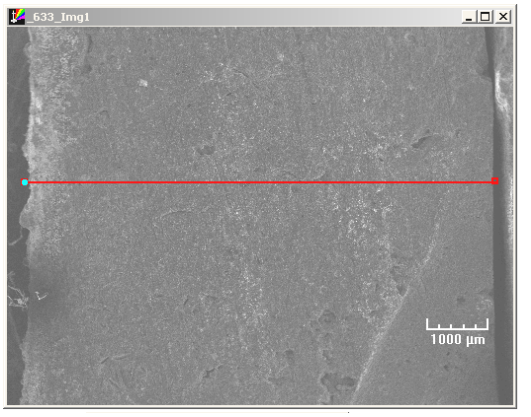

36 hour exposed Uncoated Ufala® Stick – Interface – Carbonate to Sulfide Ratio 65/25

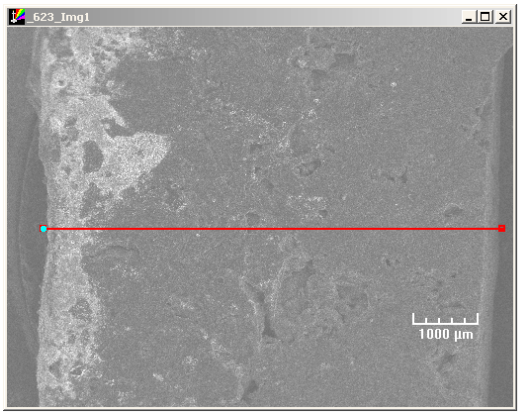

36 hour exposed Uncoated Ufala® Stick – Interface – Carbonate to Sulfide Ratio 65/20

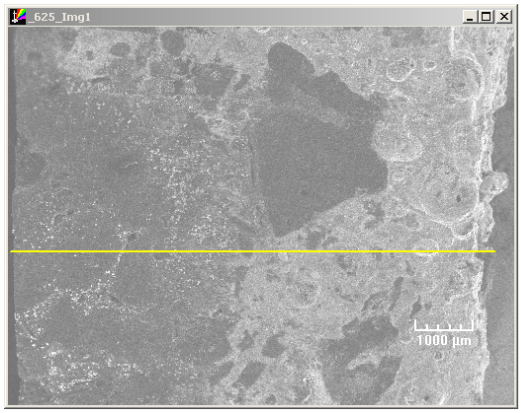

36 hour exposed Uncoated Ufala® Stick –
Liquid Exposure – Carbonate to Sulfide Ratio 65/20

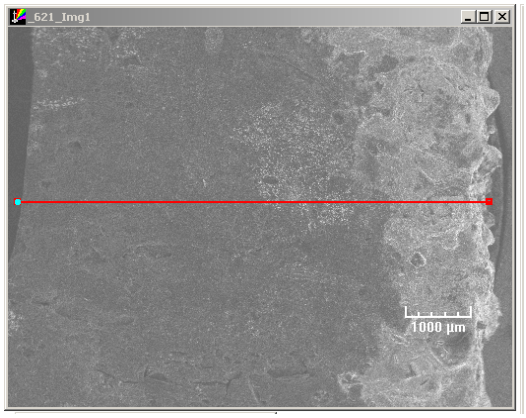

36 hour exposed Uncoated Ufala® Stick –
Liquid Exposure – Carbonate to Sulfide Ratio 65/15

WORKS CITED

1. Biermann, C.J., *Handbook of Pulping and Papermaking*. 2nd ed. 1996, San Diego, CA: Academic Press.

2. Adams, T.M., *Black Liquor Combustion*, in *Pulp and Paper Manufacture*, T.M. Grace, E.W. Malcolm, and M.T. Kocurek, Editors. 1989, TAPPI Press: Atlanta, GA.

3. Grace, T.M., *Kraft Chemical Recovery in a Low-Effluent World.* PaperAge, 1995: p. 20, 25.

4. Grace, T.M. and W.M. Timmer, *Comparison of Alternative Black Liquor Recovery Technologies.* International Chemical Recovery Conference, 1995. **2**: p. 269-275.

5. Kiiskila, E., et al., *Possibilities for New Black-Liquor Processes in the Pulping Industry: Energy and Emissions.* Bioresource Technology: Biomass, Bioenergy, Biowastes, Conversion Technologies, Biotransformations, Production Technologies, 1993. **46**(1-2): p. 129-134.

6. Saviharju, K., *Black-Liquor Gasification: Results from Laboratory Research and Rig Tests.* Bioresource Technology: Biomass, Bioenergy, Biowastes, Conversion Technologies, Biotransformations, Production Technologies, 1993. **46**(1-2): p. 145-151.

7. Peascoe, R.A., et al., *Comparison of Refractory Performance in Black Liquor Gasifiers and a Smelt Test System* International Chemical Recovery Conference, 2001: p. 297-300.

8. Erickson, D. and C. Brown, *Operating Experience with a Gasification Pilot Project.* TAPPI Journal 1999. **82**(9): p. 48-50.

9. Brown, C.A., et al., *The Chemrec Black Liquor Gasifier at New Bern - A Status Report.* International Chemical Recovery Conference, 2004. **2**: p. 1089-1093.

10. Sproul, W.D. and K.O. Legg, *Introduction to Advanced Surface Treatments*, in *Opportunities for Innovation: Advanced Surface Engineering*, W.D. Sproul and K.O. Legg, Editors. 1994, Technomic Publishing: Lancaster, PA. p. 1-5.

11. Lefebvre, B. and G. Santyr, *Chemical Recovery - Equipment*, in *Chemical Recovery in the Alkaline Pulping Process*, R.P. Green and G. Hough, Editors. 1992, TAPPI Press: Atlanta, GA. p. 79-117.

12. Smook, G.A., *Handbook for Pulp & Paper Technologists*. 2nd ed. 1992, Vancouver, British Columbia, Canada: Angus Wilde Publications.

13. Eriksson, H., S. Harvey, and T. Berntsson, *Efficient Use of Biomass in Black Liquor Gasification Plants.* International Chemical Recovery Conference, 2001(Poster Presentations): p. 75-80.

14. Finchem, K.J., *Black Liquor Gasification Research Yields Recovery Options for Future.* Pulp & Paper, 1995. **69**(11): p. 49-54.

15. Dahlquist, E. and R. Jacobs, *Development of a Dry Black Liquor Gasification Process.* Pulp & Paper Canada, 1994. **95**(2): p. 46-47.

16. Verrill, C.L., A.R.P. vanHeiningen, and J. McKenzie, *Calcium Based Sulfur Recovery Process for Kraft Black Liquor Gasification - Proof of Concept.* International Chemical Recovery Conference, 1998. **2**: p. 853-870.

17. Sinquefield, S., et al., *Black Liquor Gasification: 1. The Impact of Pressure on C-H-O-S Gas Speciation and Tar Components During Pyrolysis.* International Chemical Recovery Conference, 2001(Poster Presentations): p. 117-121.

18. Gemmer, B., D. Cicero, and R. DeCarrera. *Black Liquor Gasification Expected to Yield Energy, Environmental, and Economic Benefits*. 2001 Accessed 6/12/2005 [cited; Available from: http://eereweb.ee.doe.gov/industry/bestpractices/fall2001_black_liquor.html.

19. Kymalainen, M., et al., *Sulfate Reduction in an Entrained-Flow Black Liquor Gasifier.* International Chemical Recovery Conference, 1995. **2**: p. 251-267.

20. Larson, E.D., et al., *A Cost-Benefit Analysis of Black Liquor Gasifier/Combined Cycle Technology Integrated into a Kraft Pulp Mill.* TAPPI Journal, 1998. **1**: p. 1-18.

21. Stiggson, L.L. and B. Hesseborn, *Gasification of Black Liquor.* International Chemical Recovery Conference, 1995. **2**: p. 277-295.

22. *Materials for High-Temperature Gasification*. 2004 Accessed 10/12/2005 [cited; Available from: http://www.eere.energy.gov/industry/imf/pdfs/16540_mat_black_liquor_gas.pdf.

23. Keiser, J.R., et al. *Improved Materials for High-Temperature Black Liquor Gasification*. Accessed 10/12/2005 [cited; Available from: http://www.eere.energy.gov/industry/imf/pdfs/16540blackliquorgas.pdf.

24. Brown, C.A. and W.D. Hunter, *Operating Experience at North America's First Commercial Black Liquor Gasification Plant.* International Chemical Recovery Conference, 1998. **2**: p. 655-662.

25. Keiser, J.R., et al., *Materials Issues in Black Liquor Gasification Systems.* 11th International Symposium on Corrosion in the Pulp & Paper Industry, 2004: p. 255-270.

26. Berglin, N., L. Persson and T. Berntsson, *Energy System Options with Black Liquor Gasification.* International Chemical Recovery Conference, 1995. **2**: p. 311-315.

27. Banerjee, S., *Properties of Refractories*, in *Refractories Handbook*, C.A. Schacht, Editor. 2004, Marcel Dekker: New York, NY. p. 1-10.

28. Schacht, C.A., *Thermomechanical Considerations for Refractory Linings*, in *Refractories Handbook*, C.A. Schacht, Editor. 2004, Marcel Dekker: New York, NY. p. 369-394.

29. Brosnan, D.A., *Alumina-Silica Brick*, in *Refractories Handbook*, C.A. Schacht, Editor. 2004, Marcel Dekker: New York, NY. p. 79-107.

30. Davis, R.F. and J.A. Pask, *Mullite*, in *High Temperature Oxides - Part IV*, A.M. Alper, Editor. 1971, Academic Press: New York, NY. p. 36-71.

31. Levin, E.M., C.R. Robbins, and H.F. McMurdie, *Al_2O_3-SiO_2 System*, in *Phase Diagrams for Ceramists*, M.K. Reser, Editor. 1969, The American Ceramic Society: Columbus, OH. p. 123, Figure 314.

32. Baxendale, S., *Testing of Refractory Materials*, in *Refractories Handbook*, C.A. Schacht, Editor. 2004, Marcel Dekker: New York, NY. p. 435-474.

33. Hendrick, M.R., J.M. Hampikian, and W.B. Carter, *High Temperature Oxidation of an Alumina-Coated Ni-Base Alloy*, in *Elevated Temperature Coatings: Science and Technology II*, N.B. Dahotre and J.M. Hampikian, Editors. 1996, The Minerals, Metals, & Materials Society: Warrendale, PA. p. 287-299.

34. Brosnan, D.A., *Corrosion of Refractories*, in *Refractories Handbook*, C.A. Schacht, Editor. 2004, Marcel Dekker: New York, NY. p. 39-77.

35. Bradley, L., L. Li, and F.H. Stott, *Surface Modification of Alumina-Based Refractories Using a Xenon Arc Lamp.* Applied Surface Science, 2000. **154**: p. 675-681.

36. Anderson, J.C., *Conduction and Diffusion Processes*, in *Science and Technology of Surface Coating*, B.N. Cashman and J.C. Anderson, Editors. 1974, Academic Press: London, England. p. 22-27.

37. Hines, A.L. and R.N. Maddox, *Mass Transfer Fundamentals and Applications*. 1985, Upper Saddle River, NJ: Prentice Hall.

38. Mencke, K.M., *Assessing Refractory Coatings for Use in High-Temperature Black Liquor Gasification*, in *Materials Science and Engineering*. 2004, The Georgia Institute of Technology: Atlanta, GA.

39. Levin, E.M., C.R. Robbins, and H.F. McMurdie, *Al_2O_3-$NaAlO_2$ System*, in *Phase Diagrams for Ceramists*, M.K. Reser, Editor. 1969, The American Ceramic Society: Columbus, OH. p. 81, Figure 2284.

40. Levin, E.M., C.R. Robbins, and H.F. McMurdie, *Na_2O - SiO_2 System*, in *Phase Diagrams for Ceramists*, M.K. Reser, Editor. 1969, The American Ceramic Society: Columbus, OH. p. 81, Figure 2286.

41. Levin, E.M., C.R. Robbins, and H.F. McMurdie, *Na_2O-Al_2O_3-SiO_2 System*, in *Phase Diagrams for Ceramists*, M.K. Reser, Editor. 1969, The American Ceramic Society: Columbus, OH. p. 181, Figure 501.

42. Dettenwanger, F., et al., *Investigation of Damage Mechanisms in Thermal Barrier Coatings by Acoustic Emission*, in *Elevated Temperature Coatings: Science and Technology III*, J.M. Hampikian and N.B. Dahotre, Editors. 1999, The Minerals, Metals, & Materials Society: Warrendale, PA. p. 39-48.

43. Purdue University. Thermophysical Properties Research Center. and Y.S. Touloukian, *Thermophysical Properties of Matter*, ed. Y.S. Touloukian. Vol. 13. 1970, New York, NY: IFI/Plenum.

44. Bloom, H., *The Chemistry of Molten Salts*. The Physical Inorganic Chemistry Series, ed. M.J.S. Robert A. Plane. 1967, New York, NY: W. A. Benjamin.

45. Lovering, D.G. and R.J. Gale, *Introduction*, in *Molten Salt Techniques*, D.G. Lovering and R.J. Gale, Editors. 1983, Plenum Press: New York, NY. p. 1-17.

46. Jacobson, N.S., K.N. Lee, and T. Yoshio, *Corrosion of Mullite by Molten Salts.* Journal of the American Ceramic Society, 1996. **79**(8): p. 2161-2167.

47. Cutler, A.J.B., *Molten Sulfates*, in *Molten Salt Techniques*, D.G. Lovering and R.J. Gale, Editors. 1983, Plenum Press: New York, NY. p. 111-136.

48. Tiegs, T.N., et al., *Surface Modification of Ceramics by High Density Infrared Heating.* Ceramic Engineering and Science Proceedings, 2003. **24**(3): p. 477-482.

49. Eidelman, S. and X. Yang, *Optimization of Thermal Spray Guns and Coating Processes Using Numerical Simulations*, in *Elevated Temperature Coatings: Science and Technology II*, N.B. Dahotre and J.M. Hampikian, Editors. 1996, The Minerals, Metals, & Materials Society: Warrendale, PA. p. 47-57.

50. Richard, C., G. Beranger, and J. Lu, *Residual Stresses, Adhesion and Thermal Sprayed Coatings*, in *Elevated Temperature Coatings: Science and Technology II*, N.B. Dahotre and J.M. Hampikian, Editors. 1996, The Minerals, Metals, & Materials Society: Warrendale, PA. p. 77-86.

51. Horie, C.V., *Materials for Conservation: Organic Consolidants, Adhesives, and Coatings*. Butterworths Series in Conservation and Museology, ed. S.G. Rees-Jones and D. Linstrum. 1987, London, England: Butterworths.

52. Chen, W., et al., *Sol-Gel Preparation of Thick Titania Coatings Aided by Organic Binder Materials.* Sensors and Actuators B: Chemical, 2004. **100**(1-2): p. 195-199.

53. Okutomi, M. and K. Tsukamoto, *Application of Ceramic Coating and Spherical Ceramic Particle Synthesis Using Laser Spray Technique*, in *Elevated Temperature Coatings: Science and Technology II*, N.B. Dahotre and J.M. Hampikian, Editors. 1996, The Minerals, Metals, & Materials Society: Warrendale, PA. p. 59-67.

54. Brinker, C.J., et al., *Sol-Gel Derived Ceramic Films - Fundamentals and Applications*, in *Metallurgical and Ceramic Protective Coatings*, K.H. Stern, Editor. 1996, Chapman & Hall: London, England. p. 112-151.

55. Bunshah, R.F., *Deposition Technologies: An Overview*, in *Handbook of Deposition Technologies for Films and Coatings 2nd Edition*, R.F. Bunshah, Editor. 1994, Noyes Publications: Park Ridge, NJ. p. 1-28.

56. Chapman, B.N. and J.C. Anderson, *Introduction*, in *Science and Technology of Surface Coating*, B.N. Chapman and J.C. Anderson, Editors. 1974, Academic Press: London, England. p. ix-xvii.

57. Li, J.F., L. Li, and F.H. Stott, *Multi-Layered Surface Coatings of Refractory Ceramics Prepared by Combined Laser and Flame Spraying.* Surface & Coatings Technology, 2004. **180**: p. 500-505.

58. Triantafyllidis, D., L. Li, and F.H. Stott, *Surface Treatment of Alumina-Based Ceramics Using Combined Laser Sources.* Applied Surface Science, 2002. **186**(1-4): p. 140-144.

59. Gogotski, Y.G. and V.A. Lavrenko, *Corrosion of High-Performance Ceramics*. 1992, Berlin, Germany: Springer-Verlag.

60. Li, T.K., D.A. Hirschfeld, and J.J. Brown, *Alkali Corrosion Resistant Coatings for Si_3N_4 Ceramics.* Journal of Materials Science, 1997. **32**(16): p. 4455-4461.

61. Näfe, H. and G.M. Kale, *On the Thermodynamic Activity of Na_2O in Na-Beta-Alumina.* Materials Research Bulletin, 2002. **37**: p. 1063-1069.

62. Blachere, J.R. and F.S. Pettit, *High Temperature Corrosion of Ceramics*. 1989, Park Ridge, NJ: Noyes Data Corporation.

63. Hirata, T., K. Akiyama, and H. Yamamoto, *Corrosion Resistance of Cr_2O_3-Al_2O_3 Ceramics by Molten Sodium Sulphate-Vanadium Pentoxide.* Journal of Material Science, 2001. **36**(24): p. 5927-5934.

64. Lawson, M.G., F.S. Pettit, and J.R. Blachere, *Hot Corrosion of Alumina.* Journal of Materials Research, 1993. **8**(8): p. 1964-1971.

65. Hirata, T., S. Ota, and T. Morimoto, *Influence of Impurities in Al_2O_3 Ceramics on Hot Corrosion Resistance Against Molten Salt.* Journal of the European Ceramic Society, 2003. **23**(1): p. 91-97.

66. Paul, S., *Paint Properties and Their Evaluation*, in *Surface Coatings Science & Technology 2nd Edition*, S. Paul, Editor. 1996, John Wiley & Sons: Chichester, West Sussex, England. p. 511-651.

67. Buehler, *Tables for Knoop and Vickers Hardness Numbers*.